Antón Camilo Pérez Astray

Chemical looping combustion of biomass with negative CO2 emissions

Director/es

Mendiara Negredo, María Teresa
Diego Poza, Luis Francisco de

Universidad Zaragoza
1542

Tesis Doctoral

CHEMICAL LOOPING COMBUSTION OF BIOMASS WITH NEGATIVE CO2 EMISSIONS

Autor

Antón Camilo Pérez Astray

Director/es

Mendiara Negredo, María Teresa
Diego Poza, Luis Francisco de

UNIVERSIDAD DE ZARAGOZA
Escuela de Doctorado

2020

Departamento de Ingeniería Química y Tecnologías del Medio Ambiente
UNIVERSIDAD DE ZARAGOZA

DOCTORAL THESIS

CHEMICAL LOOPING COMBUSTION OF BIOMASS WITH NEGATIVE CO$_2$ EMISSIONS

Author: Antón C. Pérez Astray

Supervisors: M. Teresa Mendiara Negredo

Luis F. de Diego Poza

Zaragoza, December 2019

INSTITUTO DE CARBOQUIMICA

CSIC
CONSEJO SUPERIOR DE INVESTIGACIONES CIENTÍFICAS

M. Teresa Mendiara Negredo, Investigadora ''Ramón y Cajal'', y

Luis F. de Diego Poza, Investigador científico del CSIC,

CERTIFICAN:

que el trabajo titulado:

"Combustión de biomasa mediante transportadores de oxígeno con emisiones negativas de CO$_2$"

"Chemical Looping Combustion of biomass with negative CO$_2$ emissions"

Fue realizado por Antón C. Pérez Astray bajo la dirección de los abajo firmantes en el Instituto de Carboquímica (ICB-CSIC) en Zaragoza y se corresponde con el plan de investigación aceptado el 29 de septiembre de 2016 por la Comisión de Doctorado de la Universidad de Zaragoza. Así mismo, se autoriza a la presentación de la misma como compendio de publicaciones.

Y para que así conste, se firma el presente certificado,

Fdo: Dra. M. Teresa Mendiara Negredo   Fdo: Dr. Luis F. de Diego Poza

en Zaragoza, a 12 de noviembre de 2019.

Chemical Looping Combustion of biomass with negative CO_2 emissions

Abstract

CO_2 emissions to the atmosphere became an important environmental problem because of the effect on the global warming and consequently, the climate change. The climate change challenge demands a commitment of combined strategies between global institutions, governments and citizens. To reach the objectives set in the Paris Agreement (2015), greenhouse gas emissions need to be reduced. No technology is currently able to achieve the necessary reductions in greenhouse gas emissions on its own. Biomass represents an interesting alternative fuel for heat and power production as a carbon dioxide-neutral fuel. Moreover, if the CO_2 generated during biomass combustion process is captured then negative-CO_2 emissions would be reached and these are named bioenergy with Carbon Capture and Storage (BECCS) technologies.

Chemical Looping Combustion (CLC) came up as one of the most promising CO_2 capture technologies thanks to the low energy penalty of the CO_2 separation and therefore, low-cost. CLC technologies are based in two interconnected fluidized bed reactors without gas mixing. The combustion takes place in the fuel reactor where the oxygen is supplied by a solid oxygen carrier, normally metal oxides. After being reduced, the oxygen carrier goes to the air reactor without gas mixing between reactors where it is oxidized again in air, and it is able for a new redox cycle starts.

The main objective of this thesis is to evaluate the biomass combustion with CLC technologies (bioCLC). The research plan covers studies different at different scales, starting at lab scale, through a 1 kW_{th} pilot plant, to the continuous operation in a 20 kW_{th} plant to demonstrate the viability and optimizing the operation range for different low-cost oxygen carriers and different types of biomass residues.

Iron based ores as well as manganese ores has been pointed as promising oxygen carriers because of their reactivity and low cost. Under *In Situ* Gasification

Chemical Looping Combustion (iG-CLC) mode, the performance of the process was studied focusing on the effect of different important operating variables in a 1 kW$_{th}$ CLC unit. Values about 100% of carbon capture efficiency with the three types of biomass were obtained using ores as oxygen carrier and the total oxygen demand was reduced because of the different reactivity of each oxygen carrier and the operating conditions optimization. Also a synthetic iron-manganese mixed able to release molecular oxygen during the CLC process was used. The effect of the several operating variables was also studied finding a high dependency on the air excess and the temperature, both in the air reactor, on the CO_2 capture efficiency and the total oxygen demand. About 100% of CO_2 capture efficiency achieving values of total oxygen demand about 5%. The use of a mixed Cu-Mn oxide was also studied as a Chemical Looping with Oxygen Uncoupling (CLOU) oxygen carrier. High CO_2 capture efficiencies were obtained and close to null total oxygen demand was achieved.

The effect of the operating conditions on the performance of CLC was evaluated in a 20 kW$_{th}$ CLC unit using an iron ore as oxygen carrier. A Spanish biomass residue was tested achieving values close to 100% and total oxygen demands between 15-20% despite the low temperature used, supporting the consideration of the CLC process with biomass (bioCLC) as a promising bioenergy with Carbon Capture (BECCS) technology.

One of the aspects to be considered in the combustion of biomass is the formation of NO$_x$ and the possible existence of tar in the gaseous product stream. This work compares the results obtained with two different chemical looping combustion modes, iG-CLC and CLOU.

All these results show the feasibility of the integration of solid biofuels with CLC technologies achieving a negative emission technology able to produce an energy gain through a BECCS technology.

Keywords: Biomass, NET, BECCS, CLC, iG-CLC, CLOU

List of publications

I. Mendiara, T., A. Pérez-Astray, M. T. Izquierdo, A. Abad, L.F. de Diego, F. García-Labiano, P. Gayán, J. Adánez. Chemical Looping Combustion of different types of biomass in a 0.5 kW_{th} unit. Fuel. 2018, 211, 868-875.

II. Pérez-Astray A, Mendiara T, de Diego L.F., Abad A, García-Labiano F, Izquierdo M.T., Adánez J. (2019a) Manganese ores as low-cost oxygen carriers for biomass chemical looping combustion in a 0.5 kW_{th} unit. *Submitted to Fuel Processing Technology.*

III. Pérez-Astray A, Mendiara T, de Diego L.F., Abad A, García-Labiano F, Izquierdo M.T., Adánez J. (2019b) CLC of biomass as a BECCS technology using a manganese-iron mixed oxide. *Submitted to Sep. Purif. Technol.*

IV. Adánez-Rubio, I., A. Pérez-Astray, T. Mendiara, M.T. Izquierdo, A. Abad, P. Gayán, L.F. de Diego, F. García-Labiano, J. Adánez. Chemical Looping Combustion of biomass: CLOU experiments with a Cu-Mn mixed oxide. Fuel Processing Technology. 2018, 172, 179-186.

V. Adánez-Rubio, I., A. Pérez-Astray, A. Abad, P. Gayán, L.F. de Diego, J. Adánez. Chemical Looping with oxygen uncoupling: an advanced biomass combustion technology to avoid CO_2 emissions. Mitigation and Adaptation Strategies for Climate Change. 2019. Article in press. doi: 10.1007/s11027-019-9840-5.

VI. Pérez-Astray, A., I. Adánez-Rubio, T. Mendiara, M.T. Izquierdo, A. Abad, P. Gayán, L. F. de Diego, F. García-Labiano, J. Adánez. Comparative study of fuel-N and tar evolution in chemical looping combustion of biomass under both *i*G-CLC and CLOU modes. Fuel. 2019, 236, 598-607.

Contribution report

- Co-author, responsible for the experimentation, data evaluation and writing. Papers I, IV, V.
- Principal author, responsible for the experimental work, data evaluation and writing. Papers II, III, VI.

Acknowledgements

x

Index

Figure index

xiv

Table index

INTRODUCTION

1.1 Earth's energy balance

Since the beginning of life, about 4000 million years ago, the Sun has been supplying energy to the planet Earth. Autotroph organisms use the Sun energy to convert inorganic compounds into organic ones that they use for their biological functions. The deposition of organic materials into geologic formations under specific conditions and during long-term periods favored the fossil fuel formation. Therefore, the Earth can be considered a fossil battery in which the irradiancy coming from the Sun represents the only energy input of about 1353 W/m² in average (Schramski et al. 2015). Biomass acts as the solar energy accumulation, and coal, oil and natural gas correspond to different evolution states of natural biomass deposits into the earth's crust forming these diverse hydrocarbons associated to geological formations.

In the Paleolithic era, humans controlled the fire using vegetable biomass residues. Biomass is here all the organic matter susceptible to produce energy excluding that accumulated into geological formations (ISO 2014). Protection, thermal comfort, better food usability or lighting were the first energy uses of the biomass, being the first energy source controlled by humans. The agricultural practice development allowed an energy surplus generation that also facilitated animal domestication. This achievement provided food and animal work, increasing the individual energy demand as well as satisfying new energy needs. Figure 1 shows the evolution of the estimated individual human exogenous energy consumption. The sail navigation developing and water mills utilization implied the kinetic and potential energy use. The transportation and new goods and materials appeared at that time as the new needs for humans. Moreover, the continuous improvement of technologies for the use of different energy sources correspond with the major step forward from advanced agricultural to industrial societies (Malanima 2014).
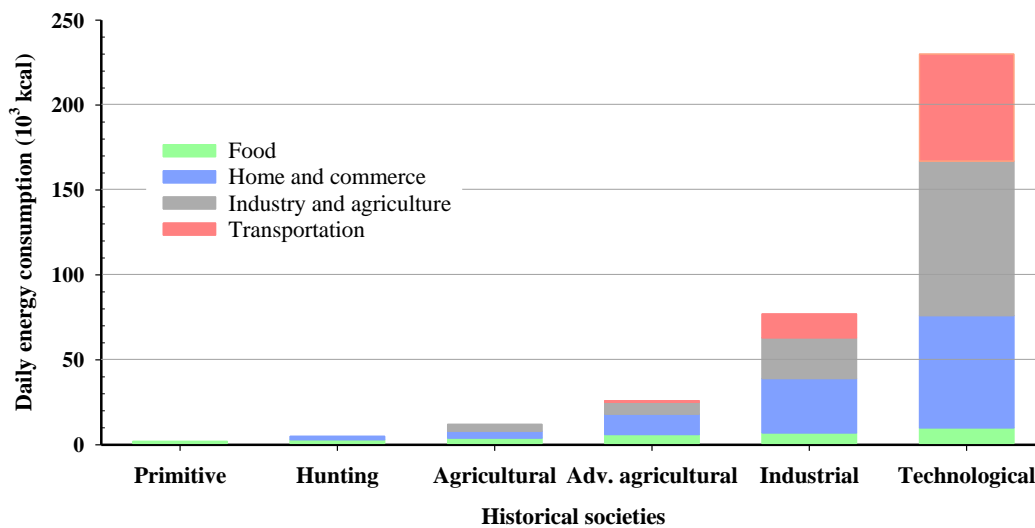
Figure 1. Evolution of estimated exogenous energy needs per capita.

Source: modified from Cook (1971).

The steam engine invention started the First Industrial Revolution. Coal began to be used for almost any mechanical activity and, in this way, the CO_2 previously captured in the fossil fuels from the ancient atmosphere during millions of years started being released modifying its concentration in the atmosphere (Schramski et al. 2015). The use of oil began the Second Industrial Revolution and

for hundreds of years the use of fossil fuels has been increasing along the increase of human energy needs. Figure 2 presents the evolution of energy consumption from Middle Ages to the present. The deployment of new more efficient and non-fossil-fueled technologies, started during the 20th century continuing until now. However, since the fire discovering, combustion processes jointly remain as the major contributors to the mix of primary energy consumption. Moreover, technological improvements allowed the use of more and more exogenous energy in different and complex activities in today's societies.
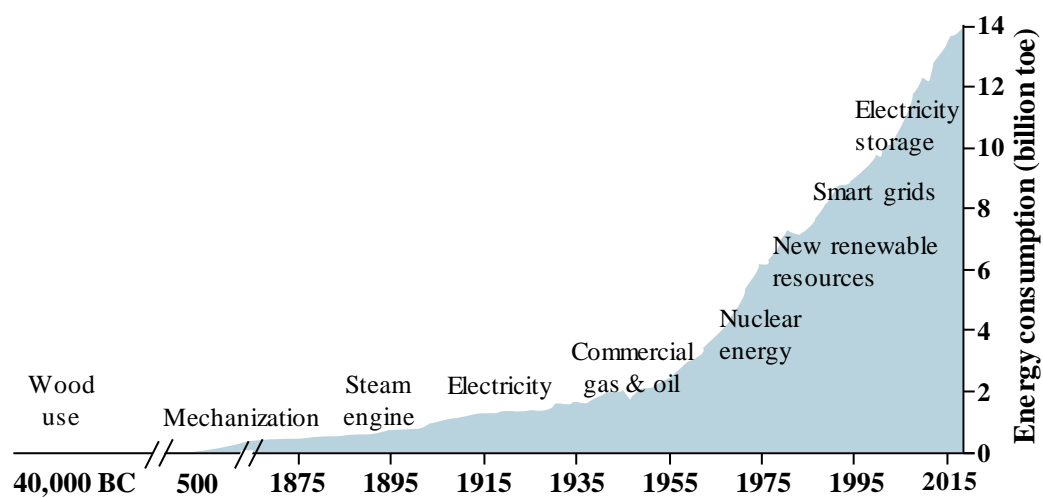
Figure 2. Evolution of energy sources consumption.

Source: modified from Belotskaia et al. (2016).

In addition to the energy source or even the technology used, human population must be considered in the analysis. Figure 3 shows the historical evolution of total energy consumption, population and energy consumption per capita. As it can be seen, the human population exponentially rose from Middle Ages to date. Similar conclusions can be extracted from the total energy consumption, During the last decades of the 20th century, the introduction of different more efficient technologies and electrification, mainly in developed countries, made the energy consumption per capita to increase less than the population or the total energy consumption.

The world's population and the energy consumption continue rising, however, this trend shows a great diversity around the world and the energy consumption has a strong dependence on the economic growth in different countries (Kander et al. 2014). Production and consumption systems need large amounts of energy and it is easy to observe the relationship between the energy consumption and the economy. Figure 4, provides an overview of the energy consumption and the Gross Domestic Product (GDP). As it can be seen, in a general trend, the economically richer a country is, the higher is the energy consumption in this territory.
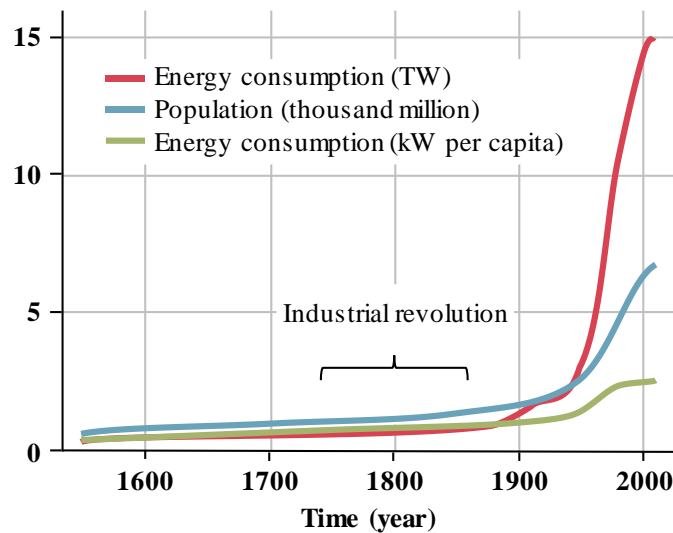
Figure 3. Evolution of total energy consumption, population and energy consumption per capita from Middle Ages.

Source: Ehrlich et al. (2012).

The Organization for Economic Co-operation and Development (OECD) is an international cooperation organization encompassing 36 States that covers about 70% of world markets and about 80% of the World Gross National Income (GNI). Since 2008, the energy consumption of non-OECD countries overcome that of OECD, moreover, the expected rising of non-OECD consumption will multiply by four that of OCDE during the next decades (BP 2019). Figure 5 gives the primary energy consumption per capita in the period 1980-2016 and the expected evolution up to 2040. A big difference between the United States of America (USA) and the

rest of the regions can be observed. A slight reduction in all the developed economies is expected changing the trend followed during the past decades. Meanwhile, the expected increase in the consumption per capita of developing economies (China and India) contrasts with the stability of the other non-OECD countries, based on the difficulty of these countries with high population growth rates to increase their energy consumption per capita.
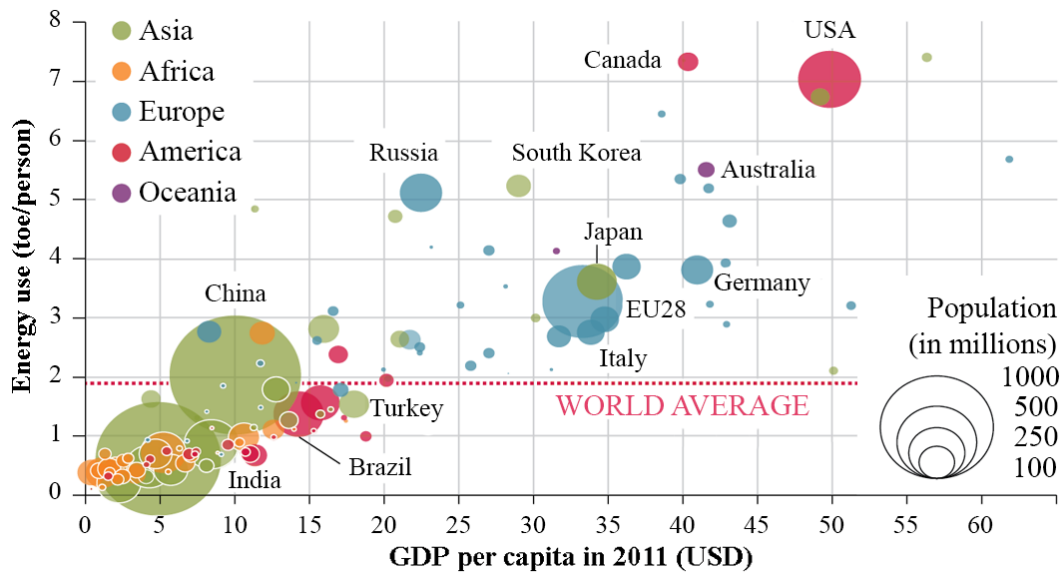
Figure 4. Energy consumption and GDP of different countries.

Source: modified from Priddle (2016).
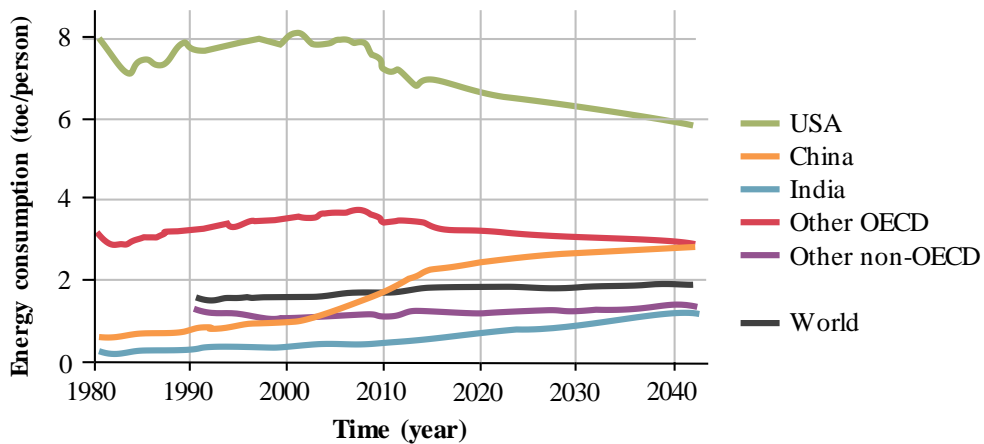
Figure 5. Total final energy consumption per capita by region.

Source: modified from Belotskaia et al. (2016).

Despite the increasing energy efficiency, the energy consumption continues increasing. Figure 6 presents the total final energy consumption from 1970 to 2016. Focusing on the increase observed since the early century, the energy consumption of the OECD countries remains constant and they are the major consumers. China and the non-OECD countries in Asia influence the increase with their contribution to the total consumption.
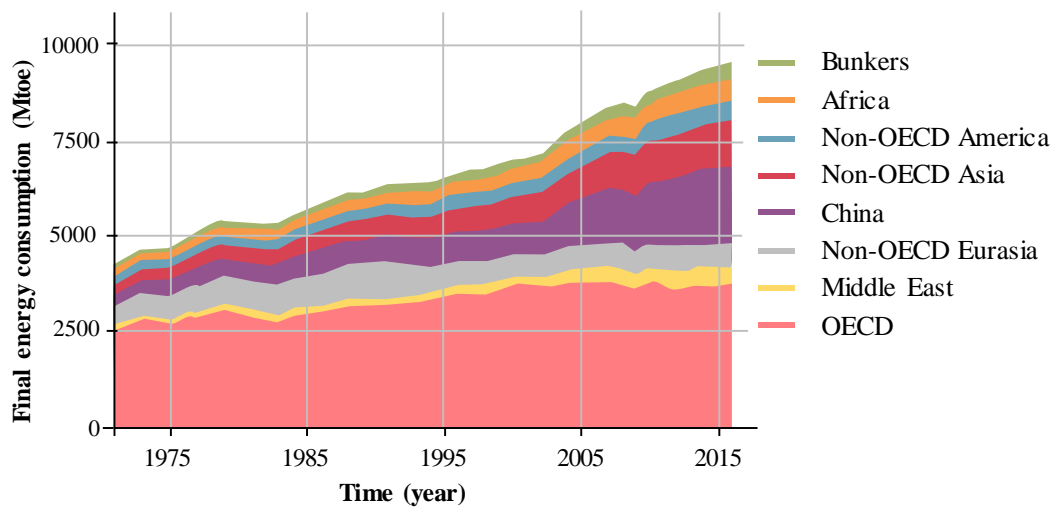
Figure 6. Total final energy consumption evolution by region.

Source: IEA (2018).

Figure 7 shows the evolution of energy balances of traded fuels in 1990 and 2017 as well as the predictions to 2040. These energy balances not only show the information about the energy import needs but it can be also understood as an indicator of the energy self-sufficiency degree of different world regions. The highly oil dependent energy system of the European Union (EU) was maintained between 1990 and 2017 while a slight decrease is observed to 2040. By that time, China, India and South-east Asia together with Oceania will top the negative energy balance of the energy foreign incoming ranking needs. Increases in the energy surplus to 2040 can be observed in Africa and the rest of Asia, while a big change stands out in America. In this case, the energy balance changed from the imports in 1990 to an energy exporter region in 2040.
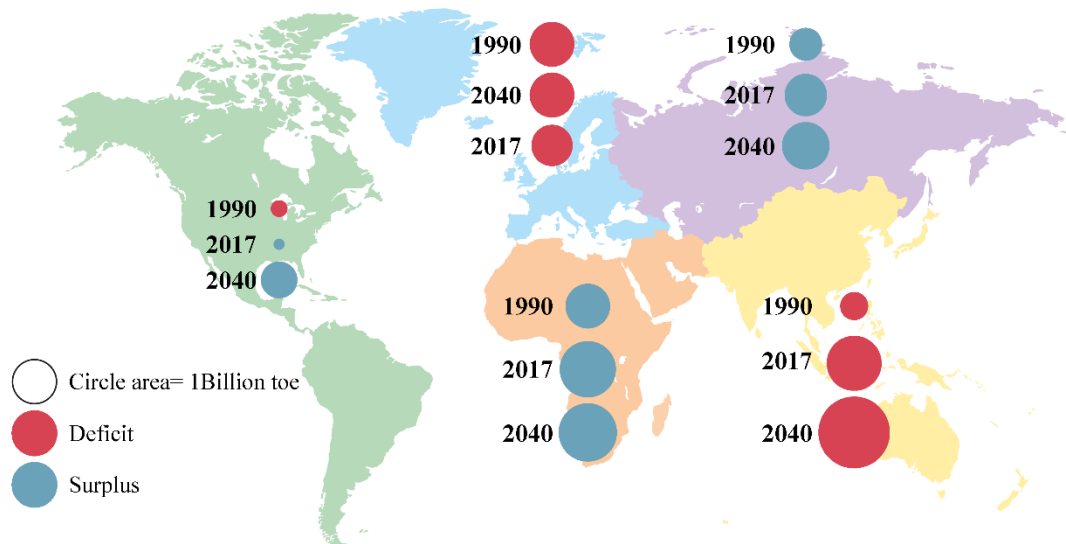
Figure 7. Energy balances of traded fuels by world regions and predictions to 2040.

Source: modified from BP (2019).

Despite the social, geographic or demographic differences, humans are making the greatest modification and exploitation of the environment, and this fact implies direct consequences to life and biodiversity. Current energy needs, raw materials availability and its incorrect use are producing resource depletion, loss of biodiversity and pollution, and consequently this is making sustainability and environmental protection getting more and more important for all the social actors.

1.2 Environmental impacts

The environment is the necessary scenario where life happens. In it, humans have developed their diverse cultures and societies, and because of that, they have produced changes in the environment which have direct impacts on the life in Earth, both positive or negative (Gaston and Spicer 2009). Different classifications of impacts are possible based on the size of the affected territory, the harm produced or the type of the affected environment, among others. Depending on the size of the

affected territory, local and global impacts can be distinguished and a general classification is here presented.

Local impacts:

- Effluents reaching soils or water bodies can harm human health but also a potential loss of biodiversity.

- Emissions. Different gas emissions (CO_2, CH_4, NO_x, SO_x or CFCs among others) and suspended particles stand out as pollutants responsible of a wide range of specific negative effects.

- Residues. The difficulty to treat different solid wastes implies their deposition under specific conditions depending on the inherent nature of the substance

- Resource depletion. The massive utilization of raw materials not considering the non-renewable characteristics of resources are a future developing constrain, with several associated problems.

- Land use changes. The change or even loss of any kind of natural ecosystem derives into the modification, or even loss, of natural functions of this ecosystem.

- Visual impact.

- Sound/noise impact.

- Electromagnetic fields.

Global impacts:

- Loss of biodiversity. This fact implies the reduction of the affected ecosystem resilience. Uncertainties derived from the ecological equilibrium appear and even cultural problems can appear in societies as a consequence of this (Gaston and Spicer 2009).

- Acid rain. The formation of sulfur and/or nitrogen acids in the atmosphere is favored by specific anthropogenic emissions (NO_x and SO_x). These acids are dispersed and fall as precipitation affecting ecosystems.

- Ozone layer depletion. The emission of different CFCs, among other substances with typically long atmospheric residence times, generates the

reaction of the stratospheric ozone with these compounds, reducing the ozone concentration in this atmospheric layer.

- Ocean acidification. CO_2 emissions to the atmosphere increase the CO_2 flows to the ocean (carbon sink) and in this way modifying oceans acidity with negative consequences on biodiversity.

- Climate change. Different substances emitted by human activities affect the natural greenhouse effect increasing it. This modification increases the global average temperature of the planet surface producing the sea level rise and the climate change.

1.2.1 The greenhouse effect modification

The greenhouse effect is the natural process whereby the earth's atmosphere maintains a thermal inertia. It is mainly produced by some gases known as greenhouse gases (GHG), capable of absorbing the infrared radiation reflected by earth surface after reaching it the solar radiation. It was pointed for the very first time by Fourier in 1824 based on his knowledge of heat transfer and ancient observations (Fourier 1824). In 1856, Foote enunciated the different heat absorption capacity of gases, thanks to the experiments with different gases inside glass closed cylinders (Jackson 2019). Nevertheless, the proper name of greenhouse effect was not used before 1896, when Arrhenius proposed the first climate model including the theoretical study of CO_2 concentration influence (Rodhe et al. (1997).

The average of the Earth surface temperature was between 13.9 and 14.2 °C during the 1981–2010 period while a temperature about -18 ºC would be achieved if no atmospheric effects would affect the Earth energy balance (Kump 2004). Figure 8 presents a scheme of the Earth radiative balance. The scheme assumes 100 arbitrary radiation units of incident solar radiation. About 30% of the total Earth high frequency energy input is reflected by surfaces, clouds and suspended particles by a process known as albedo effect. About 45% is absorbed by the Earth and about 25% is absorbed by the atmosphere. As it was mentioned in the previous section, part of this solar energy input has been accumulated by biomass through the photosynthesis

for thousands of years. Furthermore, the energy absorbed by the Earth surface and the atmosphere is dispersed as low frequency radiation. The greenhouse effect is presented in the right part of Figure 8 as 88 more arbitrary radiation units of infrared radiation. This radiation interacts with the GHG maintaining being emitted and absorbed multiple times, making internal fluxes higher than the Earth net energy balance and maintaining the Earth average temperature.
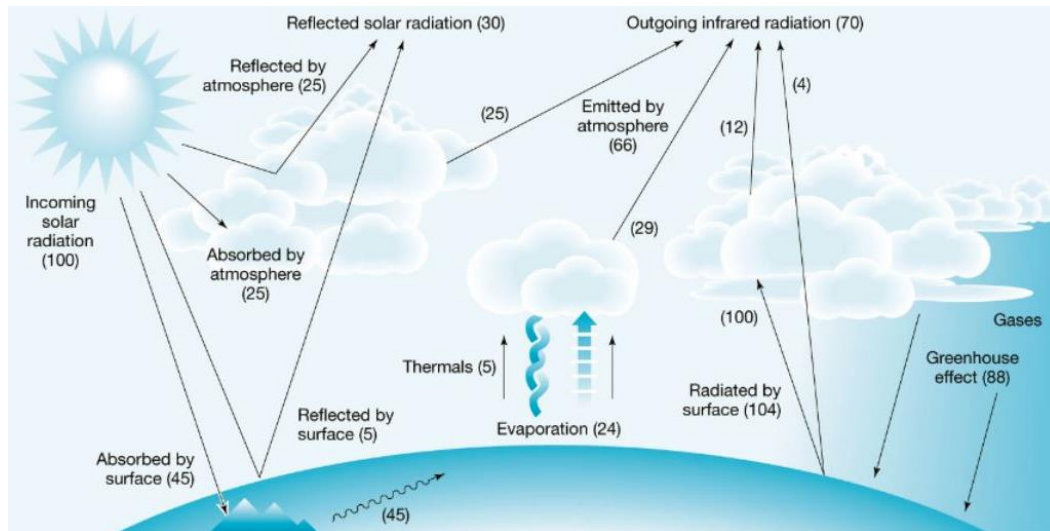
Figure 8. Radiative Earth balance, fluxes expressed as percentages.

Source: modified from Kump (2004).

1.2.2 The global warming

Table 1 presents the concentration of the main gases forming part of the atmosphere in the preindustrial period until the anthropogenic emissions began to modify the atmospheric composition. The preindustrial atmospheric gas composition establishes the needed data for comparison with anthropogenic atmospheric modifications. Earth climate models have considered slightly different variables to simulate the climate behavior with similar relevant and coherent results. As an example, the NASA's model E2 includes separately both natural and anthropogenic variables that influence the climate showing the results as temperature anomalies. This variation represents the difference between the temperature baseline distance and the predicted temperature, a more accurate than the absolute temperature because

of the intrinsic Earth's surface temperature heterogeneity. The natural effect considers variables such as Earth's orbital variations, the Sun's radiation changes (based on the Sun temperature evolution) and the escaping volcanic emissions. Among anthropogenic variables, the model considers deforestation, tropospheric ozone pollution, aerosols pollution and obviously, the GHG emissions. Figure 9 represents the observed and the simulated Earth temperature according to the Goddard Institute for Space Studies (GISS) Model E2 (Schmidt et al. 2014). As it can be seen, while no relation can be observed between the comparison of the observed temperature and the isolated effect of natural factors in the simulated temperature, the addition of all the natural and human variables approaches the observed values.

Table 1. Clean air composition.

Gas	Concentration
(-)	(%)
N_2	78.08
O_2	20.95
Ar	0.94
CO_2	0.028
Ne	$1.82 \cdot 10^{-3}$
He	$5.2 \cdot 10^{-4}$
Kr	$1.1 \cdot 10^{-4}$
Xe	$0.09 \cdot 10^{-4}$

The atmospheric composition continues changing because of human activities. The Intergovernmental Panel on Climate Change (IPCC) certified the relationship between the increase of Earth's average temperature and the increase of the atmospheric GHG concentrations because of the reinforcement of the natural greenhouse effect (IPCC 2014). In this way, the average surface temperature of the Earth was between 13.7 and 14.0°C for the 1961–1990 period, increasing to 13.9-

14.2 °C for the period 1981–2010 (Jones and Harpham 2013). Table 2 shows the main GHG together with their most important global warming characteristics, their atmospheric residence time, the contribution of each GHG to the total GHG emissions and the Global Warming Potential (GWP). This GWP represents the warming caused by the release of 1 kg of any GHG with respect to the warming caused by the release of 1 kg of CO_2 during a time horizon. Despite the large amount of H_2O emitted, the vapor-liquid equilibrium of this substance maintains a constant H_2O concentration for the constant pressure and temperature ranges, reducing the impact of H_2O emissions compared with any other GHG. The CO_2 stands out here as the world's largest contributor to the warming because of the large amount emitted along with the long atmospheric residence time of this gas in the atmosphere.
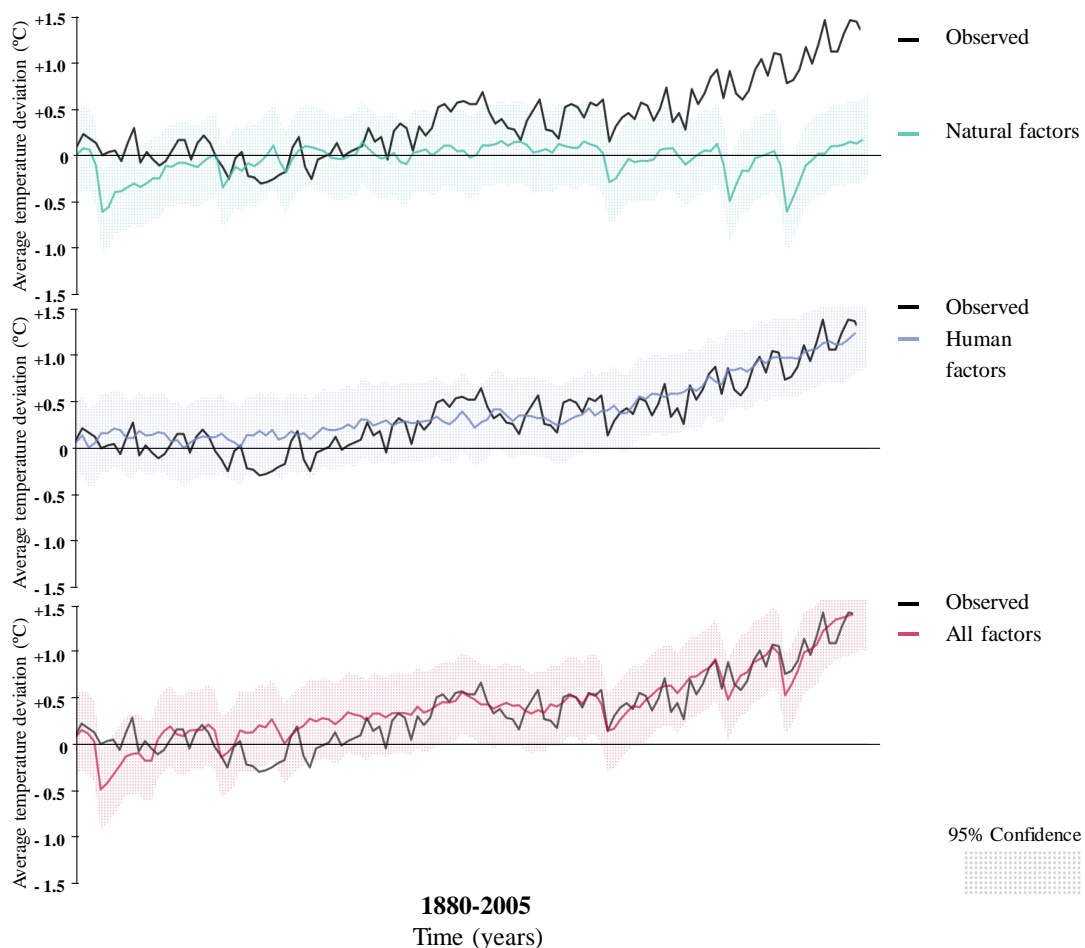
Figure 9. Observed and simulated Earth temperature according to the GISS Model E2. (Dotted area represents the 95% confidence).

Source: modified from Miller et al. (2014).

Table 2. Greenhouse gases and their atmospheric residence time together with the anthropogenic GHG emission contribution percentage and GWP.

Source: IPCC (2013).

	Residence time (years)	Contribution (%)	GWP (kg_{CO2eq})		
			20 years	100 years	500 years
H_2O	0.04	66	-	-	-
CO_2	300	20	1	1	1
CH_4	15	4	56	21	6.5
N_2O	120	1	280	310	170
CFC	$10 - 5 \cdot 10^4$	1.5	4800	7000	10100
SF_6	$10 - 5 \cdot 10^4$	1.5	16300	23900	34900

Apart from the proper increase in the temperature of the atmosphere and the hydrosphere, the main impact derived from global warming are the unpredictable consequences on global climate, producing more extreme weather phenomena, and environmental destruction, among others.

The CO_2 balance

The study of the major carbon sources and sinks contributes to the global warming understanding. The Carbon Budget analyzes the major carbon deposits to stablish an annually carbon flow study that takes into account the Fossil fuel CO_2, the land use change CO_2, the atmospheric CO_2, the ocean CO_2 sink and the terrestrial CO_2 sink, all systematically estimated for the period of 1959–2017 (Le Quéré et al. 2018). The carbon amount in the planet is constant and, from this point of view, the carbon cycle is the carbonaceous exchange process among the biosphere, geosphere, hydrosphere and atmosphere. Figure 10 shows the carbon cycle anthropogenic perturbation scheme averaged for the period 2008-2017. As it can be seen, during the decade 2008-2017 the atmospheric carbon deposit increased by 4.7 Gt_{CO2} per year, while a total amount of approximately 250 Gt_{CO2} was moved to the atmosphere from

1870 to 2017. Fossil fuel combustion since Industrial Revolution and land-use change are highlighted as the major responsible of the disruption in the natural equilibrium. According to the National Oceanic and Atmospheric Administration Earth System Research Laboratory, the CO_2 atmospheric concentration increased from the approximately 280 ppm of CO_2 in the preindustrial atmosphere to the 416 ppm on May 15, 2019 (Keeling et al. 2015).
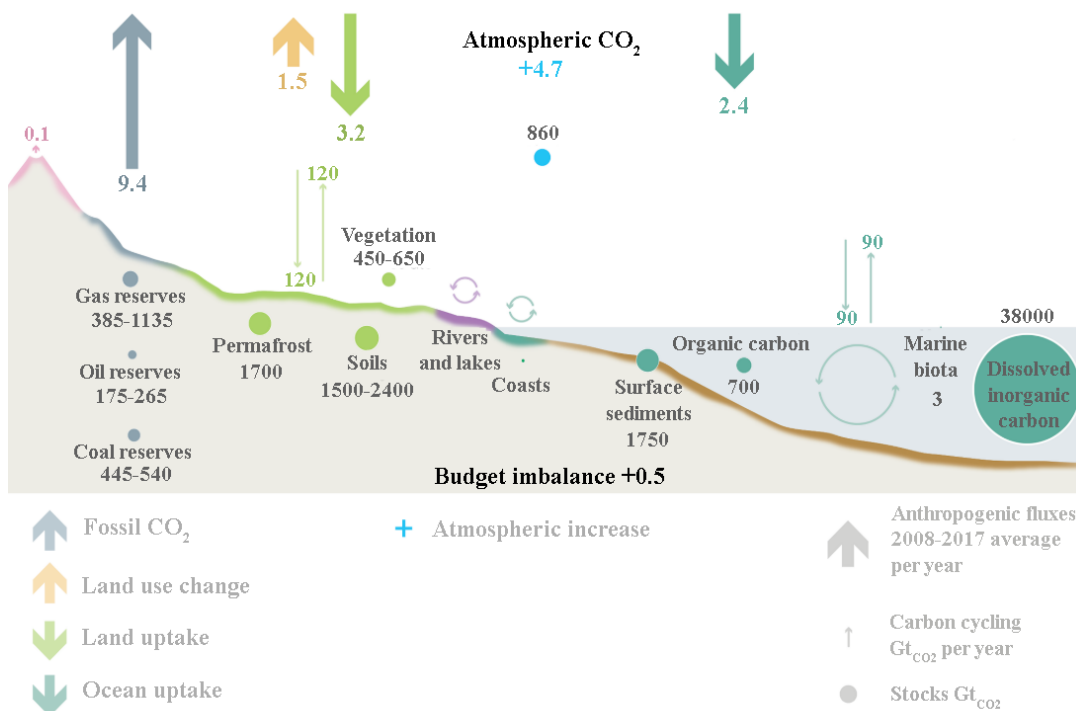
Figure 10. Carbon cycle anthropogenic perturbation scheme annually averaged for the period 2008–2017.

Source: Le Quéré et al. (2018).

Figure 11 shows the evolution of the CO_2 emissions from 1960 to 2017: (a) global emissions, (b) by fuel/process, (c) by regions and (d) per capita by region. In Figure 11 (a), a slight stabilization in CO_2 global emissions can be observed during the first years of the 2010 decade. The growth rate in the GHG emissions decreased from 4.5 % per year in the period 1960–1969 to a period of no or low growth during 2014–2016 (Le Quéré et al. 2018). Focusing in the CO_2 emitters by fuel or process, in Figure 11 (b), fossil fuels highlight as the responsible of the GHG emissions

followed by cement production. A maintained increase growth rate is observed for natural gas use, comparable with oil utilization. Since approximately the year 2000, coal combustion regained the first fuel position by CO_2 emissions, coinciding with the China CO_2 emissions increasing that made China the main GHG emitter, almost doubling USA emissions. The coal stabilization observed after the year 2010 contributed to the stabilization of the global CO_2 emissions in the same line than what can be seen with China emissions during this period (Figure 11 b). In addition, a high increase is also observed in India's emissions in contrast with USA and EU countries. Big differences can be observed in Figure 11 (d) between regions in the CO_2 emissions. The high increase of China during the 2000 decade set their CO_2 emissions per capita to EU28 comparable values. A stable increase was maintained in the CO_2 emissions per capita of India from 1960 to 2020. Moreover, the USA remains as the major contributor per capita to global CO_2 emissions.
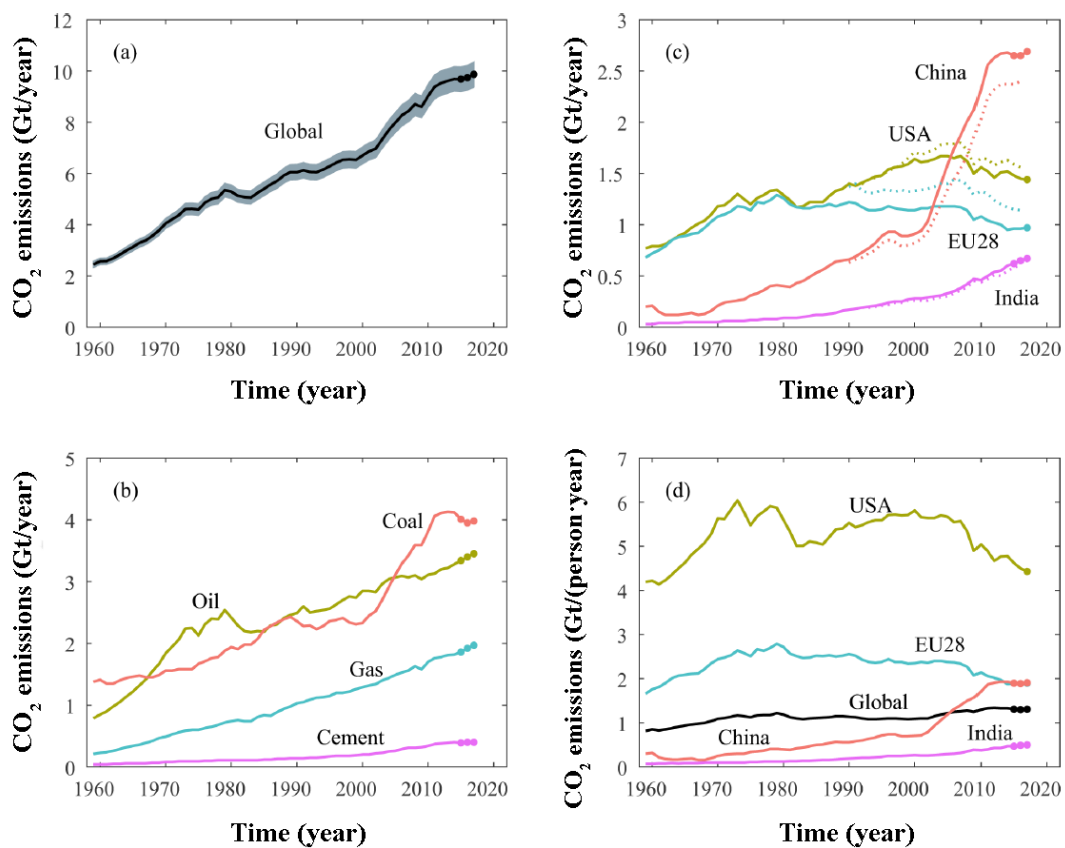
Figure 11. Evolution from 1960 to 2017 of the CO_2 emissions (a) global, (b) by fuel/process, (c) by regions, (d) per capita by region.

Source: Le Quéré et al. (2018).

1.3 The climate change

Arrhenius proposed in 1896 the first climate model including the greenhouse effect and the theoretical study of atmospheric CO_2 concentration influence (Rodhe et al. 1997). In 1972, the first environmental United Nations (UN) conference overlooked the climate change topic focusing on problems like chemical pollution or the atomic bomb consequences. The successive climate simulations reinforced the debate about the climate crisis promoting the IPCC creation in 1988 as a part of the United Nations Environmental Program (UNEP). In this way, in 1998 the Kyoto Protocol attempted to combine international efforts to reduce different GHG emissions, being the first time that GHG emission limits were stablished. In 2014, the fifth Assessment Report (AR5) presented by the IPCC highlighted the anthropogenic responsibility on the global warming and the unpredictable consequences that climate change will produce if GHG emissions continue as usual. The AR5 confirms previous evidences about extreme temperatures, increased precipitations or rising sea levels, among others, and how humans will be affected. Figure 12 shows different impacts already attributable to climate change in 2014. As it can be seen, impacts were produced all around the world affecting physical, biological and human systems. The increase of wildfires in many world areas, the decreasing food production in South-East Asia and Sub-Saharan Africa and impacts on water bodies must be highlighted. In this way, the AR5 made a call to join actions for a necessary clean development, limiting the GHG emissions combined with adaptation strategies to limit the risks of the climate crisis over sustainable and equity development.

Figure 13 shows the IPCC climate change scenarios predicted from 2014 to 2100, (a) annual global GHG emissions and (b) the temperature change for the cumulative CO_2 equivalent atmospheric concentrations. The historical data (dark line) and the Representative Concentration Pathways (RCP) are plotted in Figure 13 (a) by the different colored lines. As an example, the RCP2.6 (blue line) shows the GHG emissions mitigation trend to 2100 that corresponds with the most probable trend into the scenario area of GHG atmospheric concentrations between

430 and 530 ppm of CO_2 equivalent (blue colored areas). Looking at Figure 13 (b), the temperature increase of nearly 2 ºC produced by these cumulative GHG concentrations can be compared with the observed values for the period 2000-2009, showing the necessary reduction of GHG emissions for the coming years. The GHG emissions should be neutral during the last quarter of the 21st century and even negative GHG emissions over the end of the century for the RCP 2.6 (Figure 13 a). The RCP4.5 and RCP6.0 scenarios also presented in Figure 13 (a) show the expected intermediate GHG emissions that would cause the average temperature of 1861-1980 to be exceeded by more than 2 ºC. Finally, the RCP8.5 scenario shows a high GHG emissions that would be achieved considering the current trend of GHG emissions, without mitigation strategies, producing unpredicted consequences of the climate crisis (IPCC 2014).
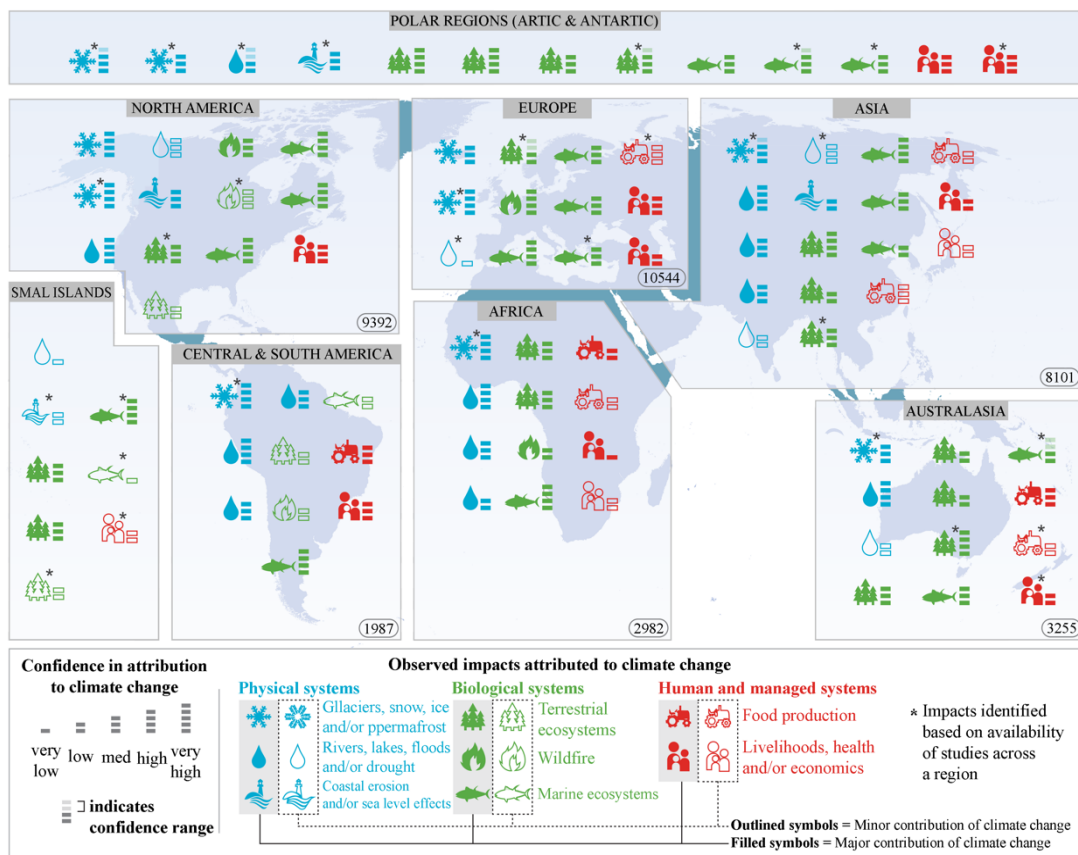
Figure 12. Climate change attributable impacts to 2014 by regions.

Source: modified from IPCC (2014).
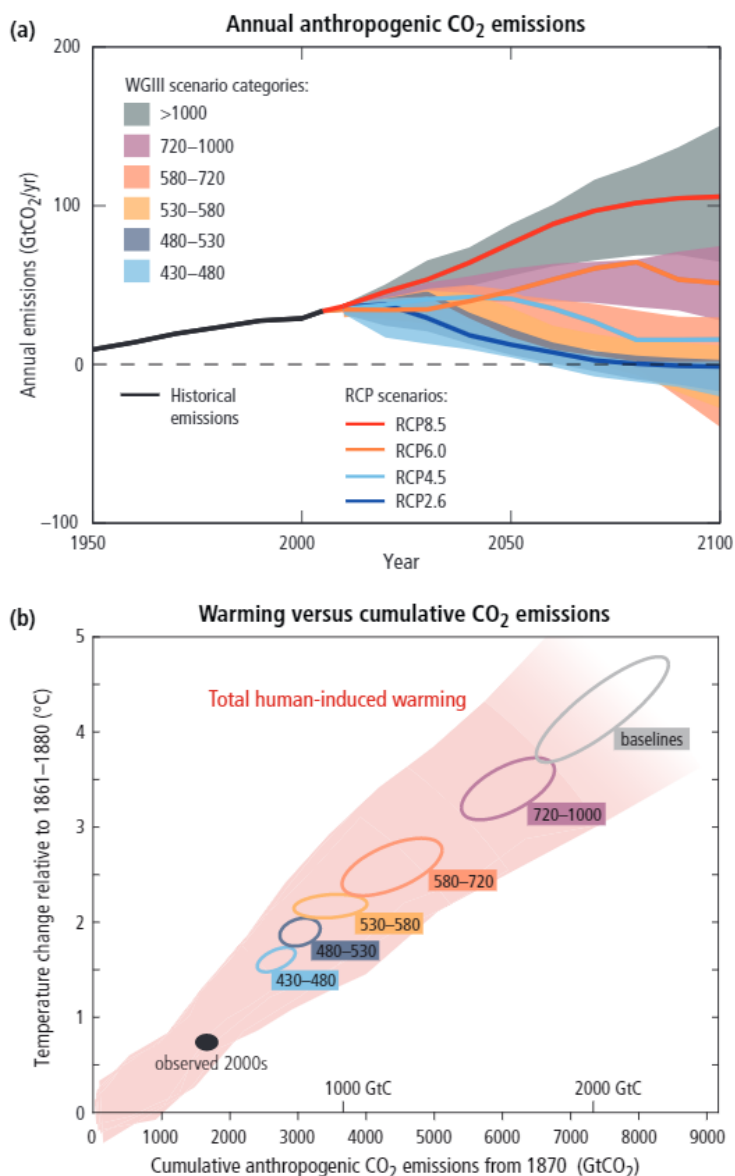
Figure 13. IPCC climate change scenarios predictions 2014-2100 (a) Annual global GHG emissions, (b) temperature change for the cumulative CO_2 atmospheric concentrations.

Source: IPCC (2014).

The social debate continued increasing meanwhile the implication of different actors also increased. The Paris Agreement set the international objective of holding the increase in the global average temperature to well below 2 ℃ above preindustrial levels and pursuing efforts to limit the temperature increase to 1.5 ℃ above preindustrial level. It would enter into force when at least 55% of the parties with at least 55% of global GHG emissions signed it. In November of 2016, 185 countries

representing more than 87% of global GHG emissions signed it entering into a force. In this agreement, each country independently decides their Nationally Determined Contributions (NDC) of GHG emissions reduction. These NDC are analyzed and revised every five years but they are not mandatory, what increases the uncertainties associated with the climate crisis mitigation. The 24th Conference of the Parties (COP24) to the United Nations Framework Convention on Climate Change (UNFCCC) celebrated in Katowice in 2018 reinforced the Paris Agreement objectives set in 2015, insisting on the emergency and the unprecedented actions needed (UNFCCC 2015). It is clear that no single solution is able to achieve the GHG necessary reduction. Furthermore, the real GHG emissions reduction will depend on the climate policies adopted by the parties, however, recent studies confirm the alarm (UNEP 2018). Figure 14 shows the number of countries achieving the GHG emission peak per decade between 1990 and 2030 as well as the percentage of global emissions covered by these countries at that time. This emissions peak could be already observed in Figure 13 (a) in the RCP 2.6 scenario. The differences among countries and climate policies are here reflected in the 40 years of difference to achieve the GHG emission peak. However, the global GHG emissions peak is expected to 2020, remaining 57 countries with about 60% of GHG emissions to 2030.
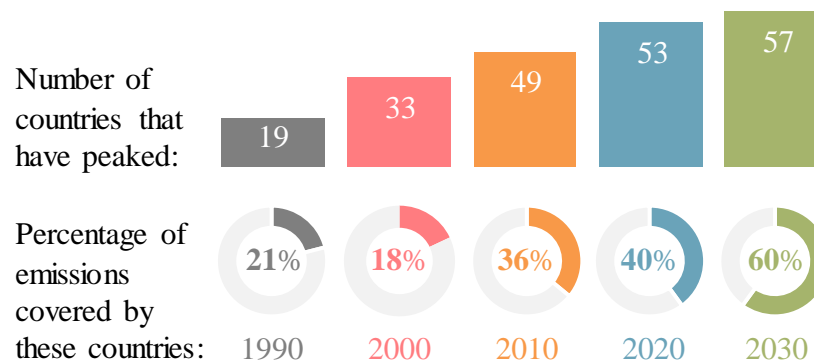
Figure 14. Global CO$_2$ emissions from fossil fuel combustion.

Source: UNEP (2018).

Differences between the GHG reduction compromise and the achieved GHG reduction have been identified in several studies. According to these studies the commitment of the countries already stablished is not enough to limit the Earth's

average temperature increase to 2 ℃. The UN Gap Report in 2018 shed light on the GHG reduction level by 2030. To this end, several scenarios were considered:

- No policy baseline. It represents the scenario without climate policies implementation since 2005.
- Current policy scenario. It shows the GHG emissions continuing the real data until 2017.
- Unconditional NDC. Contribution on the global GHG reduction objectives of each country to comply with the Paris Agreement.
- Conditional NDC. Additional efforts on the GHG reduction objectives of some countries constrained by a wide range of uncertain variables.
- 2 ℃ range. Global GHG reduction objectives to achieve about 2 ℃ of global temperature increase and to comply with the Paris Agreement.
- 1.5 ℃ range. Global GHG reduction objectives to comply with the Paris Agreement with about 1.5 ℃ of global temperature increase.
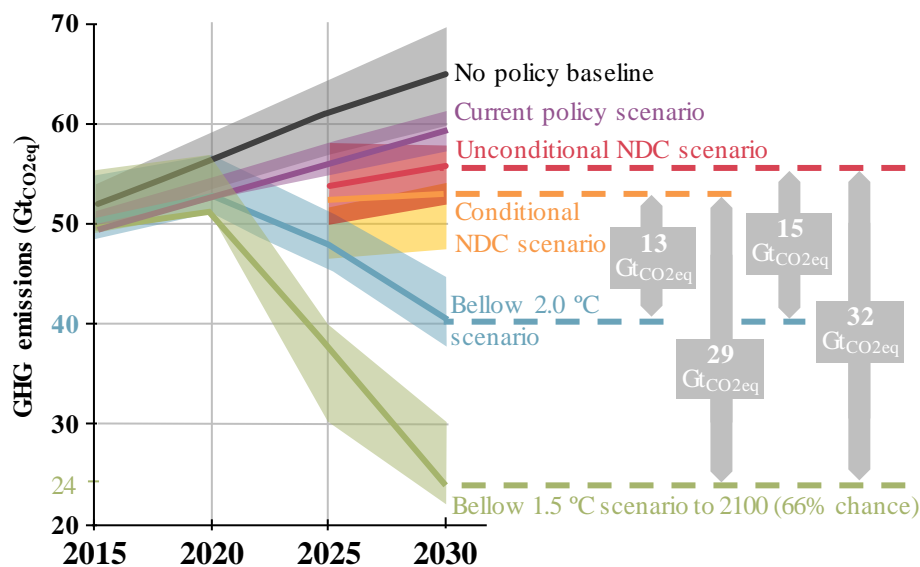
Figure 15. Global GHG emissions in different scenarios and the expected emissions gap in 2030.

Source: modified from UNEP (2018).

Figure 15 shows the global GHG emissions in different scenarios and the expected emissions gap in 2030. According to Figure 15 a large difference, of about

20

30 Gt$_{CO2eq}$, is observed among the objectives to comply with the Paris Agreement and any of the represented NDC scenarios. In this way, a major change should initiate the GHG emissions reduction. Otherwise, the climate crisis will produce more and more destructive and irreversible consequences on Earth's life.

1.3.1 Geoengineering

There is a clear scientific consensus on the anthropogenic influence in the modification of atmospheric GHG composition, and therefore, the climate crisis. The GHG emission reduction targets appear to be insufficient and a real compromise must be made effective. The Royal Society defines geoengineering as the climate modification to counter the anthropogenic global warming (Schäfer et al. 2015). The implementation of geoengineering acts on a wide range of climate variables, but also social, political, economic and technical among others (Rayner et al. 2013). Oxford University analyzed the complex context and enounced five principles that try to provide the basis for a correct deployment of climate engineering. These conclusions claim to a conscientious regulation before the implementation of geoengineering techniques (Rayner et al. 2013). The European Commission participates in the European Transdisciplinary Assessment of Climate Engineering Project (EUTRACE) analyzing the state of knowledge and deployment of geoengineering projects. It made a division of available technologies into two different main types.

- Albedo effect modifications. Solar radiation management techniques that increase solar radiation directly reflected by the deployment of reflective surfaces or specific particles injection that favor the overall temperature reduction.
- Atmospheric GHG modifications. Negative emission technologies (NET) are technologies able to remove GHG from the atmosphere.

Atmospheric GHG reduction

The GHG reduction includes a wide range of possibilities that increase natural CO_2 sinks or store the CO_2 for a long period. The NETs should be responsibly analyzed and managed to contribute to reduce the global warming and to mitigate the climate crisis effects. The main NETs are:

- Afforestation. Increasing natural CO_2 sink in forests by afforestation, as well as protecting critical forest environments and reforesting deforested areas.
- Bio char. It is a stable product for hundreds of years obtained by biomass pyrolysis or gasification. Used in soils, it contributes to their fertility while increasing the carbon sink of the earth's soil.
- Ocean fertilization. Favoring the plankton formation, the biological carbon sink would increase its contribution in the carbon cycle, contributing to the reduction of the atmospheric GHG concentration.
- Enhanced weathering. Industrial chemical methods to imitate natural mineralization of atmospheric CO_2.
- Direct air capture (DAC). An important difference must be highlighted here between technologies to absorb into solids and DAC linked with CO_2 capture and storage (CCS). CCS technologies were pointed to play an important role in carbon removal during the next century according to the IPCC AR5 report. (IPCC 2005).
- Bioenergy with CO_2 capture and storage (BECCS). This group of technologies was also highlighted in the IPCC AR5 report because of their capacity to produce energy while the negative CO_2 emissions are guaranteed. The CO_2 is captured in the sustainable managed biomass, which is transformed usually by thermochemical reactions to produce an energy gain. The CO_2 obtained is stored into safe places for a long period. A wide deployment of these technologies during the present century will be necessary (IPCC 2014). For more information about BECCS, see section 1.4.
- Other biomass-based processes: The correct management of land uses can increase the carbon soil sink. Furthermore, the use of biomass-based materials on a wide range of industries, such as buildings or new materials, should contribute to the GHG atmospheric concentration reduction.

1.3.2 The mitigation path

The first effects of the climate crisis are already evidenced in global changes in the planet's behavior. Decisions including all the social actors during coming decades lead the implementation of measures to adapt societies to these changes. Following the objectives in the Paris Agreement, if 2900 Gt_{CO2eq} were emitted by anthropogenic sources to 2011, no more than 1000 Gt_{CO2eq} should be emitted to 2100 to achieve the mitigation pathway with the goal of no more than 2 ºC of global temperature increase. Analyzing the GHG emissions reduction estimated by the IPCC's Synthesis Report (IPCC 2014) for the different sectors, power generation, industry and transportation stand out as the world's leading contributors up to date. However, different GHG emissions reduction capacities are estimated in each sector. Figure 16 shows the annual GHG emissions by sectors and predicted to 2050. A slight reduction is estimated for the period 2020-2050 in industry and transportation in the same line as what happens with buildings, transformation and agriculture. Meanwhile, the power generation sector highlights with an estimated GHG reduction of about 87% in 2050, being the sector with the highest potential of reduction.
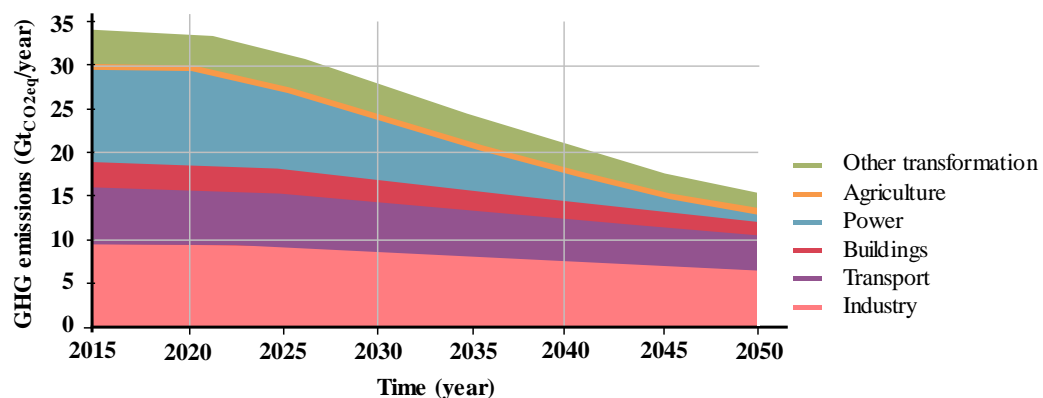
Figure 16. Annual CO₂ emissions by sectors predicted to 2050

Source: IPCC (2016).

Figure 17 shows the energy related emissions evolution and perspectives to 2100 following the trend observed to 2013, as well as the mitigation path objectives according to the IPCC's Synthesis Report (IPCC 2014). All these considerations suggest a GHG emissions reduction of about 100 Gt_{CO2eq} during the present century

and no single solution can achieve the reduction needed. The Mitigation path should include different cost-effective technologies and also a big effort on research about climate mitigation technologies. As it can be seen, the energy save together with an increase in energy efficiency should contribute about a 33% of total energy related GHG emissions reduction at the end of the century. The renewable energies deployment should contribute with about 17%, also the change to sustainable fuels (10%) and nuclear energy (6%) must be mentioned. The deployment of fossil fuel powered plants linked with CCS technologies can reduce nowadays emissions, however, a large deployment of BECCS technologies is expected after 2030. A contribution of 32% is expected for CCS associated technologies at the end of the century. In this way, a zero-emissions energy sector would be achievable about the end of the century, contributing to ensure a 22nd century with a GHG negative emission sector. The mitigation path combines strategies and measures to reduce GHG concentrations in the atmosphere by several techniques. The increase of natural carbon sinks, together with GHG emissions reduction will contribute on the climate crisis mitigation, and the decarbonization of energy sector should make special efforts while the energy supply is guaranteed.
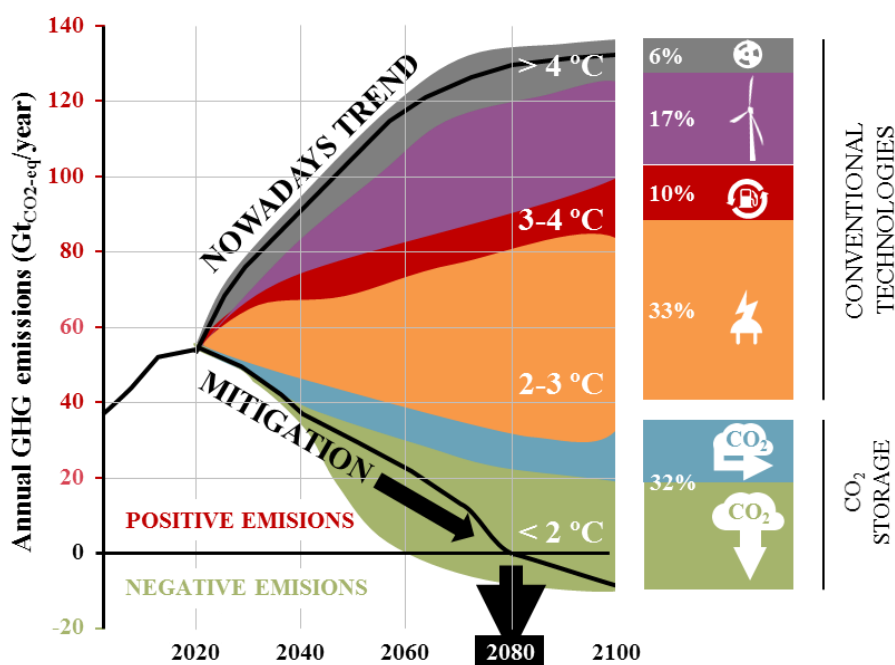
Figure 17. Energy related emissions evolution and perspectives to 2100 following nowadays trend and the mitigation path objectives.

Source: modified from IPCC (2014).

1.3.3 Other energy considerations

Air pollution includes all the emissions of gaseous, liquid and solid particles that locally or globally modify the natural atmospheric properties. Air pollution has been pointed as the fourth major factor producing premature deaths with huge estimated global derived costs. A difference between primary and secondary pollutants should be made. The first ones are those directly emitted in a process while the secondary are those formed by the primary by chemical reactions that also produce undesirable effects. In addition to CO_2, some substances among the various air pollutants derived from human activities should be especially highlighted because of their impacts (Priddle 2016). All these pollutants should also be considered when analyzing power generation processes:

- Carbon monoxide. CO_2 has been already pointed as the main contributor to anthropogenic global warming, but also CO produced by uncompleted combustion is important because of its toxicity.

- Nitrogen oxides. Both NO and NO_2 as well as ammonia favors the formation of tropospheric ozone and particulate matter. N_2O is also a GHG.

- Particulate matter. Suspended particles, usually solids with diameters lower than 10 µm, and also liquids are considered pollutants because of their impact in human health.

- Sulfur oxides. Substances related with human health undesirable effects. These compounds also favor the suspended particles formation and contribute to acid rain.

- Volatile organic compounds. Hydrocarbon vapors with a negative impact on human health and the biodiversity maintenance.

Figure 18 shows the main primary air pollutants together with the main sources where they were produced in the year 2015. As it can be seen, not only power generation, but also all energy related processes are responsible for major of the main air pollutants in all sectors, except non-energy agricultural processes.
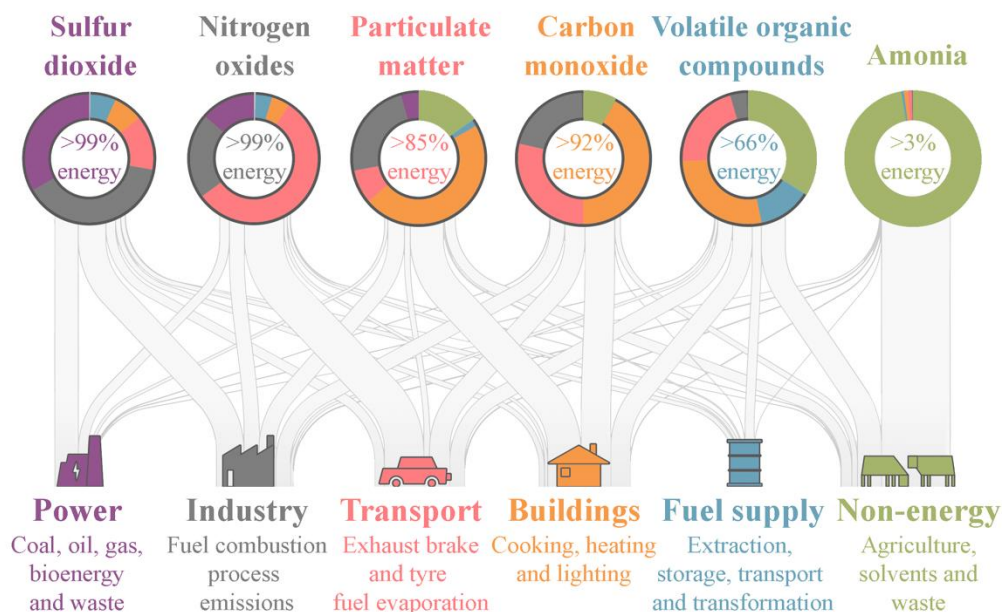
Figure 18. Main primary air pollutants and their sources in 2015.

Source: Priddle (2016).

1.4 BECCS

Social and economic growth is mainly based on energy use producing different impacts on the environment, human health and biodiversity. The generalized unsustainable way to generate energy involves a great effort in research for the correct deployment of different technologies. The whole Life Cycle Analysis (LCA) of the CO_2 emissions from various existing energy technologies, compared per unit of energy produced, is presented in Figure 19. The LCA involves the complete analysis of the process including the emissions derived from every stage from the raw materials extraction to the waste management (generation, transportation, end use, …). Almost all the technologies generate positive CO_2 emissions, and fossil fuel technologies stand out as the major contributors. The combination of traditional coal-fired power plants with CCS achieves a significant reduction in CO_2 emissions, and it is expected to play an important role prior to the deployment of BECCS. CO_2 emissions from the most common renewable energy sources are also shown. Despite their near zero emissions during operation, the CO_2

emissions are mainly emitted during their production. BECCS technologies stand out as the only group of technologies able to produce energy while GHG are removed from the atmosphere because of the CO_2 consumed during the biomass growth. Quantitatively, the reduction of atmospheric CO_2 concentrations per unit of produced energy achieves values that counteract the carbon intensity of traditional fossil fuel energy technologies.
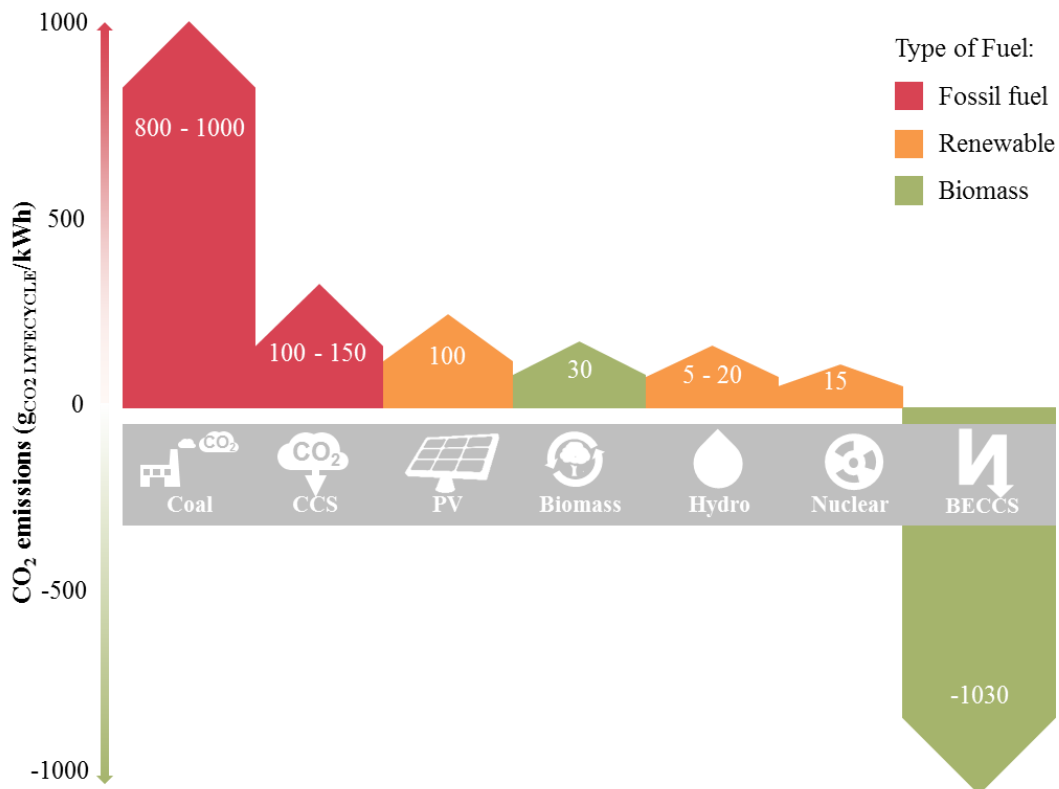
Figure 19. CO_2 emissions in different power generation systems.

Source: modified from IPCC (2014).

Regarding the expected deployment of BECCS during next decades, Figure 20 shows the necessary BECCS deployment from 2020 to 2060 by type of technology to meet the climate targets. In addition, the atmospheric CO_2 cumulative reduction is included (right axis). Biofuel sector will start a great growth around 2030, thanks to the current stage of development of these technologies. About 2040 the biomass power sector will continue growing, achieving almost half of the annual CO_2 stored associated with BECCS technologies about 2060.
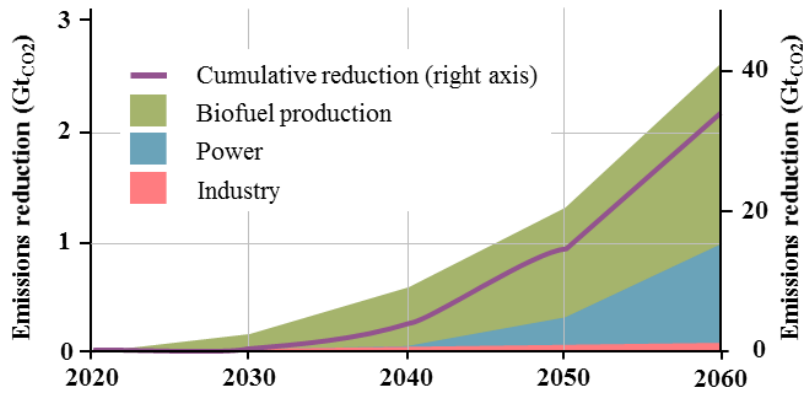
Figure 20. BECCS necessary CO_2 stored perspectives to 2060 for the B2DS scenario.

Source: Brown and Le Feuvre (2017).

Biomass has been used for thousands of years for energy purposes. Biomass fuels are usually considered CO_2 neutral, however, a sustainable management of this resource must ensure that the amount of CO_2 emitted during cultivation, harvesting, pretreatments, transportation and processing is less than the amount of CO_2 captured by the biomass during its growing. The use of CCS processes linked to bioenergy changes the CO_2 balance achieving a NET. Figure 21 presents the different BECCS potential possibilities from biomass feedstock.
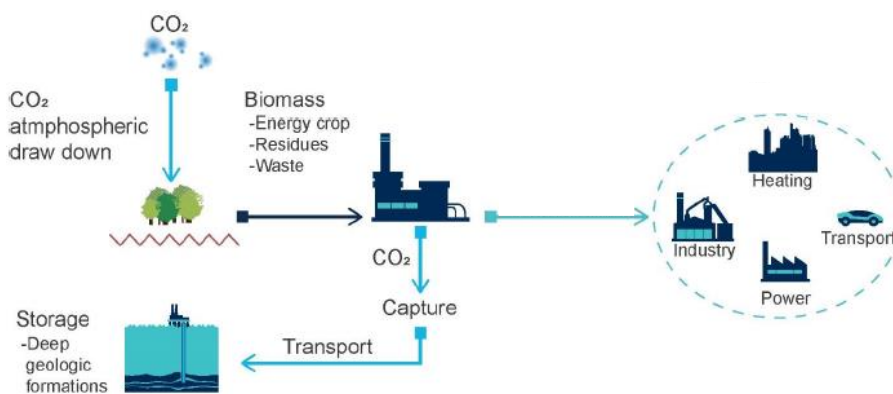
Figure 21. Scheme of different BECCS general possibilities.

Source: Consoli (2019).

As it can be seen, the scheme shows the reduction of the atmospheric CO_2 captured by the biomass. The use of different biomass-based materials, biofuels and/or bioenergy linked with CO_2 storage would contribute on the reduction of GHG emissions in the energy sector and also several industries. The general stages of BECCS processes, biomass production, CO_2 capture, transportation and storing are explained below.

- Biomass. Lignocellulose biomass supply may include starches, energy crops, algae or biomass residues. Figure 22 shows the scheme of a circular bioeconomy. Depending on the biomass origin and the characteristics, different pretreatments and processes can transform it adequately guaranteeing negative CO_2 emissions. However, environmental considerations caused by changes in land use and transportation as well as food-fuel competition must be balanced. For further information about biomass see section 1.4.1.
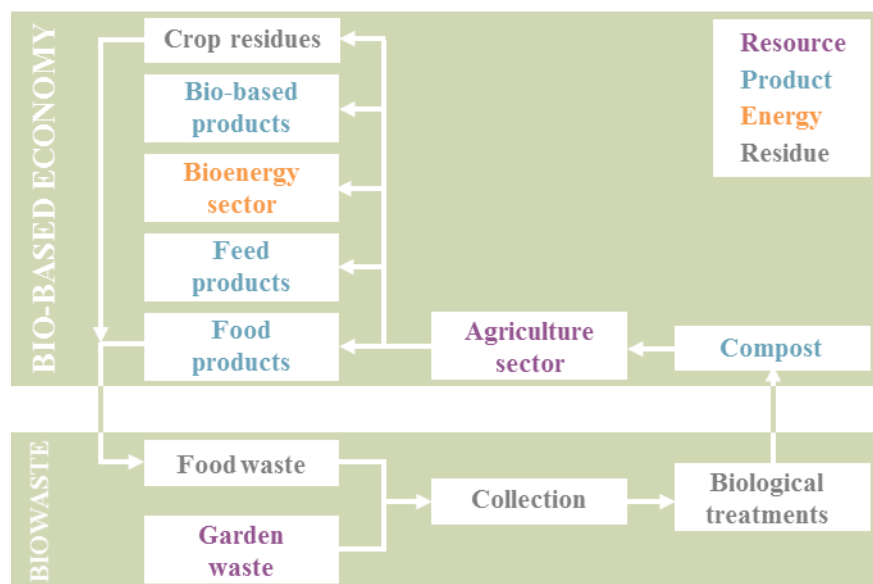
Figure 22. Scheme of a circular biomass based economy.

Source: European Commission (2018).

- CO_2 capture technology. The CO_2 capture process consists basically in the CO_2 separation process from other gases. To this, a high concentrated CO_2

29

stream is preferable, as the energy lost is reduced and, consequently, the cost of capture, transportation and storage processes. For further information about CO_2 capture technologies, see Consoli (2019).

- Transportation. The knowledge of international transport of natural gas and oil derived fuels is used for the transportation of CO_2. In this way, a dehydration and a compression stage are needed for the different cost-effective options such as maritime transportation or pipes. The quality of the CO_2 to be captured can be affected by the presence of different compounds in the outlet stream. Steam, N_2, O_2, CO, H_2, CH_4 and other hydrocarbons, SO_2, particles and also NO_x levels should be controlled in order to ensure that the captured CO_2 stream can be properly transported and safely stored. To date, there are no legal requirements on the quality of CO_2 transported and only recommendations have been outlined (de Visser et al. 2008). The limit set in the project Dynamis recommendations regarding the contents of these substances in the CO_2 stream is shown in Table 4.

Table 3. Dynamis limit recommended for different substances for CO_2 CCS.

Source: de Visser et al. (2008).

	Dynamis recommended limit
H_2O	500 ppm
H_2S	200 ppm
CO	2000 ppm
O_2	$< 4\%\,vol$
CH_4	$< 4\%\,vol$
N_2	$< 4\%\,vol$
Ar	$< 4\%\,vol$
H_2	$< 4\%\,vol$
SO_x	100 ppm
NO_x	100 ppm
CO_2	$> 95.5\%$

Table 4. Large scale and notable BECCS facilities with their main characteristics.

Source: Consoli (2019).

Name	CO₂ capture	Industry	Location	Status	Storage	Operation (year)	Capacity (tpa)
Large scale							
Illinois Industrial CCS	ADM corn to etanol	Ethanol production	US	Operating Completed	Dedicated Dedicated	2017 2011-2014	1,000,000 300,000
Norway full chain CCS	Brevik (Norcem AS)	Cement production and bioenergy	Norway	Advanced Completed		2023 2013	800,000 Variable
Occidental White Energy	Hereford and Plainview bioenergy	Ethanol production	US	Evaluation		-	650,000
Notable facilities							
Russel CO₂ injection plant	ICM ethanol plant	Ethanol production	US	Completed		2003-2005	7,700 (total)
Arkalon CO₂ compression facility	Bioernergy ethanol plant	Ethanol production	US	Operating	EOR	2009	290,000
Bonanza Bioenergy CCUS EOR	Bioernergy ethanol plant	Ethanol production	US	Operating	EOR	2012	100,000
Husky Energy Lashburn	Lloydminter ethanol plant	Power generation	Canada	Operating	EOR	2012	90,000
Mikawa Post combustion 49 MWth	Mikawa cofired thermal power plant	Power generation	Japan	Advanced Completed		2020 2009	180,000 3,000
Drax bioenergy BECCS	North Yorkshire power station	Ethanol production	England	Operating		2018	330
CPER Artenay	Sugar refinery in the Loiret	Ethanol production	France	Advanced		-	45,000
Biorecro/EERC	Biomass gasification plant	Biomass gasification	US	Advanced		-	1,000-5,000
OCAP	Abengoa's ethanol plant	Ethanol production and oil refinery	Netherlands	Planned Operating	Dedicated CCU	2025 2011	100,000 100,000
Lantmannen etanol purification	Lantmannen agroetanol plant	Ethanol production	Sweden	Operating		2015	200,000
Calgren renewable fuels CO₂ recovery	Calgren renewable ethanol plant	Ethanol production	US	Operating		2015	150,000
ABF biorefinery CO₂ recovery	Biorefinery	Ethanol production	Belgium	Operating		2016	100,000
Cargill wheat processing CO₂ purification	Wheat processing plant	Ethanol production	England	Operating		2016	100,000
Saga city waste incineration plant	Municipal waste incineration plant	Waste to energy	Japan	Operating		2016	3,000
Saint-Felicien pulp mill and greenhouse carbon capture	Resolute softwood kraft pulp mill	Pulp and papers	Canada	Operating		2018	11,000

- Storage. After the capture and transport of CO_2, the last stage of BECCS processes is the permanent and safe storage in geological deposits. Three different types of deposits are proposed: depleted oil or natural gas deposits, coal deposits or mines that cannot be exploited and salt aquifers. Figure 25 shows the CCS potential capacity by countries. The growing interest on CCS has led more and more studies to analyze the storage capacity, increasing the accurately of CCS global potential capacity. The CO_2 storage values projected to meet the climate targets quantify about 100 billion tons of accumulated CO_2 to 2060 and about 3.3 Gt per year by the end of the century. In this sense, CCS potential capacity will not constrain the BECCS deployment.

A wide range of industries and sectors can be combined with the use of biomass-based materials or bioenergy. Biomass can be used for the production of bioenergy power or power and heat. The main technologies are based in thermochemical conversion processes. There is a high variability in the maturity of the different technologies used, with technologies that are in the research phase to large-scale commercial facilities. Figure 23 shows the operating BECCS facilities in 2019. As it can be seen, all the operating BECCS plants are installed in OECD countries, mainly North America and Europe, and mostly associated to fossil fuel deposits. Ethanol facilities at different scales were installed during the early years of the 21st century as the first dedicated BECCS plants. The largest BECCS scale operating plant, placed in USA, captures 1 Mt of CO_2 per year during the fermentation process for the ethanol production and the CO_2 generated is stored in dedicated geological formations. Also, some facilities are linked to enhancing oil recovery (EOR), where the CO_2 is injected into fossil fuel deposits for a more efficient oil extraction and the proper CO_2 storage. A large deployment of BECCS processes is expected for the next decades. Further information about these facilities is presented in Table 3. Also, biomass can be used for biofuel production. Figure 24 shows the scheme of the production of different biofuels from various biomass feedstock with chemical or biological processes. A wide range of usable biofuels can be produced for road transportation or aviation, among other sectors that produce diffuse emissions that are difficult to storage.
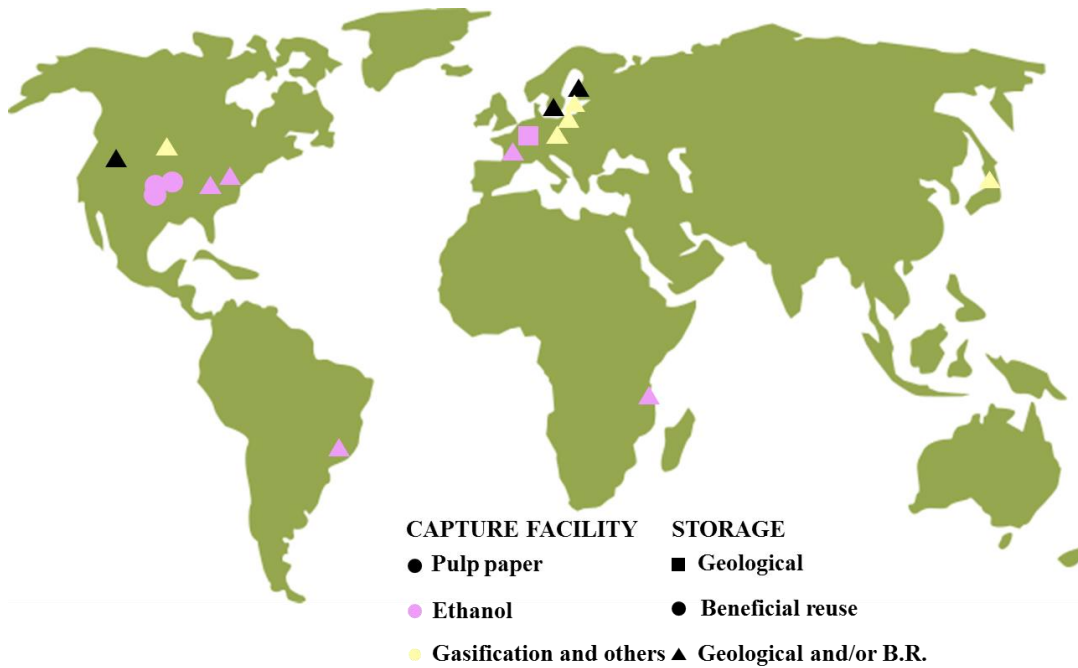
Figure 23. BECCS operating facilities in 2019.

Source: Consoli (2019).
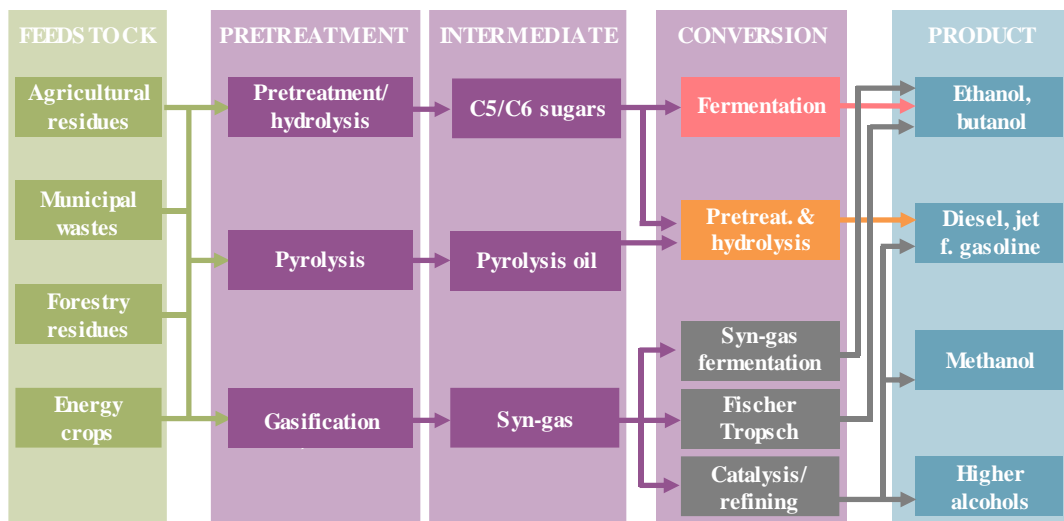
Figure 24. Scheme of different biofuels production possibilities from various biomass feedstock.

Source: modified from Consoli (2019).

Fuss et al. (2018) have analyzed the perspectives of each BECCS technology focusing in the 2100 horizon. The CCS deployment together with the correct

management of the biomass feedstock have been identified as critical variables for the BECCS deployment. Furthermore, the necessary BECCS implementation will require cost-effective technologies.
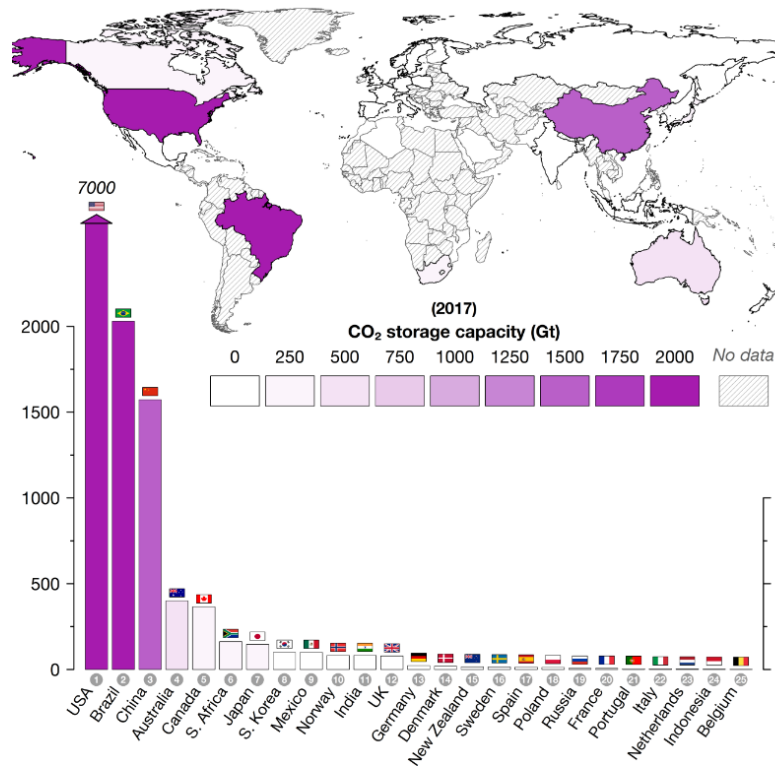
Figure 25. CCS global potential capacity by countries in 2017.

Source: Staffell et al. (2018).

1.4.1 Biomass

Biofuels represent an important fuel sources to guarantee environmental and economic sustainability. They are considered a carbon neutral (CO_2 is captured from the atmosphere and stored by biomass through photosynthesis and then emitted again into the atmosphere during biofuel combustion), renewable and abundant energy resource. Biofuels are generally classified as primary and secondary biofuels (Nigam and Singh 2011). Primary biofuels are used in an unprocessed form (woody biomass, biomass coming from forestry and agriculture, fishery products, municipal wastes, ...). Secondary biofuels are derived from primary biofuels by chemical,

biological or thermal processes to yield a fuel with suitable characteristics for a determined use (ethanol, biodiesel, dimethyl ether) (Sikarwar et al. 2017). Biofuels can be also classified according to their physical characteristics such as solid (woody biomass, …), liquid (ethanol, pyrolysis oils, …), and gaseous (biogas, pyrolysis gases, …). Gaseous and solid biofuels are normally used for heat and power production, whereas liquid biofuels are generally employed in the transport sector.

Among the solid biofuels, biomass has the greatest potential as an energy source. Biomass describes the natural tridimensional polymeric networks formed mainly by cellulose, hemicellulose and lignin of biological origin. The natural origin confers biomass a wide variability of composition. This renewable fuel source can be divided generally into three primary classes: 1. wood and woody materials, 2. herbaceous and other annual growth materials such as straws, grasses, leaves, and 3. agricultural by-products and residues including shells, hulls, pits, and animal manures. The general advantages of using biomass as fuel are: low ash, sulfur and mercury contents and high reactivity for conversion process.

Currently, some economically underdeveloped countries (mainly in sub-Saharan Africa) obtain about 90% of their energy from wood, among other biofuels, and are estimated at around 30% in Asia, Africa and Latin America. However, due to low levels of development and poor technological advances in many of these areas, biofuel consumption can contribute to deforestation rather than sustainable use. Globally, traditional energy sources worldwide declined from 98% in 1800 to 50% in 1900 and by approximately 14% in 2000 (Kander et al. 2014). Figure 26 shows the evolution from 1800 to 2017 of the consumption of various energy resources. Despite the decrease in the contribution of traditional energy uses of biomass, biomass has always remained at a steady consumption rate, while fossil fuels were constantly increasing.
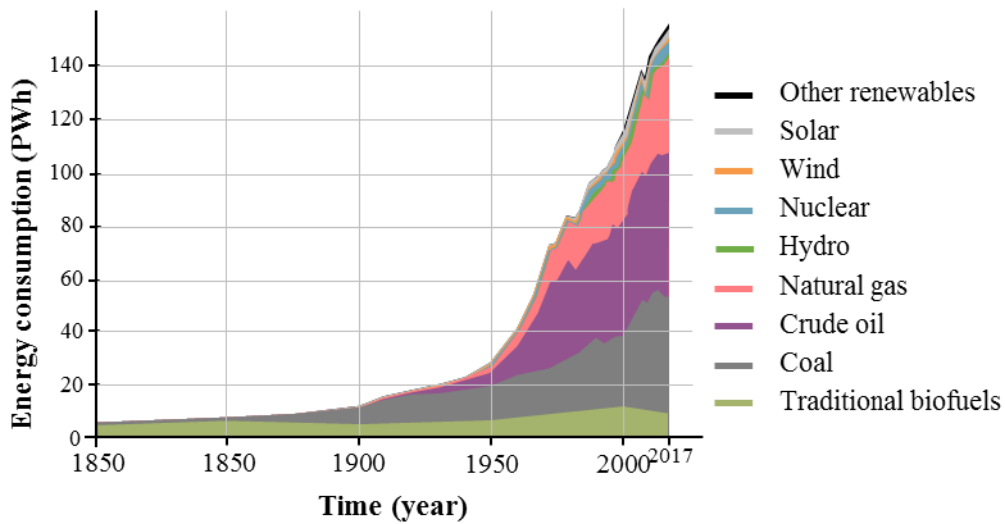
Figure 26. Energy consumption evolution from 1800 to 2017 by sources.

Source: Brown and Le Feuvre (2017).

Figure 27 shows the distribution of solid biofuels consumption by end use in 2015. As it can be seen, traditional uses remain the major consumer of biomass, accounting for more than half of the use of biomass that was around 51 EJ in 2015. Heat in the industry follows the list that continues with power generation and modern bioenergy processes. The use of biomass is maintained and new uses should be deployed with sustainable management of this resource.
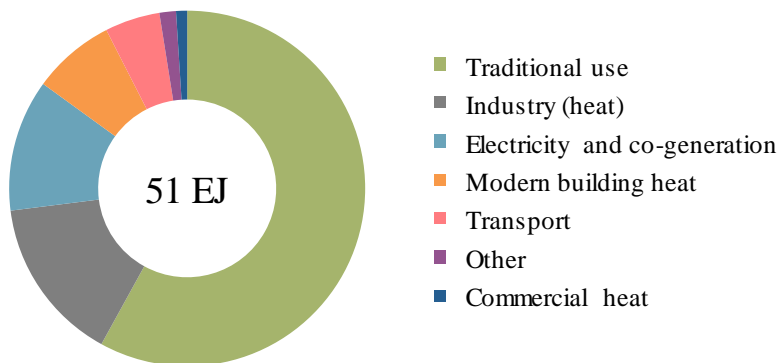
Figure 27. Biomass and waste resources by end use in 2015.

Source: modified from Brown and Le Feuvre (2017).

The use of biomass in the energy mix is nowadays limited compared to fossil fuels. However, the use of biomass in bioenergy could be increased to reduce dependence on fossil fuels. The renewable potential of this resource contrasts with the depletion of other energy resources. Fossil fuels and other energy-related raw materials are being used unsustainably, thus approaching its limit. However, biomass production will require fields with a water supply, so that it could go into competition with food production. Therefore, for sustainable development, the supply of energy from biomass should ensure environmental protection with responsible and sustainable use of water, while food production is guaranteed. In this way, the biomass supply chain would not produce impacts affecting the sustainability of resources.

Figure 28 shows the potential biomass production range of the main biomass sources. As it can be seen, according to Brown and Le Feuvre (2017), agriculture and residual biomass clearly show greater potential for sustainable biomass production than forestry operations or municipal solid waste (MSW). The minimum and maximum values of potential sustainable biomass showed in Figure 28 also include different minor biomass sources. Comparing the total sustainable biomass deployment required to achieve climate targets, the necessary value of sustainable biomass deployment enters in the range of the global potential of sustainable biomass production.
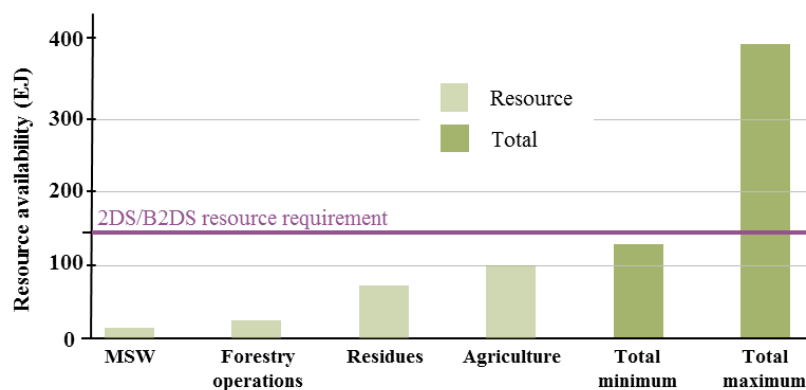
Figure 28. Main biomass sources potential, minimum and maximum potential of sustainable biomass.

Source: modified from Brown and Le Feuvre (2017).

1.4.2 Resources for BECCS in Spain

Different types of biomass can be used for bioenergy purposes. However, the sustainability of the biomass production should be considered in order to guarantee the global process sustainability. An increase in the european sustainable biomass production was pointed by the European Environmental Agency from about 190 Mtoe in 2010 to about 293 Mtoe in 2030. Figure 29 presents the environmentally compatible primary bioenergy potential in the EU-25. Various biomass types were considered and, furthermore, an additional agricultural potential was estimated by Wiesenthal et al. (2006) for Germany and France consequence of the posible rising prices paid for bioenergy. As it can be seen, a general increase in sustainable biomass potential is showed from 2010 to 2030 and basically corresponds to the agricultural potential increase. Meanwhile, maintained waste and forestry sustainable biomass production are shown.
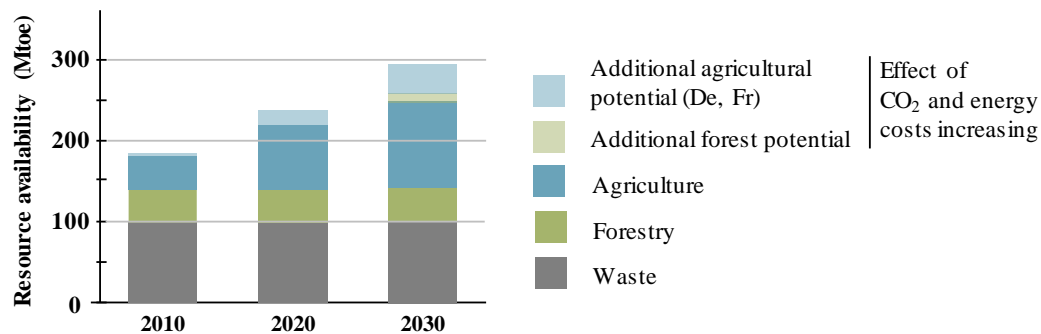
Figure 29. EU primary bioenergy potential environmentally compatible.

Source: Wiesenthal et al. (2006).

Focusing in Spain, an increment from about 17 Mtoe in 2010 to about 25 Mtoe in 2030 (Wiesenthal et al. 2006) was reported. The Spanish Renewable Energy Plan (PER) 2011-2020 shows that about 18066 kt/year of non industrial biomass are available in Spain, covering the objectives of biomass production needed for bioenergy and energy demand set in the plan IDAE (2011), and about 9639 kt/year of biomass from forestry and 5908 kt/year of agricultural waste should be used for energy uses in 2020.

Olive stones (*Olea europaea*) and almond shells (*Prunus dulcis*) are two agricultural residues with high annual production. In 2016 world olive production reached 3.3 million tons and Spanish production represented about 38% of the total production (IOOC 2018). Almond production in the world increased about 43% during the period 2007-2017, achieving at the end of the period about 1.2 million tons. Spanish almond production represented about the 5% of total production (INC 2018).

Biomass production covers the expected biomass demand increase for energy purposes, however, the deployment of NET processes associated to energy generation will need the deployment of transport and storage facilities for the CO_2 produced. In fact, all the considered strategies to mitigate the climate change effects include CCS technologies. The Geocapacity project estimated the CO_2 storage capacity of most of the European countries about 356500 Mt including saline aquifers as well as hydrocarbon and coalfields. In this study, the potential locations for a long and safe CO_2 storage are considered together with the main CO_2 emitters that guarantee the cost-effective implementation. In this sense, sources with emissions higher than 0.1 Mt of CO_2 per year were considered as well as existing natural gas pipelines were taken into account because of the transport similarities (Vangkilde-Pedersen et al. 2009). Spanish CO_2 storage capacity was estimated about 14179 Mt, analyzing 103 geological formations (Zapatero et al. 2008). No large CCS projects are installed in Spain, however, the various small projects will store about 6.5 Mt of CO_2 at the end of the period 2015-2020. Moreover, 20.2 Mt/year are expected to be stored in Spain during the period 2021-2030 (ALINNE 2019). These expected numbers point to the good perspectives for a large-scale deployment of BECCS technologies.

1.5 Chemical Looping Combustion

The CLC concept was developed for pure CO_2 production in 1954 by Lewis and Gilliland (Lewis and Gilliland 1954). Decades later, in 1980s, the CLC process was proposed as a highly efficient technology for power generation (Richter and Knoche 1983; Ishida et al. 1987) and later it was also recognized the possibility of being used as a combustion process with inherent CO_2 capture (Ishida et al. 1996).

The good perspectives of CLC brought attention on these technologies. Initially the process was developed for gaseous fuels, due to its easy handling and high energy density, but in the last years its use has spread to liquid and solid fuels. Moreover, Chemical Looping (CL) processes open up a wide range of biofuels utilization through different processes. Figure 30 presents the general scheme of Chemical Looping Processes showing the different biofuels and products. Depending on the type of biofuel used and the product obtained, different CL processes can be distinguished:

- Chemical Looping Combustion (CLC) implies the combustion of gaseous, liquid or solid fuels obtaining heat and/or power. If the biofuel is solid, two reaction mechanisms are possible: In situ gasification Chemical Looping Combustion (*i*G-CLC) and Chemical Looping with Oxygen Uncoupling (CLOU). Both mechanisms will be described in section 1.5.1.
- Chemical Looping Reforming (CLR) implies partial oxidation reforming of gas or liquid biofuels to produce syngas ($H_2 + CO$).
- Chemical Looping Gasification (CLG) allows obtaining syngas using solid biofuels.

In these processes, a solid oxygen carrier, usually a metal oxide, provides the oxygen needed for the fuel oxidation or partial oxidation. A wide range of reactor configurations has been proposed for solid, liquid and gaseous biofuels also depending on the oxygen carrier reactivity and the scale of the CL prototype. For

further information about different CL process configurations see Adánez and Abad (2019). Interconnected fluidized bed reactors are commonly the preferred option for CL processes thanks to the good and homogeneous contact between solids and gases (Kramp 2014). Fluidized bed reactors are known because of the good gas/solid contact and the homogeneous temperature distribution.
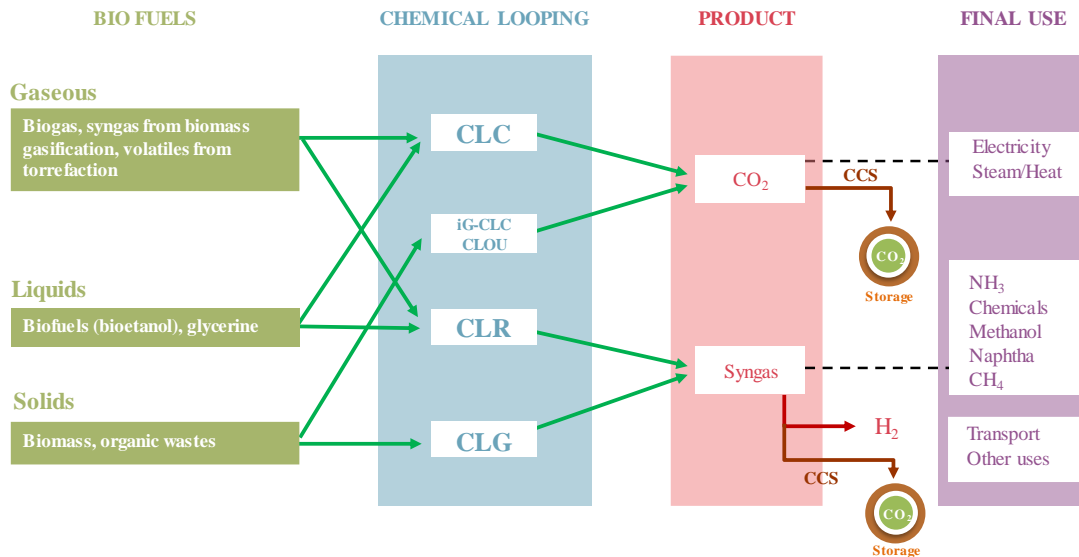
Figure 30. General scheme of Chemical Looping Processes.

Source: modified from Mendiara et al. (2018a).

The CLC process is mainly based in two interconnected fluidized bed reactors, the fuel and air reactors. A simple scheme of the process is shown in Figure 31. The solid oxygen carrier circulates between the fuel and air reactors without gas mixing. In the fuel reactor, the oxygen carrier is reduced providing the oxygen needed for the fuel oxidation to CO_2 and H_2O. After H_2O condensation, an almost pure CO_2 stream is produced during fuel conversion, ready for transportation and storage. Meanwhile, in the air reactor, the oxygen carrier is oxidized again in air to start a new cycle. Loop seals are placed between both reactors to prevent the mixing of fuel and air reactor atmospheres.

The energy balance of CLC process can be calculated as the combination of the reduction and oxidation reactions (R1 and R2), obtaining the traditional

combustion equivalent reaction (R3). The oxygen carrier oxidation in the air reactor is always an exothermic reaction, however, the oxygen carrier reduction in the fuel reactor can be exothermic or endothermic reaction depending on the redox system of the oxygen carrier and the fuel used. In this sense, under endothermic reduction reactions, the oxygen carrier also acts as energy vector by transporting heat from the air reactor to the fuel reactor to maintain constant the temperature in the fuel reactor. Regarding the kinetics of CLC process, the oxygen carrier reduction is usually slower than the oxygen carrier oxidation, however, each reaction can be affected by several variables such as the reactor temperatures, the oxygen carrier used and the gas concentrations.
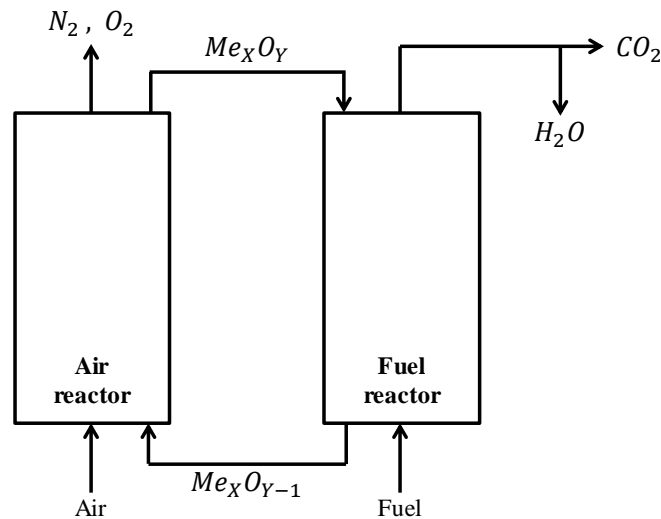
Figure 31. Simplified scheme of a CLC process.

Reduction reaction $\qquad \Delta H^0_{Red} < 0 \ or > 0 \ kJ/mol$ $\qquad$ (R1)

$$(2n + m - p)Me_xO_y + C_nH_{2m}O_p \rightarrow (2n + m - p)Me_xO_{y-1} + nCO_2 + mH_2O$$

Oxidation reaction $\qquad \Delta H^0_{Oxi} < 0 \ kJ/mol$ $\qquad$ (R2)

$$(2n + m - p)Me_xO_{y-1} + \left(n + \frac{m}{2} - \frac{p}{2}\right)O_2 \rightarrow (2n + m - p)Me_xO_y$$

Global combustion reaction $\qquad \Delta H^0_T < 0 \ kJ/mol$ $\qquad$ (R3)

$$C_nH_{2m}O_p + \left(n + \frac{m}{2} - \frac{p}{2}\right)O_2 \rightarrow nCO_2 + mH_2O$$
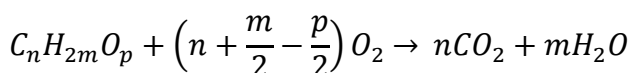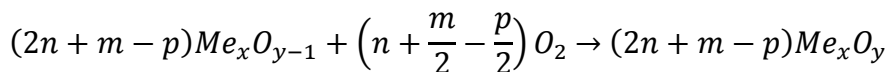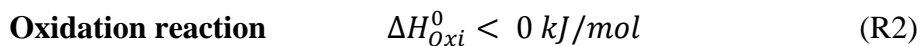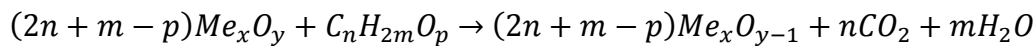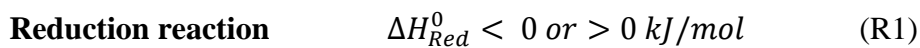
Guandalini et al. (2019) used a simplified method of costs sequential approach over different CO_2 capture technologies. The results were validated using the results of a coal-fired plant and among various pre-combustion, oxy-fuel, post combustion or absorption processes, CLC stood out with the lowest cost of avoided CO_2. Using biofuels, CLC was pointed as one of the most suitable CO_2 capture technologies to obtain bioenergy (heat and/or electricity) from energetic and economic points of view, producing a negative CO_2 balance (Lyngfelt and Leckner 2015). The inherent CO_2 capture, thanks to the two-stage reaction, makes any separation step unnecessary.
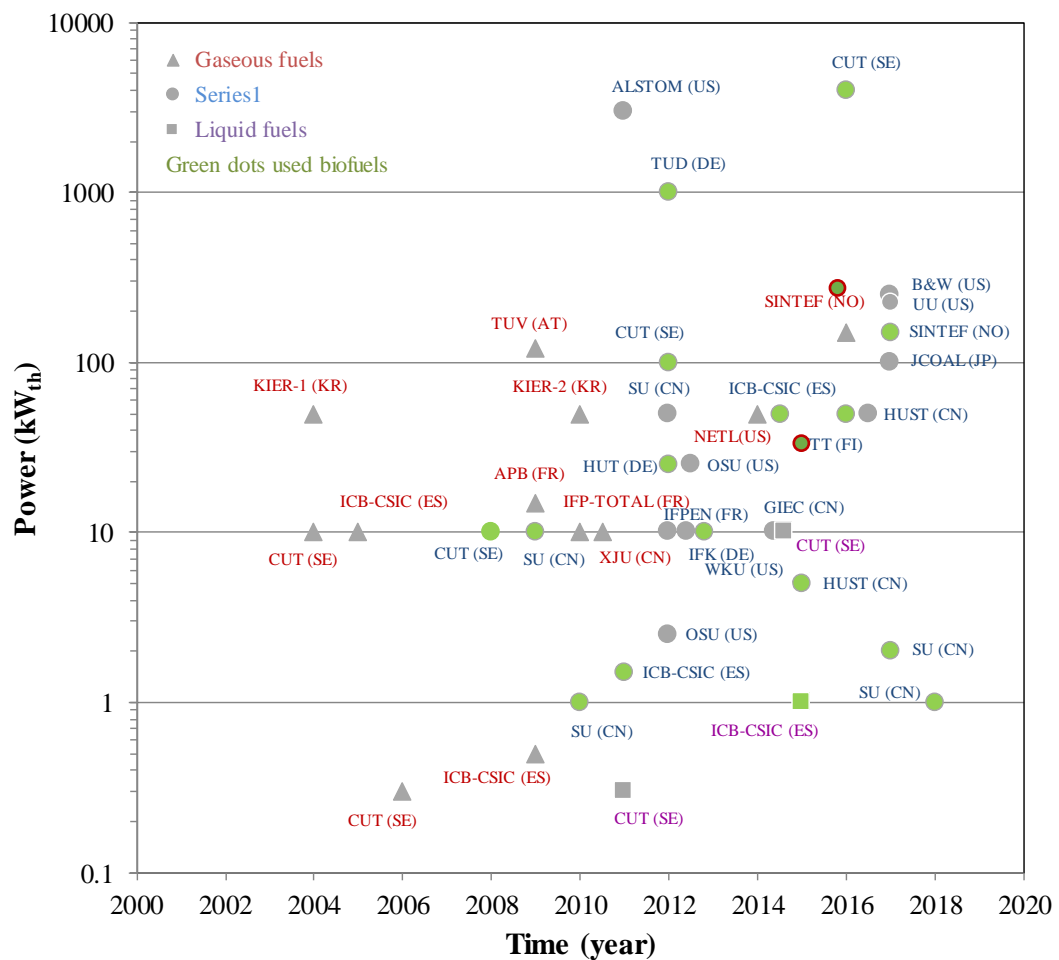
Figure 32. CLC units by power and operation date.

Source: Mendiara et al. (2018a).

Figure 32 presents the CLC units operated since year 2000 to date by power and the type of fuel used. As it can be seen, different CLC sizes were implemented

from bench scale to 4 MW$_{th}$. Bio fueled units to achieve a considered as NET (specially powered by solid biomass), highlighted in green, began to be operated around 2008 and have shown great development in recent years.

1.5.1 Chemical Looping Combustion of solid fuels

Figure 33 shows the scheme of a typical CLC unit for solid fuels. The reactor system used has large similarities with conventional circulating fluidized bed (CFB) boiler. Fuel is introduced into the fuel reactor where it is converted by the oxygen carrier to produce CO_2 and H_2O. The spent oxygen carrier is transported to the air reactor to be oxidized by air in order to start a new cycle. H_2O or CO_2 can be used to fluidize the fuel reactor and air is used in the air reactor as fluidizing gas producing a depleted air.
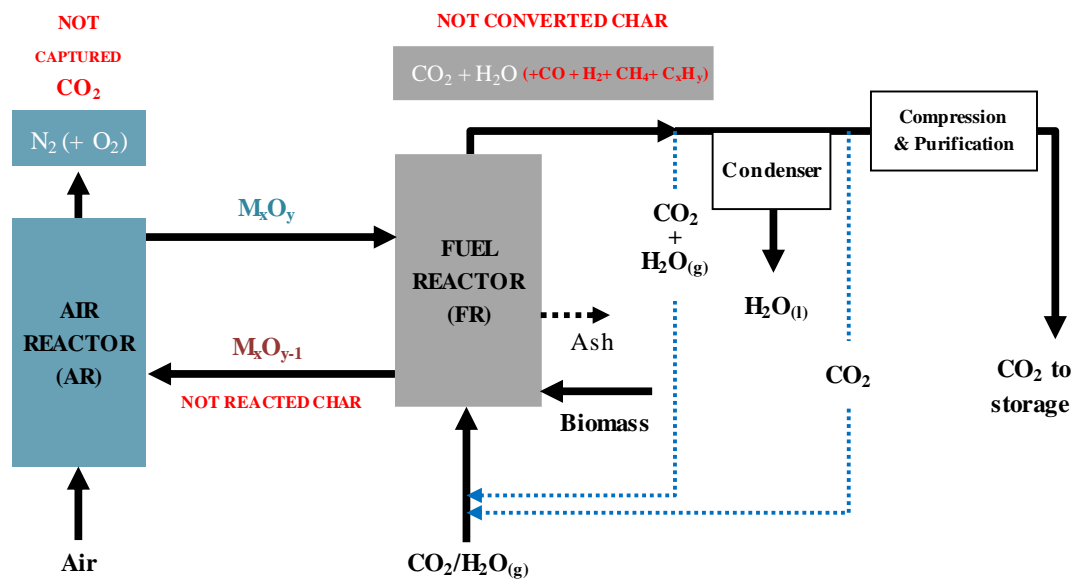
Figure 33. General scheme of a CLC process for solids fuels.

When the solid fuel is introduced into the fuel reactor, the high temperature produces the fuel drying followed by the devolatilization, generating the volatile matter and the char. This char is mainly formed by carbon. Two options have been proposed depending on how the solid fuel is converted to CO_2 and H_2O: in situ

44

Gasification CLC (*i*G-CLC) and Chemical Looping with Oxygen Uncoupling (CLOU). Figure 34 shows the *i*G-CLC and CLOU reaction schemes.
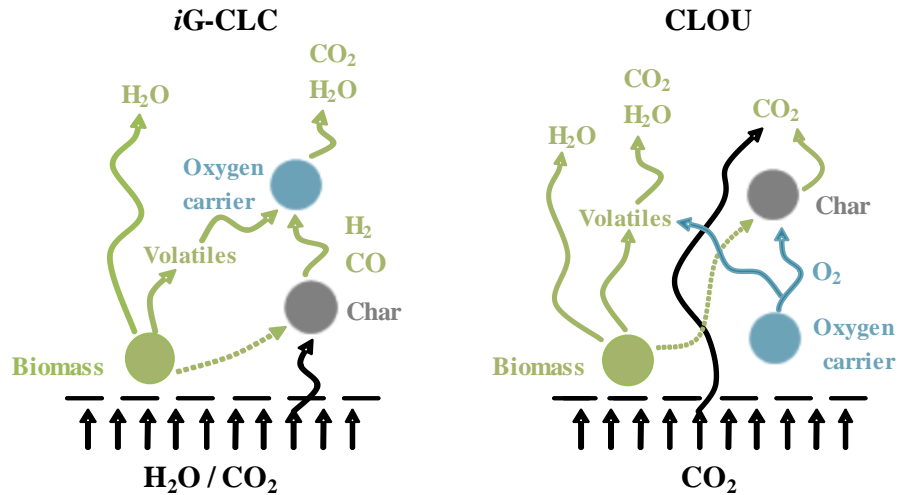
Figure 34. In-situ Gasification CLC (iG-CLC) and Chemical Looping with Oxygen Uncoupling (CLOU) reaction schemes.

Under *i*G-CLC, the steam or CO_2 supplied to the fuel reactor as fluidizing agent also acts as char gasifying agent producing combustible gases according to the following reaction scheme, reactions (R4) to (R6).

$$Solid\ fuel \rightarrow char + volatile\ matter \qquad \text{(R4)}$$

$$Char + x\ H_2O \rightarrow x\ H_2 + x\ CO + ash \qquad \text{(R5)}$$

$$Char + y\ CO_2 \rightarrow 2y\ CO + ash \qquad \text{(R6)}$$
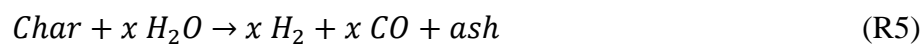
The lattice oxygen in the solid oxygen carrier reacts with the volatile matter and the gasification products of the char to produce CO_2 and H_2O as final products. The prevailing reaction between the oxygen carrier and the fuel is a solid-gas reaction. In this process the CO_2 capture efficiency is reduced by char particles by-passed to the air reactor together oxygen carrier when these particles are burnt. Char gasification has been identified as the limiting step of this process (Adánez et

al. 2018). Thus, char particles need high residence time in the fuel reactor to be gasified. Also the fluidizing agent (H_2O or CO_2) used in the fuel reactor plays an important role in the reactivity, enhancing the char gasification rate. Other characteristic of *i*G-CLC process is that unburnt compounds can be found in the gas stream from the fuel reactor (Adánez et al. 2018). These unburnt compounds should be burnt by using pure O_2 (oxygen demand). Finally, because of the ashes present in the solid fuels it is necessary the drainage of ashes from the system to avoid its accumulation in the reactors. Most of the experience gained in biomass combustion was under this mechanism.

CLOU process is based on the capacity of some specific oxygen carriers to release molecular oxygen at the common operating temperatures in the fuel reactor (about 800-1000 ºC). The O_2 generated reacts with volatiles and char as in conventional combustion with air. In CLOU, the prevailing reaction became a gas-gas reaction. This process was proposed in 2009 by Mattisson, et al. (2009a) and the proof of concept was demonstrated with coal in a 1.5 kW_{th} unit located at ICB-CSIC (Abad et al. 2012). The materials used as oxygen carriers in this process must have suitable thermodynamic properties for oxygen uncoupling at temperatures of interest. The suitable materials that have the property of release oxygen are limited. Three metal oxide systems have so far been identified (Mattisson et al. 2009): CuO/Cu_2O, Mn_2O_3/Mn_3O_4, Co_3O_4/CoO and mixed oxides (Fe-Mn, Mn-Cu, Cu-Fe or Perovskites).

The CLC technology for solid fuels was initially developed for coal use. In this sense, the biomass has significant differences with respect to coal that will affect to its performance in CLC: Firstly, a high fraction of volatile matter is released during devolatilization, which contains 70-80% of the biomass heating value. Thus, a good conversion of the generated volatile matter during biomass devolatilization is a key point for a good process performance. On the other hand, a low fraction of char is produced, which has high gasification reactivity with steam and CO_2. Moreover, the sulfur content is low and also the ash fraction present in biomass is usually lower than that of coal.

The higher fraction of volatiles, compared to coal, could be a disadvantage due to unburnt volatile matter can increase the amount of unburned compounds in the outlet of the fuel reactor, increasing the total oxygen demand. The lower fraction and much higher reactivity of biomass char in steam and CO_2 gasification is a great advantage because a much smaller fraction of char would be by-passed to the air reactor. Its low ash content is a great advantage because the impact of ash-removal on oxygen-carrier lifetime and thus oxygen-carrier cost will be much less. However, biomass ash components, such as alkali metals and chlorine, are problematic in normal biomass combustion, mainly due to corrosion and agglomeration issues. In CLC, biomass ash could be problematic as several components, alone or together, could cause deactivation of the oxygen carrier particles and, in the worst case, cause agglomeration in the fluidized bed system due to the interaction of oxygen carrier materials and fuel ashes.

Tar compounds can be also produced during the biomass oxidation in the fuel reactor, reducing the biomass conversion efficiency and causing operational problems as fouling (Kobayashi and Fan 2011). However, the use of different oxygen carriers and the operating conditions should be analyzed because of the different tar formation and/or cracking (Virginie et al. 2012; Ge et al. 2016). Other aspect to be considered during biomass processing is the NO_x emissions. Although there is no gas-phase N_2 present during the CLC in the fuel reactor, biomass could contain certain amounts of organically bound nitrogen. This nitrogen may form harmful species, like NO, N_2O, HCN, and NH_3, that can be released in the fuel reactor, affecting the quality of the CO_2 stream produced. In addition, NO_x emissions can be released in the air reactor due to the combustion of the char coming from the fuel reactor. These emissions must be lower than those indicated by the EU regulations.

Compared to gaseous fuels or coal, the direct conversion of biomass in CLC processes is a relatively new subject. At the time of beginning this thesis, the experience that existed related to CLC processes with biomass combustion was very limited. Works published under CLC conditions using biomass had been carried out on laboratory-scale discontinuous reactors with small amounts of oxygen carriers and fuel fed. Mainly wood char or pine sawdust were used in these experiments, showing

the combustion efficiency a great dependence on the reduction temperature (Leion et al. 2009a; Leion et al. 2011). Subsequently, progress has been made in this technology by conducting experiments on continuous prototypes. As a summary, Table 5 presents an overview of the experience accumulated in different bioCLC facilities, indicating the specific fuel and oxygen carrier used among other operating variables. As can be seen, most correspond to work carried out in the framework of this thesis or works published during the period of realization of this thesis.

In any case, to date, most of the biomass fueled CLC studies used mineral oxygen carriers for iG-CLC. The natural origin of this type of materials, typically iron or manganese oxides, confers them a low cost. Synthetic oxygen carriers based on Cu and/or Mn have been used for the CLOU process. Different biofuels have been tested at the different pilot plants from 0.5 kW$_{th}$ to 4 MW$_{th}$. Pine sawdust and pine wood pellets have been usually used as reference materials thanks to the large world production and world distribution. Among other biofuels, agricultural wastes or sewage sludge have also been considered. In general, high carbon capture efficiencies were obtained but also high oxygen demands.

Table 5. Summary of the experience accumulated in bioCLC continuous units. Results highlighted in grey were obtained prior to the beginning of the research carried out in this Ph.D. Thesis.

Research group	Year of publication	Nominal power (kW)	Oxygen carrier	Fuel	FR design	FR Temperature (ºC)	Carbon capture (%)	Oxygen demand (%)	Operation (h)	Ref.
					iG-CLC					
SU	2009	10	Iron oxide	Pine sawdust	SB	740-920	*n.a*	*n.a*	30	(Shen et al. 2009)
SU	2011	1	Australian iron ore	Shenhua bituminous coal/ Sawdust	SB	720-930	95.5-98.5	*n.a.*	-	(Haiming et al. 2011)
SU	2015	1	Hematite	Sewage sludge	SB	800-900	~ 100	8.5-23.5	10	(Jiang et al. 2016)
ICB-CSIC	2013	0.5	Tierga iron ore	Pine sawdust	BFB	880-980	90-100	3.8-14.1	37	(Mendiara et al. 2013a)
CUT	2014	100	Ilmenite	Wood char	CFB	929-973	91-97	4.7-15.5	31	(Linderholm et al. 2014)
SU	2016	1	Hematite	Sewage sludge (SS) / Zhundong (ZD) coal	SB	800-930	94-96	13.5-35	5	(Jiang et al. 2016)
SU	2017	2	Hematite	Sewage sludge	2-stage SB	800-900	~ 100	*n.a.*	8	(Yan et al. 2017)
SU	2018	1	Australian hematite	Sawdust	5-stage BFB	840-920	> 95	*n.a.*	*n.a.*	(Jiang et al. 2018)
SU	2018	1	Australian hematite	Rice husk	5-stage BFB	840-920	> 95	*n.a.*	*n.a.*	(Jiang et al. 2018)
ICB-CSIC	2018	0.5	Tierga iron ore	Pine sawdust	BFB	880-980	90-100	7-34.6	14	(Mendiara et al. 2018b)
ICB-CSIC	2018	0.5	Tierga iron ore	Olive stones	BFB	905-980	90-100	20-30	13.4	(Mendiara et al. 2018b)
ICB-CSIC	2018	0.5	Tierga iron ore	Almond shells	BFB	905-985	90-100	18-28	10.8	(Mendiara et al. 2018b)
ICB-CSIC	2019	0.5	Manganese minerals	Pine sawdust	BFB	891-966	~ 100	9.1-34.8	65	(Pérez-Astray et al. 2019a)
ICB-CSIC	2019	0.5	Manganese-iron mixed oxide	Pine sawdust	BFB	887-951	~ 100	5-21.8	41	(Pérez-Astray et al. 2019b)
ICB-CSIC	2018	20	Tierga iron ore	Olive stones	CFB	900	95-99.9	15-20	20	(García-Labiano et al. 2018)
CUT	2016	10	Manganese ores	Wood char	BFB	887-1000	76.0-96.4	5.8-11.4	32	(Schmitz et al. 2016)
CUT	2016	100	Tierga iron ore	Wood char	CFB	880-960	> 96	7.4-8.5	26	(Linderholm and Schmitz 2016)
CUT	2018	10	Sintered manganese ore	Biochar and black wood pellets	BFB	900-970	92.8-99	6.5-30	20	(Schmitz and Linderholm 2018)

CUT	2018	100	Sintered manganese ore	Biochar and black wood pellets	CFB	940-981	99-100	10-35	28	(Schmitz and Linderholm 2018)
CUT	2019	10	Steel converter slag	Wood char, biochar and black pellets	BFB	920-985	~ 99	*n.a.*	28	(Moldenhauer et al. 2019)
CUT	2019	100	CaMn$_{0.775}$Ti$_{0.125}$Mg$_{0.1}$O$_{3-\delta}$ + Ilmenite (10-20 /80-90 wt%)	Wood char and black wood pellets	CFB	933-954	99.3-99.5	10.5-20.2	3	(Gogolev et al. 2019)
CUT	2017	4000*	Australian ilmenite or Brazilian manganese ore	Spruce tree wood pellets	CFB	~830	n.a.	~ 40	>1000	(Berdugo Vilches et al. 2017)
VTT	2016	50	Ilmenite	White and black pellets	BFB	~850	83-96	29-41	16+20	(Pikkarainen et al. 2016)
VTT	2017	50	Braunite	White and black pellets, Wood char	BFB	838-897	72-96	11-31	20	(Pikkarainen and Hiltunen 2017)
HUT	2018	25	CuO/Al$_2$O$_3$	Hard wood	Two-step BFB	850	93	1.6	*n.a.*	(Haus et al. 2018)
SINTEF	2018	150	Ilmenite	Black wood pellets	CFB	960-980	94-97	23-28	3	(Langørgen and Saanum 2018)
TUD	2017	1000	Tierga iron ore	Hard coal and torrefied biomass	CFB	900-950	Up to 66	38-45	6	(Ohlemüller et al. 2017)
CLOU										
ICB-CSIC	2014	1.5	CuO/MgAl$_2$O$_4$	Pine sawdust	BFB	900-935	98-100	0	10	(Adánez-Rubio et al. 2014)
ICB-CSIC	2018	1.5	Cu$_{1.5}$Mn$_{1.5}$O$_4$	Pine sawdust	BFB	775-850	86-100	0	20	(Adánez-Rubio et al. 2018)
ICB-CSIC	2018	1.5	Cu$_{1.5}$Mn$_{1.5}$O$_4$	Olive stones	BFB	775-850	78-91	0	10	(Adánez-Rubio et al. 2018)
ICB-CSIC	2018	1.5	Cu$_{1.5}$Mn$_{1.5}$O$_4$	Almond shells	BFB	775-850	73-93	0	10	(Adánez-Rubio et al. 2018)
CUT	2016	10	CaMn$_{0.9}$Mg$_{0.1}$O$_{3-\delta}$	Biochar	BFB	917-970	82-95.2	2.1-4.9	37	(Schmitz and Linderholm 2016)
CUT	2018	10	MnSiTi mixed oxide	Wood char	BFB	900-970	81.3-95.5	3.4-6.7	7.5	(Schmitz et al. 2018)
CUT	2019	100	CaMn$_{0.775}$Ti$_{0.125}$Mg$_{0.1}$O$_{3-\delta}$ + Ilmenite (80-90/10-20 wt%)	Black wood pellets	CFB	946-957	> 99.5	3-5	3	(Gogolev et al. 2019)

* Corresponds to the gasifier acting as fuel reactor in the Chalmers boiler/gasifier loop (with inputs of 12 MW$_{th}$ and 2–4 MW$_{th}$, respectively)

(SB= Spouted bed, BFB= Bubbling fluidized bed, CFB= Circulating fluidized bed)

1.5.2 Oxygen Carriers

The oxygen carrier particles are responsible of the oxygen exchange from the air in the air reactor to the fuel in the fuel reactor. Furthermore, depending on the thermodynamics of the process, the oxygen carrier acts as heat vector between the reactors. Several properties of the oxygen carriers should be considered for a suitable CLC performance: 1. A correct fluidization behavior should be guaranteed (no agglomeration problems). 2. The oxygen transport capacity of the oxygen carrier (R_{oc}) must be enough to allow the complete combustion of the fuel. 3. A high reactivity and its maintenance over a high number of redox cycles. 4. High selectivity to CO_2 and H_2O during combustion. 5. High mechanical resistance of the particles and its maintenance over a high number of redox cycles. In general, the lower chemical stress affects the of oxygen carrier particles, the longer their lifetime should be (Adánez et al. 2012). 6. Low price of the materials. Oxygen carrier origin (synthetic or natural) will affect the oxygen carrier cost. 7. The low toxicity of the oxygen carrier and residues generated must be taken into account (Mendiara et al. 2012).

Figure 35 presents the oxygen transport capacity of the most important redox pairs used in CLC. Different colors were used to classify the oxygen carriers depending on their capacity to release molecular oxygen under specific conditions. Hundreds of oxygen carriers (natural or synthetic) have been tested for years in CLC, most of them using gaseous fuels (Adánez et al. 2012). Minerals, or ores, usually are low cost oxygen carriers. Even some mining residues have been used as oxygen carriers with good results. On the contrary, synthetic oxygen carriers, usually more reactive carriers than ores, need a preparation processes that increases the cost. Synthetic oxygen carriers are normally formed by an active phase, actually able to react with the fuel, and an inert support that increases resistance. The variability in the price of the oxygen carrier feedstock can greatly influence the total cost. Different oxygen carrier preparation methods can be used. Among them, spray drying, impregnation and granulation processes are the most commonly used. Cobalt based and nickel based oxygen carriers present high costs as well as toxicity effects, what

disregard their use in CLC units. Meanwhile, iron, manganese, and copper oxygen carriers generate inert residues that can be disposed as nonhazardous materials.
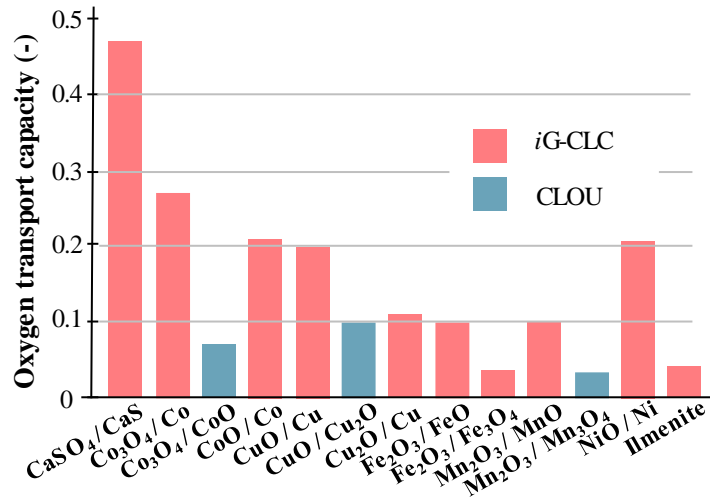
Figure 35. Oxygen transport capacity (R_{OC}) of various redox pairs.

The majority of the CLC units for combustion of solid fuels, including biomass, have been operated under the *i*G-CLC mode using minerals or residues. Despite the lower ash content of solid bio fuels compared with coal, the necessary ash removal associated with the use of solid fuels implies the oxygen carrier drainage. Because of this oxygen carrier purge, the oxygen carrier price can greatly affect the total costs, being low-cost oxygen carriers the preferable option for the CLC of biomass. In this sense, the natural origin of ores, typically iron or manganese oxides, confers them a low-cost appropriate for this use. Moreover, synthetic oxygen carriers based on Cu and/or Mn have been used for the CLOU process.

First results using biomass (pine sawdust) and iron ore as oxygen carrier were obtained by Shen et al. (2009) in a 10 kW$_{th}$ unit during about 30 h of operation. They evaluated the influence of the fuel reactor temperature on the gas products of the fuel reactor and they found a higher influence of the temperature on the CO formation than the observed on the CO oxidation. Pine sawdust was also used in the experiments performed at *Instituto de Carboquímica* by Mendiara et al. (2013a) with a Fe-based iron ore (Tierga ore) as oxygen carrier. The influence of the fuel reactor

temperature on the CO_2 capture and combustion efficiencies and the oxygen demand was assessed. In the interval 880–915 ºC, high carbon captures (> 95%) were achieved using both steam and CO_2 as gasifying agents and the total oxygen demand decreased by increasing the fuel reactor temperature. Moreover, no interaction of biomass ashes with the oxygen carrier was observed after 78 h of continuous operation. The same oxygen carrier was also used by Linderholm and Schmitz (2016) in a 100 kW$_{th}$ CLC plant located at Chalmers University of Technology (CUT) using wood char as fuel. The highest combustion efficiency observed in these experiments was 93% (Linderholm and Schmitz 2016). Gogolev et al. (2019) used a mixture of synthetic calcium manganite (10 - 20%) and natural ilmenite (80 - 90%) as oxygen carrier in a 100 kW$_{th}$ during an experimental campaign with black pellets of steam-exploded stem wood, straw pellets and wood char. Close to 100% of CO_2 capture efficiency and about 95% gas conversion was achieved for black pellets. Pikkarainen et al. (2016), at the VTT Technical Research Centre in Finland, built a 10-50 kW$_{th}$ CLC plant for biomass combustion, which was operated with ilmenite during 16 h. They found high oxygen demands during the combustion of wood pellets due to an insufficient bed temperature of the fuel reactor, as the unit was originally designed for gasification. Ohlemüller et al. (2017) presented the results with hard coal mixed with biomass in their 1 MW$_{th}$ pilot plant. High total oxygen demands were obtained using the Tierga ore as oxygen carrier. Low CO_2 capture efficiencies were reached, however, no carbon stripper was used. Langørgen and Saanum (2018) used black pellets with ilmenite in a 150 kW$_{th}$ CLC pilot unit. CO_2 capture efficiencies over 90% were achieved while a minimum total oxygen demand about 23% was reached.

More recently, Mn-ores are being considered as an alternative to Fe-based materials due to its relatively high reactivity and its positive effect on the char conversion rate (Abad et al. 2018). A wide number of manganese ores with different origins all around the world and different characteristics have been studied during recent years for their use as oxygen carriers at various laboratory scales. The researcher group from Chalmers University of Technology (Schmitz el al. 2016; Schmitz and Linderholm 2018) has used several manganese ores as oxygen carriers in two different 10 and 100 kW$_{th}$ CLC units with wood pellets and wood char. The influence of several operating conditions was studied and, in general, high carbon

capture and combustion efficiencies (> 90%) and low oxygen demands were obtained. However, the lifetime of the oxygen carrier was not very high.

A major step in the scale-up of the biomass CLC process was recently presented by Berdugo-Vilches et al. (2017). Several experimental campaigns were carried out in a semi-commercial dual fluidized bed unit at Chalmers University consisting of a 12 MW_{th} boiler coupled to a 2-4 MW_{th} bubbling bed gasifier. The gasifier can be assimilated to a fuel reactor of a conventional CLC unit and the boiler to the air reactor. More than 1000 hours of combustion were reported using commercial wood pellets as fuel and ilmenite and a manganese ore as oxygen carriers. Combustion efficiencies up to 60% were achieved although the temperature in the gasifier was not high, about 830 ºC (Berdugo Vilches et al. 2017). Despite this pilot plant represents a non-optimized reactor design for CLC applications, these results highlight the strong potential of the CLC technology for biomass combustion and reinforce its possibilities as BECCS technology.

Current experience in biomass combustion under CLOU mode is quite limited. As it is shown in Figure 36, few metal oxides present adequate partial pressure of oxygen at conditions relevant for combustion processes (CuO/Cu_2O, Mn_2O_3/Mn_3O_4 and Co_3O_4/CoO) (Mattisson et al. 2009). Assuming similar oxygen excess (about 20%) to those used in traditional biomass boilers, about 4% of oxygen would be preferable at the air reactor outlet for a CLOU process, and therefore different temperatures in the air reactor would be needed depending on the redox pair used. Regarding the fuel reactor temperature, the increase of the fuel reactor temperature favours the oxygen release.

Table 6 shows the temperature operating window for CuO/Cu_2O and Mn_2O_3/Mn_3O_4 redox pairs. The difference between the fuel reactor and the air reactor temperatures can difficult CLC energy integration, however the low differences on the operating windows for each reaction of the considered oxygen carriers can be easily managed. Despite the CLOU capacity of Co_3O_4/CoO, the energy balance of this redox reaction difficulties the integration of reduction and oxidation reactors

(Leion et al. 2009a) since the reduction reactions are endothermic. In addition, Co-based materials are toxic.
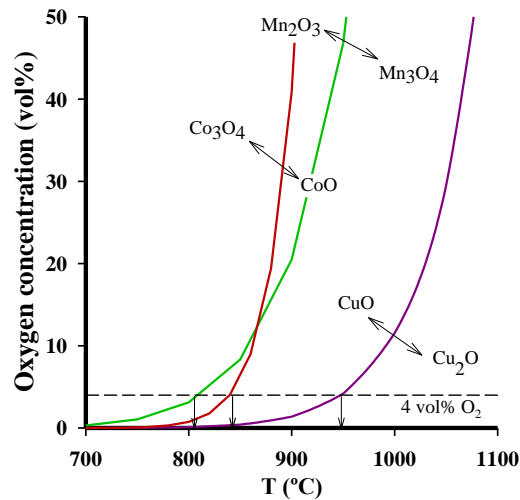
Figure 36. O_2 equilibrium concentration of CuO/Cu₂O, Mn₂O₃/Mn₃O₄ and

Co₃O₄/CoO redox pairs.

Source: Abad et al. (2012).

Table 6. Operating window for the CuO/Cu₂O and Mn₂O₃/Mn₃O₄ redox pairs.

	Fuel reactor temperature (°C)	Air reactor temperature (°C)
CuO/Cu₂O	900-950	900-950
Mn₂O₃/Mn₃O₄	850-900	800-825

Among them, Cu-based materials have been the focus of research as their oxygen release is greater and faster than that of Mn-based oxides, and their temperature window for oxygen release is higher than in the case of Mn oxides. Adánez-Rubio et al. (2014) demonstrated the feasibility of CLOU with biomass using a Cu-based oxygen carrier in a 1.5 kW$_{th}$ continuous unit. In this work, almost 100% CO_2 capture and combustion efficiencies were achieved at 935 °C.

In order to improve the thermodynamic restrictions associated with manganese, mixed oxides (Mn-Si, Mn-Mg, Mn-Fe, Mn-Cu) have been proposed

(Azimi et al. 2013; Jing et al. 2014). Adding another metal to manganese oxide enables oxidation of the material to be used at higher temperatures (Shulman et al. 2009, 2011; Pour et al. 2013; Adánez-Rubio et al. 2016; Hosseini et al. 2015; Rydén et al. 2014; Sajen et al. 2016). Hanning et al. (2016) studied the combustion of wood char in a batch fluidized with Mn-Si and Mn-Si-Ti oxygen carriers. They found the *i*G-CLC reaction to be more important than CLOU with these oxygen carriers. On the contrary, a natural mixed oxide based on Cu-Mn (Hopcalite) has shown high oxygen uncoupling capability (Adánez-Rubio et al. 2016). Also, a synthetic Cu-Mn mixed oxide material was tested by Adánez-Rubio et al. (2017a, 2018) in a 1.5 kW_{th} continuous unit using coal as fuel. With this oxygen carrier, combustion efficiencies close to 100% were reached, which qualified this oxygen carrier as a potential material for testing in experiments with biomass. Schmitz and Linderholm (2016) tested in a 10 kW_{th} unit a perovskite ($CaMn_{0.9}Mg_{0.1}O_{3-\delta}$) during about 37 h using as fuel a bio char with a very low sulfur content. They achieved high combustion efficiencies and CO_2 capture efficiencies of up to 98%. These results confirmed, for the first time, the utilization of non-copper oxygen carriers for CLOU combustion using a biomass based fuel.

1.5.3 Next challenges on biomass fueled CLC

Next challenges on biomass fueled CLC involves both operational and design solutions to improve the performance of this technology, reducing the unburnt matter at the outlet of the fuel reactor and the char reaching the air reactor. Some of the operational and design improvements proposed for solid fuel CLC are briefly discussed below.

Operational improvements:

- Temperature. An increase in the fuel reactor temperature favors the gasification rate of the char and the combustion kinetics of the gases generated during the gasification.

- Oxygen availability. For each oxygen carrier, the oxygen availability in the fuel reactor depends on the solids circulation rate. Increasing the solids circulation rate, the oxygen availability is increased. However, the increase of the solids circulation rate can reduce the residence time of solids in the reactor and counteract the desired effect.

- Oxygen carrier. The use of an oxygen carrier appropriate for their oxygen transport capacity, molecular oxygen releasing capacity, reactivity or even the selectivity should be considered to improve the CLC process (Lyngfelt and Leckner 2015; Gayán et al. 2013).

Design improvements:

- Carbon stripper. Implementation of a solid particles separator (carbon stripper) to recirculate char particles in the fuel reactor and in this way avoid the char combustion in the air reactor (Gayán et al. 2013).

- Distributors. Introduction of internals (Figure 37-1a) or distributor plates (Figure 37-1b) can improve the homogeneity of the fluidized bed increasing the contact among reactants. Also different fuel reactor designs were suggested to increase the contact of the oxygen carrier and the biomass products (Gayán et al. 2013).

- Secondary fuel reactor (Figure 37-2). Implementation of a secondary fuel reactor was pointed as a potential solution for typically high volatile matter content of the fuel reactor outlet (Gayán et al. 2013). Some technological alternatives have been already tested and results published in literature (Yan et al., 2017; Haus et al. 2018; Jiang et al. 2018).

- Recycling of the fuel reactor outlet steam. The recycling of the fuel reactor outlet stream to the fuel reactor (Figure 37-3) or even to the carbon stripper increases the contact time between biomass gasification products and the oxygen carrier particles. This would reduce the unburnt compounds and therefore would increase the combustion efficiency (Lyngfelt and Leckner 2015; Gayán et al. 2013).

- Unburnt compounds separation during the CO_2 purification and compression steps can be recycled to the fuel reactor (Figure 37-4).

- Change of the fuel feeding to the carbon stripper (Figure 37-5), which will act as a first fuel reactor, or to the entrance of the fuel reactor (Figure 37-6). Both options would increase the contact time between biomass gasification products and the oxygen carrier.
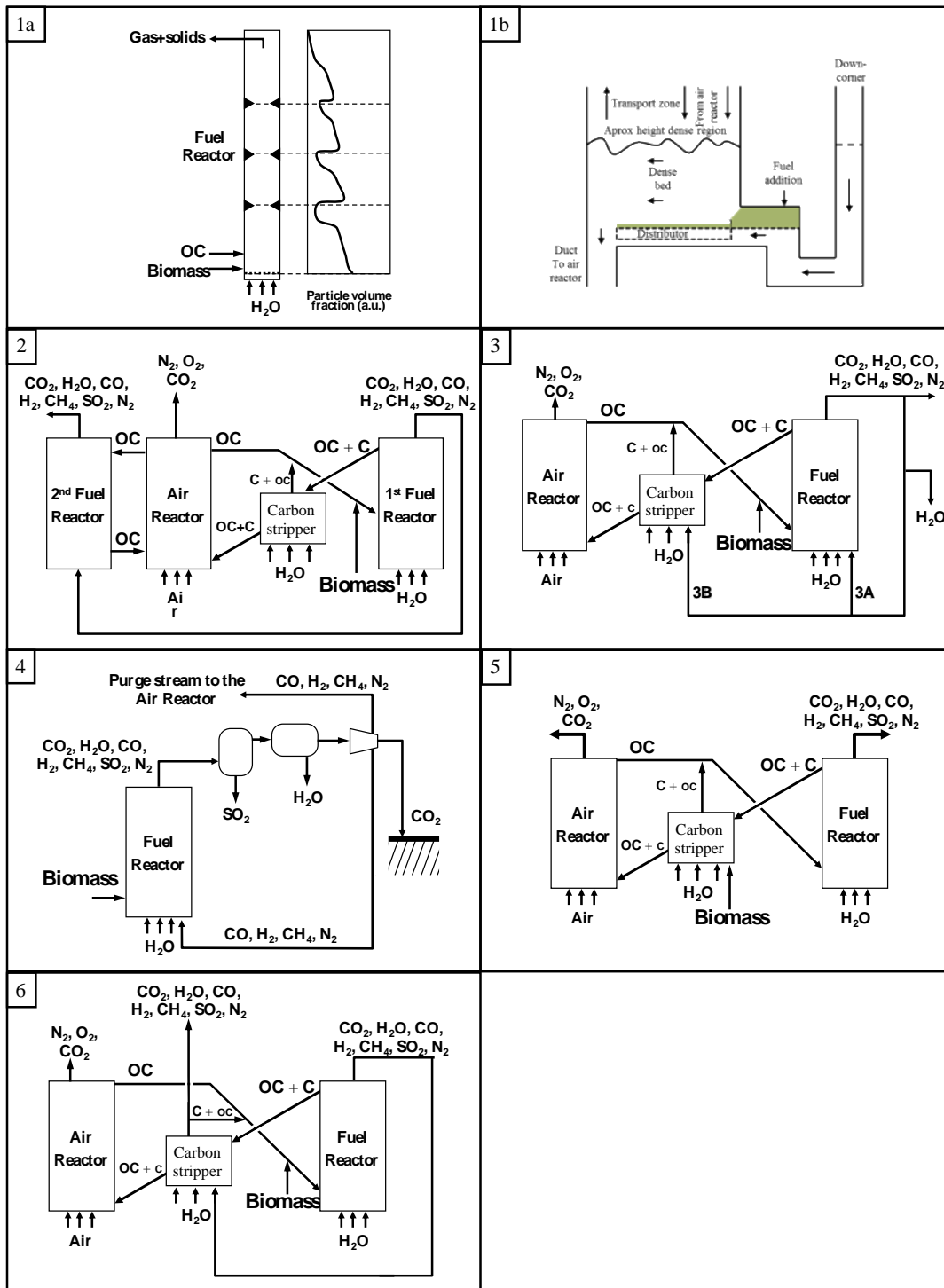
Figure 37. Main technical CLC proposed improvements.
Source: Adánez et al. (2018).

1.6 Scope of study

Biomass is considered a carbon neutral fuel since the CO_2 released in biomass combustion has previously been removed from the atmosphere during its growth. For this reason, biomass is being used for partial replacement of fossil fuels in many thermo-chemical processes. Moreover, if the CO_2 generated during biomass combustion is captured, this would lead to negative CO_2 emissions. A power plant that integrates both biomass and Carbon Capture and Storage (CCS) technologies will receive carbon credits, potentially making this process economically attractive.

The main objective of this Thesis was to evaluate the integration of solid biofuels in the Chemical Looping Combustion technology (bioCLC). The whole combustion process can then be considered as Bioenergy with CCS (BECCS) technology allowing to achieve negative CO_2 emissions while energy is produced. The Thesis was carried out at the *Instituto de Carboquímica* in Zaragoza (Spain), including a four-month stay at the Institute of Solids Process Engineering and Particle Technology in the *Technische Universität Hamburg* (TUHH) in Hamburg (Germany).

The specific objectives defined for this Thesis were:

1. To identify suitable oxygen carriers for the biomass-fueled CLC process and to validate their performance under relevant operating conditions.
2. To investigate the influence of operating conditions on the overall process performance for different types of biomass.
3. To demonstrate the technology performance at scale of 20 kW_{th}.
4. To assess the effect of biomass ash constituents on the oxygen carrier behavior (deactivation and agglomeration).
5. To evaluate the presence of different pollutants (tar and NO_x) generated during combustion in the CLC system

The investigation performed during the Thesis covered from basic research at particle level to continuous operation in 1 kW_{th} and 20 kW_{th} units to demonstrate the

process concepts. Focus was made on the analysis of the effect of the operating conditions on the performance of the bioCLC process as well as on the determination of a window of suitable operating conditions for different oxygen carriers.

Results obtained throughout this Thesis were presented in six papers. **Paper I and II** summarize the results reached with low-cost oxygen carriers based on iron and manganese oxides named as Tierga ore, MnGBHNE and MnSA. All were tested in the 1 kW_{th} CLC unit working under the so-called iG-CLC mode. The influence of operating conditions such as gasifying agent, temperature in the fuel reactor, solids inventory in the fuel reactor and solids circulation rate between reactors was assessed. Moreover, the influence of the type of biomass used as biofuel was included. Pine sawdust, olive stones and almond shells were chosen based on their wide use for energy purposes as well as large availability. **Paper III** shows the evaluation as oxygen carrier for the bioCLC process of a synthetic mixed manganese and iron-based oxygen carrier (Mn66FeTi7). This oxygen carrier shows the ability to release molecular oxygen under specific conditions, what could improve the combustion efficiency of the bioCLC process. The influence of the operating conditions on the oxygen release capability of the material and therefore on the performance of the bioCLC process was studied in the 1 kW_{th} CLC unit using pine sawdust as fuel. **Paper IV and V** continue the analysis of different types of oxygen carriers for the bioCLC process and evaluate the performance of a synthetic Cu-based CLOU oxygen carrier (Cu34Mn66) characterized by its higher and faster oxygen release capability. The effect of different operating conditions on the performance of the process was studied and the operating window for the biomass combustion was determined in the 1 kW_{th}. Another aspect to be considered in the combustion of biomass is the NO_x formation and the possible existence of tar in the gaseous product stream. **Paper VI** presents a comparison between the iG-CLC and CLOU operating modes regarding the NO_x and tar formation when different types of biomass are considered. Finally, results concerning the demonstration of the bioCLC process at higher scale in 20 kW_{th} CLC unit are shown (**Conference paper J**) (García-Labiano et al. 2018) using olive stones as biofuel and the Tierga ore as oxygen carrier.

1.7 List of papers

I. Mendiara, T., A. Pérez-Astray, M. T. Izquierdo, A. Abad, L. F. de Diego, F. García-Labiano, P. Gayán, J. Adánez. Chemical Looping Combustion of different types of biomass in a 0.5 kW$_{th}$ unit. *Fuel* 2018, 211, 868-875.

II. Pérez-Astray A, T. Mendiara, L. F. de Diego, A. Abad, F. García-Labiano, M. T. Izquierdo, J. Adánez (2019) Manganese ores as low-cost oxygen carriers for biomass chemical looping combustion in a 0.5 kW$_{th}$ unit. *Submitted to Fuel Processing Technology.*

III. Pérez-Astray A, T. Mendiara, L. F. de Diego, A. Abad, F. García-Labiano, M. T. Izquierdo, J. Adánez. (2019a) CLC of biomass as a BECCS technology using a manganese-iron mixed oxide. *Submitted to Separation and Purification Technology.*

IV. Adánez-Rubio, I., A. Pérez-Astray, T. Mendiara, M. T. Izquierdo, A. Abad, P. Gayán, L. F. de Diego, F. García-Labiano, J. Adánez. Chemical Looping Combustion of biomass: CLOU experiments with a Cu-Mn mixed oxide. *Fuel Processing Technology* 2018, 172, 179-186.

V. Adánez-Rubio, I., A. Pérez-Astray, A. Abad, P. Gayán, L. F. de Diego, J. Adánez. Chemical Looping with oxygen uncoupling: an advanced biomass combustion technology to avoid CO$_2$ emissions. *Mitigation and Adaptation Strategies for Climate Change* 2019. (In press). doi: 10.1007/s11027-019-9840-5.

VI. Pérez-Astray, A., I. Adánez-Rubio, T. Mendiara, M. T. Izquierdo, A. Abad, P. Gayán, L. F. de Diego, F. García-Labiano, J. Adánez. Comparative study of fuel-N and tar evolution in chemical looping combustion of biomass under both *i*G-CLC and CLOU modes. *Fuel* 2019, 236, 598-607.

Conference papers:

A. Mendiara, T., P. Gayán, F. García-Labiano, L. F. de Diego, A. Pérez-Astray, M. T. Izquierdo, A. Abad, J. Adánez.

Chemical looping combustion of biomass: an approach to BECCS.

13th Conference on Greenhouse Gas Control Technologies (GHGT), 14-18 November 2016, Lausanne, Suisse.

B. Mendiara, T., M. T. Izquierdo, A. Pérez-Astray, A. Abad, L. F. de Diego, F. García-Labiano, P. Gayán, J. Adánez.

Biomass with CO_2 capture using CLC: results in a 500 W_{th} unit.

4th International Conference on Chemical Looping, 26-28 September 2016, Nanjing, China.

C. Mendiara, T., P. Gayán, F. García-Labiano, L. F. de Diego, A. Pérez-Astray, M. T. Izquierdo, A. Abad, J. Adánez.

Combustión de biomasa con captura de CO_2.

7ª Jornada de Jóvenes Investigadores (Física y Química) de Aragón, 24 November 2016, Zaragoza, Spain.

D. Mendiara, T., I. Adánez-Rubio, A. Pérez-Astray, M. T. Izquierdo, A. Abad, P. Gayán, L. F. de Diego, F. García-Labiano, J. Adánez.

Chemical Looping Combustion of biomass: CLOU experiments with a Cu-Mn mixed oxide.

10th conference on Sustainable Energy and Environmental Protection (SEEP) 2017, 27-30 June 2017, Bled, Slovenia.

E. Pérez-Astray, A., T. Mendiara, M. T. Izquierdo, L. F. de Diego, F. García-Labiano.

Combustión de diferentes tipos de biomasa mediante transportadores de oxígeno.

XIV Reunión del Grupo Español del Carbón. 22-25 October 2017, Malaga, Spain.

F. Pérez-Astray, A., T. Mendiara, M.T. Izquierdo, A. Abad, L. F. de Diego, F. García-Labiano, P. Gayán, J. Adánez.

In Situ Gasification Chemical Looping Combustion of different biomass types.

10th World congress of Chemical Engineering. 1-5 October 2017, Barcelona. Spain.

G. Abad, A., R. Pérez-Vega, <u>A. Pérez-Astray</u>, T. Mendiara, L. F. de Diego, F. García-Labiano, P. Gayán, M. T. Izquierdo, J. Adánez.

Biomass Combustion with CO_2 Capture by Chemical Looping: Experimental results in a 50 kW_{th} Pilot plant.

I International Conference on CO_2 Negative Emissions. 22-24 May 2018, Goteborg, Sweeden.

H. Adánez-Rubio, I., A. Pérez-Astray, A. Abad, P. Gayán, L. F. de Diego, <u>J. Adánez.</u>

Biomass combustion by Chemical Looping with Oxygen Uncoupling process: experiments with Cu-based and Cu-Mn mixed oxide as oxygen carriers.

I International Conference on CO_2 Negative Emissions. 22-24 May 2018, Goteborg, Sweeden.

I. Adánez-Rubio, I., R. Pérez-Vega, A. Pérez-Astray, T. Mendiara, <u>J. Adánez</u>.

Coal and biomass combustion by Chemical Looping with Oxygen Uncoupling (CLOU) with a Cu and Cu-Mn materials.

5th International Conference on Chemical Looping. 24-27 September 2018, Park City, Utah, USA.

J. <u>García-Labiano</u>, F., R. Pérez-Vega, A. Pérez-Astray, T. Mendiara, L. F. de Diego, M. T. Izquierdo.

Chemical Looping Combustion of Biomass in a 50 kW_{th} unit.

5th International Conference on Chemical Looping. 24-27 September 2018, Park City, Utah, USA.

K. Abad, A., R. Pérez-Vega, <u>A. Pérez-Astray</u>, T. Mendiara, L. F. de Diego, F. García-Labiano, P. Gayán, M. T. Izquierdo, J. Adánez.

Biomass combustion with CO_2 capture by CLC: Experimental results in a 50 kW_{th} unit.

XXXVI Jornadas Nacionales de Ingeniería Química, September 2019, Zaragoza, Spain.

EXPERIMENTAL

2.1 Oxygen carriers

Different promising oxygen carriers, both ores and synthetic, were selected for operation in the CLC prototypes. The selection was based on the previous experience reached in CLC by the Combustion and Gasification Group at the *Instituto de Carboquímica* (ICB-CSIC) working with gaseous fuels and especially with coal. All the selected oxygen carriers were physically and chemically characterized and their main properties are shown in Table 7.

Reactivity analyses of the oxygen carriers were performed in a thermogravimetric analyzer (TGA) in sequential redox cycles using different gaseous fuels (H_2, CO or CH_4) for the reduction reaction and air for the oxidation reaction. The TGA was also used to determine the oxygen transport capacity of the oxygen carriers. The identification of crystalline chemical species in each material was carried out by powder X-ray diffraction (XRD) patterns acquired in a Bruker D8 Advance diffractometer equipped with a linear detector. The force needed to fracture a particle of oxygen carrier was measured in a Shimpo FGE-5X dynamometer. Then,

the crushing strength was calculated as the average value of twenty measurements of individual particles randomly chosen. A three-hole air jet attrition tester ATTRI-AS (Ma. Tec. Materials Technologies Snc.) configured according to the ASTM-D-5757 standard was used to determine the Air Jet Index (AJI) of the different samples (Cabello et al. 2016). The oxygen carrier density was determined using a Micrometrics AccuPyc II helium pycnometer. The BET surface area was measured in a Micromeritics Autopore V, whereas a Quantchrome PoreMaster 33 mercury pycnometer was used to measure the porosity of the oxygen carrier particles. Finally, a Hitachi S 3400 N scanning electronic microscopy (SEM) was used to evaluate changes in the microstructure of the oxygen carrier particles.

Table 7.Main physical and chemical properties of the selected oxygen carriers.

	Tierga	MnGBHNE	MnSA	Mn66FeTi7	Cu$_{34}$Mn$_{66}$
Composition	Fe_2O_3, SiO_2, Al_2O_3, CaO, MgO	Mn_2O_3, Fe_2O_3	Mn_2O_3, Fe_2O_3	$(Mn_xFe_{1-x})_2O_3$, $(Mn_xFe_{1-x})_3O_4$, TiO_2	$Cu_{1.5}Mn_{1.5}O_4$, Mn_3O_4
XRD active phases, Me$_x$O$_y$ (wt%)	76.5 (Fe_2O_3)	Mn_2O_3 (68.2) Fe_2O_3 (10.6)	Mn_2O_3, (65.6) Fe_2O_3 (4.4)	$(Mn_xFe_{1-x})_2O_3$ (81.0) $(Mn_xFe_{1-x})_3O_4$ (13.4) TiO_2 (5.6)	$Cu_{1.5}Mn_{1.5}O_4$ (72.0)
Crushing strength (N)	5.8	1.8	4.6	2.0	1.9
Oxygen transport capacity, R_{OC} (wt%)	2.5	5.1	4.7	9.4	4.0
Porosity (%)	26.3	38.7	12.3	9.5	12.1
Skeletal density of particles (kg/m³)	4216	2800	3510	4630	4100
Specific surface area, BET (m²/g)	1.4	12.3	0.6		< 0.5

2.1.1 Iron ore

An iron ore obtained from a hematite mine in Tierga (Zaragoza, Spain) was selected to be used as oxygen carrier. This oxygen carrier, named Tierga ore, showed the highest reactivity in the combustion of coal as well as stability and durability, in a comparative study among different Fe-based oxygen carriers, highlighting its low cost (Mendiara et al. 2014a). The ore was crushed and sieved to a particle size of 100-300 µm and subsequently calcined in air atmosphere at 950 ℃ during 12 hours to increase its mechanical strength. The ferrite-magnetite (Fe_2O_3-Fe_3O_4) redox pair was considered for the reaction of this material. Reactions (R7) to (R10) show the main iron oxide redox reactions.

$$3Fe_2O_3 + H_2 \Longleftrightarrow 2Fe_3O_4 + H_2O \tag{R7}$$

$$3Fe_2O_3 + CO \Longleftrightarrow 2Fe_3O_4 + CO_2 \tag{R8}$$

$$12Fe_2O_3 + CH_4 \Longleftrightarrow 8Fe_3O_4 + CO_2 + 2H_2O \tag{R9}$$

$$4\,Fe_3O_4 + 0.5\,O_2 \Longleftrightarrow 3Fe_2O_3 \tag{R10}$$
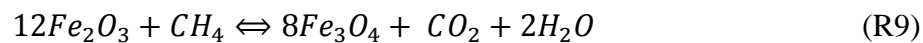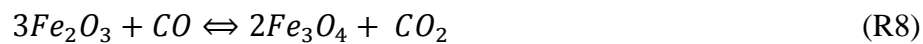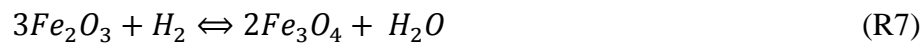
2.1.2 Manganese ores

Tests performed in a batch fluidized bed reactor with different manganese ores showed good fluid dynamics properties as well as an estimated long lifetime (Mei et al. 2015; Mei et al. 2016). Also, a previous study carried out at the *Instituto de Carboquímica* using a manganese based oxygen carrier with coal as fuel showed comparable results to those obtained with a highly reactive iron-based oxygen carrier (Tierga ore) working in a CLC continuous unit under similar operating conditions (Abad et al. 2018). Based on these previous studies, two manganese-based ores have been used in the present work as oxygen carriers. One came from Gabon (hereafter named MnGBHNE) and another one from South Africa (hereafter named MnSA), both supplied by *Hidro Nitro Española S.A*. After received, both materials were crushed and sieved to 100–300 µm. Then, a thermal treatment was carried out in air at 800 °C during 2 h to ensure the complete oxidation of the particles and also to increase the crushing strength of the oxygen carriers. For more information about the oxygen carriers see Mei et al. (2015). The redox pairs considered for the reaction of

these materials, both MnGBHNE and MnSA, were Mn_3O_4-MnO and Fe_2O_3-Fe_3O_4, reactions (R11) to (R14) and (R7) to (R10), respectively.

$$Mn_3O_4 + H_2 \Longleftrightarrow 3\ MnO + H_2O \tag{R11}$$

$$Mn_3O_4 + CO \Longleftrightarrow 3\ MnO + CO_2 \tag{R12}$$

$$4\ Mn_3O_4 + CH_4 \Longleftrightarrow 3\ MnO + CO_2 + 2\ H_2O \tag{R13}$$

$$3\ MnO + 0.5\ O_2 \Longleftrightarrow Mn_3O_4 \tag{R14}$$
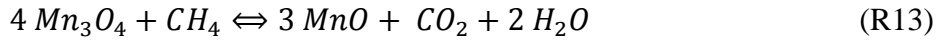
2.1.3 Mn66FeTi7

Manganese and iron mixed oxides have received attention because of their relatively low cost and high reactivity. Previous results working with these materials showed high reactivity with H_2, CO and CH_4 thanks to their capacity to release a small amount of molecular oxygen during the reduction phase under specific operating conditions (Pérez-Vega et al. 2020). This ability has been named Chemical Looping assisted by Oxygen Uncoupling (CLaOU). Reactions (R15) to (R18) describe the reduction reactions of the iron-manganese mixed oxides in CLC. The bixbyite phase, $(Mn_xFe_{1-x})_2O_3$, decomposes into a spinel phase, $(Mn_xFe_{1-x})_3O_4$, and molecular oxygen (R15) at specific operating conditions. Furthermore, the spinel phase oxidizes the biomass gasification products with lattice oxygen, (R16) to (R18). The oxygen release capacity of these oxygen carriers is affected by the kinetics and the thermodynamics (Pérez-Vega et al. 2019).

$$3(Mn_xFe_{1-x})_2O_3 \leftrightarrow 2(Mn_xFe_{1-x})_3O_4 + 0.5O_2 \tag{R15}$$

$$(Mn_xFe_{1-x})_3O_4 + H_2 \rightarrow 3(Mn_xFe_{1-x})O + H_2O \tag{R16}$$

$$(Mn_xFe_{1-x})_3O_4 + CO \rightarrow 3(Mn_xFe_{1-x})O + CO_2 \tag{R17}$$

$$4(Mn_xFe_{1-x})_3O_4 + CH_4 \rightarrow 12(Mn_xFe_{1-x})O + CO_2 + 2H_2O \tag{R18}$$
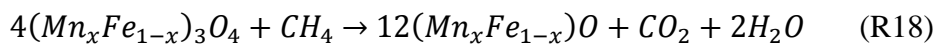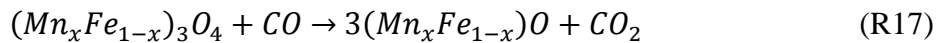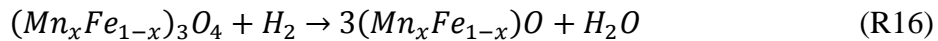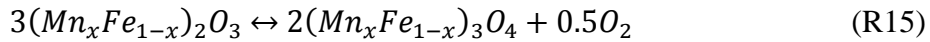
For this Thesis, a synthetic oxygen carrier, named Mn66FeTi7, based on manganese and iron oxides doped with TiO_2 was selected. The oxygen carrier was prepared at the ICB-CSIC in Zaragoza (Spain) using 60 wt% of Mn_3O_4 (Elkem),

33 wt% of Fe_2O_3 (Chemlab) and 7 wt% of TiO_2 (Panreac), achieving a stoichiometric formula of the particles of $(Mn_{0.66}Fe_{0.34})_2O_3(TiO_2)_{0.15}$. The powder mixture was converted into a solution with suitable viscosity by heating at 80 ℃. The particles were manufactured by spray granulation in a Glatt spouted bed system, model Procell5. After that, particles were thermally processed during 2 h at 1050 ℃ and then, sieved to the particle size distribution 100-300 µm. For more information about the oxygen carrier preparation see Pérez-Vega et al. (2020).

2.1.4 Cu34Mn66

In this Thesis, a Cu-Mn mixed oxide was selected as oxygen carrier for the CLOU process. The oxygen carrier was prepared at the ICB-CSIC using 34 wt% of CuO (Chemlab) and 66 wt% of Mn_3O_4 (Micromax®, Elkem). The powder mixture was converted into a solution with an adequate viscosity for the spray granulator and the particles were manufactured by spray granulation in a Glatt spouted bed system, model Procell5. Finally, the particles were calcined for 2 h at 1125 ℃ and then sieved to a particle size of 100-300 µm. The active phase in the mixed oxide was $Cu_{1.5}Mn_{1.5}O_4$. The excess of Mn_3O_4 in the particles acted as an inert (Adánez-Rubio et al. 2017b). Reaction (R19) describes the release of gaseous oxygen by the oxygen carrier.

$$2Cu_{1.5}Mn_{1.5}O_4 \Leftrightarrow 3CuMnO_2 + O_2 \qquad\qquad (R19)$$
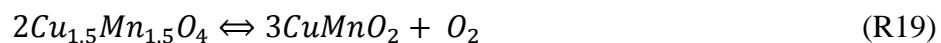
Figure 38 shows the O_2 equilibrium concentrations as a function of the temperature for the redox systems CuO/Cu_2O and Mn_2O_3/Mn_3O_4 together the O_2 concentrations measured in tests carried out in a batch fluidized bed reactor with the prepared oxygen carrier.
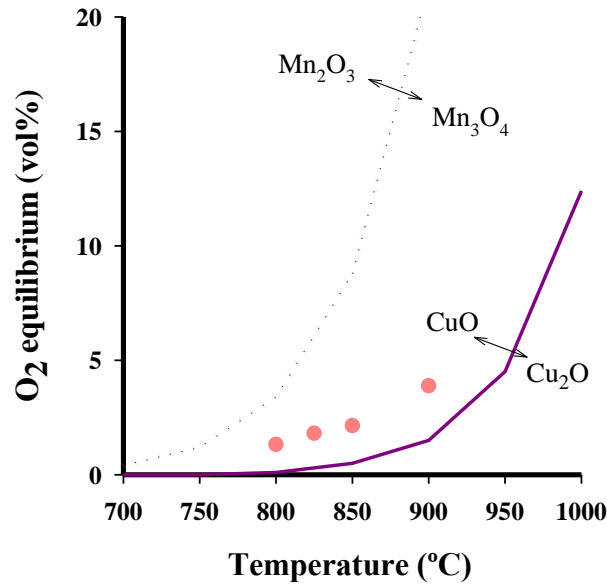
Figure 38. O₂ concentrations at equilibrium as a function of the temperature for the systems: (—)CuO/Cu₂O,(·⋯) Mn₂O₃/Mn₃O₄ and experimental points obtained for (●) Cu₁.₅Mn₁.₅O₄/CuMnO₂.

2.2 Solid biofuels

Three Spanish biomass wastes were used as fuels for the CLC experiments: Pine sawdust (*Pinus sylvestris*), olive stones (*Olea europaea*) and almond shells (*Prunus dulcis*). Pine sawdust was chosen as the reference material because of its large use and wide distribution. Olive stones and almond shells are two agricultural residues used for energy production with high annual production in Spain.

Raw materials were ground and sieved to adequate their size particle distribution between 0.5 - 2 mm. Table 8 shows the proximate and ultimate analyses of the three types of biomass including the low heating value and the value of the oxygen demand of the solid fuel (Ω_{sf}), which represents the amount of oxygen needed to burn the biomass.

Biomass ashes were prepared by controlled combustion in a muffle at 900 ºC. An inductively coupled plasma optical emission spectrometry equipment and a fusibility equipment were used for the ash characterization. Table 9 presents the content on sodium (Na), potassium (K) and calcium (Ca), the three major alkali and alkaline earth metal (AAEM) components, of the three types of biomass. It is worth noting the high potassium content of the almond shells, as well as the high calcium content of the pine sawdust and olive stones. Melting temperatures for biomass ashes in reducing atmosphere were about 1000 ºC for the pine sawdust and about 780 ºC for the olive stones and the almond shells.

Table 8. Proximate and ultimate analyses of the various biomass types used.

	Pine sawdust	Olive stones	Almond shells
Proximate analysis (wt%)			
Moisture	4.2	9.4	2.3
Ash	0.4	0.8	1.1
Volatile matter	81.0	72.5	76.6
Fixed carbon	14.4	17.3	20.0
Ultimate analysis (wt%)			
C	51.3	46.5	50.2
H	6.0	4.8	5.7
N	0.3	0.2	0.2
S	0.0	0.0	0.0
O	37.8	38.3	40.5
LHV (kJ/kg)	19158	16807	18071
Ω_{sf} (kg oxygen/kg fuel)	1.5	1.2	1.4

Table 9. Na, K y Ca content of the different types of biomass used (mg/kg$_{dry\ fuel}$).

	Pine sawdust	Olive stones	Almond shells
Na	4	17	12
K	152	1053	2157
Ca	1194	1334	749

2.3 Experimental installations

2.3.1 Thermogravimetric analyzer

The reactivity of the different oxygen carriers, before and after their utilization in the CLC pilot plants, was determined in a TGA CI Electronics. For that, the sample weight variation versus time during reaction with gases under well-defined conditions and during successive redox cycles was measured. About 50 mg of oxygen carrier sample were loaded in a platinum wire mesh basket. The basket design reduced the mass transfer resistance and improved the contact of the oxygen carrier sample with the gaseous reactants. The sample was heated to the operating temperature in air atmosphere with an electric furnace. After stabilization, the sample was successively exposed to reducing and oxidizing reactive atmospheres. For reduction, 25 L/h (STP) of CH_4, CO_2 were used. For oxidation, 25 L/h (STP) of air were used. In order to avoid the mixing of combustible gas and air, nitrogen was introduced for 2 min between the oxidizing and the reducing periods. Figure 39 shows the TGA scheme and a picture of the experimental set-up. For more information about the TGA characteristics and utilization procedure see Adánez et al. (2004).
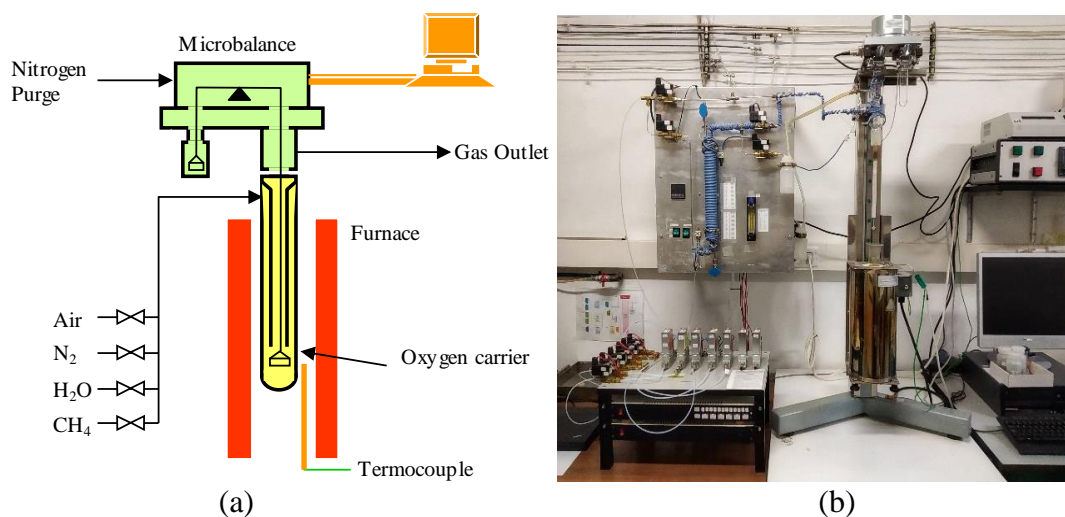
Figure 39. (a) Scheme of the TGA CI Electronics and (b) picture of the experimental set-up.

Data evaluation

Reactivity data were obtained from the oxygen carrier weight evolution measurements in TGA during successive redox cycles as a function of the time. The oxygen carrier conversions during the reduction and oxidation reactions were calculated by Equation (1) and Equation (2), respectively, where m is the mass of the sample at any time, m_{Ox} is the mass of the fully oxidized oxygen carrier sample and m_{Red} is the mass of the reduced oxygen carrier sample.

$$X_{Red} = \frac{m_{Ox} - m}{m_{Ox} - m_{Red}}$$
(1)

$$X_{Ox} = 1 - \frac{m_{Ox} - m}{m_{Ox} - m_{Red}}$$
(2)

The oxygen transport capacity, R_{OC}, which evaluates the total amount of oxygen that the material can exchange in each redox cycle, was obtained by Equation (3).

$$R_{OC} = \frac{m_{Ox} - m_{Red}}{m_{Ox}}$$
(3)

2.3.2 Batch fluidized bed reactor

A batch fluidized bed reactor was used for the analysis of agglomeration as well as changes in reactivity of the oxygen carrier samples under successive redox cycles due to the isolated effect of the presence of alkali and alkaline earth metals (AAEM) in the biomass. This experimental work was carried out in the Institute of Solids Process Engineering and Particle Technology at Hamburg (Germany). The experimental set-up consisted of a fluidized bed reactor, a gas feeding system, a solids feeding system, a calibrating system, a sampler and gas analyzers. Figure 40 shows the scheme of the batch fluidized bed reactor and the solids feeding system and the online sampling design. The oxygen carrier sample, used as bed material, was introduced in a 53 mm internal diameter fluidized bed reactor. An electric furnace heated the sample to the operating temperature while air was introduced

through a distributor plate at the bottom part of the reactor. Different mass flow controllers allowed the use of different fluidizing agents. Four thermocouples and five pressure taps allowed the measurement of the temperatures and pressures at the different parts of the reactor. A valve system allowed the AAEM salt introduction into the fluidized bed as well as the online bed sampling. A ceramic filter placed inside the bed material allowed the gas measuring preventing the fine particle. A nondispersive infrared analyzer (NDIR) was used for the CO, CH_4 and CO_2 measurements while a thermal conductivity analyzer was used for the H_2 measurement using a four-channel measurement system TAD GmbH type GME.84-K4. A paramagnetic cell (ABB Magnos 3K) was used for the O_2 measurement.

Experimental procedure

About 250 g of oxygen carrier sample were loaded as bed material in the batch fluidized bed reactor and heated to the desired temperature. An air flow was used for fluidization during the heating up of the bed material. After reaching the operating temperature of 950 ºC, as no biomass was added, the oxygen carrier was partly reduced with 15 vol% of H_2 (N_2 balance) during a specific time to reach the desired oxygen carrier reduction degree (50 and 75%). The reduction degrees were chosen to adapt oxygen carrier characteristics to the normal operation behaviour of a CLC plant. After the reduction of the oxygen carrier, pure nitrogen was fed for fluidization and salt batches of approximately 0.1–0.2 g each, with a separation among them of 5 minutes, were added to bed. The fluidization conditions were maintained at 0.1 m/s, analysing the fluidization properties by using differential pressure measurements. For each salt tested (NaCl, KCl or $CaCl_2$) and for each oxygen carrier, a total of 30 batches of salt were added. Finally, the bed was oxidized in air to start a cycle. In each experiment, oxygen carrier samples, both reduced and oxidized, were extracted after salt additions for characterization.
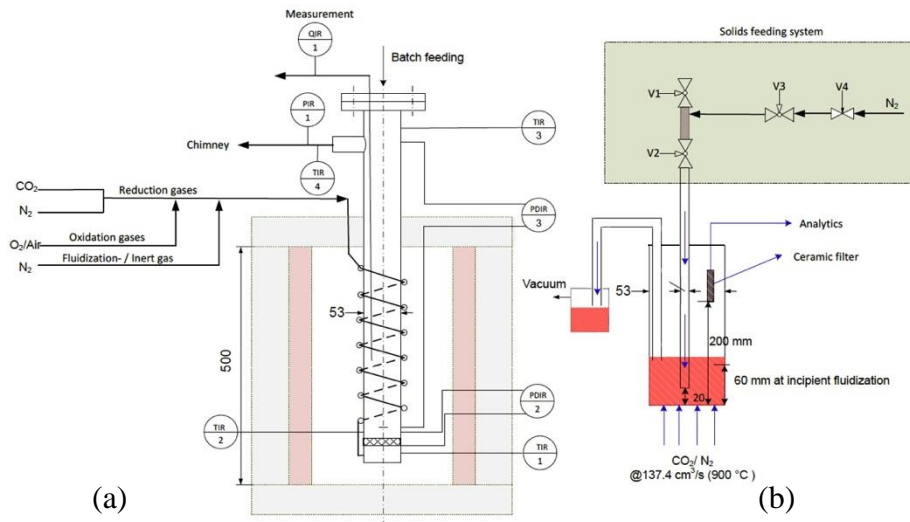
Figure 40. Scheme of (a) the batch fluidized bed reactor and (b) the solids feeding system and the online sampling design.

2.3.3 Continuous pilot plants

2.3.3.1   1 kW$_{th}$ prototype (ICB-CSIC-s1)

A scheme of the ICB-CSIC-s1 experimental unit is shown in Figure 41. It consists of the fuel (1) and the air (3) reactors, both bubbling fluidized bed type. The biomass is fed into the fuel reactor (50 mm ID) at the bottom of the bubbling fluidized bed through a series of two screw feeders (9). It is fed just above the fuel reactor distributor plate in order to maximize the time that the fuel and volatile matter are in contact with the bed material. CO_2 or steam can be used as gasifying agents. Steam is produced by heating up in an evaporator the corresponding water flow supplied by a peristaltic pump. The fuel reactor is connected to the air reactor by a U-shaped bubbling fluidized bed reactor (30 mm ID) placed as loop seal (2) to prevent the mixture of the gases between them. There is no carbon stripper between the fuel and the air reactors. The loop seal is fluidized with nitrogen and, during operation, the percentage of the loop seal fluidizing agent reaching the fuel reactor can be calculated. The reduced oxygen carrier is transferred to the air reactor (80 mm ID). Once re-oxidized, the oxygen carrier leaves the air reactor through a riser (4) helped by a secondary air flow. The oxygen carrier is then collected by a cyclone (5) and

sent to a deposit (7) that keeps both reactor atmospheres separated. A diverting solid valve (6) is used to measure the solids circulation rate between reactors during the experiment. The flow of oxygen carrier fed to the fuel reactor from this deposit is controlled by a solids valve (8). The temperature in both reactors is controlled with electrical furnaces (11). Figure 42 shows a picture of the 1 kW_{th} ICB-CSIC-s1 CLC unit.
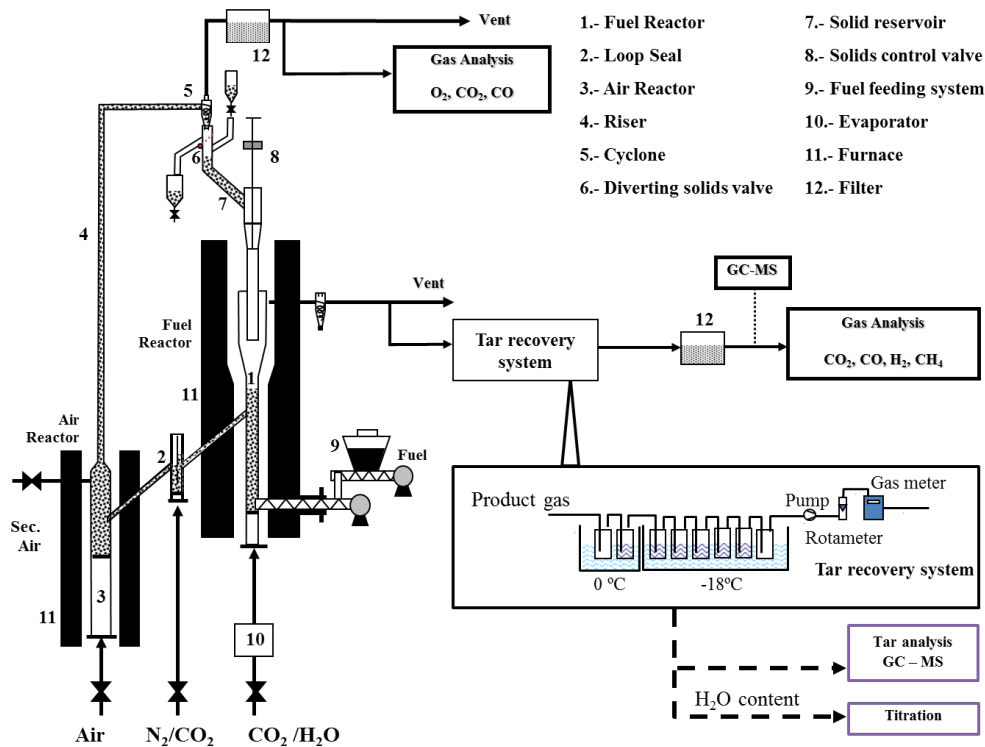
Figure 41. Scheme of the 1 kW (ICB-CSIC-s1) experimental set-up.

Different electronic mass flow controllers allow the use of various fluidizing gases. The fluidization velocities in each reactor were kept constant, about 0.1 m/s for the fuel reactor and 0.5 m/s, for the air reactor during all the experiments. The reactor temperatures, independently controlled thanks to the electric furnaces, and the pressure drops in the reactors were recorded during all the experiments. The gas outlet composition of both reactors was measured and recorded. A non-dispersive infrared analyzer (Siemens Ultramat 23) was used for the CO_2, CO and CH_4 online analysis and a thermal conductivity detector (Siemens Calomat 6) for the H_2. The O_2 concentration was measured with a paramagnetic analyzer (Siemens Ultramat 23 and Oxymat 6). A non-dispersive infrared analyzer Siemens Ultramat 23 was used for

76

the NO_x determination. Gas samples were taken in order to analyze gaseous C_2-C_4 hydrocarbons at the fuel reactor outlet with an HP 5890 gas chromatograph (GC) coupled with a Thermal Conductivity Detector (TCD). More detailed information about the design and operation of the unit can be found elsewhere (Cuadrat et al. 2011).

Figure 42. Picture of the 1 kW (ICB-CSIC-s1) experimental set-up.

Tar can appear as a biomass gasification byproduct reducing the combustion performance of the process and causing operational problems. Tar compounds at the fuel reactor outlet were collected in impingers filled with isopropanol according to the standard tar protocol (Simell et al. 2000). The quantitative determination of the concentrations of the different tar compounds in the samples was done by a gas chromatograph (Agilent 7890A) fitted with a capillary column (HP-5) and a Flame Ionization Detector (FID). Furthermore, the gas chromatograph was coupled with a mass spectrometer (Agilent 5975C). Naphthalene and phenanthrene were selected for the external calibration procedure. The quantitative values were obtained assuming a similar response factor to naphthalene for tar compounds of 1–2 rings and similar to phenanthrene for 3-rings compounds.

2.3.3.2   20 kW$_{th}$ prototype (ICB-CSIC-s50)

A scheme of the ICB-CSIC-s50 experimental unit is shown in Figure 43. This facility was designed to operate in both *i*G-CLC and CLOU modes. The nominal thermal power was 20 kW$_{th}$ for *i*G-CLC mode and 50 kW$_{th}$ for CLOU mode. In this work, the unit was operated in *i*G-CLC mode by using Tierga ore as oxygen carrier.

The CLC unit mainly consists of two circulating fluidized bed reactors, the fuel and the air reactors, interconnected by different loop seals, and one carbon stripper. The fuel reactor was designed with two parts: bottom bed (0.10 m inner diameter, 1.2 m height) and upper part (0.08 m inner diameter, 2.8 m tall). The gas velocities in both sections of the fuel reactor are fitted to operate in the turbulent regime. The solids circulation rate can be independently controlled by handling the fluidization conditions in each reactor and loop-seals. Furthermore, two different solids diverting valves allow the measurement of the solids circulation rate. The global solids circulation rate evaluates the amount of oxygen carrier leaving the air reactor while the fuel reactor solids circulation rate includes the fraction recycled to the fuel reactor in the double loop seal. A bubbling bed reactor acting as a carbon stripper, installed between the fuel and the air reactors, allows the char and the oxygen carrier particles separation and, in this way, the char particles are recycled to the fuel reactor while the oxygen carrier particles reach the air reactor to be reoxidized. The air reactor, 4.8 m height was also designed with two parts: the bottom bed (0.30 m inner diameter) and the upper part (0.10 m inner diameter). Figure 44 shows a picture of the ICB-CSIC-s50 CLC unit.

The solid fuel is fed into the fuel reactor at the bottom part with two screw feeders. CO_2 or H_2O can be used as gasifying agents. When H_2O is used, an evaporator is installed for the steam production. Different mass flow controllers allow fluidizing gases to be fed in reactors, loop-seals and carbon stripper. The reactor temperatures were independently controlled thanks to the electric furnaces. These temperatures and the pressure drop at the different parts of the unit were recorded during all the experiments. The gas outlet composition of each reactor was measured online and recorded. The same gas analyzers described for the 1 kW$_{th}$ unit

were used. More detailed information about the design and operation of the unit can be found elsewhere (Abad et al. 2015a).
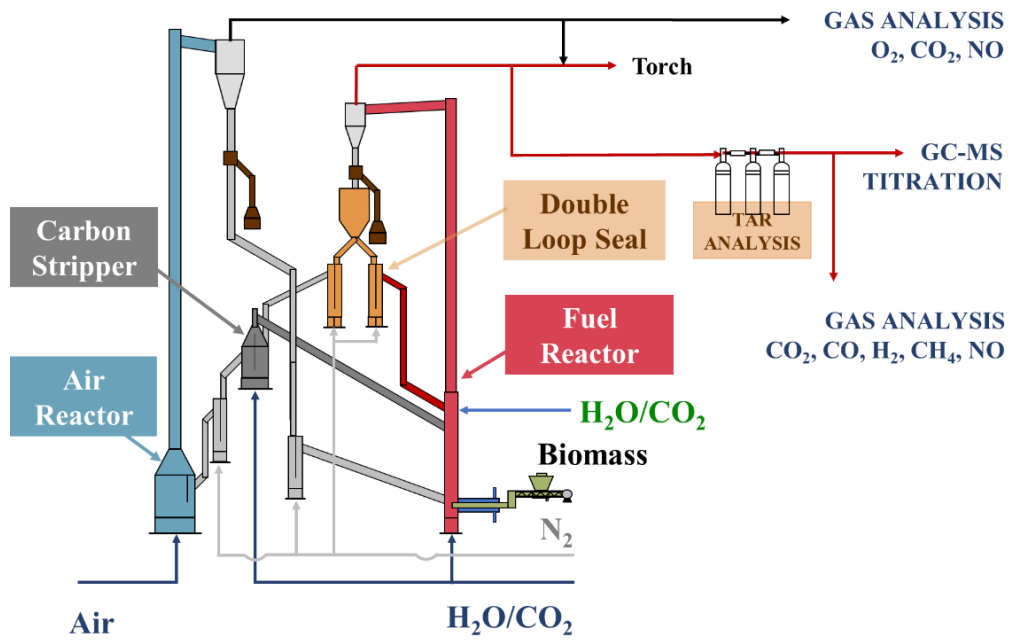
Figure 43. Scheme of the 20 kW$_{th}$ experimental set-up.

Figure 44. Picture of the 20 kW$_{th}$ experimental set-up.

2.3.3.3 Data evaluation

To analyze the performance of the CLC process in the continuous prototypes using different types of biomass and oxygen carriers the main parameters evaluated are the CO_2 capture efficiency, the combustion efficiency, and the oxygen demand. All of them as a function of the oxygen carrier to fuel molar ratio.

The oxygen carrier to fuel molar ratio (ϕ) compares the oxygen that is transported by the oxygen carrier with the oxygen needed for the complete combustion of the fed fuel. A value of $\phi = 1$ corresponds to the stoichiometric flow of oxygen carrier needed to fully convert the fuel to CO_2 and H_2O. ϕ was calculated by Equation (4)

$$\phi = \frac{\dot{m}_{OC} \cdot R_{OC}}{\dot{m}_{sf} \cdot \Omega_{sf}} \tag{4}$$

Where $\dot{m}_{OC}$ is the solids circulation flow rate in the completely oxidized state, R_{OC} is the oxygen transport capacity, $\dot{m}_{sf}$ the mass-based flow of fuel fed in to the reactor, and Ω_{sf} the stoichiometric kg of oxygen to convert 1 kg of fuel to CO_2 and H_2O.

The CO_2 capture efficiency (η_{CC}) is defined as the fraction of the carbon introduced in the fuel reactor which was converted to gas in this reactor. The converted carbon was calculated from the concentrations of CH_4, CO and CO_2 measured at the exit of the fuel reactor and the CO_2 concentration measured at the exit of the air reactor. Considering the low amounts of C_2-C_4 detected in the tests, the amounts of hydrocarbons heavier than CH_4 were considered negligible for the calculations. The CO_2 capture efficiency was calculated by Equation (5).

$$\eta_{CC} = \frac{\left[F_{CO_2,FR} + F_{CO,FR} + F_{CH_4,FR}\right]_{out}}{\left[F_{CO_2,FR} + F_{CO,FR} + F_{CH_4,FR} + F_{CO_2,AR}\right]_{out}} \tag{5}$$

The CO_2 capture efficiency calculated according Equation (5) depends on the fraction of char that is gasified in the fuel reactor. The char conversion (X_{char}), defined

as the fraction of carbon in the char which is gasified and released to the fuel-reactor exhaust gas stream, was calculated by Equation (6):

$$X_{char} = \frac{[F_{CO_2,FR}+F_{CO,FR}+F_{CH_4,FR}-F_{C,vol}]_{out}}{[F_{CO_2,FR}+F_{CO,FR}+F_{CH_4,FR}+F_{CO_2,AR}-F_{C,vol}]_{out}} \qquad (6)$$

The combustion efficiency in the fuel reactor ($\eta_{comb,FR}$) evaluates the gas conversion in the fuel reactor. It was defined in Equation (7), as the fraction of oxygen demanded by the fuel that is supplied by the oxygen carrier in the fuel reactor, where M_{O_2} represents the molecular weight of O_2 (kg/mol).

$$\eta_{comb,FR} = 1 - \frac{[4F_{CH_4,FR}+F_{CO,FR}+F_{H_2,FR}]_{out}}{\frac{1}{M_{O_2}}2\Omega_{sf}\dot{m}_{sf}-2F_{CO_2,outAR}} \qquad (7)$$

The total oxygen demand (Ω_T), Equation (8), was calculated as the quotient between the oxygen required in order to reach complete combustion of the unconverted gases (CH$_4$, CO and H$_2$) and the oxygen needed for the complete combustion of the biomass fed.

$$\Omega_T = \frac{4 \cdot F_{CH_4,FR}+F_{CO_{FR}}+F_{H_2,FR}}{\frac{1}{M_O} \cdot \dot{m}_{sf} \cdot \Omega_{sf}} \qquad (8)$$

Similarly, the tar oxygen demand (Ω_{tar}) was calculated, Equation (9), as the quotient between the oxygen required in order to reach complete combustion of the tar and the oxygen needed for the complete combustion of the biomass fed.

$$\Omega_{tar} = \frac{(j+k/4) \cdot F_{C_jH_k,FR}}{\frac{1}{M_O} \cdot \dot{m}_{sf} \cdot \Omega_{sf}} \qquad (9)$$

Other parameters that can help to analyze the performance of the CLC process in the continuous prototypes are:

The specific solids inventory in the fuel reactor (m^*_{FR}) allows the comparison of the CLC performance among different oxygen carriers and the used power input. It was calculated by Equation (10), where P_{th} is the power input of the unit, $m_{OC,FR}$ is the mass of oxygen carrier in the fuel reactor, ΔP is the pressure drop in the fuel reactor and S is the reactor surface area.

$$m^*_{FR} = \frac{1}{P_{th}} m_{OC\,FR} = \frac{1}{P_{th}} \left[\left(\frac{\Delta P \cdot S}{g} \right)_{bottom} + \left(\frac{\Delta P \cdot S}{g} \right)_{riser} \right] \tag{10}$$

The carbon mass balance allows an accurate analysis of the CLC performance. It was calculated by Equations (11) and (12), where $F_{C,sf}$ is the carbon flow in the solid fuel, $F_{C,char}$ is the carbon flow as derived char and $F_{C,vol}$ was calculated from the biomass analyses as the difference between the total carbon in the biomass and the fixed carbon.

$$F_{C,sf} = F_{C,char} + F_{C,vol} = \left(F_{C,FR\,out} - F_{CO_2\,in} \right) + F_{C,elu} + F_{C,AR_{out}} \tag{11}$$

$$F_{C,FR\,out} = (F_{CO_2} + F_{CO} + F_{CH_4})_{FR,out} \tag{12}$$

The solid fuel conversion (X_{sf}) is a measurement of the amount of solid fuel, biomass in this case, converted in the CLC unit, including both the fuel and air reactors. According to the carbon mass balance showed in Equation (13), this parameter was calculated as:

$$X_{sf} = \frac{(F_{C,FR,out} - F_{CO2,in}) + F_{C,AR,out}}{F_{C,sf}} \tag{13}$$

RESULTS AND DISCUSSION

3.1 Performance of the bioCLC in a 1 kW$_{th}$ continuous unit

The objective of this first section (**Papers I, II, III, IV, V and VI**) was to evaluate the performance of different types of oxygen carriers in the bioCLC process. As it was mentioned in the previous chapter, the evaluation process consisted in the combustion of different types of biomass in a 1 kW$_{th}$ continuous combustion unit and the subsequent analysis of the results obtained following several parameters already defined, mainly the CO$_2$ capture efficiency (η_{CC}) and the total oxygen demand (Ω_T).

Both natural (minerals/ores) and synthetic materials were considered. First of all, low-cost oxygen carriers for the *i*G-CLC process were tested (**Papers I, II and III**). The potential of iron and manganese ores as oxygen carriers for the bioCLC process was evaluated and compared.

3.1.1 Combustion under *i*G-CLC: low-cost oxygen carriers

3.1.1.1 Fe-based oxygen carrier

The first tested low-cost oxygen carrier was an iron-based ore denoted as Tierga ore (**Paper I**). Previous experiments with this oxygen carrier had already been performed using pine sawdust as fuel (Mendiara et al. 2013a). The oxygen carrier showed good performance and adequate lifetime. The experimental campaign accomplished in the present work aimed at complementing these results previously published, in which higher specific solids inventories were used (> 1000 kg/MW$_{th}$). Theoretical studies dedicated to CLC scaling-up (Abad et al. 2015b; Cuadrat et al. 2012) established that specific solids inventories larger than 1000 kg/MW$_{th}$ were not recommended since they would only slightly improve the combustion efficiency while the pressure drop in the fuel reactor would excessively increase. A compromise should be reached between enlarging reactors to allow higher solids inventories and the increase of the combustion efficiency. Thus, in the present study, the specific solids inventories considered were in all cases below 1000 kg/MW$_{th}$.

Table 10 summarizes the experiments carried out with Tierga iron ore. Three types of forest and agricultural residues (pine sawdust, olive stones and almond shells) were tested at a fuel reactor temperature between 900-980 ºC. A total of 78 h of hot fluidization corresponding to 40 h of biomass combustion were registered.

Figure 45 presents the temporal evolution of the different gas concentrations as well as the temperatures in both fuel and air reactors for a typical experiment during 50 min of steady state operation. Data correspond to pine sawdust combustion experiment at 950 ºC, although similar profiles were obtained for the rest of the types of biomass. CO_2 appeared as the major compound, with about 70% in all cases, followed by the unburnt compounds: H_2 (10-15 vol%), CO (10-12 vol%) and CH_4 (6-8 vol%). The amount of other light hydrocarbons, C2-C4, was negligible.

Table 10. Operating conditions with the Tierga ore in the 1 kW$_{th}$ experimental unit.

Test	FA (-)	T$_{FR}$ (ºC)	T$_{AR}$ (ºC)	ϕ (-)	$\dot{m}_{OC}$ (kg/h)	$\dot{m}_{sf}$ (kg/h)	P$_{th}$ (W$_{th}$)	m^*_{FR} (kg/MW$_{th}$)	$norm.\dot{m}_{OC}$ ((kg/s)/MW$_{th}$)
					Pine sawdust				
T1	H$_2$O	**895**	950	1.1	10.1	0.152	809	475	3.5
T2	H$_2$O	**910**	950	1.3	9.2	0.113	601	750	4.2
T3	H$_2$O	**950**	950	1.1	6.7	0.098	522	785	3.6
T4	H$_2$O	**985**	950	1.1	6.7	0.098	522	780	3.6
					Olive stones				
T5	H$_2$O	**905**	950	1.0	8.8	0.164	766	600	3.2
T6	H$_2$O	**955**	950	1.0	7.6	0.141	658	600	3.2
T7	H$_2$O	**980**	950	1.0	7.6	0.141	658	590	3.2
					Almond shells				
T8	H$_2$O	**905**	950	1.2	13.0	0.190	954	370	3.8
T9	H$_2$O	**955**	950	1.2	7.0	0.102	512	550	3.7
T10	H$_2$O	**985**	950	1.2	5.9	0.088	442	890	3.7
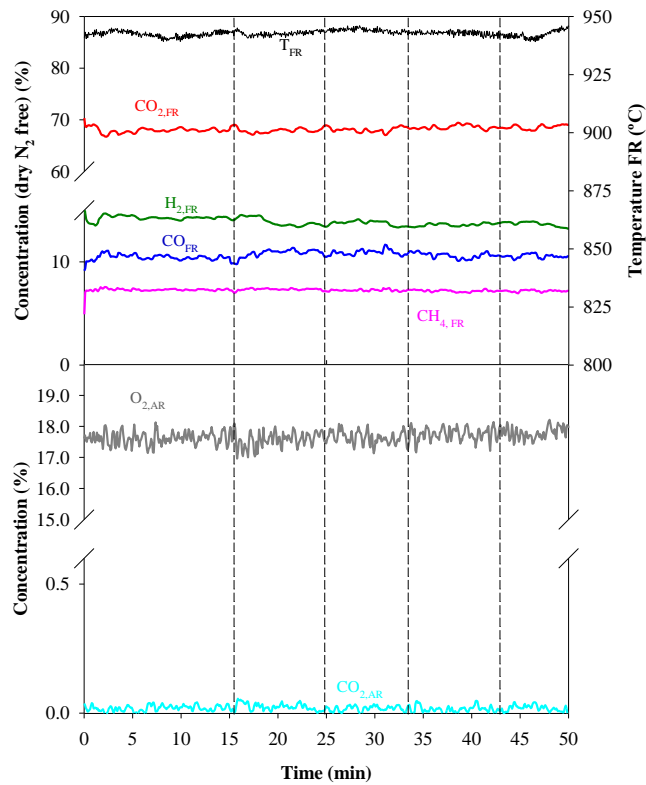
Figure 45. Example of temporal evolution of gas concentrations and temperatures at steady state operation in a normal test in the 1 kW$_{th}$ CLC unit (pine sawdust at 950 ºC, norm.$\dot{m}_{OC}$≈ 3.6 kg/(s·MW$_{th}$).

Figure 46 presents the obtained values for the CO$_2$ capture efficiency and the char conversion for the three types of biomass. Both parameters increased with the fuel reactor temperature, reaching values of about 100% from 950 ºC in the case of

pine sawdust and almond shells and from 985 ºC for the olive stones. This could be due to their higher volatile content of pine sawdust and almond shells compared to olive stones, see Table 8. It is interesting to highlight that 100% CO_2 capture was achieved with the three types of biomass at 980 ºC even in the absence of a carbon stripper between the fuel and the air reactors in this experimental unit.
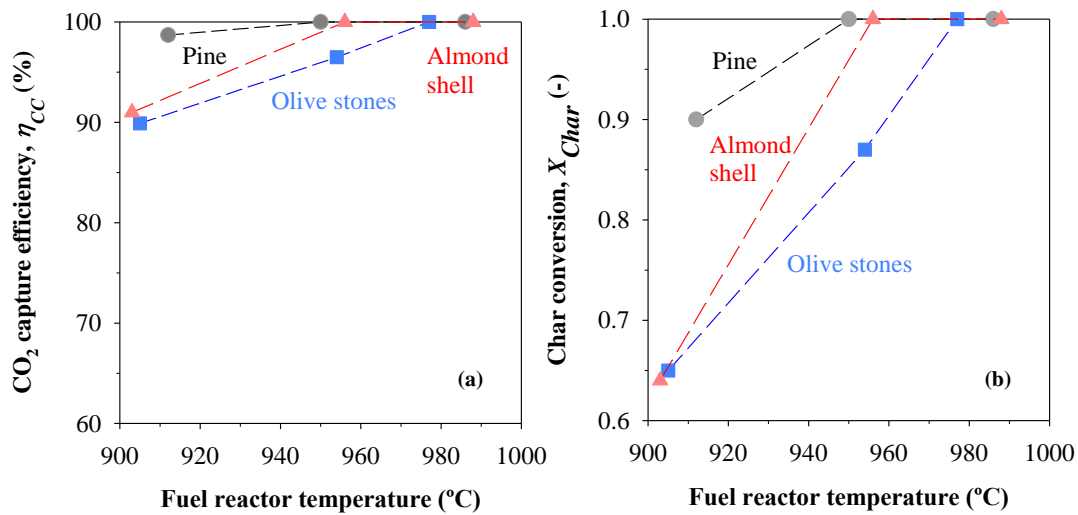
Figure 46. Effect of the fuel reactor temperature on the (a) CO_2 capture efficiency and (b) char conversion for the three types of biomass norm.$\dot{m}_{OC} \approx 3.7 \ kg/(s \cdot MW_{th})$.

Previous experiments with Tierga ore and different types of coal, such as anthracite, bituminous and lignite, reached lower CO_2 capture efficiencies at temperatures in the range 900-930ºC (Mendiara et al. 2014a). The volatile matter of those coals represented about 7.5% for the anthracite, 33.0% for the bituminous coal and 28.6% for the lignite. Therefore, it can be concluded that the higher volatile content of biomass and the reactivity of biomass char compared to coal makes the use of a carbon stripper not as decisive as in the combustion of coal.

Figure 47 presents the total oxygen demand obtained in the combustion of the three types of biomass with the Tierga ore at different fuel reactor temperatures. No clear trend was observed with the fuel reactor temperature increase. In general, the total oxygen demand for these types of biomass was similar and about 20-30%.
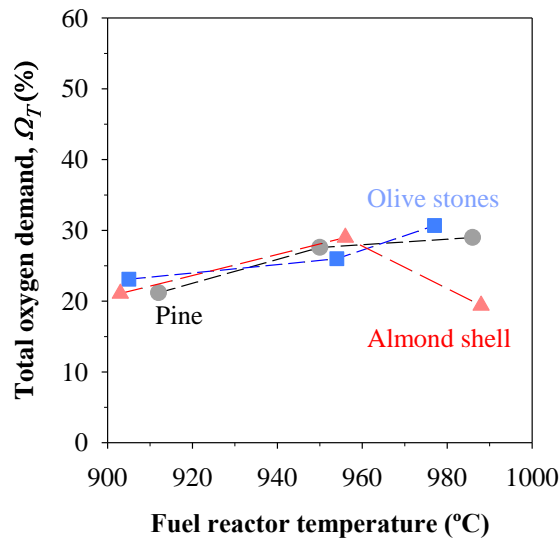
Figure 47. Effect of the fuel reactor temperature on the total oxygen demand for the different types of biomass and $norm.\dot{m}_{OC} \approx 3.7 \ kg/(s \cdot MW_{th})$.

It is realistic to assume that most of the oxygen demand is generated by the volatiles that escape the fuel reactor bed without interacting with the oxygen carrier particles. This aspect was more deeply analysed by the estimation of the conversion of the biomass volatiles in this bed. Only CH_4 at the fuel reactor outlet was considered as coming from the volatile matter since both the CO and H_2 in this outlet stream could also come from char gasification.

In order to estimate the volatile conversion, an empirical model by Neves et al. (2011) for the prediction of biomass pyrolysis products was used. The model does not consider the physical-chemical processes occurring within the biomass particles. It is based on mass balances to the overall pyrolysis processes and experimentally-based closing parameters obtained after the compilation of a significant amount of experimental data for different types of biomass and pyrolysis conditions. It should be pointed out that only mass balances to carbon, hydrogen and oxygen were considered. Those corresponding to nitrogen, sulphur and chlorine were not included in the original model.

The input data required by the model were the CHO composition of the parent fuel (dry-ash-free) and the temperature of pyrolysis in ºC. As output, the model calculates the dry-ash-free composition of resulting tar, C_xH_y, CH_4, CO, CO_2, H_2O

and H_2. An extra assumption was herein made in order to adapt this composition to the reacting conditions existing in the CLC process. It must be remarked that steam is used as gasifying agent in the fuel reactor in order to convert the char produced during biomass pyrolysis to CO and H_2. The presence of steam would facilitate the conversion of most of the tar and C_xH_y formed during biomass pyrolysis to CH_4 and carbon. Considering this, the amounts of the different species resulting from biomass pyrolysis predicted by the model were recalculated.

As it was mentioned, CH_4 was used as volatile reference compound to calculate volatile conversion. Thus, the flow of methane at the fuel reactor outlet was compared to that predicted by the model at the corresponding fuel reactor temperature. Table 11 shows the estimated volatile conversion based on CH_4 at 900 ºC for the three types of biomass tested. An average volatile conversion about 70% was estimated for the three types of biomass. These values are in line with the oxygen demand about 20-30% showed in Figure 47.

Table 11. Volatile conversion referred to methane in the experiments with Tierga ore at about 900 ºC in the fuel reactor.

	Pine sawdust	Olive stones	Almond shells
Fuel reactor	910	905	905
Air reactor	950	950	950
CH_4 conversion (%)	73.5	65.1	71.0

Other studies found in literature also used Tierga ore as oxygen carrier in the combustion of biomass. Linderholm and Schmitz (2016) performed experiments using wood char as fuel in a 100 kW_{th} CLC unit in a temperature interval (880-960 ºC) close to that in the present study and specific solids inventories between 400-600 kg/MW_{th}. High CO_2 capture efficiencies were also attained, although the 100 kW_{th} unit is equipped with a carbon stripper. Besides, values of the total oxygen demand were reported between 7.4-8.5 %. These values were lower than those obtained in the present work, which can be attributed to two reasons. First the used fuel was wood char, with a lower volatile content (16.7 %) compared to pine sawdust. Second, the fuel reactor in the 100 kW_{th} unit is a circulating fluidized bed where a

better contact between volatiles and oxygen carrier particles is expected and therefore lower total oxygen demands.

3.1.1.2 Mn-based oxygen carriers

One of the options to improve the volatile conversion, and this way, to reduce the high values of total oxygen demand found in the experiments with Tierga ore is the use of more reactive low-cost oxygen carriers. This possibility was investigated using different manganese ores (**Paper II**), which had been identified in previous studies of the research group as potential alternatives to Tierga ore considering their high reactivity and their estimated lifetime (Mei et al. 2015; Mei et al. 2016; Abad et al. 2018). Thus, two manganese-based ores were used (MnGBHNE and MnSA) in the combustion of the three different types of biomass.

Table 12 summarizes the experiments carried out with MnGBHNE and MnSA with pine sawdust, olive stones and almond shells under similar conditions to those previously used with Tierga ore. The experimental campaign involved more than 160 h of hot fluidization with more than 63 h of biomass combustion. Neither agglomeration, nor fluidization problems were detected with any of the oxygen carriers and the three types of biomass used during all the experimental campaign.

The first series of experiments (G1-G17) in Table 12 evaluated the performance of MnGBHNE oxygen carrier in a range of specific solids inventories of 520-775 kg/MW$_{th}$. Tests G1 to G7 corresponded to the evaluation of the effect of the fuel reactor temperature. Tests G8-G11 analyzed the influence of the gasifying agent. Finally, the influence of the variation of the solids circulation rate normalized per MW$_{th}$, ($norm. \dot{m}_{OC}$) was addressed (G12-G17). The second series of experiments used MnSA as oxygen carrier and pine as fuel at different fuel reactor temperatures (S1-S4). In the discussion of the results obtained with manganese ores, some tests in Table 10 identified as T1-T6 were considered for comparison.

Evaluation of MnGBHNE: Influence of the fuel reactor temperature and the gasifying agent

Figure 48 presents the effect of the fuel reactor temperature (G1 to G7) on both the CO_2 capture efficiency (η_{CC}) and the total oxygen demand (Ω_T) using the different types of biomass (pine sawdust, olive stones and almond shells). These experiments were done using steam as fluidizing agent and values of normalized solids circulation rates ($norm.\dot{m}_{OC}$) close to 3 kg/(s·MW$_{th}$). Also previous experimental results obtained with the Tierga ore are presented (open symbols) to facilitate the comparison between both oxygen carriers

Table 12. Operating conditions with the manganese ores in the 1 kW$_{th}$ experimental unit.

Test	FA (-)	T_{FR} (ºC)	T_{AR} (ºC)	ϕ (-)	$\dot{m}_{OC}$ (kg/h)	$\dot{m}_{sf}$ (kg/h)	P_{th} (W$_{th}$)	m^*_{FR} (kg/MW$_{th}$)	$norm.\dot{m}_{OC}$ ((kg/s)/MW$_{th}$)
					Pine sawdust				
G1	H_2O	**935**	950	2.0	7.2	0.120	639	605	3.1
G2	H_2O	**900**	950	2.0	7.2	0.120	639	625	3.1
G3	H_2O	**855**	950	2.0	7.2	0.120	639	590	3.1
G4	H_2O	**890**	950	1.8	7.2	0.135	718	555	2.8
					Olive stones				
G5	H_2O	**900**	950	1.9	6.2	0.132	610	700	2.8
					Almond shells				
G6	H_2O	**905**	950	1.9	6.5	0.124	617	675	2.9
G7	H_2O	**940**	950	1.5	5.0	0.124	617	650	2.3
					Pine sawdust				
G8	**CO_2**	910	950	2.9	9.8	0.115	612	775	4.5
G9	**CO_2**	915	950	2.7	9.8	0.123	655	715	4.2
G10	**CO_2**	900	950	2.9	9.7	0.115	612	665	4.4
G11	**CO_2**	950	950	3.3	12.4	0.128	681	520	5.0
G12	H_2O	935	950	1.0	3.8	0.128	681	700	**1.6**
G13	H_2O	920	950	3.5	12.0	0.120	639	685	**5.4**
G14	H_2O	925	950	3.5	12.0	0.117	623	675	**5.4**
G15	H_2O	950	950	1.0	3.8	0.117	623	650	**1.6**
G16	H_2O	950	950	3.5	12.0	0.128	681	670	**5.4**
G17	H_2O	965	950	0.7	2.8	0.117	623	530	**1.2**
S1	CO_2	910	950	2.5	9.2	0.116	617	**770**	4.4
S2	CO_2	930	950	2.7	9.6	0.116	617	**730**	4.0
S3	CO_2	900	950	1.9	7.2	0.120	639	**970**	3.1
S4	CO_2	890	950	2.2	8.4	0.120	639	**970**	3.7
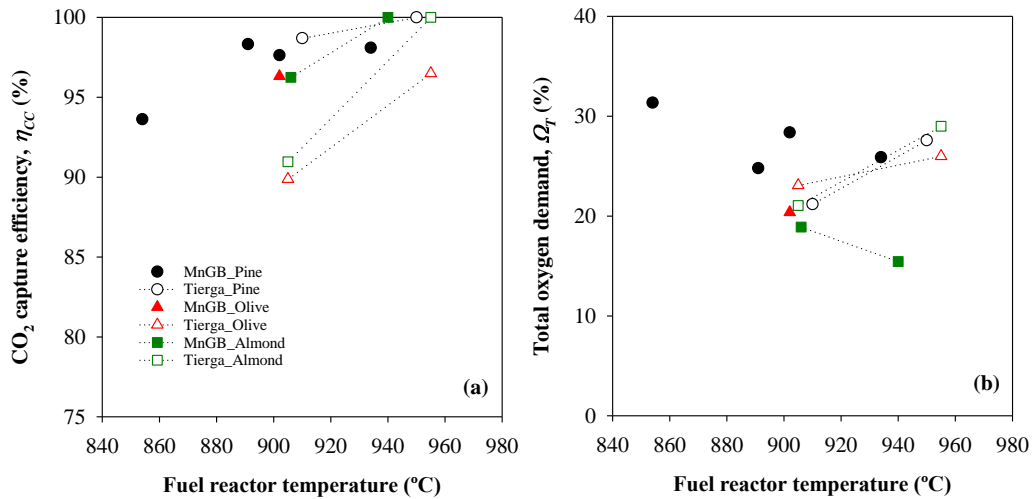
Figure 48. Effect of the fuel reactor temperature on (a) the CO₂ capture efficiency and (b) the total oxygen demand with the three types of biomass norm.$\dot{m}_{OC} \approx$ 3 kg/(s·MW$_{th}$).

Following the trend previously shown in Figure 46 with Tierga ore, the CO_2 capture efficiencies obtained with the MnGBHNE oxygen carrier increased with the increase of the fuel reactor temperature reaching values higher than 90% regardless the biomass used. It should be here again reminded that these results were obtained in the absence of a carbon stripper. Nevertheless, differences can be observed in Figure 48 (a) among oxygen carriers and types of biomass. While similar values of CO_2 capture efficiency were observed for pine, olive stones and almond shells using the MnGBHNE in the temperature range between 855 and 935 ºC (> 95%), in the experiments with the Tierga ore, lower CO_2 capture efficiencies were reached in the experiments with olive stones and almond shells compared to pine. This different behaviour would indicate that the conversion of biomass char would be more favoured using the MnGBHNE as oxygen carrier, as it has been previously reported using coal as fuel (Abad et al. 2018). Figure 48 (b) shows the values obtained for the total oxygen demand with the different types of biomass. The MnGBHNE results showed a clear decrease with the increase of the fuel reactor temperature. Nevertheless, the oxygen demand values reached were in line to those previously obtained for Tierga ore working under similar conditions (**Paper I**). Higher total oxygen demand values were determined for the experiments with pine compared to those obtained with olive stones and almond shells, which may be attributed to the different composition of the volatiles/gasification products depending on the biomass

considered. In order to further investigate the differences between the two oxygen carriers, Figure 49 shows the contribution to the total oxygen demand of the different unburnt compounds measured at the fuel reactor exit (H_2, CO and CH_4) for the experiments performed with pine and Tierga ore and MnGBHNE under similar operating conditions.
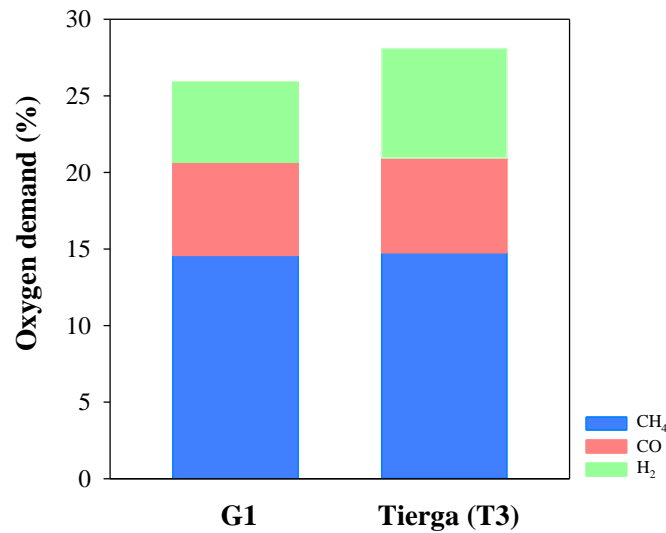
Figure 49. Comparison of partial oxygen demand for H_2, CO and CH_4 at similar conditions using Tierga ore and MnGBHNE as oxygen carriers in experiments with pine sawdust, norm.$\dot{m}_{OC} \approx 3.4 \ kg/(s \cdot MW_{th})$.

As it can be seen in Figure 49, the partial oxygen demands for CO and CH_4 were similar at comparable specific solids circulation rates for MnGBHNE and Tierga ores in experiments using H_2O as gasifying agent and pine sawdust as biomass. However, a reduced contribution to the total oxygen demand of the H_2 partial demand is observed in the experiments with MnGBHNE in comparison to Tierga.

The influence of the gasifying agent used in the fuel reactor had been previously addressed with Tierga ore (Mendiara et al. 2013a) and no significant differences were found in the performance of the process when CO_2 replaced steam as the gasifying agent. Similar conclusions were obtained with MnGBNHNE, as it is shown in Figure 50. CO_2 capture efficiencies near to 100% were obtained in Figure 50 (a) in all the experiments with CO_2, working at the temperatures higher than 900 ºC in the fuel reactor. The total oxygen demand values obtained with H_2O

and CO_2 as gasifying agents, in Figure 50 (b), follow the same decreasing trend with the fuel reactor temperature increase, reaching a value of 17% at 950ºC. Therefore, it is possible to conclude that it is possible to use dry recirculated CO_2 as feed in the fuel reactor, which is an important advantage since the energy required to produce steam is avoided.
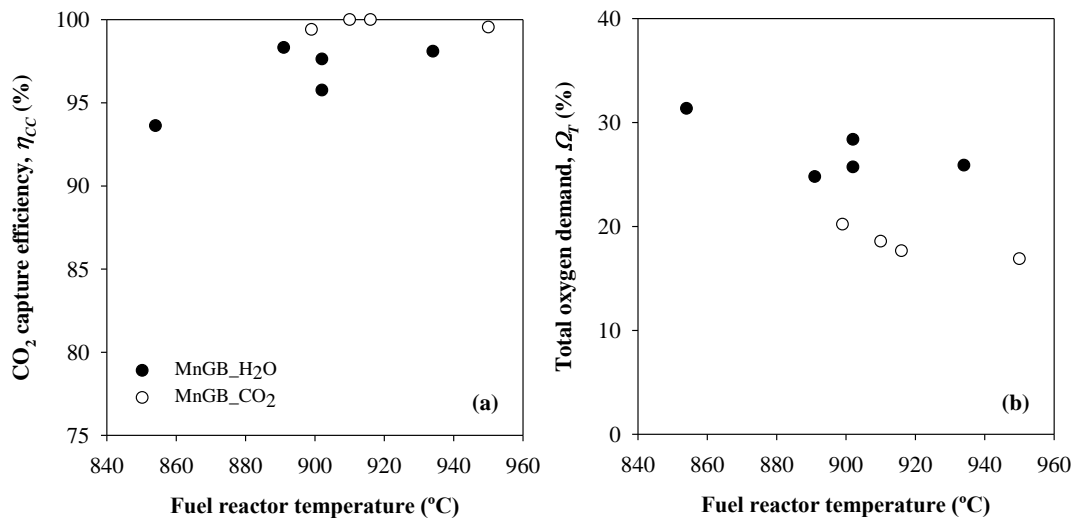
Figure 50. Effect of the gasifying agent at different fuel reactor temperatures on (a) the CO_2 capture efficiency and (b) the total oxygen demand for experiments with MnGBHNE.

Evaluation of MnGBHNE: Influence of the normalized solids circulation rate ($norm.\dot{m}_{OC}$)

The normalized solids circulation rate ($norm.\dot{m}_{OC}$) is defined as the solids circulation rate normalized per MW_{th}. This parameter is related with the amount of oxygen available in the fuel reactor for the combustion, i.e. the oxygen carrier to fuel ratio (ϕ), and can influence the total oxygen demand. Figure 51 shows the CO_2 capture efficiency and the total oxygen demand at various normalized solids circulation rates burning pine sawdust and using H_2O as gasifying agent at temperatures of about 940 ºC in the fuel reactor. Although the CO_2 capture efficiency was not clearly affected by the specific solids circulation rate (> 98% in all cases) the total oxygen demand decreased when the normalized solids circulation rate

increased, reaching a value about 20% at 5.4 kg/(s·MW$_{th}$). A higher solids circulation rate implies higher oxygen supply in the fuel reactor, increasing the combustion of volatiles and gasification products and, therefore, decreasing the total oxygen demand values.
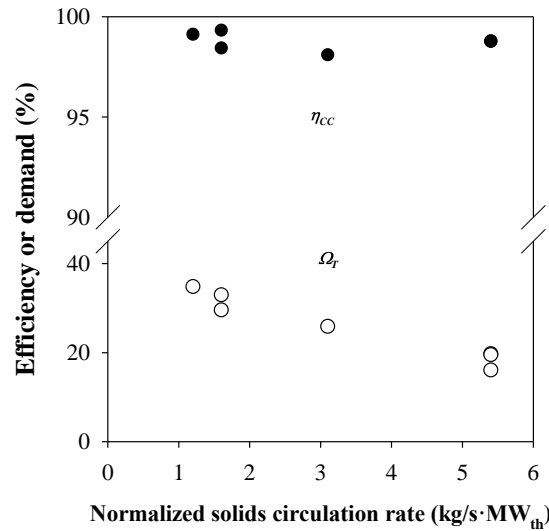
Figure 51. Effect of the normalized solids circulation rate on the CO$_2$ capture efficiency and the total oxygen demand with the MnGBHNE and pine sawdust, T$_{FR}$≈ 940 ºC.

The comparison of the results obtained with the MnGBHNE ore and the Tierga ore under similar conditions, showed that both oxygen carriers performed similarly in CLC of biomass and there was no clear advantage of one carrier over the other. For this reason it was evaluated another pre-selected manganese mineral, i.e. MnSA, which had been previously found by the authors as especially reactive to CO (Mei et al. 2015). Moreover, it presented adequate fluidization properties and lifetime.

Evaluation of MnSA

The comparison between MnGBHNE and MnSA was made with the in experiments carried out at different fuel reactor temperatures maintaining almost constant the rest of the operating conditions (tests G8-G11 and S1-S4). Figure 52 presents the CO$_2$ capture efficiencies and the total oxygen demands obtained with both oxygen carriers under similar conditions.

94
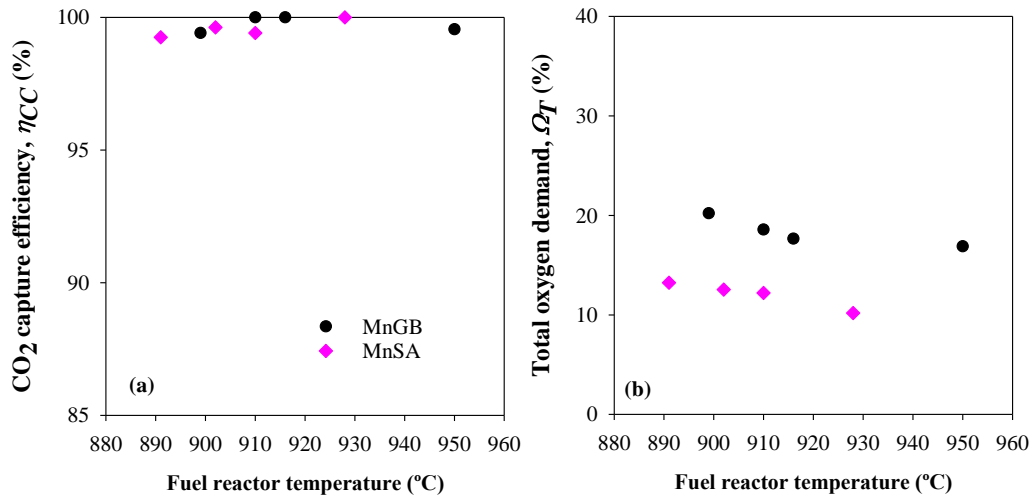
Figure 52. Effect of the fuel reactor temperature on (a) the CO₂ capture efficiency and (b) the total oxygen demand with the MnGBHNE and the MnSA with pine sawdust, norm. $\dot{m}_{OC} \approx 4\ kg/(s \cdot MW_{th})$.

Regarding the CO_2 capture efficiency values showed in Figure 52 (a), no differences were found between oxygen carriers. Despite the different fuel reactor temperatures, CO_2 capture efficiencies higher than 99% were reached with both oxygen carriers in a CLC unit without a carbon stripper. In Figure 52 (b) the total oxygen demand decreased with the fuel reactor temperature increase for both materials. In the comparison between MnGBHNE and MnSA it was observed that total oxygen demands obtained with MnSA were clearly lower than those corresponding to MnGBHNE, reaching a value as low as 10.2% at 930 °C. Moreover, to obtain oxygen demand values about 10% working with Tierga ore, it was necessary to increase the solids inventory to about 1400 kg/MW$_{th}$ and decrease the normalized solids circulation rate (Mendiara et al. 2013a). Therefore, it can be concluded that the MnSA had a better performance than the other two minerals and it can be considered a better alternative for the bioCLC process. The analysis of the partial contributions to the total oxygen demand made in Figure 53 with the two manganese ores and for two fuel reactor temperatures revealed that the major contribution to the oxygen demand came from unburned methane. However, the contribution of all unburned compounds is clearly diminished in the case of MnSA compared to that found for MnGBHNE since MnSA seems to be more reactive to the combustion of these gases than MnGBHNE. It should be highlighted that complete H_2 combustion at a fuel reactor temperature as low as 910 °C was reached with the MnSA.
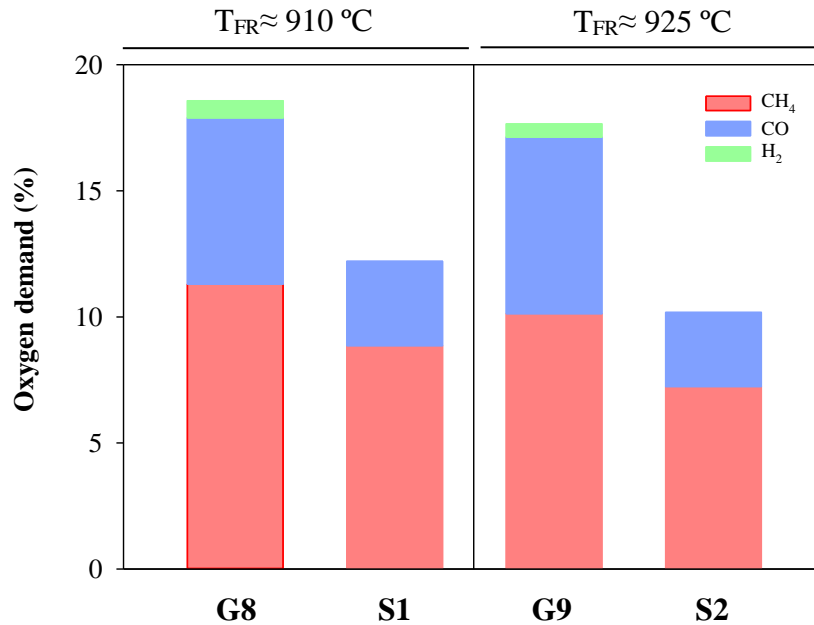
Figure 53. Comparison of partial oxygen demand for H_2, CO and CH_4 using MnGBHNE and MnSA as oxygen carriers in experiments with pine at fuel reactor temperatures between 910 and 925 ºC and norm. $\dot{m}_{OC} \approx 4$ (kg/s)/MW$_{th}$.

The results obtained with MnSA are quite remarkable when they are compared to other results reported in literature with different manganese ores. Recently, Schmitz and Linderholm (2018) reported the results obtained with a sintered manganese ore as oxygen carrier burning different types of biomass: Swedish and German wood char and black pellets. They performed experiments in a 10 kW$_{th}$ and in a 100 kW$_{th}$ continuous CLC units. The fuel reactor in the 10 kW$_{th}$ unit was a bubbling fluidized bed. In this unit and using black pellets as fuel they reported combustion efficiencies between 65 and 70% working at a fuel reactor temperature of 970 ºC and high specific solids inventories (> 1200 kg/MW$_{th}$), which would correspond to oxygen demands about 30%, higher than those reported in the present work. The same authors reported results using the same sintered manganese ore and black pellets in a 100 kW$_{th}$ unit where the fuel reactor was a circulating fluidized bed. In this case, the fuel reactor temperature varied between 910 and 981 ºC and the specific solids inventories were lower (300-600 kg/MW$_{th}$). The reached combustion efficiencies oscillated between 81 and 90%, similar to those reached in the present work with MnSA, although in the present work, results were obtained in a bubbling fluidized bed fuel reactor, where volatile combustion may not be as favored as in a circulating fluidized bed. Higher oxygen demand values than those reported here for

MnSA were obtained in experiments with braunite as oxygen carrier and white/black pellets in a 50 kW$_{th}$ unit operating at 900 ºC. (Pikkarainen and Hiltunen 2017).

3.1.1.3 Recycling of the fuel reactor outlet stream

Results obtained in the present work and those reported under similar conditions in literature pointed to one of the main cornerstones in the development of the bioCLC technology: the high values obtained for the total oxygen demand associated to the high volatile content of biomass when compared to other fuels such as coal (Mendiara et al. 2018a). The existence of an elevated amount of unburned products at the fuel reactor outlet makes necessary the incorporation of a polishing step to complete the combustion. This oxygen polishing implies an energy penalization for the CLC process and therefore it should be either minimized or even avoided (Adánez et al. 2018). Several strategies have been proposed in literature to avoid this oxygen polishing step (Gayán et al. 2013), most of them commented in section 1.5.3. One of them is the use of highly reactive oxygen carriers. A higher reactivity of the oxygen carrier would facilitate the combustion of H_2, CO and CH_4 in the fuel reactor and would decrease the total oxygen demand. This strategy was already considered in the present work with the testing of MnSA, searching for an improvement of the results obtained with MnGBHNE or Tierga ore.

Among the technical solutions commented in section 1.5.3 to reduce the total oxygen demand values, the fuel reactor outlet recycling is considered. In the present work, the effect of the recirculation to the fuel reactor of the fuel reactor outlet stream has been evaluated assuming a simulated recycled stream. The methodology used for this purpose was to simulate a recycled stream and to analyze the behavior of the different unburned compounds (i.e. H_2, CO and CH_4), see **Paper II**. For that, tests identified in Table 12 as G8 and S1 were selected and individual flows of each unburned compound corresponding to gas concentrations from 0-10% in the inlet stream were introduced while the total flow at the fuel reactor inlet was kept constant at 130 L/h (STP). Then, the composition of the new gas outlet stream leaving the fuel reactor was analyzed once the steady state was again reached. Knowing the amount of gas introduced and the gas concentrations before and after the gas introduction,

the degree of conversion (χ) in the fuel reactor were estimated for each of the introduced gases in Table 13. Hydrogen was completely converted regardless the molar flow introduced to the fuel reactor. In the case of CO and CH_4, about 80% and 70% conversion, respectively, were reached for the different molar flows of each compound that were tested.

Table 13. Conversion χ (%) for each recycled unburned compound gas in the fuel reactor at 900 ºC

	MnGBHNE	MnSA
H₂	100	100
CO	81	78
CH₄	67	70

After the experimental tests, the behavior of a CLC unit was simulated with different gas recirculation (*R*), see Figure 54.
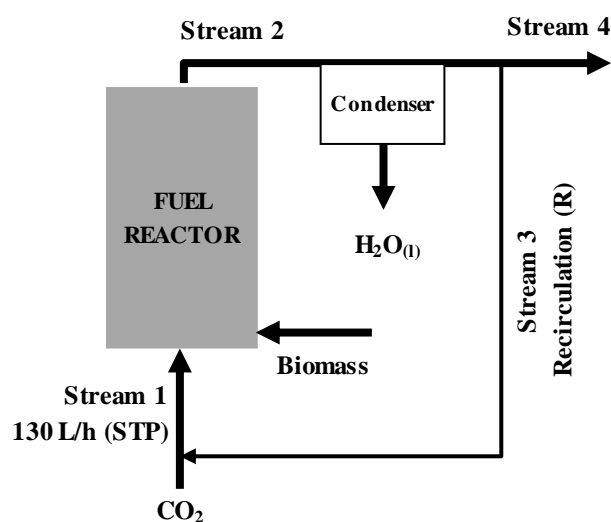
Figure 54. Fuel reactor outlet recycling scheme.

Dry recycling (stream 3) was assumed in the calculations. The recirculation (R) is defined as the percentage of the outlet stream (stream 2) being recycled to the fuel reactor (stream 3). The iterative process started considering the composition of stream 3 which is the same than that in stream 2 when recirculation is R = 0 %. Then, a value of R is assumed and the molar flows of each component calculated. The value

of χ in Table 13 for each gaseous compound was considered in order to recalculate the composition in the new stream 2. These values were compared to those calculated in the previous iteration. If the molar flows are similar, then the iterative process is stopped and the total oxygen demand at the fuel reactor outlet calculated based on these molar flows. If they are not similar, the process is repeated.
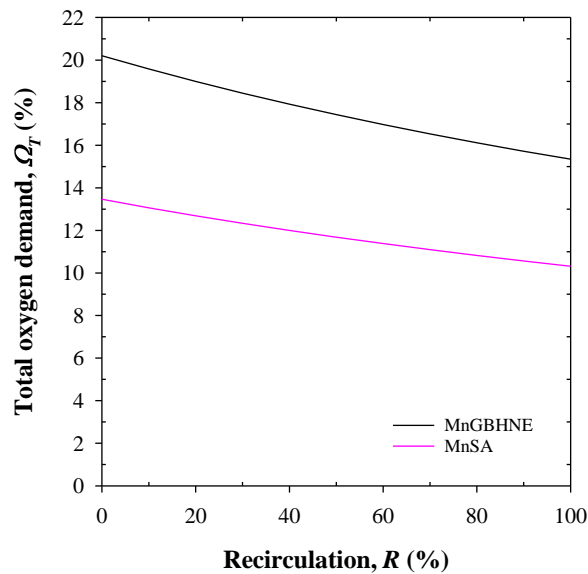
Figure 55. Fuel reactor outlet recycling simulation (data used for the iG-CLC simulation with MnGBHNE and MnSA burning at 900 ºC, about 4 (kg/s)/MW$_{th}$ and about 770 kg/MW$_{th}$.

The simulation was carried out with a molar $CO_2/C_{biomass}$ ratio ~ 1.2, similar to the ratio in the experiments G8 and S1 and assuming in the first iteration the composition of those tests. Figure 55 represents the total oxygen demand values obtained through the application of the iterative simulation as a function of the recirculation for both MnGBHNE and MnSA oxygen carriers in the combustion of pine sawdust. As it can be observed, the total oxygen demand is reduced when the gas recirculation is increased. In the limit case, that is, when the fuel reactor is fluidized with only recirculated gas (R~50%), values close to 30% of total oxygen demand reduction were observed for both oxygen carriers, pointing to the promising possibilities of this technical improvement.

3.1.1.4 Improved oxygen carrier: Mn66FeTi7

Manganese-iron mixed oxides have received attention because of their ability to release oxygen during the reduction under specific operating conditions. Their use had led to a new process, denoted as Chemical Looping assisted by Oxygen Uncoupling (CLaOU), that allows to obtain better results in the oxygen demand without expensive scheme modifications, such as using distributor plates at the bottom part of the fuel reactor for a better volatile distribution or a second fuel reactor to convert the unburnt matter at the exit of the first fuel reactor. As it was mentioned in the experimental chapter, a synthetic oxygen carrier, named Mn66FeTi7, based on manganese and iron oxides doped with TiO_2 has been used in the present work to test its effect on the oxygen demand reduction (**Paper III**). The bixbyite phase, $(Mn_xFe_{1-x})_2O_3$, present in this oxygen carrier decomposes into a spinel phase, $(Mn_xFe_{1-x})_3O_4$, and molecular oxygen is released at specific operating conditions.

Table 14 summarizes the experiments carried out with Mn66FeTi7 with pine sawdust under similar conditions to those previously used with Fe and Mn based ores/minerals. About 180 hours of hot fluidization were accomplished, 41 h of which corresponded to biomass combustion. Good fluid dynamic performance and no agglomeration problems were observed during all the experiments. Steady state was usually reached after 20 min and maintained at least during 60 min.

The effect of different operating variables on the CO_2 capture efficiency and the total oxygen demand was analyzed, including the temperature in the air reactor and the air excess ratio, λ^*, calculated in Equation (14). Previous results using coal as fuel concluded the importance of these two particular variables on the molecular oxygen release of this oxygen carrier, since both variables affected the oxidation from spinel in the air reactor to bixbyite (Pérez-Vega et al. 2020).

$$\lambda^* = \frac{1 - y_{O_2\ AR\ out}}{1 - \frac{y_{O_2\ AR\ out}}{y_{O_2\ AR\ in}}} \tag{14}$$

In the first series (M1-M3), conditions in the air reactor were set to about 880 ℃ and low air excess ratio while the solid inventory in the fuel reactor was changed. In the second series (M4-M7) the solids inventory in the fuel reactor was maintained constant and the air excess ratio in the air reactor was changed while temperature remained at 880 ℃. The third series (M8-M11) analyzed the effect of the air excess ratio at two different specific solids inventories. Finally, the fourth series (M12-M16) set the values of air excess ratio and solids inventory while the temperature in the air reactor was increased to 930 ℃.

Table 14. Operating conditions with the Mn66FeTi7 in the 1 kW$_{th}$ experimental unit.

Test	T_{FR} (℃)	T_{AR} (℃)	λ^* (-)	ϕ (-)	$\dot{m}_{OC}$ (kg/h)	$\dot{m}_{sf}$ (kg/h)	P_{th} (W$_{th}$)	m^*_{FR} (kg/MW$_{th}$)	$norm.\dot{m}_{OC}$ ((kg/s)/MW$_{th}$)
					Mn66FeTi7				
M1	930	880	**1.2**	2.6	5.3	0.130	692	**600**	2.1
M2	925	880	**1.1**	3.5	3.5	0.063	335	**1420**	2.9
M3	935	880	**1.2**	6	4.3	0.060	245	**1870**	4.9
M4	900	880	**1.4**	1.8	1.7	0.059	314	1575	1.5
M5	950	880	**1.4**	5	4.7	0.059	314	1515	4.1
M6	900	880	**1.8**	2.9	3	0.065	346	1330	2.4
M7	930	880	**1.9**	3.1	3	0.062	330	1400	2.5
M8	890	880	1.6	2.1	2.6	0.086	458	**1110**	2.1
M9	905	880	1.6	2.1	2.6	0.086	458	**1075**	2.1
M10	900	880	1.9	2.9	2.9	0.048	255	**1855**	3.1
M11	930	880	1.9	3.5	3.5	0.048	255	**1890**	3.8
M12	935	**930**	1.2	3.8	3.6	0.046	319	1310	3.1
M13	905	**930**	1.8	3	3.7	0.066	351	1240	3.0
M14	960	**930**	1.8	3.1	3.9	0.066	351	1240	3.1
M15	925	**930**	1.8	4	4	0.064	341	1485	3.3
M16	940	**930**	1.8	4	4	0.064	341	1385	3.3

Evaluation of Mn66FeTi7: CO$_2$ capture efficiency

The values of CO$_2$ capture efficiency under the different conditions in Table 14 were so close to 100 % that no influence of the operating conditions could be found. The high values of CO$_2$ capture efficiency reached were attributed to the almost full char conversion in the fuel reactor since almost no CO$_2$ was measured at the outlet of the air reactor.

Evaluation of Mn66FeTi7: Total oxygen demand

EFFECT OF THE SOLIDS INVENTORY

Figure 56 shows the results obtained with the Mn66FeTi7 oxygen carrier working under similar conditions of air excess ratio and solids inventory (M1) to those used with the Tierga ore and the manganese ores (MnGBHNE and MnSA). In this case, the temperature in the air reactor was maintained at 880 ℃. Working with specific solids inventories about 600-800 kg/MW$_{th}$ (M1), the Mn66FeTi7 oxygen carrier performed similarly to Tierga (T2-T3) and MnGBHNE (G1-G2), yielding also high values of total oxygen demand (21-28%). Increasing the solids inventory to values about 1000-1400 kg/MW$_{th}$ in the fuel reactor and keeping the rest of operating conditions constant, a further reduction in the oxygen demand was reached, as it is shown in Figure 56, point (M2). Working with 1870 kg/MW$_{th}$ (M3) in the fuel reactor, an oxygen demand of about 12% was obtained. The increase in the solids inventory in the fuel reactor can be used as a measure for the oxygen demand reduction. However, similar results were obtained compared with the MnSA (S4-S3) despite the lower inventories used for this manganese ore, about 1000 kg/MW$_{th}$. Therefore, further optimization of the operating conditions of Mn66FeTi should be investigated in order to enhance the oxygen release potential of the Mn66FeTi7 material and a significant reduction in the oxygen demand compared to best values reached with iron or manganese ores could be expected.

EFFECT OF THE AIR EXCESS RATIO

In the second and third series of experiments in Table 14 several operating conditions affecting Mn66FeTi7 regeneration in the air reactor were analyzed. In the second series (M4-M7), the air excess in the air reactor was increased from 1.4 (M2) to 1.9 (M7) while the temperature in the air reactor was maintained at 880 ℃ with an average solids inventory of about 1455 kg/MW$_{th}$. The results in Figure 57 show that the oxygen demand decreased when the air excess ratio was increased. The largest reductions in the oxygen demand were observed for $\lambda^* = 1.8$-1.9. Under these conditions, total oxygen demand values of 10.4 % (M7) were reached, which represents reductions of 35% with respect to the reference value with $\lambda^* = 1.1$ (M2).
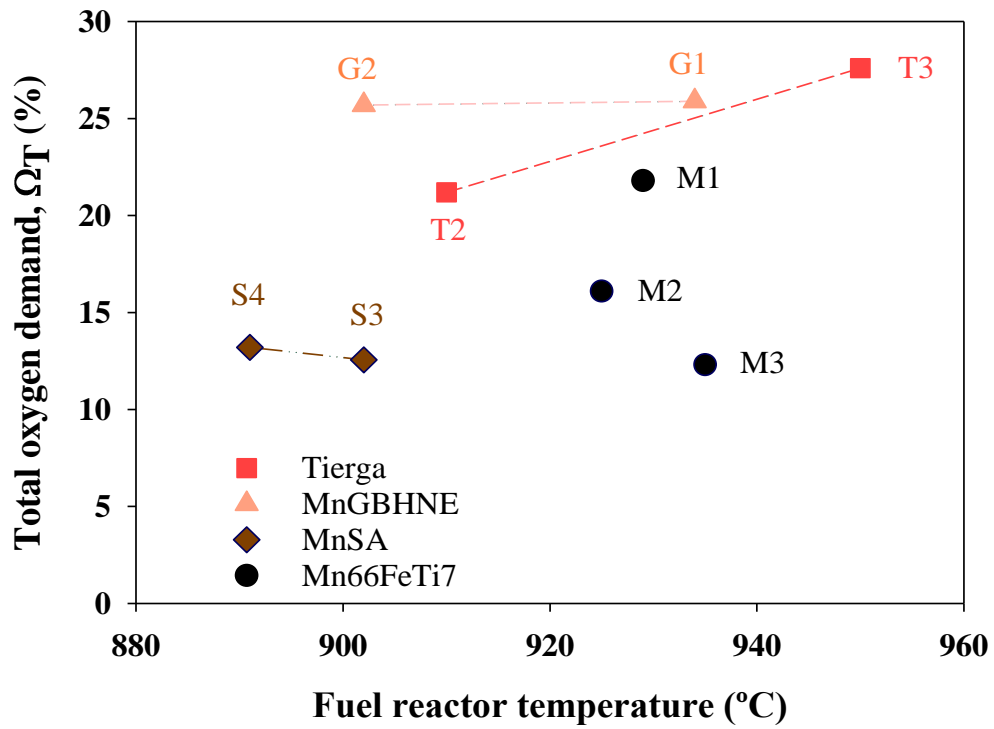
Figure 56. Effect of the specific solids inventory on the total oxygen demand with the Mn66FeTi7 with pine sawdust and comparison with Mn and Fe ores.
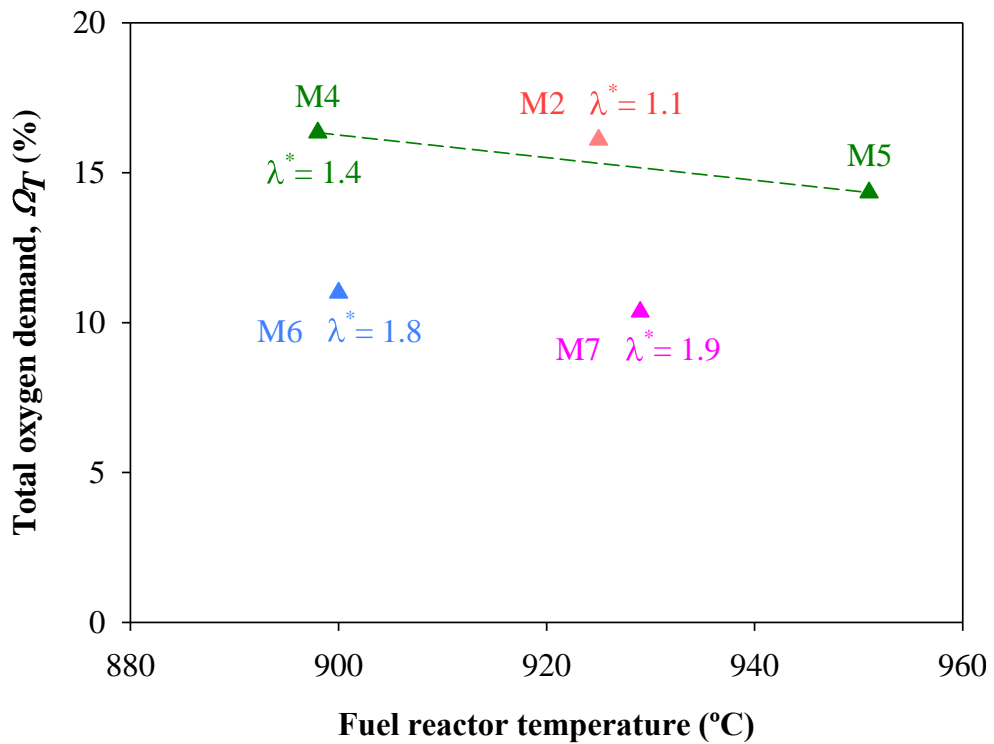
Figure 57. Effect of the air excess (λ^*) on the total oxygen demand with the Mn66FeTi7 with pine sawdust, $T_{AR} \approx 880$ ºC, $m^*_{FR} \approx 1450$ kg/MW$_{th.}$(M4-M7).

The effect of the air excess air ratio has been also assessed in the third series of the experimental campaign (M8-M11).The results shown in Figure 58 correspond to experiments performed under similar conditions to those shown in Figure 57 but with two different averaged values of solids inventories, i.e. 1095 kg/MW$_{th}$ and 1875 kg/MW$_{th}$. When M4-M5 are compared to M8-M9 it can be observed that lower values of total oxygen demand were obtained despite the lower solids inventory available in the fuel reactor (1095 kg/MW$_{th}$). The combination of high air excess ratios ($\lambda^* = 1.9$) and high solids inventories (1875 kg/MW$_{th}$) can led to values of total oxygen demand as low as 4.6 % at 930 ºC (M11).
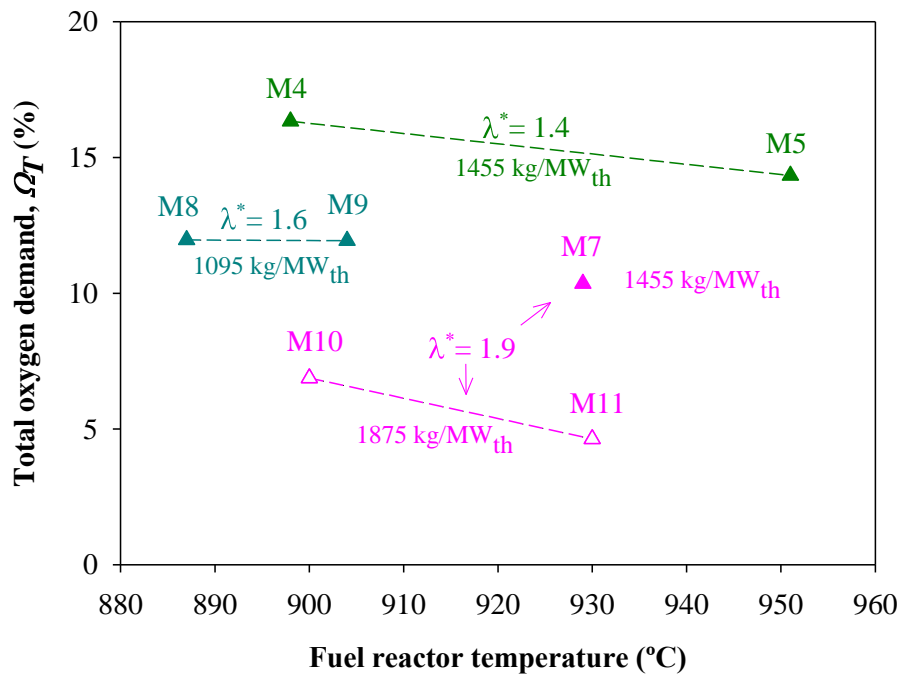
Figure 58. Effect of the air excess (λ^*) on the total oxygen demand with the Mn66FeTi7 with pine sawdust, T_{AR}=880 ºC (M8-M11).

EFFECT OF THE AIR REACTOR TEMPERATURE

All the experimental results shown in Figure 56 to 58 were obtained maintaining the temperature in the air reactor at approximately 880 ºC. The fourth experimental series, (M12-M16) was carried out increasing the temperature in the air reactor to 930 ºC. Under this conditions, two different air excess ratios were tested, i.e. 1.1-1.2 and 1.8. Results are shown in Figure 59. Tests corresponding to M2 and M12 were performed with a low air excess ratio ($\lambda^* = 1.1$-1.2) and an averaged solids

104

inventory about 1365 kg/MW$_{th}$. In this case, a slightly lower total oxygen demand was attributed to the experiment at 880 ºC in the air reactor. A similar comparison can be performed at higher air excess ratio, namely ($\lambda^* = 1.8$) and similar solids inventories for the tests M6 (1455 kg/MW$_{th}$), M13-M14 (1240 kg/MW$_{th}$) and M15-M16 (1435 kg/MW$_{th}$). Working at 930 ºC in the air reactor, a decrease in the total oxygen demand was observed from M13-M14 to M15-M16 when the solids inventory in the fuel reactor was slightly increased. Nevertheless, the lowest oxygen demand value was again obtained when the air reactor was operated at 880 ºC (M6-M7).
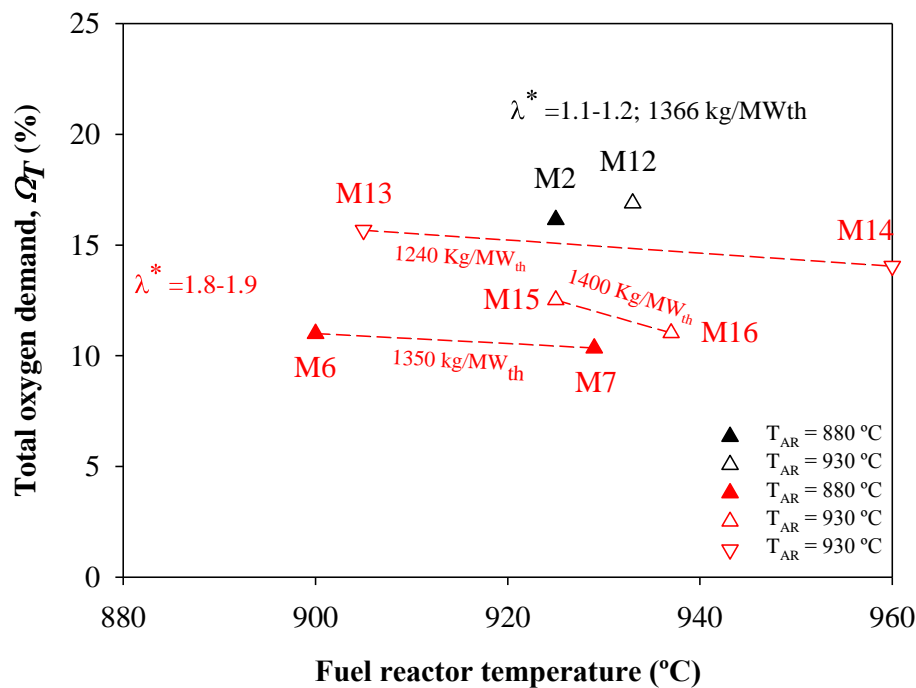
Figure 59. Effect of the air reactor temperature (T$_{AR}$) on the total oxygen demand with the Mn66FeTi7 with pine sawdust.

Further analysis of the total oxygen demand values obtained in the experimental series presented in Table 14 is shown in Figure 60 representing the total and partial oxygen demands attributed to each of the unburned compounds found at the fuel reactor exit, i.e. H$_2$, CO and CH$_4$ in the different experimental tests in Table 14. In Series I, the main contribution to the total oxygen demand value came from methane followed by CO regardless the solids inventory in the fuel reactor. In Series II and III this trend changed. When the air excess ratio was increased, methane

was better burned and its contribution to the total oxygen demand decreased and became closer to that of CO or even lower in some cases (see M10 and M11). These results demonstrate how the increased presence of molecular oxygen in the fuel reactor improved the oxygen demand by improving methane combustion.
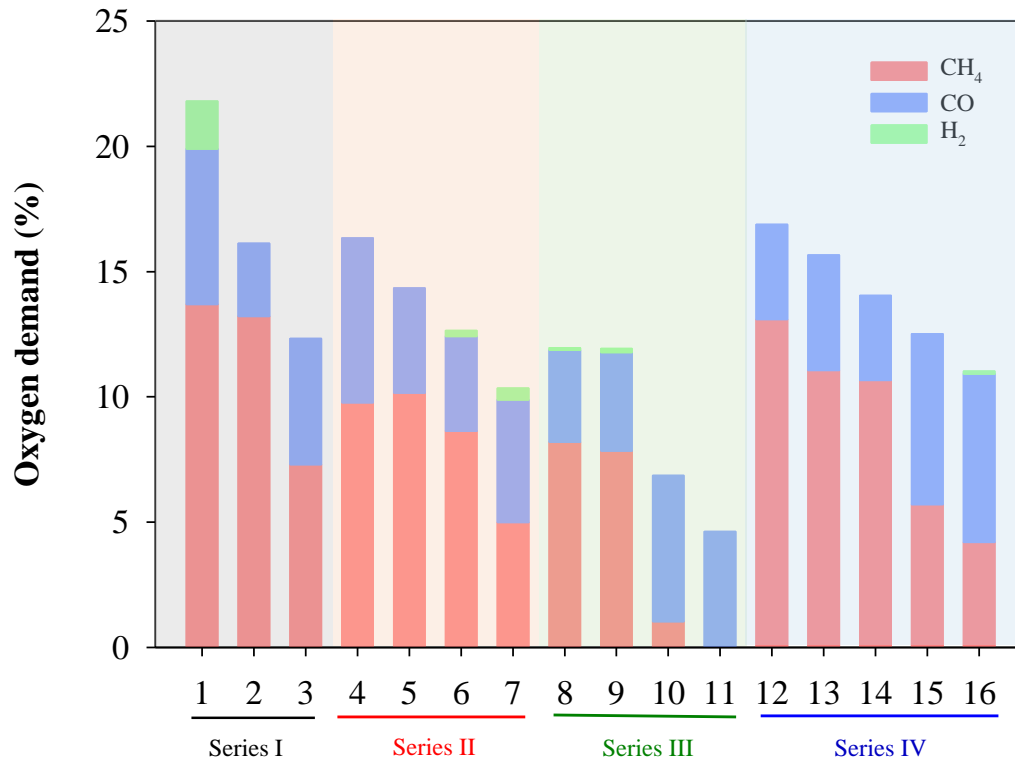
Figure 60. Comparison of partial oxygen demands for H_2, CO and CH_4 found at the fuel reactor exit in the different experimental tests in Table 14.

As a summary of the results shown in Figures 56 to 60, it was concluded that in order to maximize the oxygen release capacity of Mn66FeTi7 oxygen carrier in the fuel reactor and decrease the oxygen demand in biomass combustion, the air reactor should be operated with temperatures about 880 ºC and high air excess ratio, preferably about 1.8 or higher. Working under these operating conditions and using an averaged solids inventory of 1875 kg/MW$_{th}$ in the fuel reactor, total oxygen demand values as low as 4.6% have been reached. Comparable values for the oxygen demand (3.4-6.7%) were reached recently by Schmitz et al. (2018) using a manganese-silicon-titanium oxygen carrier with the ability to release molecular oxygen. However, in this case, the fuel used was a low-volatile fuel (wood char).

3.1.2 Combustion under CLOU: Cu34Mn66

Biomass combustion under the CLOU mode has been reported to significantly reduce the total oxygen demand of the biomass combustion process compared to results under iG-CLC. Under the CLOU mode, the oxygen carrier releases molecular oxygen (O_2) that is able to easily react with the biomass devolatilization products in a similar way than in a conventional combustion. However, the oxygen carriers developed for the CLOU process (mainly based on copper oxides or perovskites) are commonly more expensive and with lower mechanical properties than those used under iG-CLC mode (Adánez et al. 2018). To reduce the high costs associated to copper oxides, mixed oxides have been proposed and among them, mixed oxides based on Cu-Mn have shown high oxygen uncoupling capability (Adánez-Rubio et al. 2016). Moreover, Cu-Mn mixed oxides have shown a lower temperature operating window than Cu-based oxygen carriers (750-850 ℃), see Figure 38, section 2.1.4.

In the present work, a mixed Cu-Mn oxide (Cu34Mn66) was used as oxygen carrier (**Papers IV and V**). Table 15 summarizes the experiments carried out with Cu34Mn66 with the three types of biomass (pine sawdust, olive stones and almond shells). A total of 65 h of biomass combustion were carried out with this oxygen carrier, without problems of agglomeration.

Figure 61 shows the gas concentrations in the outlet stream of the fuel and air reactors (dry basis) as a function of the operation time in the pine sawdust experiments, where the effect of the fuel reactor temperature was analysed (C5–C8). The fuel reactor temperature varied between 775 ℃ and 850 ℃, and each temperature was maintained at a steady state for at least 60 min. No unburnt products (CH_4, CO or H_2) were detected in the gas outlet stream of the fuel reactor, even at the lower temperature (775 ℃). Therefore, all the volatiles were completely converted inside the fuel reactor by the molecular oxygen released by the oxygen carrier. It can be seen that an increase in the fuel reactor temperature resulted in an increase in the CO_2 concentration in the fuel reactor outlet gas stream. This was

caused by the increase in the char conversion inside the fuel reactor that decreased the CO_2 concentration at the air reactor outlet. Also worthy of note is the fact that that no gaseous oxygen was measured at the fuel reactor outlet which could be associated with the low fuel reactor temperature, together with the large proportion of volatiles in the biomass composition.

Table 15. Experimental conditions with Cu34Mn66 in the 1 kW$_{th}$ experimental unit.

Test	FA (-)	T_{FR} (°C)	T_{AR} (°C)	$y_{O_2\,in\,AR}$ (%)	ϕ (-)	$\dot{m}_{OC}$ (kg/h)	$\dot{m}_{sf}$ (kg/h)	P_{th} (W$_{th}$)	m^*_{FR} (kg/MW$_{th}$)	$norm.\,\dot{m}_{OC}$ ((kg/s)/MW$_{th}$)
					Pine sawdust					
C1	CO_2	850	800	21	**7.6**	**27.2**	0.082	435	2200	17.4
C2	CO_2	850	800	21	**5.3**	**19.3**	0.082	435	2200	12.3
C3	CO_2	850	800	21	**4.7**	**16.8**	0.082	435	2200	10.7
C4	CO_2	850	800	21	**2.3**	**8.7**	0.082	435	2200	5.6
C5	CO_2	**775**	800	21	3.9	22.5	0.14	740	1200	8.4
C6	CO_2	**800**	800	21	3.9	22.5	0.14	740	1200	8.4
C7	CO_2	**825**	800	21	3.9	22.5	0.14	740	1200	8.4
C8	CO_2	**850**	800	21	3.9	22.5	0.14	740	1200	8.4
C9	CO_2	800	800	10	3.9	22.5	**0.14**	740	1200	8.4
C0	CO_2	800	800	10	3.4	28.5	**0.19**	1000	900	7.9
C11	CO_2	800	800	10	2.6	28.5	**0.25**	1330	715	6.0
					Olive stones					
C12	CO_2	**775**	800	21	3.0	20.3	0.173	860	1150	6.6
C13	CO_2	**800**	800	21	3.0	20.3	0.173	860	1150	6.6
C14	CO_2	**825**	800	21	3.0	20.3	0.173	860	1150	6.6
C15	CO_2	**850**	800	21	3.0	20.3	0.173	860	1150	6.6
					Almond shells					
C16	CO_2	**775**	800	21	3.3	22.5	0.225	1040	760	6.0
C17	CO_2	**800**	800	21	3.3	22.5	0.225	1040	760	6.0
C18	CO_2	**825**	800	21	3.3	22.5	0.225	1040	760	6.0
C19	CO_2	**850**	800	21	3.3	22.5	0.225	1040	760	6.0

Figure 62 shows the combustion and CO_2 capture efficiencies, as well as the char conversion as a function of the fuel reactor temperature in experiments with the three types of biomass used in this work. It is remarkable that complete combustion of volatiles in the fuel reactor was obtained at such a low fuel reactor temperature as 775 °C. The pine sawdust contained 81% volatile matter, therefore, even with this high volatile matter content, the results showed full combustion of the biomass in all the tests. The CO_2 capture efficiency with pine sawdust increased from 86% to about 98% when temperature in the fuel reactor increased from 775 to 850 °C even without the use of carbon stripper in the 1 kW$_{th}$ unit. However, the CO_2 capture efficiencies

obtained for almond shells and olive stones, were lower than those obtained for the pine sawdust. So, it seems that for types of biomass with lower reactivity than the pine sawdust, it would be necessary to increase the fuel reactor temperature or to install a carbon stripper to increase char conversion and thus reduce the amount of unburnt char transferred to the air reactor.
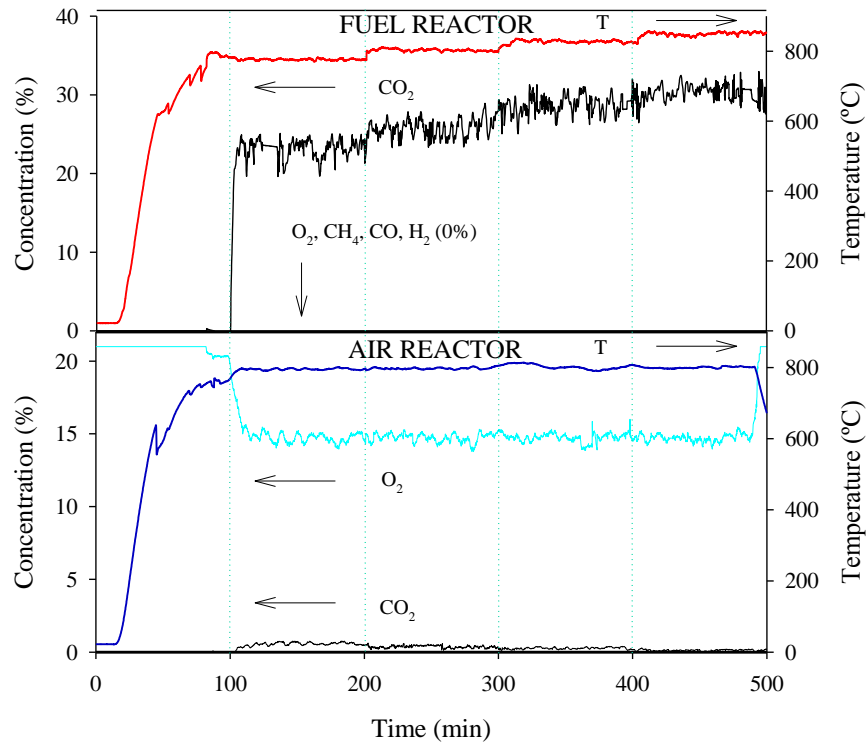
Figure 61. Evolution of the fuel and air reactors temperatures and gas outlet compositions in the 1 kW$_{th}$ CLC unit. (Tests C5-C8).

Figure 63 shows the effect of the oxygen carrier-to-fuel ratio, ϕ, on the combustion and the CO_2 capture efficiencies (a) and on the char conversion (b) burning pine sawdust (C1–C4). Complete combustion to CO_2 and H_2O was always obtained in the fuel reactor. Therefore, the oxygen carrier under these conditions was able to generate enough oxygen, even with excess, in the fuel reactor stream to reach combustion efficiencies near to 100%. CO_2 capture efficiencies near 100% were also achieved. It was necessary to use ϕ values higher than 7 to observe a small reduction of the CO_2 capture efficiency from 100% to 99.6%, due to some unconverted char passed to the air reactor. It must be considered that the increase of ϕ was produced

by increasing the solids circulation rate, and then decreasing the residence time of char and oxygen carrier in the fuel reactor.
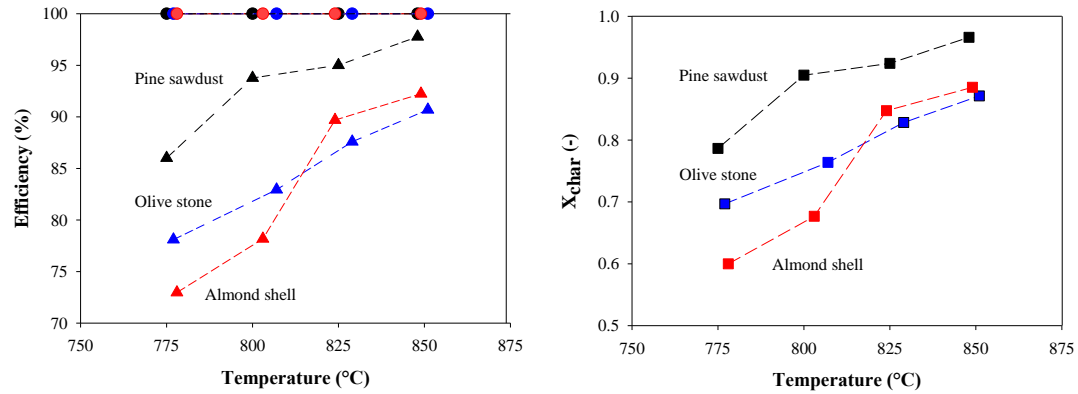
Figure 62. Effect of the fuel reactor temperature on the Combustion (●) and CO_2 capture (▲) efficiencies, and char conversion (■) for the three types of biomass: pine sawdust (C5–C8), almond shells (C12–C15) and olive stones (C16–C19).
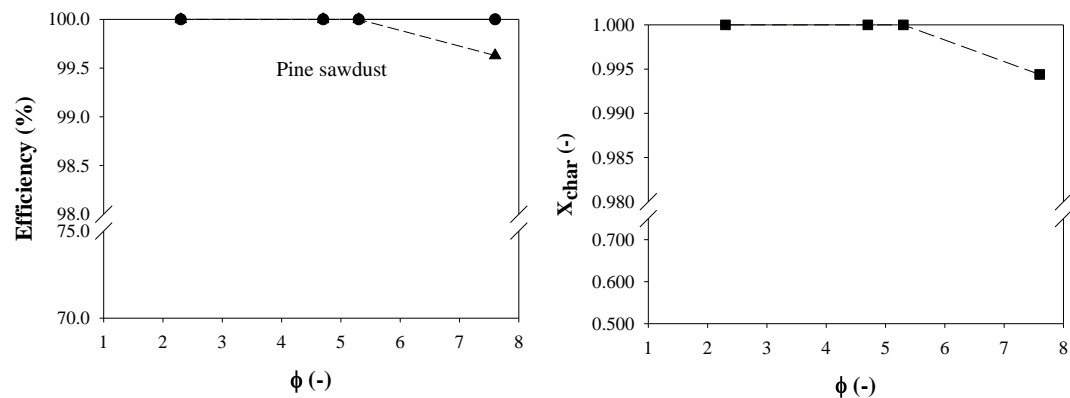
Figure 63. Effect of the oxygen to fuel ratio on the Combustion (●) and CO_2 capture (▲) efficiencies, and char conversion (■) in the 1 kW_{th} CLC unit (tests C1-C4, $T_{FR}= 850$ ºC).

Figure 64 shows the effect of the power input on the combustion and CO_2 capture efficiencies, and also on the char conversion at 800 ºC in the combustion of pine sawdust. It can be seen that the CO_2 capture efficiency decreased by increasing the power input from about 700 to 1300 W_{th}. When the biomass feeding rate increased, the CO_2 capture efficiency decreased as a result of the reduction in the

char conversion in the fuel reactor. Under these conditions, when the biomass feeding rate is increased, the ϕ value and the specific oxygen carrier inventory decreases. A decrease in the oxygen carrier-to-fuel ratio value increases oxygen carrier conversion in the fuel reactor, decreasing the rate at which O_2 is released by the Cu-Mn mixed oxide. Higher CO_2 capture efficiencies can be obtained increasing the fuel reactor temperature to 850 °C, as it was seen, an optimum temperature to operate the fuel reactor with the Cu34Mn66 oxygen carrier (Adánez-Rubio et al. 2017a). It is important to highlight that even with a power input of 1330 W_{th} and a fuel reactor temperature as low as 800 °C, a combustion efficiency near 100% was achieved.
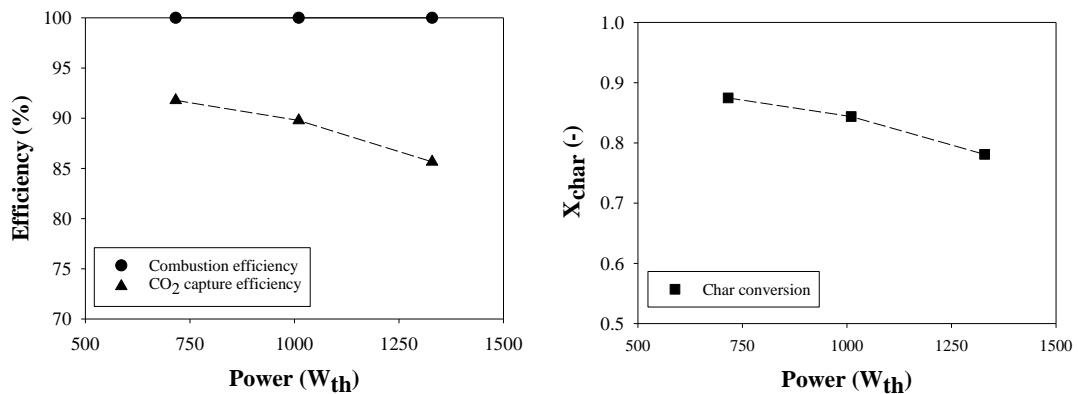
Figure 64. Effect of the power input on the Combustion (●) and CO_2 capture (▲) efficiencies, and char conversion (■) in the 1 kW_{th} CLC unit (C9–C11). T_{FR}=800 °C, 10% O_2 in air reactor).

The results presented with the Cu34Mn66 synthetic oxygen carrier represent an important advance in the study of biomass fueled CLC. Throughout the experimental campaign, no unburnt gaseous compounds appeared at the fuel reactor outlet, despite the low temperatures used with this oxygen carrier, showing complete combustion efficiency in the fuel reactor, that is, the oxygen demand was near 0%. Compared to the number of studies concerning biomass combustion under iG-CLC, the number of studies under CLOU mode reported in literature is significantly less. Most of them use perovskite type oxygen carriers based on calcium manganates. Schmitz and Linderholm (2016) burned biochar in a 10 kW_{th} continuous unit with a bubbling fluidized bed reactor. Working at about 970 °C, they reached values of CO_2

capture efficiency between 82 and 95.2% and the reported oxygen demand values were between 2.1 a 4.9%. Recently, Gogolev et al. (2019) also used a mixture of 80-90 wt% calcium manganite with 10-20 wt% ilmenite in the combustion of black wood pellets in a 100 kW_{th} continuous unit at temperatures close to 950 ºC. In this case, the fuel reactor was a circulating fluidized bed. Under these conditions, the lowest oxygen demand reported was about 3%.

3.1.3 Comparison of 1 kW_{th} experimental results

From the experimental results already presented, the high values obtained for the total oxygen demand can be pointed as the crucial parameter to be improved for the development of the bioCLC process as a BECCS technology. In this respect, a comparison of the oxygen demand values, obtained in the 1 kW_{th} CLC unit at comparable operating conditions for the different oxygen carriers (the Tierga ore, the manganese ores -MnGBHNE and MnSA- and the synthetic materials -Mn66FeTi7 and Cu34Mn66-) and using pine sawdust as fuel, is presented in Figure 65. CO_2 was used as fluidizing gas for all oxygen carriers, except for Tierga ore experimental campaign, which was carried out with water steam. However, no significant differences were observed in results using these two gasifying agents.

Figure 65 presents the total oxygen demand of the different oxygen carriers and also the partial oxygen demand of the different unburnt compounds (CH_4, CO and H_2). Starting with the ores results, lower amounts of hydrogen were obtained with the MnGBHNE compared to Tierga ore, achieving a total oxygen demand reduction despite the slightly higher amounts of CO measured. Total oxygen demand values continued decreasing using the MnSA oxygen carrier because of the negligible hydrogen detected as well as the CH_4 favoured oxidation (compared with both the Tierga and the MnGBHNE ores). Focusing on the synthetic Mn66FeTi7 oxygen carrier, initially similar oxygen demands to those obtained working with MnSA were reached. However, after optimization of the operating conditions, the oxygen demands with the Mn66FeTi7 oxygen carrier slightly decreased because this oxygen was able to release molecular oxygen, which improved the reaction rate with the unburnt compounds. Finally, the CLOU capacity of the Cu34Mn66 oxygen

carrier allowed to reach complete combustion of the volatiles in the fuel reactor, reaching an oxygen demand near to 0%.
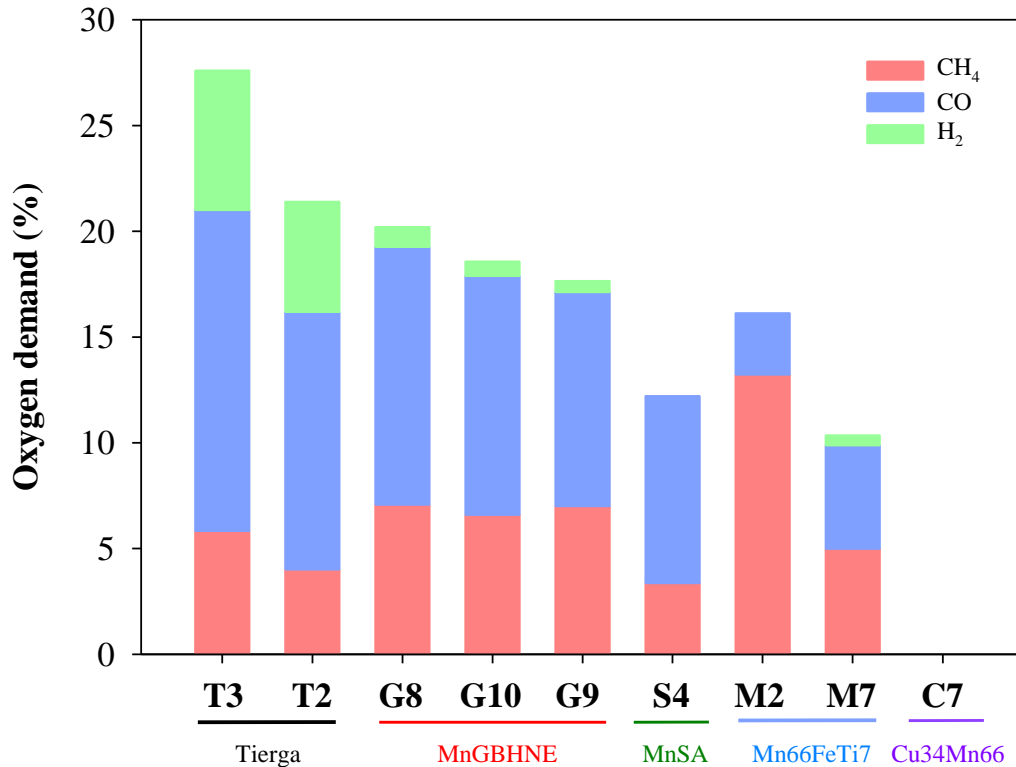
Figure 65. Effect of the different oxygen carrier used on the total oxygen demand (Ω_T) and the partial oxygen demands for the different oxygen carriers ($T_{FR} \approx 900$-950 °C, $m^*_{FR} \approx 650$-1100 kg/MW$_{th}$, norm.$\dot{m}_{OC}$=3.9-4.9 kg/(s·MW$_{th}$)).

3.1.4 Other aspects of the bioCLC process

3.1.4.1 Ash formation during combustion

The experience accumulated in the operation in fluidized bed boilers burning biomass shows that the characteristics of the biomass ash are important for the correct operation of the system. Alkali in biomass ash is released during combustion and could lead to problems such as corrosion and fouling of the boiler tubes. Moreover, some alkali present in biomass (mainly potassium) could react with the silica sand in the fluidized bed boiler forming sticky ash compounds, which can lead to

agglomeration of the bed. The most common configuration for a CLC system is two interconnected fluidized beds. Therefore, some of these problems previously encountered in biomass combustion in fluidized bed boilers can affect the performance of the bioCLC process. Nevertheless, as it was pointed by Pikkarainen et al. (2016) the risk of high-temperature corrosion of superheater tubes may be lower in bioCLC than in conventional biomass combustion since they might be placed in the air reactor and the alkali release would happen in the fuel reactor. Under this assumption, it would be possible to use higher steam values (temperature, pressure) in bioCLC improving the power generation efficiency from biomass.

There are many references available in literature concerning the effect of biomass ash in the bioCLC process. These studies refer to two aspects: effect on oxygen carrier reactivity and alkali emissions from the fuel/air reactors. The latter has been recently addressed by Gogolev et al. (2019) who explored the fate of alkali in the gaseous streams from fuel and air reactors from a 100 kW_{th} unit by on-line surface ionization measurements. The effect on the oxygen carrier reactivity has been evaluated with different types of oxygen carrier (mainly Mn and Fe-based) both in fixed (Haiming et al. 2015; Leion et al. 2017; Zevenhoven et al. 2018) or batch fluidized bed reactor (Song et al. (2016)) as well as continuous CLC units of different size (Haiming et al. 2011; Mendiara et al. 2013a; Adánez-Rubio et al. 2014; Niu et al. 2015; Schmitz et al. 2016; Sun et al. 2018; Gogolev et al. 2019; Hildor et al. 2019; Hanning et al. 2018).

The interaction of the oxygen carriers with alkali compounds in biomass ash showed widely different behavior. Mattison et al. (2019) impregnated two manganese ores and an iron-based waste material with alkali (K) in order to explore the behavior of oxygen carriers. The two manganese ores retained almost all alkali after redox testing in a batch fluidized bed reactor but the iron-based waste lost most alkali to the gas phase during testing. In the operation in continuous units, some authors found evidences of ash deposition on the oxygen carrier surface affecting its reactivity (Haiming et al. 2015), although some others did not report changes in the reactivity of the oxygen carriers used (Mendiara et al. 2013a; Adánez-Rubio et al.

2014; Pikkarainen et al. 2016). Regarding agglomeration, Haiming et al. (2015) found that SiO_2-rich biomass ash was likely to be converted into potassium silicates being the cause of serious particle sintering of oxygen carrier. Leion et al. (2017) also pointed to this effect of SiO_2 in the biomass ash. However, Zevenhoven et al. (2018) established from experiments with ilmenite in a fixed bed (crucible) that the agglomeration mechanisms depend on the major potassium compound found in the ash: KCl glued the particles together, whereas K_2CO_3 reacted with the bed particles. KH_2PO_4 reacted with the bed material and glued the particles together. K_2SO_4 remained non-reactive and did not influence the agglomeration of ilmenite bed particles.
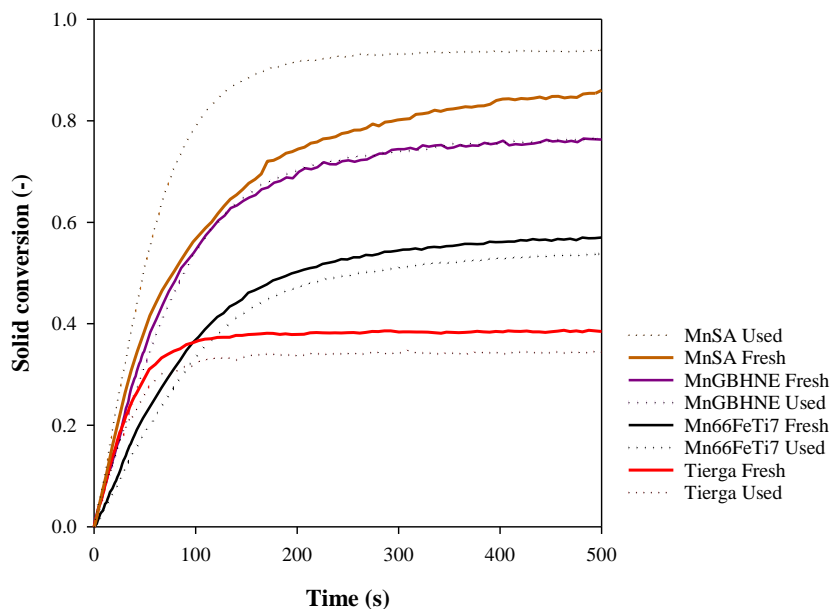
Figure 66. Conversion versus times curves obtained for fresh and used samples of the different oxygen carriers (T = 950 ºC, 15% CH_4 + 20 % H_2O).

In the present work, neither ash deposition on the oxygen carrier particles nor agglomeration problems during operation was found within the experimental campaigns in the 1 kW_{th} unit with any of the oxygen carriers tested. Moreover, the reactivity of the different oxygen carrier materials before and after the corresponding experimental campaigns carried out in the 1 kW_{th} CLC unit was evaluated in the TGA, already described in the experimental section. Figure 66 shows conversion versus time curves obtained with the different oxygen carriers. No significant

115

deactivation changes could be observed for any of the analyzed oxygen carriers. Slight reductions in the oxygen transport capacity can be observed in the case of the Tierga ore and the Mn66FeTi7 while similar behavior was obtained in the case of the MnGBHNE ore. Higher differences were found in the case of MnSA, this manganese ore presented activation reaching solid conversions about 0.92.

Nevertheless, the influence of the presence in the biomass ash of alkali and alkaline earth metals on the fluidization behaviour and reactivity of the oxygen carriers tested was investigated in a batch fluidized bed reactor described in the experimental section during a 4-month stay at the Institute of Solids Process Engineering and Particle Technology in Hamburg Technological University (Germany). In a previous study carried out in the same batch fluidized bed reactor used at Hamburg University, Song et al. (2016) studied the effect of the addition of NaCl to the oxygen carrier fluidization at temperatures over the salt's melting point. Pressure drop variations in the fluidized bed were analyzed as an important and representative variable of the fluidization behavior. In this study, about 280 g of iron ore were used as bed material and three additions of 0.5 g each of sodium chloride were carried out at 900°C. It was observed an important pressure drop variation during the experimental procedure and agglomerates were found in the analysis of the samples. It was assumed that the salt acted as glue for the iron ore particles, causing agglomeration that produced the pressure drop. Moreover, sodium chloride was found in SEM analysis presented by Song et al. (2016) on the oxygen carrier particles surfaces.

During the research stay at Hamburg University similar experiments were performed with Tierga ore, ilmenite, MnGBHNE and a synthetic iron-based oxygen carrier (Fe20γAl) and three different salts (NaCl, KCl and CaCl$_2$). A total of 5 g of each salt were gradually added to each oxygen carrier, using two different oxygen carrier reduction conversion degrees (50 and 75 %) at 950 ºC. Figure 67 presents an example of the pressure drop variations measured in the fluidized bed in a test at 950 ºC during three CaCl$_2$ additions to a Tierga ore bed identified by (a). As it can be observed, high-pressure drop oscillations were observed just during the salt

introduction. After that, a slight increase of the pressure drop of the fluidized bed was measured to finally return to previous values. No significant changes were found for the bed pressure drop despite the higher salt amounts added compared to Song et al. (2016). This behaviour was observed for all the salt additions and all the oxygen carriers tested. In this way, no defluidization problems were found analysing the fluidized bed pressure drop variations.
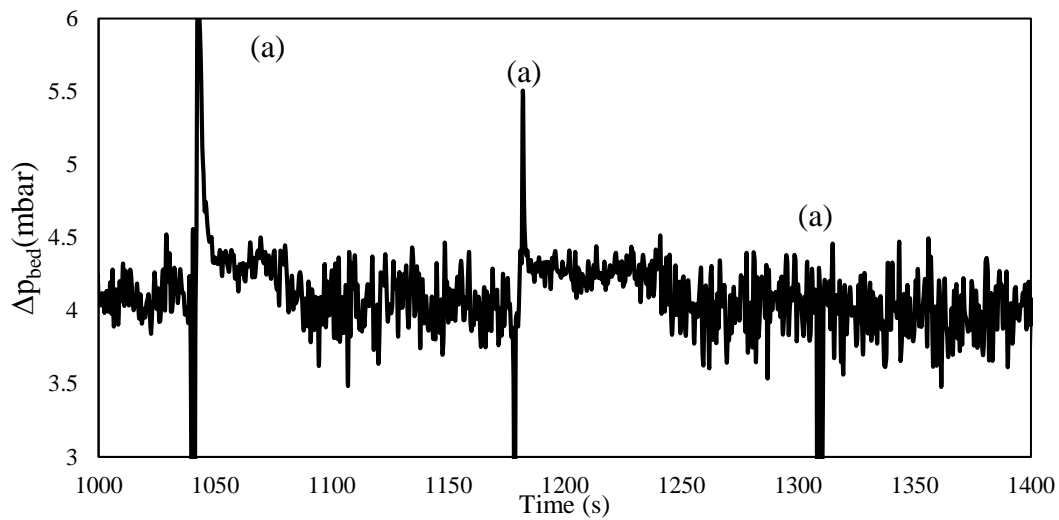
Figure 67. Fluidized bed pressure drop using 250 g of iron ore (Tierga) at 950ºC with CaCl$_2$

In addition to fluidization properties, no significant changes in the reactivity for any of the oxygen carriers used during the redox cycles carried out for the salt addition experiments were observed. Moreover, no visible agglomeration for any tested oxygen carrier and salt was observed, neither in the oxygen carrier samples extracted online from the fluidized bed nor after the experiments during the oxygen carrier batch change nor in the SEM analyses carried out to the samples extracted from the bed. SEM images also show no salt deposition on the oxygen carrier particles surface. As an example, Figure 68 presents the SEM image (a) and an element mapping (b) for the Fe20γAl oxygen carrier after KCl addition, where it can be observed that K on the surface of the oxygen carrier is almost not detected.

It should be considered that results reported to date in batch fluidized bed reactors or continuous CLC units regarding biomass ash effect on bioCLC performance may be limited by the number of hours of continuous operation reached (Mendiara et al. 2018a). Longer operating periods under similar conditions to those existing in a chemical looping unit would be needed in order to establish solid conclusions. In this respect, the oxygen carrier-aided combustion (OCAC) process can be of great interest. In the OCAC process, biomass is combusted in a fluidized bed using an oxygen carrier as bed material. In this case, the combustion efficiency of the process is improved, although combustion is performed with air, and therefore CO_2 capture is not achieved. The operational experience gained through the OCAC process can offer information on what happens to the oxygen carrier particles during their long exposure to ash in a combustion environment. Recent results were obtained in a 12 MW_{th} CFB boiler at Chalmers University where a Fe-based waste material from the steel industry and a manganese ore were tested as oxygen carriers and the effect of biomass ash evaluated. In both cases potassium as well as silicon and calcium were found to be deposited on the oxygen carrier surface (Hanning et al. 2019; Hildor et al. 2019).
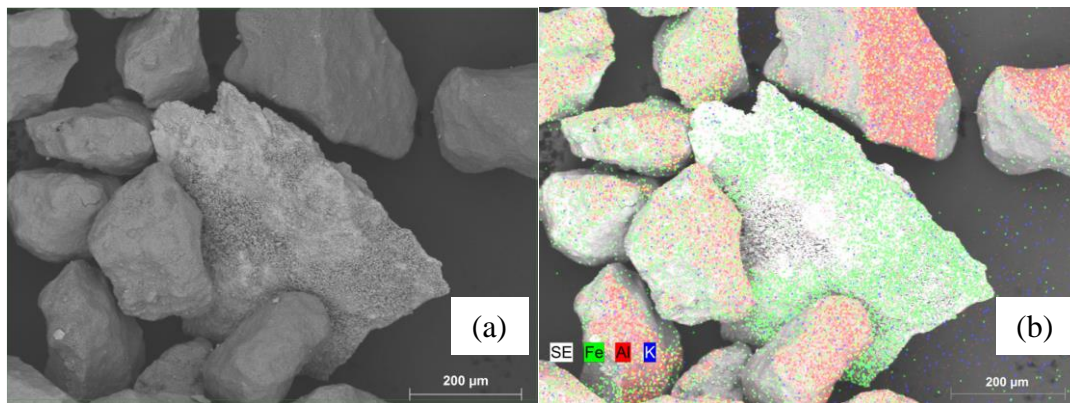
Figure 68. SEM image after the addition of about 5 g of KCl for the Fe20γAl.

3.1.4.2 NO$_x$ emissions

During the experimental campaigns carried out with the different oxygen carrier materials attention was paid to the possible emissions generated in the bioCLC process, especially NO$_x$ emissions. One of the advantages of CLC over conventional

combustion is the reduction in NO_x (Ishida and Jin 1996) formation due to two reasons. First, the lower combustion temperatures used in the bioCLC process compared to conventional combustion avoid thermal NO_x formation. Thus, NO_x emission will mainly come from the fuel nitrogen. Second, since the nitrogen fuel released to the fuel reactor stream will be capture, the only NO_x considered as emissions would be those appearing in the air reactor outlet stream. This NO_x would be formed in the combustion of the unconverted char that may reach the air reactor. In the specific case of the bioCLC process, the unconverted char in the air reactor is minimal since high CO_2 capture efficiencies are reached in the process, as it has been outlined before. Considering this, the presence of NO_x in both fuel and air reactor streams has been analysed in all the experimental campaigns performed with the five oxygen carriers and the three types of biomass studied. The main results and conclusions about NO_x emissions are summarized next. Some of these conclusions were already outlined in **Paper VI**.

The first consideration when analysing NO_x emissions results is the operating mode under which they were obtained, i.e. *i*G-CLC or CLOU. The optimal temperature range for each process used in the fuel reactor is different and this fact can affect the nitrogen chemistry occurring in the fuel reactor. Performance results from the experiments were discussed in detail in Figure 69 for the experiments with Tierga ore (as reference results for the *i*G-CLC mode) and with Cu34Mn66 (CLOU mode) in order to be afterwards correlated to the results obtained in the analysis of pollutant emissions. It can be seen under the *i*G-CLC mode high values of CO_2 capture efficiencies were obtained with all the types of biomass. The values increase with the fuel reactor temperature reaching almost 100% at 980ºC. These values for CO_2 capture efficiencies are correlated to those calculated for the char conversion in the fuel reactor, which also increase with the fuel reactor temperature from 70-80 to almost 100%. In *i*G-CLC, low combustion efficiencies (about 70%) were found for all the types of biomass tested mainly due to the fraction of volatiles released by the biomass that are not burnt by the oxygen carrier. In the CLOU experiments also shown in Figure 69, the CO_2 capture efficiencies increased with temperature because of the char reactivity increase at higher temperatures in the fuel reactor and therefore, less unconverted char reaches the air reactor. With this Cu-Mn based oxygen carrier

values of CO_2 capture efficiencies about 98% at 850ºC were obtained. In order to increase the values of the CO_2 capture efficiencies a carbon stripper would be needed. The combustion efficiencies for CLOU experiments in Figure 69 were always close to 100% even at the lowest temperature (775ºC), due to the release of gaseous oxygen in the fuel reactor.
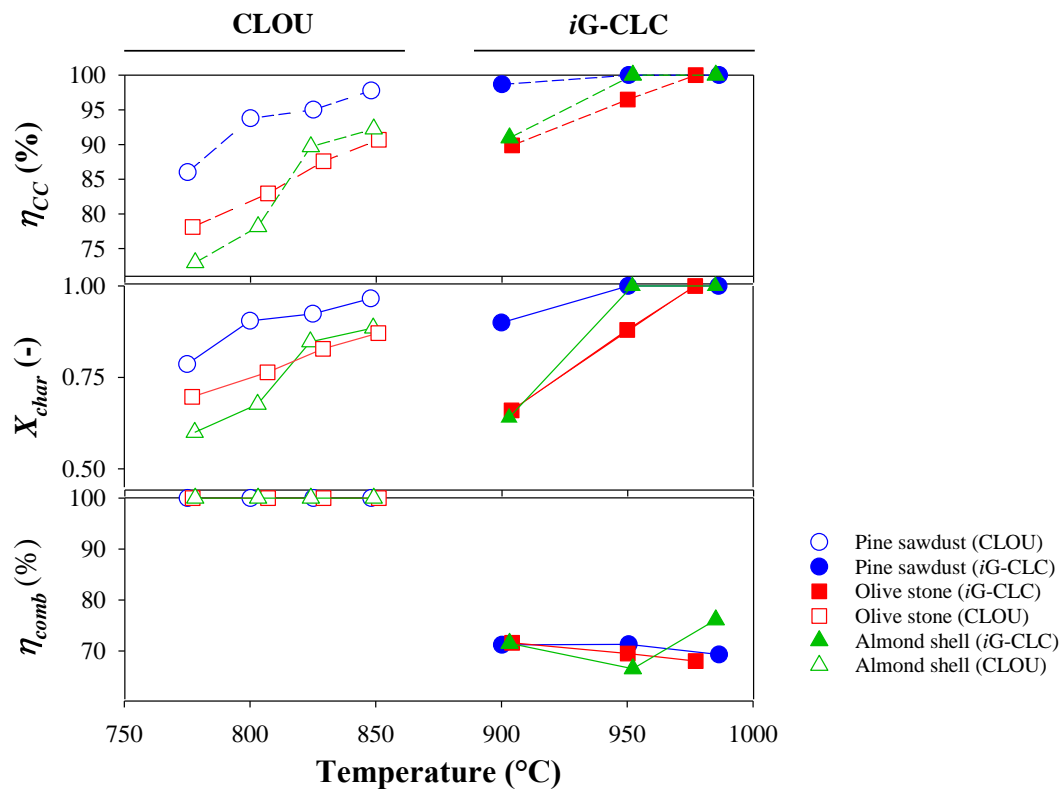
Figure 69. Effect of the fuel reactor temperature on the combustion ($\eta_{comb,FR}$) and CO_2 capture efficiencies (η_{CC}) and char conversion ($X_{char,FR}$) for iG-CLC (filled symbols) and CLOU (open symbols) burning pine sawdust, olive stones and almond shells.

Fuel-N distribution _between fuel and air reactors_

There is some information in literature about the fate of fuel-N in CLC processes, mainly referred to coal as fuel (Adánez et al. 2018). The majority of the iG-CLC studies carried out conclude that most of fuel-N is released in the fuel reactor as N_2 and only low amounts of NO_x can be found (Mendiara et al. 2014b). In the air reactor, the fuel-N in the unconverted char that may reach the air reactor is released

as NO. According to the composition of the different types of biomass in Table 8, the highest nitrogen content is observed for pine sawdust (0.3 wt%), while olive stones and almond shells are reported 0.2 wt%. Fuel-N in biomass is released during biomass devolatilization. The dominant nitrogenous volatile species are NH_3 and HCN (Werther et al. 2000). Both can evolve to either N_2 or NO, depending on the combustion conditions. On the other hand, char-bound nitrogen can evolve to NO, N_2O or N_2. However, at temperatures higher than 900ºC N_2O decomposes to N_2 (Glarborg et al. 2003). In the experiments performed under both *i*G-CLC and CLOU modes, different atmospheres can be found in the fuel reactor when biomass devolatilization takes place. In the experiments with NO_x measurement, CO_2 was supplied to the fuel reactor as gasifying/fluidizing agent. Therefore, in *i*G-CLC a reducing environment is generated due to the presence of gasification products (H_2 and CO). However, oxygen is present in the reacting atmosphere under CLOU operation. In both processes, N_2 from air is not present, which is an important difference compared to the conventional combustion in air.

Figure 70 presents fuel-N distribution between fuel and air reactors in the experiments under *i*G-CLC and CLOU modes with the different oxygen carrier using pine sawdust, although similar conclusions could be obtained with the olive stones and almond shells (**Paper VI**). Despite the different operating temperature under *i*G-CLC and CLOU, 900 ºC were chosen for comparison in *i*G-CLC and 850 ºC for the CLOU mode of operation. As a general conclusion shown in Figure 70, for both operating modes, the most of the nitrogen in the fuel was released in the fuel reactor, in line with the results previously reported in literature for CLC using coal as fuel (Adánez et al. 2018). Moreover, nitrogen emissions in the air reactor were only measured using the Tierga ore and the Cu34Mn66 at those conditions. In this way, the high CO_2 capture efficiencies reached with all the oxygen carriers used avoided the nitrogen emissions at these conditions with the manganese ores and the Mn66FeTi7. Moreover, the temperature increase slightly reduces the amount of char achieving the air reactor, being necessary temperatures higher than 850 ºC with the Cu34Mn66 and 900 ºC with the rest of the used oxygen carriers (Tierga, MnGBHNE, MnSA and Mn66FeTi7) to obtain negligible nitrogen emissions in the air reactor.
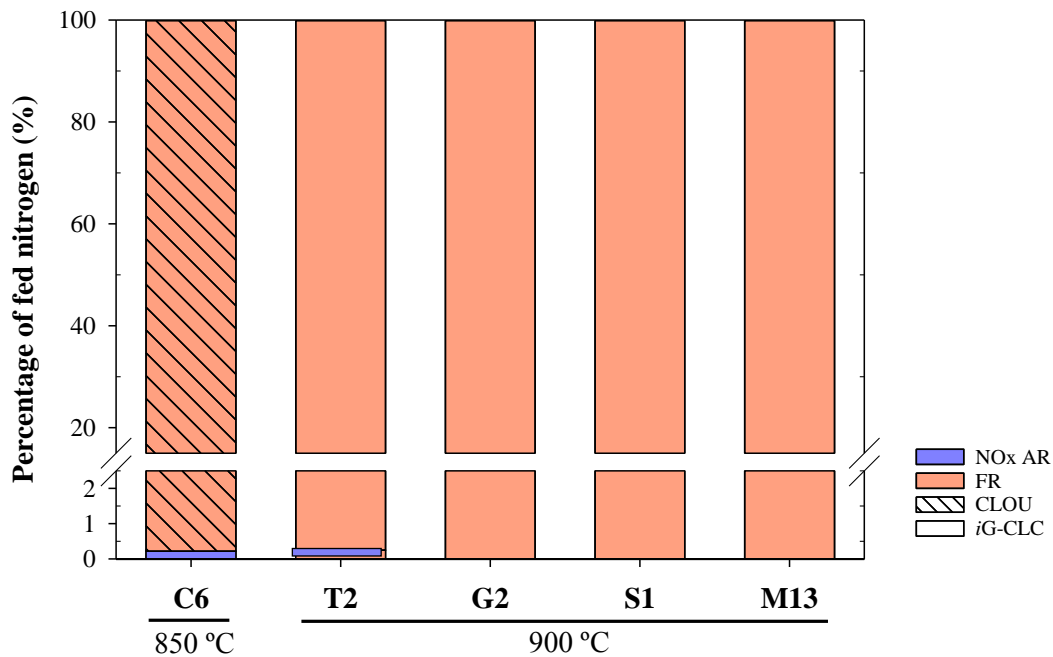
Figure 70. Fuel-N distribution between the fuel and the air reactor for iG-CLC and CLOU processes burning pine sawdust ($m_{FR}^*\approx$ 650-1250 kg/MW$_{th}$, norm. $\dot{m}_{OC}$=2.5-3.9 kg/(s·MW$_{th}$)).

Evolution of nitrogen species in the **fuel reactor**

Neither under *i*G-CLC nor under CLOU mode the presence of NH$_3$ or HCN was detected at the fuel reactor outlet. As it is shown in Table 16, only N$_2$, NO$_x$ and N$_2$O were identified depending on the conditions. This indicated that all the nitrogen released as NH$_3$ or HCN in the devolatilization was converted via homogenous or heterogeneous reactions.

Table 16. Nitrogen species found at the fuel reactor outlet in the iG-CLC and CLOU experiments.

iG-CLC	N$_2$, NO$_x$
CLOU	N$_2$, NO$_x$, N$_2$O

Both under *i*G-CLC and CLOU, the major nitrogen species found in the fuel reactor was N$_2$, followed by NO$_x$ and by certain amounts of N$_2$O, the later only in the case of CLOU experiments with the Cu34Mn66. The presence of N$_2$O can be

122

attributed to the temperature range of operation (775-850ºC) and the release of molecular oxygen in the fuel reactor atmosphere (Glarborg et al. 2003). Nevertheless, the concentration of N_2O in the fuel reactor outlet stream in the CLOU experiments decreased with temperature to values close to zero at 850ºC.

Among de different types of biomass, the nitrogen measured in the fuel reactor as N_2 in the experiments at the highest temperature (980 ºC) with the pine sawdust, olive stones and almond shells, were respectively, 97.2, 96.7 and 94.6 wt% with the Tierga ore under iG-CLC. The corresponding percentages under the CLOU mode with the Cu34Mn66 operating at 850ºC were respectively 97.3, 92.0 and 81.5 wt%, maintaining the same order of biomass types.

Regarding the amount of NO present in the fuel reactor outlet stream the value of the NO_x/C molar ratio was calculated in the experiments with pine sawdust in order to determine whether this ratio was lower than that recommended for CO_2 concentrated streams to be transported and stored with each oxygen carrier. The quality of the CO_2 to be captured can be affected by the presence of different compounds in the outlet stream from the fuel reactor. Steam, N_2, O_2, CO, H_2, CH_4 and other hydrocarbons, SO_2, particles and also NO_x levels should be controlled in order to ensure that the captured CO_2 stream can be transported and safely stored. To date, no legal requirements exist and only recommendations have been outlined for the quality of CO_2 (de Visser et al. 2008). The limit marked by these recommendations regarding NO_x/C molar ratio content in the CO_2 stream is 280 ppm, calculated with values in Table 4, see section 1.4. Figure 71 shows the different trends in the evolution of the molar ratio NO_x/C (expressed in ppm) with the fuel reactor temperature for both iG-CLC and CLOU. All the experiments presented were performed at comparable conditions with any of the oxygen carriers used, the ratio was well below the recommended value. The NO_x/C ratio increased with temperature in CLOU since more oxygen was released by the oxygen carrier with the increase of the fuel reactor temperature (Adánez-Rubio et al. 2017a). The presence of gaseous oxygen in the fuel reactor atmosphere favours fuel-N oxidation to NO (Williams et al. 2012).
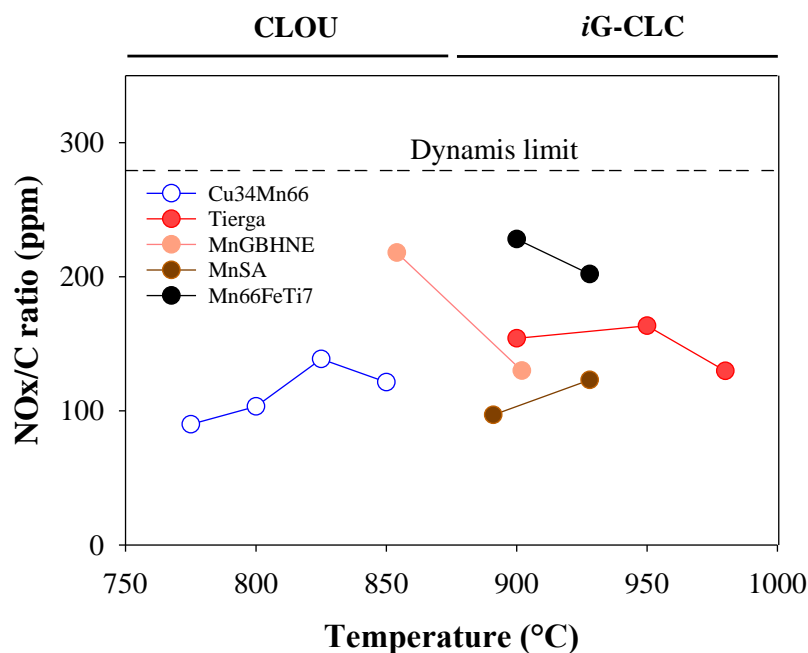
Figure 71. Effect of the fuel reactor temperature on the molar ratio NO$_x$/C for CLOU (open symbols) and iG-CLC (filled symbols) in experiments using pine sawdust (norm. $\dot{m}_{OC}$=3.1-3.9 kg/(s·MW$_{th}$)).

Evolution of nitrogen species in the **air reactor**

Both during *i*G-CLC and CLOU operation, the main nitrogen species besides N$_2$ found at the air reactor outlet was NO. In this case, no N$_2$O was detected. This NO is originated in the oxidation of the fuel-N present in the unconverted char that reaches the air reactor. Figure 72 shows the evolution of the NO concentration with the fuel reactor temperature. The NO concentrations have been normalized to 6% O$_2$ in the stream, as it is indicated in the legal emission limit. Results in Figure 72 correspond to pine sawdust but the trends for both operating modes, *i*G-CLC and CLOU, are the same for all the types of biomass tested. The NO emissions decreased when the fuel reactor temperature was increased. The reason for this trend is that an increase in the fuel reactor temperature enhances the char gasification. If more char is converted, less unconverted char is transferred to the air reactor. Thus, the fuel-N released in the air reactor is decreased. It should be taken into account that the NO present in the outlet stream of the air reactor can be considered an emission to the atmosphere and therefore, the levels should fulfil those specified in the current

124

legislation (European Council 2010). The Directive 2010/75/EU on industrial emissions (integrated pollution prevention and control) sets the NO_x emission most restrictive limit to 150 mg/Nm^3 (normalized to 6% O_2) for new installations in the EU and for the highest power (> 300 MW). Values shown in Figure 72 presented NO_x levels at the air reactor outlet in the range of 0-10 mg/Nm^3 for the CLOU and *i*G-CLC experiments with pine sawdust, then lower than legal limits. Thus, no emission problems could be anticipated when biomass was used as fuel in a CLC system. Moreover, these values were obtained in the absence of a carbon striper. If there was a carbon stripper, this would decrease the unconverted char bypassed to the air reactor and hence the NO_x formed in the air reactor.
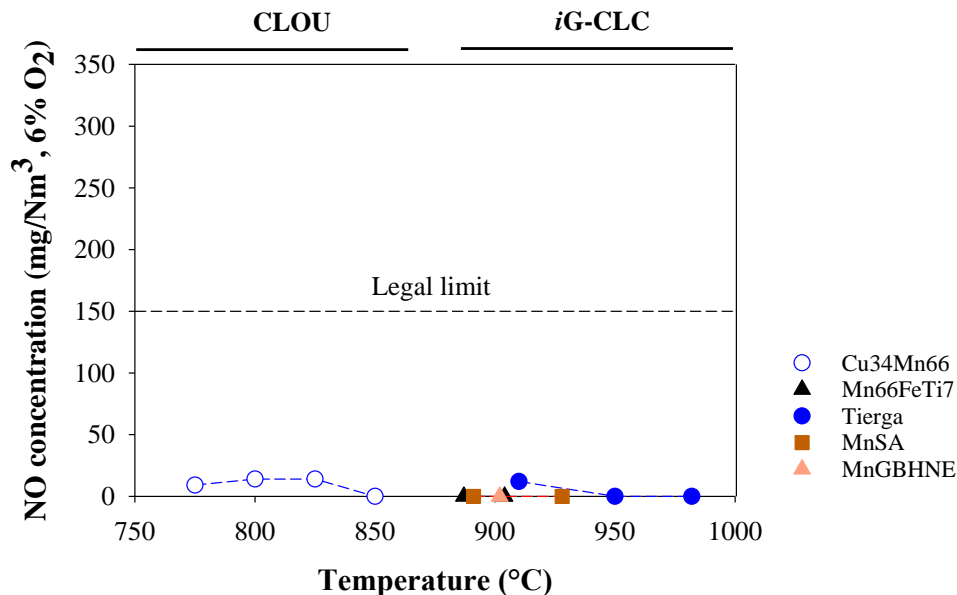
Figure 72. Effect of the fuel reactor temperature on the NO_x concentrations in mg/Nm^3 (6% O_2) at the air reactor outlet for CLOU (open symbols) and iG-CLC (filled symbols) processes burning pine sawdust.

3.1.4.3 Tar formation

Another aspect of the bioCLC process that was analysed in the present work was tar formation. Traditionally, tar formation control during gasification represented one of the main challenges in the use of biomass. Tar has been reported to cause fouling problems downstream of the gasification chamber and strict limits have been imposed for its presence when the syngas produced is intended to be used

for energy generation or chemicals production. In the case of the CLC process, scarce information about tar formation can be found. The presence of tar is limited to the fuel reactor outlet and it is therefore affecting the quality of the CO_2 stream there generated and the further operations prior to CO_2 storage (compression and transport). In the recommendations summarized by de Visser about CO_2 quality (de Visser et al. 2008), there is no clear reference to tar. Nevertheless, in order to set a range of values for safe operation, the limit given by (Reed et al. 1987) for compressing and piping any distance a biomass gasification gas can be used. According to these authors, the tar content should be lower than 0.5 g/Nm^3. The main results and conclusions about tar formation are summarized next. Some of these conclusions were already outlined in **Paper VI**.

In the experiments under *i*G-CLC and CLOU modes, the tar compounds at the fuel reactor outlet were detected and quantified. In these experiments, steam was used in the fuel reactor as fluidizing agent in *i*G-CLC and nitrogen in CLOU. Figure 73 plotted the tar compounds grouped as primary, secondary tertiary and alkyl-tertiary tars (Evans and Milne 1987a, 1987b) and also includes lineal hydrocarbons. Figure 73 shows the concentration values in the experiments with the different oxygen carriers tested, the three ores (iron and manganese based) and the Mn66FeTi7 at about 900-950 ℃ and the synthetic Cu34Mn66 at the highest temperature evaluated (825 ℃), all using pine sawdust.

Focusing in the *i*G-CLC measurements, Figure 73, it can be seen that similar types of compounds were obtained for both iron and MnGBHNE ores. Moreover, tertiary compounds were the major tar compounds followed by the alkyl-tertiary and secondary tars with both oxygen carriers. At these conditions, the total tar values obtained for the iron ore almost doubled those obtained for the MnGBHNE (3.8 g/Nm^3 and 1.9 g/Nm^3) mostly because of the reduction in the presence of alkyl-tertiary tar compounds. Furthermore, in the case of the iron ore, no significant differences were found among types of biomass, see (**Paper VI**). Similar behavior was found in the tar formation between S4 and P15, obtaining similar tar types despite the lower amount produced with the Mn66FeTi7 (0.4 g/Nm^3 and 0.2 g/Nm^3 respectively).

Recently, results from operation the in a boiler/gasifier loop (12 and 2-4 MW$_{th}$, respectively) at Chalmers University of Technology using ilmenite and a manganese ore as oxygen carriers with wood pellets reported 21-22 g tar per kg dry-ash-free fuel at 830 ºC (Berdugo Vilches et al. 2017). The values obtained in the present work were 8-13 times lower than those previously reported. Besides the different methodology employed in the tar collection and analysis, the differences can be also attributed to the higher temperatures used in the fuel reactor during gasification in the present work.
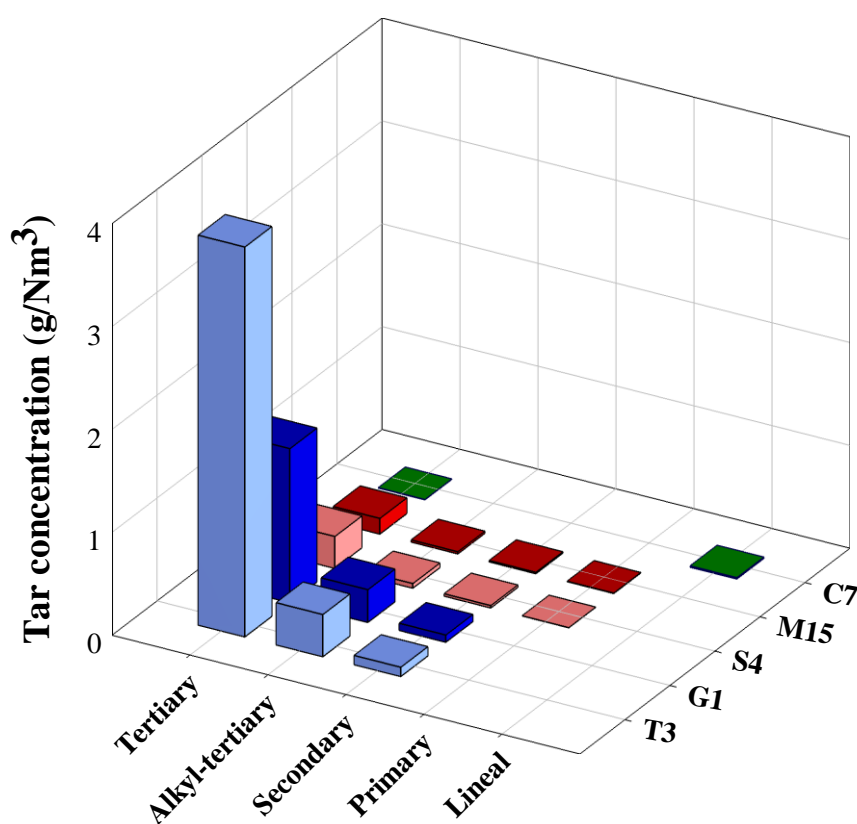
Figure 73. Effect of the fuel reactor temperature on the tar concentration using pine sawdust under CLOU and iG-CLC.

The tar concentration values obtained under *i*G-CLC were higher than those considered adequate to avoid operational problems derived from tar condensation and subsequent polymerization leading to fouling. Nevertheless, no fouling problems downstream can be anticipated in CLC due to the tar presence. In an industrial CLC unit tar compounds would be burned in the oxygen polishing step after the fuel

reactor. The amount of tar found in the experimental campaign performed, < 5 g/Nm^3, would represent an increase of about 1% in the total oxygen demand from the unburnt compounds in the fuel reactor outlet. Tertiary tars showed the higher concentrations with all the oxygen carriers used, showing also the major differences among oxygen carriers. Comparing both operating CLC modes, significant differences were found. First of all, the different levels of tar found. The values determined for CLOU were about two orders of magnitude lower (< 0.02 g/Nm^3) in a lower fuel reactor temperature interval (775-850ºC). These tar levels are so low that it should not represent a problem in the CO_2 transport-storage chain. Tar composition obtained in CLOU experiments showed some differences with respect to that obtained in *i*G-CLC. In the CLOU experiments, low amounts of naphthalene were found but certain quantities of linear or branched hydrocarbons are detected, such as dodecane or tetradecane. This may indicate a different mechanism for the consumption/reforming of the tar under CLOU environment when it is compared to *i*G-CLC. In any case, the combustion of biomass using both of any combustion modes results in lower tar content in the product gas stream than in conventional processes such as biomass air-fired gasification. Note that for an air-blown circulating fluidized bed (CFB) gasifier a typical tar content of about 10 g/Nm^3 has been reported (Anis and Zainal 2011).

3.2 Scale-up of the bioCLC process: Operation in a 20 kW$_{th}$ unit

The experience gained in the evaluation of the bioCLC process in the 1 kW$_{th}$ continuous unit is of great value for the scaling-up of the technology. The principal conclusion drawn from the experimental campaigns carried out was the need to reduce the high oxygen demand values obtained in the bioCLC process. This high oxygen demand values found, associated to the high volatile content of biomass. The high oxygen demand is a drawback in the development of the bioCLC process as costly measures should be taken in order to reach complete combustion of the fuel.

Bearing this idea in mind, an experimental campaign based on the Tierga ore as oxygen carrier was designed to be performed at the 20 kW$_{th}$ CLC unit existing at the *Instituto de Carboquímica* (ICB-CSIC) (García-Labiano et al. 2018). As it was mentioned, this unit consists of two interconnected circulating fluidized beds acting as fuel and air reactors, respectively. Table 17 summarizes the experiments carried out with Tierga ore and olive stones. The solid fuel conversion values obtained were in the range of 75-91%, which means that about 9-25% of the carbon in biomass leaked from the fuel reactor cyclone as elutriated char particles. A total of 60 hours of continuous hot fluidization were carried out, of which 20 hours corresponded to biomass combustion by *i*G-CLC mode using both H_2O and CO_2 as gasifying agent.

Table 17. Experimental conditions with the Tierga ore in the 20 kW$_{th}$ experimental unit.

Test	FA (-)	T_{FR} (ºC)	T_{AR} (ºC)	ϕ (-)	τ_{FR} (s)	$\dot{m}_{OC}$ (kg/h)	$\dot{m}_{sf}$ (kg/h)	P_{th} (kW$_{th}$)	m_{FR}^* (kg/MW$_{th}$)	$norm.\dot{m}_{OC}$ ((kg/s)/MW$_{th}$)
H1	H_2O	900	1000	1.1	164	60	1.1	5.1	540	3.1
H2	H_2O	900	1000	1.8	122	115	1.3	6.1	630	2.9
H3	H_2O	900	1000	1.8	158	90	1.0	4.8	850	4.9
H4	CO_2	900	1000	**1.8**	212	115	1.4	6.5	1000	1.5
H5	H_2O	900	1000	2.4	230	115	1.0	4.8	1550	4.1
H6	CO_2	900	1000	**2.4**	135	170	1.4	6.5	1035	3.0
H7	CO_2	900	1000	5.4	65	375	1.4	6.5	1050	3.1

Figure 74 shows the time evolution with the temperature and gas concentrations in both the fuel (dry and nitrogen free) and air reactors during tests H2-H4. The unit operation was smooth and the response to a gas flow change was quite quick. Solid flows and pressure drops were kept stable during the steady state operation. Steady state was usually reached on 20-30 min after operating conditions modification for every test, with roughly stable concentration values of CO_2, CO, H_2 and CH_4 in the fuel reactor, and O_2 and CO_2 in the air reactor. H4 uses CO_2 as gasifying agent, this explains the strong gap of unburned products (H_2, CO and CH_4) in the fuel reactor only because of the dilution process. It has to be considered that plots in Figure 74 correspond to dry and nitrogen free basis.
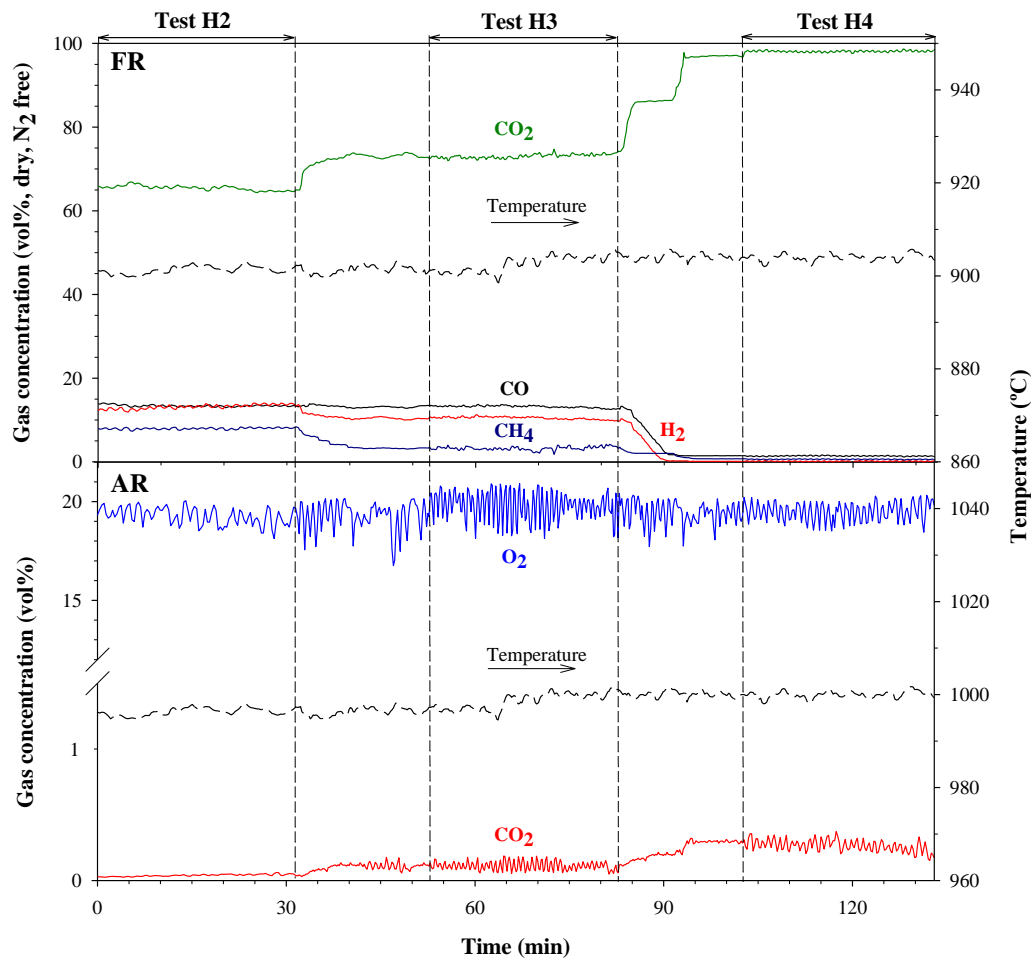
Figure 74. Time evolution of the temperature and gas concentrations in both fuel and air reactors during test H2, H3 and H4. Gas concentration values in the fuel reactor are given in dry basis and N2-free.

Evaluation of the CO2 capture efficiency

CO_2 capture efficiency is usually affected by several operating conditions in *i*G-CLC mode, such as the fuel reactor temperature, the carbon stripper separation efficiency and the solids circulation rate. It should be remembered that during the experimental campaign both the fuel reactor temperature and the carbon stripper separation efficiency were maintained. The fuel reactor temperature was set to 900 ºC to clearly observe changes on total oxygen demand as a consequence of the variations in the ϕ parameter and the specific solids inventory in the fuel reactor. In the latter case, the carbon stripper separation efficiency was set keeping constant the gas velocity at 0.35 m/s. This value should be enough to separate and return the

unconverted char particles to the fuel reactor (Abad et al. 2015a). Therefore, the CO_2 capture efficiency could only be affected by the solids circulation rate during this experimental campaign.

The solids circulation rate was modified in the range 60-375 kg/h, see Table 17. Figure 75 shows the variation of CO_2 capture efficiency as a function of the solids circulation rate in experiments using olive stones as solid fuel. Clearly, the CO_2 capture efficiency in the unit decreased as the solids circulation rate was increased, independently of the gasifying agent used. This is because a lower circulating solids flux entails higher residence times for the char particles in the fuel reactor, see Table 17. In addition, the type of gasifying agent used was also considered when CO_2 capture efficiency was assessed. No clear differences were found for the CO_2 capture efficiency in those tests where steam was introduced both to the fuel reactor and the carbon stripper in comparison with similar tests carried out with CO_2. Therefore, the use CO_2 as gasifying agent seems cannot be discarded considering the energy penalty of the use of H_2O. In this sense, solids circulation rates up to 150 kg/h should be maintained at 900 ºC to achieve CO_2 capture efficiencies above 95%, although these values would be improved operating at higher temperatures.
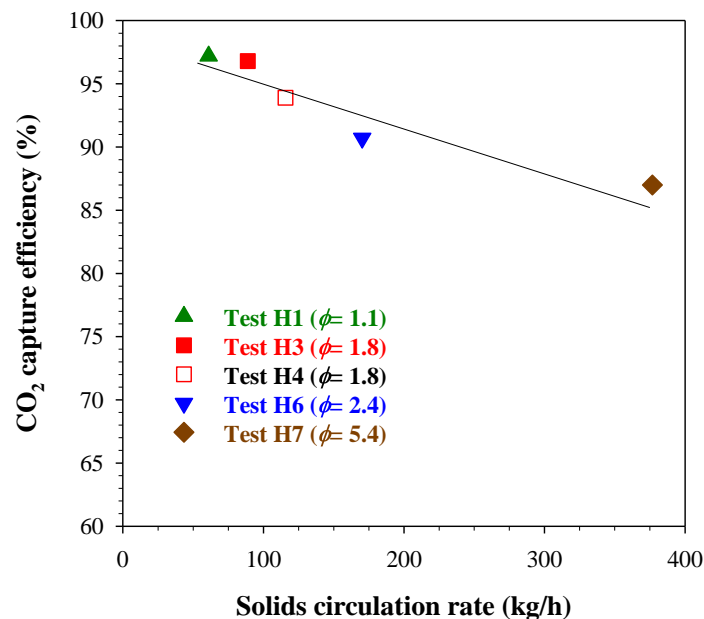
Figure 75. Effect of solids circulation rate on CO₂ capture efficiency during tests burning olive stones.

<u>*Evaluation of the Total oxygen demand*</u>

The total oxygen demand depends mainly of both the availability of oxygen and the solids inventory into the fuel reactor (Cuadrat et al. 2012; García-Labiano et al. 2013). Therefore, the effect of the oxygen carrier to fuel ratio (ϕ) and the specific solids inventory in the fuel reactor (m^*_{FR}) on the total oxygen demand was analyzed, see Figure 76.
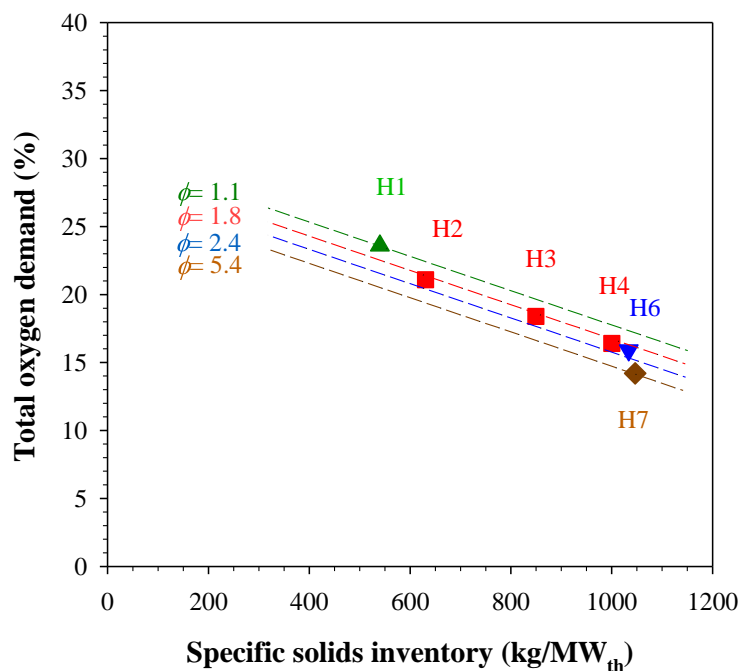
Figure 76. Effect of oxygen carrier to fuel ratio (ϕ) and specific solids inventory in the fuel reactor (m^*_{FR}) on total oxygen demand (Ω_T).

It was observed that when both the ϕ parameter and the specific solids inventory in the fuel reactor were increased, the total oxygen demand decreased. This can be observed comparing the tests H1 and H3, since they were performed feeding similar biomass to the CLC unit (~1 kg/h) and using steam as gasifying agent. The total oxygen demand decreased by 5 points (from 23.6% to 18.4%) when increasing the ϕ parameter from 1.1 to 1.8 and the solids inventory in the fuel reactor from 540 kg/MWth to 850 kg/MWth. The lowest total oxygen demand value ($\Omega_T = 14.8\%$) was obtained in test H7, which represents one of the lowest oxygen demand value

obtained during biomass combustion by iG-CLC in a continuous CLC unit (Schmitz and Linderholm 2018; Pikkarainen and Hiltunen 2017), excepting those tests using wood char as fuel (Linderholm and Schmitz, 2016; Schmitz et al. 2016).

Effect of the oxygen carrier to fuel ratio on the total oxygen demand

Figure 76 shows that the total oxygen demand was clearly decreased when the oxygen carrier to fuel ratio was increased. For a correct evaluation of the isolated effect of the ϕ parameter on the total oxygen demand, the rest of the operating conditions must be maintained constant. It was previously observed that the specific solids inventory in the fuel reactor greatly affected the total oxygen demand. But it should be also considered that other operating conditions such as the biomass feeding rate (m_{sf}) could affect the total oxygen demand by modifying the amount of unburned gases inside the fuel reactor. Thus, test H4, tests H6 and H7 were selected, since they were carried out at same fuel power input (6.5 kW$_{th}$), using the same gasifying agent (CO_2), and with a similar specific solids inventory (m_{OC}^* ~1000kg/MW$_{th}$). Increasing the ϕ value from 1.8 (test H4) to 2.4 (test H6) a decrease of the total oxygen demand by 2.5 points was achieved. Subsequently, the increase in the ϕ value from 2.4 to 5.4 in test H7 allowed a decrease of 1 additional point. Considering that volatile matter is the most influencing parameter on total oxygen demand, these results confirm that the decrease of the total oxygen demand observed when the ϕ parameter was increased was mainly due to the improvement on the volatile matter conversion to CO_2 and H_2O. This is in agreement with the work of Pérez-Vega et al. (2016), who observed a similar behavior burning coal by in the same CLC unit.

Effect of the fuel reactor specific solids inventory on the total oxygen demand

The isolated analysis of the effect of the specific solids inventory in the fuel reactor on the oxygen demand would require modifying other operating conditions, such as solids circulation rate, fuel power input, or total solids inventory in the CLC unit. Thus, the results obtained are consequence of the combined effect of several operating conditions. However, it should be kept in mind that the operating parameter

that mainly affects to the total oxygen demand is the oxygen carrier to fuel ratio. Thus, tests H2, H3 and H4 were selected because of the oxygen carrier to fuel ratio was set to 1.8 and the solids inventory in the fuel reactor was varied between 630 and 1000 kg/MW$_{th}$.

In test H2, a total oxygen demand of 21.1% was obtained for a specific solids inventory in the fuel reactor of 630 kg/MW$_{th}$. Figure 76 shows that total the oxygen demand decreased by 2.5 points in test H3 when increasing the specific solids inventory up to 850 kg/MW$_{th}$. In this case, the effect could be increased by the lower fuel power input used in test H3. It should be considered that a lower biomass feeding rate generates a lower amount of unconverted gases inside the fuel reactor, which could cause a decrease of the total oxygen demand. However, in test H4 the total oxygen demand decreased by 2 points with respect to test H3, in spite of the increase the biomass feeding rate in the CLC rig.

Further improvement in the performance of the 20 kW$_{th}$ unit will look for an increase of the CO$_2$ capture efficiency. For that, it would be necessary to raise both the fuel reactor temperature and the carbon stripper separation efficiency (e.g., by increasing the gas velocity). The increase of the fuel reactor temperature will drive to higher biomass char gasification rate but it will also to increase the reaction rate between the oxygen carrier and the gases present into the fuel reactor, which could reduce the total oxygen demand.

CONCLUSIONS

One of the actions for climate change mitigation is the substitution of fossil fuels by biofuels such as biomass in many thermo-chemical processes. Furthermore, when biofuels are combined with CCS processes, a negative emission technology known as BECCS is obtained. This group of technologies are able to produce energy while the CO_2 is captured, thus obtaining and selling carbon credits. The present work focused on the use of solid biofuels in a combustion technology with inherent carbon capture such as Chemical Looping Combustion (CLC) technology- the bioCLC process. A correct management of biomass resources converts biomass in an almost neutral fuel regarding CO_2 emissions. The work was carried out at the *Instituto de Carboquímica* in Zaragoza (Spain), including a four-month stay at the Institute of Solids Process Engineering and Particle Technology in the *Technische Universität Hamburg* (TUHH) in Hamburg (Germany). The experimental campaigns performed with different oxygen carriers and three types of biomass (pine sawdust, olive stones and almond shells) involved more than 220 h of continuous biomass combustion in both 1 kW_{th} and 20 kW_{th} continuous CLC units. This way, both *i*G-CLC and CLOU

operation modes were studied and the integration of biomass in CLC processes was assessed.

Five oxygen carriers were tested: three ores based in Fe or Mn (Tierga ore, MnGBHNE and MnSA) and the other two synthetic oxygen carriers (Fe-Mn and Mn-Cu mixed oxides: Mn66FeTi7 and Cu34Mn66). In this sense, the evaluation of the bioCLC performance was carried out and the effect of different operating variables was analyzed. Despite the different behavior of the oxygen carriers any of them could be dismissed for the bioCLC. Among types of biomass, no significant differences were obtained in the CLC performance with both CO_2 and steam as gasifying agents.

Almost 100% of CO_2 capture efficiency was obtained with all the low-cost oxygen carriers (Tierga, MnGBHNE and MnSA ores) without carbon stripper in the 1 kW_{th} CLC unit at different operating conditions. Focusing on the synthetic oxygen carriers, values about 100% of CO_2 capture efficiency were obtained during all the experimental campaign with the Mn66FeTi7 between 890 and 960 ºC into the fuel reactor. This fact confirmed the higher reactivity of the Mn66FeTi7 with the char since no CO_2 was measured in the air reactor outlet. CO_2 capture efficiency reached values up to 98% at operating temperatures in the fuel reactor as low as 850 ºC with Cu34Mn66.

High values of total oxygen demand (20-30 %) were observed for the Tierga ore. Slightly better values were obtained working the MnGBHNE at similar conditions, mainly because of the higher reactivity of with H_2. The higher reactivity of the MnSA compared with the MnGBHNE further contributed on the total oxygen demand reduction, reaching the lowest values in the present study working under iG-CLC mode (10.2 % with about 750 kg/MW_{th} and 930 ºC). Thus, this newly identified manganese mineral can be thought as an interesting low-cost oxygen carrier for further scale up. The molecular oxygen releasing capacity of Mn66FeTi7 could reduce the total oxygen demand values achieved with the Fe or Mn-based minerals. The oxygen release was favored by a low temperature of operation in the air reactor (880 ºC) and a high air excess ratio (λ^*=1.9). Under these conditions, oxygen demand

values of 4.6% were obtained with averaged solids inventories of 1875 kg/MW$_{th}$. The best results regarding oxygen demand were obtained with the Cu34Mn66 working under CLOU mode. In this case, no gaseous unburnt compounds were present in the fuel reactor outlet, even at the lowest temperature studied (775 ºC).

The possibility of dry recycling the outlet stream of the fuel reactor to the fuel reactor was evaluated in this work as a design solution for further oxygen demand reduction. In the conditions evaluated in this work, it is possible about a 30% reduction in the oxygen demand when the fuel reactor outlet stream is recirculated.

The presence of NO$_x$ and tar in the outlet streams of fuel and air reactor was studied under both iG-CLC and CLOU operation modes. During all the experiments, most the fuel-N appeared as N$_2$ at the fuel reactor outlet with only little presence of NO. About air reactor emissions, NO$_x$ concentrations never exceeded the legal limits for power plants. Working under iG-CLC mode, naphthalene was the major tar compound found in all the studied cases and for all the types of biomass. The tar contribution to the total oxygen demand was estimated about 1% of the oxygen needed to fully burn the fuel. Under CLOU mode, insignificant tar amounts were found although in this case also linear or branched hydrocarbons were detected.

Finally, biomass fueled CLC was demonstrated in a 20 kW$_{th}$ unit at 900 ºC using the Tierga iron ore with olive stones. CO$_2$ capture efficiencies above 95% were commonly obtained achieving values about 99.9% in some specific conditions. Total oxygen demands about 15-20% with specific solids inventory in the fuel reactor about 1000 kg/MW$_{th}$ were achieved. All these results demonstrate the promising possibilities of biomass fueled CLC (bioCLC) as a BECCS technology.

ABBREVIATIONS

AAEM	*Alkali and alkaline earth metals*
AR5	*Fifth Assessment Report*
BECCS	*Biomass energy with CO_2 Capture and Storage*
BET	*Brunauer-Emmett-Teller*
BFB	*Bubbling fluidized bed*
BP	*British Petroleum*
B2DS	*Beyond the two degrees scenario*
CCS	*CO_2 Capture and Storage*
CCU	*CO_2 Capture and Utilization*
CFB	*Conference of the Parties*
CFB	*Circulating Fluidized bed*
CFCs	*Chlorofluorocarbon Substances*
CL	*Chemical Looping*
CLC	*Chemical Looping Combustion*
CLG	*Chemical Looping Gasification*
CL*a*OU	*Chemical Looping Combustion assisted by Oxygen Uncoupling*
CLOU	*Chemical Looping Combustion with Oxygen Uncoupling*
CLC	*Chemical Looping Reforming*
COP	*Conference of the parties*
CUT	*Chalmers University of Technology*
DAC	*Direct Air Capture*
DACCS	*Direct Air CO_2 Capture and Storage*
EOR	*Enhancing Oil Recovery*
EU	*European Union*
EuTrace	*European Transdisciplinary Assessment on Climate Engineering*

FA	*Fluidizing Agent*
FID	*Flame ionization detector*
GDP	*Gross Domestic Product*
GHG	*Greenhouse Gases*
GISS	*Goddard Institute for Space Studies*
GNI	*Gross National Income*
GWP	*Global Warming Potential*
HUT	*Hamburg University of Technology*
ICB-CSIC	*Instituto de Carboquímica – Consejo Superior de Investigaciones Científicas*
IEA	*International Energy Agency*
*i*G-CLC	*In situ Gasification-Chemical Looping Combustion*
IPCC	*Intergovernmental Panel on Climate Change*
LCA	*Life Cycle Analysis*
LHV	*Low Heating Value (kJ/kg)*
MSW	*Municipal Solid Waste*
NDC	*Nationally Determined Contribution*
NDIR	*Nondispersive infrared sensor*
NET	*Negative Emission Technology*
OECD	*Organization for Economic Co-operation and Development*
RCP	*Representative Concentration Pathway*
SEM	*Scanning electronic microscopy*
SINTEF	*Stiftelsen for industriell og teknisk forskning*
SRM	*Solar Radiation Management*
STP	*Standard temperature and pressure*
SB	*Spouted bed*
SU	*Southeast University*

TCD	*Thermal conductivity* detector
TGA	*Thermogravimetric Analyzer*
TUD	*Darmstadt* University *of Technology*
UN	*United Nations*
UNEP	*United Nations Environmental Program*
UNFCCC	*United Nations Framework Convention on Climate Change*
USA	*United States of America*
VTT	VTT *Technical Research Centre of Finland*
XRD	*X-Ray Diffractometer*
2DS	*Two degrees scenario*

SYMBOLS

F_i	mol/s	Molar flow of component i in the air reactor outlet
g	m/s^2	Gravity
m	kg	Oxygen carrier mass at any time
m^*	kg/MW_{th}	Specific solids inventory
m_{OC}	kg	Mass of oxygen carrier
m_{Ox}	kg	Oxygen carrier mass fully oxidized
m_{Red}	kg	Oxygen carrier mass fully reduced
$\dot{m}_{OC}$	kg/s	Oxygen carrier circulating rate
$\dot{m}_{sf}$	kg/s	Solid fuel mass flow
M_i	kg/mol	Molecular mass of component i
$norm.\dot{m}_{OC}$	$kg/(s \cdot MW_{th})$	Normalized solids circulation rate
P_{th}	MW_{th}	Power input
R_{OC}	-	Oxygen transport capacity
S	m^2	Surface area
t	s	Time
T	K	Temperature
X_{char}	-	Char conversion
X_{Ox}	-	Oxygen carrier conversion for oxidation
X_{Red}	-	Oxygen carrier conversion for reduction
χ	-	Conversion
y_{O_2}	-	Oxygen concentration

143

Greek letters

ΔP	Pa	Pressure drop
ϕ	-	Oxygen carrier to fuel molar ratio
λ^*	-	Air excess in the air reactor
η_{CC}	-	CO_2 capture efficiency
$\eta_{comb,FR}$	-	Combustion efficiency
τ_{FR}	s	Mean residence time of particles in the fuel reactor
Ω_{sf}	kg/kg	Stoichiometric oxygen for the solid fuel full conversion
Ω_T	-	Total oxygen demand
Ω_{tar}	-	Tar oxygen demand

Subscripts

AR	Air reactor
elu	Elutriated
FR	Fuel reactor
in	Inlet
OC	Oxygen carrier
out	outlet
sf	Solid fuel
vol	Volatiles

REFERENCES

Abad, A., Adánez-Rubio, I., Gayán P., García-Labiano, F., de Diego, L. F. and Adánez, J. **2012**. "Demonstration of Chemical-Looping with Oxygen Uncoupling (CLOU) Process in a 1.5 kW$_{th}$ Continuously Operating Unit Using a Cu-Based Oxygen-Carrier." International Journal of Greenhouse Gas Control 6 (January): 189–200.

Abad, A., Pérez-Vega, R., de Diego, L. F., García-Labiano, F., Gayán, P. and Adánez, J. **2015a**. "Design and Operation of a 50 kW$_{th}$ Chemical Looping Combustion (CLC) Unit for Solid Fuels." Applied Energy 157: 295–303.

Abad, A., Adánez, J., Gayán, P., de Diego, L. F., García-Labiano, F. and Sprachmann, G. **2015b**. "Conceptual Design of a 100 MW$_{th}$ CLC Unit for Solid Fuel Combustion." Applied Energy 157: 462–74 .

Abad, A., Gayán, P., Mendiara, T., Bueno, J. A., García-Labiano, F., de Diego, L. F. and Adánez, J. **2018**. "Assessment of the Improvement of Chemical Looping Combustion of Coal by Using a Manganese Ore as Oxygen Carrier." Fuel Processing Technology 176 (July): 107–18.

Adánez, J., de Diego, L. F., García-Labiano, F. and Gayán, P., Abad, A. and Palacios, J. M. **2004**. "Selection of Oxygen Carriers for Chemical-Looping Combustion." Energy Fuels 18: 371–77.

Adánez, J., Abad, A., García-Labiano, F., Gayán, P. and L. F. de Diego. **2012**. "Progress in Chemical-Looping Combustion and Reforming Technologies." Progress in Energy and Combustion Science 38 (2): 215–82.

Adánez, J., Abad, A., Mendiara, T., Gayán, P., de Diego, L. F. and García-Labiano, F. **2018**. "Chemical Looping Combustion of Solid Fuels." Progress in Energy and Combustion Science 65 (March): 6–66.

Adánez, J., and Abad, A. **2019**. "Chemical-Looping Combustion: Status and Research Needs." Proceedings of the Combustion Institute 37 (4): 4303–17.

Adánez-Rubio, I., Abad, A., Gayán, P., de Diego, L. F., García-Labiano, F. and Adánez, J. **2014**. "Biomass Combustion with CO_2 Capture by Chemical Looping with Oxygen Uncoupling (CLOU)." Fuel Processing Technology 124 (August): 104–14.

Adánez-Rubio, I., Abad, A., Gayán, P., Adánez I., de Diego, L. F., García-Labiano, F. and Adánez, J. **2016**. "Use of Hopcalite-Derived Cu–Mn Mixed Oxide as Oxygen Carrier for Chemical Looping with Oxygen Uncoupling Process." Energy & Fuels 30 (7): 5953–63.

REFERENCES

Adánez-Rubio, I., Abad, A., Gayán, P., García-Labiano, F., de Diego, L. F., and Adánez, J. **2017a**. "Coal Combustion with a Spray Granulated Cu-Mn Mixed Oxide for the Chemical Looping with Oxygen Uncoupling (CLOU) Process." Applied Energy 208 (December): 561–70.

Adánez-Rubio, I., Izquierdo, M. T., Abad, A., Gayán, P., de Diego, L. F. and Adánez J. **2017b**. "Spray Granulated Cu-Mn Oxygen Carrier for Chemical Looping with Oxygen Uncoupling (CLOU) Process." International Journal of Greenhouse Gas Control 65 (October): 76–85.

Adánez-Rubio, I., Abad, A., Gayán, P., de Diego, L. F. and Adánez, J. **2018**. "CLOU Process Performance with a Cu-Mn Oxygen Carrier in the Combustion of Different Types of Coal with CO_2 Capture." Fuel 212 (January): 605–12.

ALINNE. **2019**. "Análisis Del Potencial de Desarrollo de Tecnologías Energéticas. Captura, Transporte, Almacenamiento, Usos y Transformación Del CO_2." Ejercicio APTE 2017-2018, 1–45.

Anis, S. and Zainal Z. A. **2011**. "Tar Reduction in Biomass Producer Gas via Mechanical, Catalytic and Thermal Methods: A Review." Renewable and Sustainable Energy Reviews 15 (5): 2355–77.

Azimi, G., Rydén, M., Leion, H., Mattisson, T. and Lyngfelt, A. **2013**. "$(Mn_zFe_{1-z})_yO_x$ Combined Oxides as Oxygen Carrier for Chemical-Looping with Oxygen Uncoupling." AIChE Journal 59 (2): 582–88.

Berdugo Vilches, T., Rydén, M. and Thunman, H. **2017**. "Experience of More than 1000 h of Operation with Oxygen Carriers and Solid Biomass at Large Scale." Applied Energy 190 (March): 1174–83.

BP. **2019**. "BP Energy Outlook 2019 Edition." BP Energy Outlook 2019. https://www.bp.com/content/dam/bp/business-sites/en/global/corporate/pdfs/energy-economics/energy-outlook/bp-energy-outlook-2019.pdf.

Brown, A. and Le Feuvre, P. **2017**. "Technology Roadmap: Delivering Sustainable Bioenergy." International Energy Agency (IEA), 94.

Cabello, A., Gayán, P., García-Labiano, F., de Diego, L.F., Abad, A. and Adánez, J. **2016**. "On the Attrition Evaluation of Oxygen Carriers in Chemical Looping Combustion." Fuel Processing Technology 148 (July): 188–97.

Consoli, C. **2019**. "2019 Perspective. Bioenergy and Carbon Capture and Storage." Global CCS Institute, 1–14.

Cook, E. L. **1971**. "The Flow of Energy in an Industrial Society." Scientific American 225 (3): 135-42.

Cuadrat, A., Abad, A., García-Labiano, F., Gayán, P., de Diego, L. F. and Adánez, J. **2011**. "The Use of Ilmenite as Oxygen-Carrier in a 500 W_{th} Chemical-Looping

Coal Combustion Unit." International Journal of Greenhouse Gas Control 5: 1630–42.

Cuadrat, A., Abad, A., García-Labiano, F., Gayán, P., de Diego, L. F. and Adánez J. **2012**. "Effect of Operating Conditions in Chemical-Looping Combustion of Coal in a 500 W_{th} Unit." International Journal of Greenhouse Gas Control 6: 153–63.

Ehrlich, P. R., Kareiva, P. M. and Daily, G. C. **2012**. "Securing Natural Capital and Expanding Equity to Rescale Civilization." Nature 486 (7401): 68–73.

European Commission. **2018**. Final Report of the High-Level Panel of the European Decarbonisation Pathways Initiative. 978–92–79–96826–6.

European Council. **2010**. "Directive 2010/75/EU Industrial Emissions." Official Journal of the European Union. https://doi.org/10.3000/17252555.L_2010.334.eng.

Evans, R. J. and Milne, T. A. **1987a**. "Molecular Characterization of the Pyrolysis of Biomass." Energy & Fuels 1 (2): 123–37.

Evans, R. J. and Milne, T. A. **1987b**. "Molecular Characterization of the Pyrolysis of Biomass. 2. Applications." Energy & Fuels 1 (4): 311–19.

Fourier, J. B. J. **1824**. "Remarques Générales Sur Les Températures Du Globe Terrestre Et Des Espaces Planétaires." Annales de Chimie et de Physique 27: 136–67.

Fuss, S., Lamb, W. F., Callaghan, M. W., Hilaire, J., Creutzig, F., Amann, T., Beringer, T. et al. **2018**. "Negative Emissions—Part 2: Costs, Potentials and Side Effects." Environmental Research Letters 13 (6): 063002.

García-Labiano, F., de Diego, L. F., Gayán, P., Abad A. and Adánez, J. **2013**. "Fuel Reactor Modelling in Chemical-Looping Combustion of Coal: 2-Simulation and Optimization." Chemical Engineering Science 87: 173–82.

García-Labiano, F., Pérez-vega, R., Pérez-Astray, A., Mendiara, T., de Diego, L. F. and Izquierdo, M. T. **2018**. "Chemical Looping Combustion of Biomass in a 50 kW_{th} Unit." In 5th CLC Conference, Park City, Utah, USA.

Gaston, K. J. and Spicer, J. I. **2009**. Biodiversity: An Introduction. Planet Earth. Second edition. University of Chicago Press, Chicago, 2008 . 217 pp. https://doi.org/10.1111/j.1442-9993.2009.01985.x.

Gayán, P., Abad, A., de Diego, L. F., García-Labiano, F. and Adánez, J. **2013**. "Assessment of Technological Solutions for Improving Chemical Looping Combustion of Solid Fuels with CO_2 Capture." Chemical Engineering Journal 233 (November): 56–69.

REFERENCES

Ge, H., Guo, W., Shen, L., Song, T. and Xiao, J. **2016**. "Biomass Gasification Using Chemical Looping in a 25 kW_{th} Reactor with Natural Hematite as Oxygen Carrier." Chemical Engineering Journal 286 (February): 174–83.

Glarborg, P, Jensen, A. D. and Johnsson, J. E. **2003**. "Fuel Nitrogen Conversion in Solid Fuel Fired Systems." Progress in Energy and Combustion Science 29 (2): 89–113. https://doi.org/10.1016/S0360-1285(02)00031-X.

Gogolev, I., Linderholm, C., Gall, D., Schmitz, M., Mattisson, Pettersson, T., J. B. C. and Lyngfelt, A. **2019**. "Chemical-Looping Combustion in a 100 kW Unit Using a Mixture of Synthetic and Natural Oxygen Carriers – Operational Results and Fate of Biomass Fuel Alkali." International Journal of Greenhouse Gas Control 88 (September): 371–82.

Guandalini, G., Romano, M. C., Ho, M., Wiley, D., Rubin, E. S. and Abanades, J. C. **2019**. "A Sequential Approach for the Economic Evaluation of New CO_2 Capture Technologies for Power Plants." International Journal of Greenhouse Gas Control 84 (May): 219–31.

Haiming G., Shen, L., Xiao, J., Zhang, S. and Song, T. **2011**. "Chemical Looping Combustion of Biomass/Coal with Natural Iron Ore as Oxygen Carrier in a Continuous Reactor." Energy & Fuels 25 (1): 446–55.

Haiming, G., Shen, L., Zhong, Z., Zhou, Y., Liu, W., Niu, X., Ge, H., Jiang, S. and Wang L. **2015**. "Interaction between Biomass Ash and Iron Ore Oxygen Carrier during Chemical Looping Combustion." Chemical Engineering Journal 277 (October): 70–78.

Hanning, M., Frick, V., Mattisson, T., Rydén, M. and Lyngfelt, A. **2016**. "Performance of Combined Manganese–Silicon Oxygen Carriers and Effects of Including Titanium." Energy & Fuels 30 (February): 1171–82.

Hanning, M., Corcoran, A., Lind, F. and Rydén, M. **2018**. "Biomass Ash Interactions with a Manganese Ore Used as Oxygen-Carrying Bed Material in a 12 MW_{th} CFB Boiler." Biomass and Bioenergy 119 (December): 179–90.

Haus, J., Feng, Y., Hartge, E. U., Heinrich, S. and Werther, J. **2018**. "High Volatiles Conversion in a Dual Stage Fuel Reactor System for Chemical Looping Combustion of Wood Biomass." In , 1–13. I International Conference on CO_2 Negative Emissions. 22-24 May 2018, Goteborg, Sweeden.

Hildor, F., Mattisson, T., Leion, H., Linderholm, C. and Rydén, M. **2019**. "Steel Converter Slag as an Oxygen Carrier in a 12 MW_{th} CFB Boiler – Ash Interaction and Material Evolution." International Journal of Greenhouse Gas Control 88 (September): 321–31.

Hosseini, D., Imtiaz, Q., Abdala, P. M., Yoon, S., Kierzkowska, A. M., Weidenkaff, A. and Müller, C. R. **2015**. "CuO Promoted Mn_2O_3 -Based Materials for Solid Fuel Combustion with Inherent CO_2 Capture." Journal of Materials Chemistry A 3 (19): 10545–50.

IDAE. **2011**. "Plan de Energías Renovables 2011-2020." Instituto para la Diversificación y Ahorro de la Energía: 1–824.

IEA. **2016**. "Energy Technology Perspectives 2016: Towards Sustainable Urban Energy Systems" OECD/IEA, no. May. 1–418.

IEA. **2018**. "Global Energy and CO_2 Status Report." OECD/IEA, no. March. 1–28 https://www.iea.org/publications/freepublications/publication/GECO2017.pdf

INC. **2018**. "Nuts and Dried Fuits Statistical Yearbook 2017/2018.". International Nut and Dried Fruit Council Foundation. 1–80.

IOOC. **2018**. International Olive Oil Council. http://www.internationaloliveoil.org

IPCC. **2005**. B. Metz, O. Davidson, H. de Coninck, M. Loos and L. Meyer (Eds.) "Carbon Dioxide Capture and Storage" Cambridge University Press, UK. 431 pp. Cambridge University Press, The Edinburgh Building Shaftesbury Road, Cambridge.

IPCC. **2013**. "Summary for Policymakers. In: Climate Change 2013: The Physical Science Basis." Contribution of Working Group I to the Fifth Assessment Report of the Intergovernmental Panel on Climate Change.

IPCC. **2014**. Climate Change 2014: Synthesis Report. Contribution of Working Groups I, II and III to the Fifth Assessment Report of the Intergovernmental Panel on Climate Change. Core Writing Team, Pachauri, R.K. and Meyer, L.A. Geneva, Switzerland. 1–151.

Ishida, M., Zheng, D. and Akehata, T. **1987**. "Evaluation of a Chemical-Looping-Combustion Power-Generation System by Graphic Exergy Analysis." Energy 12 (2): 147–54.

Ishida M. and Jin, H. **1996**. "A Novel Chemical-Looping Combustor without NO_x Formation." https://doi.org/10.1021/IE950680S.

Ishida M., Jin, H. and Okamoto, T. **1996**. "A Fundamental Study of a New Kind of Medium Material for Chemical-Looping Combustion." Energy & Fuels 10 (4): 958–63.

Jackson, R. **2019**. "Eunice Foote, John Tyndall and a Question of Priority." Notes and Records: The Royal Society Journal of the History of Science, February.

Jiang, S., Shen, L., Niu, X., Ge, H. and Haiming G. **2016**. "Chemical Looping Co-Combustion of Sewage Sludge and Zhundong Coal with Natural Hematite as the Oxygen Carrier." Energy and Fuels 30: 1720–29.

Jiang, S. Shen, L., Yan, J., Ge H. and Song, T. **2018**. "Performance in Coupled Fluidized Beds for Chemical Looping Combustion of CO and Biomass Using Hematite as an Oxygen Carrier." Energy & Fuels 32 (12): 12721–29.

Jing, D, Arjmand, M., Mattisson, T., Rydén, M., Snijkers, F., Leion, H. and Lyngfelt, A. **2014**. "Examination of Oxygen Uncoupling Behaviour and Reactivity towards Methane for Manganese Silicate Oxygen Carriers in Chemical-Looping Combustion." International Journal of Greenhouse Gas Control 29 (October): 70–81.

Jones, P. D. and Harpham, C. **2013**. "Estimation of the Absolute Surface Air Temperature of the Earth." Journal of Geophysical Research: Atmospheres 118 (8): 3213–17.

Kander, A., Malanima, P. and Warde, P. **2014**. Power to the People: Energy in Europe over the Last Five Centuries. Princeton and Oxford: Princeton University Press, 457 pp.

Keeling, C. D., Piper, S. C., Bacastow, R. B., Wahlen, M., Whorf, T. P., Heimann, M. and Meijer, H. A. Atmospheric CO_2 and $^{13}CO_2$ exchange with the terrestrial biosphere and oceans from 1978 to 2000: observations and carbon cycle implications, 83–113, in "A History of Atmospheric CO_2 and its effects on Plants, Animals, and Ecosystems", **2005**. Ed. Ehleringer, J.R., T. E. Cerling, M. D. Dearing, Springer, New York.

Kobayashi, N. and Fan, L. S. **2011**. "Biomass Direct Chemical Looping Process: A Perspective." Biomass and Bioenergy 35 (3): 1252–62.

Kramp, M. **2014**. "Chemical Looping Combustion in Interconnected Fluidized Bed Reactors: Simulation and Experimental Validation." 181 pp, Dissertation Technische Universität Hamburg-Harburg (2014). Ed. Dr. Hut.

Kump, L. R., Kasting, J. F. and Crane R. G. **2004**. "The Earth System. " Prentice Hall; 2 edition (August 16, 2003), 432 p.

Langørgen, Ø., and Saanum, I. **2018**. "Chemical Looping Combustion of Wood Pellets in a 150 kW_{th} CLC Reactor." In, 1–10. Gothemborg, Sweeden.

Leion, H., Jerndal, E., Steenari, B. M., Hermansson, S., Israelsson, M., Jansson, E., Johnsson, M., et al. **2009a**. "Solid Fuels in Chemical-Looping Combustion Using Oxide Scale and Unprocessed Iron Ore as Oxygen Carriers." Fuel 88 (10): 1945–54.

Leion, H., Larring, Y., Bakken, E., Bredesen, R., Mattisson, T. and Lyngfelt, A. **2009b**. "Use of $CaMn_{0.875}Ti_{0.125}O_3$ as Oxygen Carrier in Chemical-Looping with Oxygen Uncoupling." Energy & Fuels 23 (10): 5276–83.

Leion, H., Mattisson, T. and Lyngfelt A. **2011**. "Chemical Looping Combustion of Solid Fuels in a Laboratory Fluidized-Bed Reactor." Oil & Gas Science and Technology – Revue d'IFP Energies Nouvelles 66 (2): 201–8.

Leion, H., Knutsson P. and Steenari B.M. **2017**. "Experimental Evaluation of Interactions between K, Ca, and P and Mn/Si-Based Oxygen Carriers." In 25th

European Biomass Conference and Exhibition Proceedings. Stockholm (Sweden).

Lewis, W. K., and Gilliland, E. R. **1954**. "Production of Pure CO_2," November. https://patents.google.com/patent/US2665972A/en.

Linderholm, C., Schmitz, M., Knutsson, P., Källén, M. and Lyngfelt A. **2014**. "Use of Low-Volatile Solid Fuels in a 100 KW Chemical-Looping Combustor." Energy and Fuels 28: 5942–52.

Linderholm, C. and Schmitz, M. **2016**. "Chemical-Looping Combustion of Solid Fuels in a 100 kW Dual Circulating Fluidized Bed System Using Iron Ore as Oxygen Carrier." Journal of Environmental Chemical Engineering 4: 1029–39.

Lyngfelt, A. and Leckner, B. **2015**. "A 1000 MW_{th} Boiler for Chemical-Looping Combustion of Solid Fuels – Discussion of Design and Costs." Applied Energy 157: 475–87.

Malanima, P. **2014**. "The Basic Environmental History." Edited by Mauro Agnoletti and Simone Neri Serneri. Springer International, Environmental History, 4 (10): 52-5302-52–5302.

Mattisson, T., Lyngfelt, A. and Leion, H. **2009**. "Chemical-Looping with Oxygen Uncoupling for Combustion of Solid Fuels." International Journal of Greenhouse Gas Control 3 (1): 11–19.

Mattison, T., Hildor, F., Li, Y. and Linderholm, C. **2019**. "Negative Emissions of Carbon Dioxide through Chemical-Looping Combustion (CLC) and Gasification (CLG) Using Oxygen Carriers Based on Manganese and Iron." Mitigation and Adaptation Strategies for Global Change, April, 1–21.

Mei, D., Mendiara, T., Abad, A., de Diego, L. F., García-Labiano, F., Gayán, P., Adánez, J. and Zhao, H. **2015**. "Evaluation of Manganese Minerals for Chemical Looping Combustion." Energy and Fuels 29 (10): 6605–15.

Mei, D., Mendiara, T., Abad, A., de Diego, L. F., García-Labiano, F., Gayán, P., Adánez, J. and Zhao, H. **2016**. "Manganese Minerals as Oxygen Carriers for Chemical Looping Combustion of Coal." Industrial and Engineering Chemistry Research. 8 June 201655, (22): 6539–46.

Mendiara, T., Pérez, R., Abad, A., de Diego, L. F., García-Labiano, F., Gayán, P. and Adánez, J. **2012**. "Low-Cost Fe-Based Oxygen Carrier Materials for the *i*G-CLC Process with Coal. 1." Industrial and Engineering Chemistry Research 51: 16216–29.

Mendiara, T., Abad, A., de Diego, L. F., García-Labiano, F., Gayán, P. and Adánez, J. **2013a**. "Biomass Combustion in a CLC System Using an Iron Ore as an Oxygen Carrier." International Journal of Greenhouse Gas Control 19: 322–30.

REFERENCES

Mendiara, T., de Diego, L. F., García-Labiano, F., Gayán, P., Abad, A. and Adánez, J. **2013b**. "Behaviour of a Bauxite Waste Material as Oxygen Carrier in a 500 W_{th} CLC Unit with Coal." International Journal of Greenhouse Gas Control 17: 170–82.

Mendiara, T., de Diego, L.F., García-Labiano, F., Gayán, P., Abad, A. and Adánez, J. **2014a**. "On the Use of a Highly Reactive Iron Ore in Chemical Looping Combustion of Different Coals." Fuel 126 (June): 239–49.

Mendiara, T., Izquierdo, M.T., Abad, A., de Diego, L.F., García-Labiano, F., Gayán, P., and Adánez, J. **2014b**. "Release of Pollutant Components in CLC of Lignite." International Journal of Greenhouse Gas Control 22 (March): 15–24.

Mendiara, T., García-Labiano, F., Abad, A., Gayán, P., de Diego, L. F., Izquierdo, M. T. and Adánez J. **2018a**. Negative CO_2 emissions through the use of biofuels in chemical looping technology: A review, 232 Applied Energy 657–84.

Mendiara, T., Pérez-Astray, A., Izquierdo, M.T., Abad, A., de Diego, L. F., García-Labiano, F., Gayán, P. and Adánez J. **2018b**. "Chemical Looping Combustion of Different Types of Biomass in a 0.5 kW_{th} Unit." Fuel 211 (January): 868–75.

Miller, R. L., Schmidt, G. A., Nazarenko, L. S., Tausnev, N., Bauer, S. E., del Genio, A. D. Kelley, M. et al. **2014**. "CMIP5 Historical Simulations (1850-2012) with GISS ModelE2." Journal of Advances in Modeling Earth Systems 6 (2): 441–78.

Mohammad P., N., Leion, H., Rydén, M. and Mattisson T. **2013**. "Combined Cu/Mn Oxides as an Oxygen Carrier in Chemical Looping with Oxygen Uncoupling (CLOU)." Energy & Fuels 27 (10): 6031–39.

Moldenhauer, P, Linderholm, C., Rydén, M. and Lyngfelt A. **2019**. "Avoiding CO_2 Capture Effort and Cost for Negative CO_2 Emissions Using Industrial Waste in Chemical-Looping Combustion/Gasification of Biomass." Mitigation and Adaptation Strategies for Global Change, March, 1–24.

Neves, D., Thunman, H., Matos, A., Tarelho, L. and Gómez-Barea A. **2011**. "Characterization and Prediction of Biomass Pyrolysis Products." Progress in Energy and Combustion Science 37 (5): 611–30.

Nigam, P. S. and Singh A. **2011**. "Production of Liquid Biofuels from Renewable Resources." Progress in Energy and Combustion Science 37 (1): 52–68.

Niu, X., Shen, L., Haiming G., Jiang, S. and Xiao J. **2015**. "Characteristics of Hematite and Fly Ash during Chemical Looping Combustion of Sewage Sludge." Chemical Engineering Journal 268: 236–44.

152

Ohlemüller, P., Ströhle, J. and Epple B. **2017**. "Chemical Looping Combustion of Hard Coal and Torrefied Biomass in a 1 MW$_{th}$ Pilot Plant." International Journal of Greenhouse Gas Control 65: 149–59.

Pérez-Astray, A, Mendiara T, Abad A, García-Labiano F, de Diego L. F., Izquierdo M. T., Adánez J. **2019a**. "Manganese Ores as Low-Cost Oxygen Carriers for Biomass Chemical Looping Combustion in a 0.5 kW$_{th}$ Unit". Submitted to Fuel Processing Technology.

Pérez-Astray, A, Mendiara T, Abad A, García-Labiano F, de Diego L. F., Izquierdo M. T., Adánez J. **2019b**. "CLC of Biomass as a BECCS Technology Using a Manganese-Iron Mixed Oxide". Submitted to Sep. Purif. Technol.

Pérez-Vega, R., Abad, A., Izquierdo, M. T., Gayán, P., de Diego, L. F. and Adánez J. **2019**. "Evaluation of Mn-Fe Mixed Oxide Doped with TiO$_2$ for the Combustion with CO$_2$ Capture by Chemical Looping Assisted by Oxygen Uncoupling." Applied Energy 237: 822–35.

Pérez-Vega, R., Abad A., García-Labiano, F., Gayán, P., de Diego, L. F., Adánez, and Adánez J. **2016**. "Coal Combustion in a 50 kW$_{th}$ Chemical Looping Combustion Unit: Seeking Operating Conditions to Maximize CO$_2$ Capture and Combustion Efficiency." International Journal of Greenhouse Gas Control 50 (July): 80–92.

Pérez-Vega, R., Abad, A., Gayán, P., García-Labiano, F., Izquierdo, M. T., de Diego, L. F. and Adánez J. **2020**. "Coal Combustion via Chemical Looping Assisted by Oxygen Uncoupling with a Manganese‑iron Mixed Oxide Doped with Titanium." Fuel Processing Technology 197 (January): 106184.

Pikkarainen, T., Teir, S. and Hiltunen I. **2016**. "Piloting of Bio-CLC for BECCS." 4th International Conference on Chemical Looping. Nanjing (China).

Pikkarainen, T., Hiltunen, I. **2017**. "Chemical Looping Combustion of Solid Biomass Performance of Ilmenite and Braunite as Oxygen Carrier Materials." European Biomass Conference and Exhibition Proceedings 2017 (June): 1837–44.

Priddle, R. **2016**. "World Energy Outlook- Special Report Energy and Air Pollution." IEA, 266. https://doi.org/10.1021/ac00256a010.

Quéré, C. Le, Andrew, R. M., Friedlingstein, P., Sitch, S., Hauck, J., Pongratz, J., Pickers, P. A. et al. **2018**. "Global Carbon Budget 2018." Earth System Science Data 10 (4): 2141–94.

Rayner, S., Heyward, C., Kruger, T., Pidgeon, N., Redgwell, C. and Savulescu, J. **2013**. "The Oxford Principles." Climatic Change 121 (3): 499–512.

Reed, T. B., Levie, B. and Graboski, M. S. **1987**. "Fundamentals, Development and Scaleup of the Air-Oxygen Stratified Downdraft Gasifier." Richland, WA (United States).

REFERENCES

Richter, H. J. and Knoche K. F. **1983**. "Reversibility of Combustion Processes." American Chemical Society. Chapter 3, 71–85.

Rodhe, H., Charlson, R., and Crawford E. **1997**. "Svante Arrhenius and the Greenhouse Effect." Ambio. vol. 26: 2-5.

Rydén, M., Leion, H., Mattisson, T. and Lyngfelt A. **2014**. "Combined Oxides as Oxygen-Carrier Material for Chemical-Looping with Oxygen Uncoupling." Applied Energy 113: 1924–32.

Sajen, S., Singh, S. K., Mungse, P., Rayalu, S., Watanabe, K., Saravanan, G. and Labhasetwar N. **2016**. "Mechanically Stable Mixed Metal Oxide of and Mn as Oxygen Carrier for Chemical Looping Syngas Combustion." Energy & Fuels 30 (9): 7596–7603.

Schäfer, S., Lawrence, M., Stelzer, H., Born, W., Low, S., Schäfer, S., Lawrence, M., et al. **2015**. "The European Transdisciplinary Assessment of Climate Engineering (EuTRACE) Away from Earth," 170. http://www.iass-potsdam.de/sites/default/files/files/rz_150715_eutrace_digital.pdf.

Schmidt, G. A., Kelley, M., Nazarenko, L., Ruedy, R., Russell, G. L., Aleinov, I., Bauer, M. et al. **2014**. "Configuration and Assessment of the GISS ModelE2 Contributions to the CMIP5 Archive." Journal of Advances in Modeling Earth Systems 6 (1): 141–84.

Schmitz, M. Linderholm, C., Hallberg, P., Sundqvist, S. and Lyngfelt, A. **2016**. "Chemical-Looping Combustion of Solid Fuels Using Manganese Ores as Oxygen Carriers." Energy & Fuels 30 (2): 1204–16.

Schmitz, M. and Linderholm C. J. **2016**. "Performance of Calcium Manganate as Oxygen Carrier in Chemical Looping Combustion of Biochar in a 10 KW Pilot." Applied Energy 169 (May): 729–37.

Schmitz, M. and Linderholm C. J. **2018**. "Chemical Looping Combustion of Biomass in 10- and 100-KW Pilots − Analysis of Conversion and Lifetime Using a Sintered Manganese Ore." Fuel 231 (November): 73–84.

Schmitz, M., Linderholm, C. J. and Lyngfelt, A.. **2018**. "Chemical Looping Combustion of Four Different Solid Fuels Using a Manganese-Silicon-Titanium Oxygen Carrier." International Journal of Greenhouse Gas Control 70 (March): 88–96.

Schramski, J. R., Gattie, D. K. and Brown J. H. **2015**. "Human Domination of the Biosphere: Rapid Discharge of the Earth-Space Battery Foretells the Future of Humankind." Proceedings of the National Academy of Sciences 112 (31): 9511–17.

Shen, L., Wu, J., Xiao, J., Song, Q. and Xiao R. **2009**. "Chemical-Looping Combustion of Biomass in a 10 kW$_{th}$ Reactor with Iron Oxide as an Oxygen Carrier." Energy and Fuels 23: 2498–2505.

154

Shulman, A., Cleverstam, E., Mattisson, T.and Lyngfelt A. **2009**. "Manganese/Iron, Manganese/Nickel, and Manganese/Silicon Oxides Used in Chemical-Looping With Oxygen Uncoupling (CLOU) for Combustion of Methane." Energy & Fuels 23 (10): 5269–75.

Shulman, A., Cleverstam, E., Mattisson, T. and Lyngfelt A. **2011**. "Chemical – Looping with Oxygen Uncoupling Using Mn/Mg-Based Oxygen Carriers – Oxygen Release and Reactivity with Methane." Fuel 90 (3): 941–50.

Sikarwar, Vi. S., Zhao, M., Fennell, P. S., Shah, N. and Anthony E. J. **2017**. "Progress in Biofuel Production from Gasification." Progress in Energy and Combustion Science 61 (July): 189–248.

Simell, P., Ståhlberg, P., Kurkela, E., Albrecht, J., Deutsch, S. and Sjöström K. **2000**. "Provisional Protocol for the Sampling and Anlaysis of Tar and Particulates in the Gas from Large-Scale Biomass Gasifiers. Version 1998." Biomass and Bioenergy 18 (1): 19–38.

Song, T., Hartge, E. U., Heinrich, S., Shen, L. and Werther J. **2016**. "Chemical Looping Combustion of High Sodium Lignite in the Fluidized Bed: Combustion Performance and Sodium Transfer." In 4th International Conference on Chemical Looping, 70:22–31.

Staffell, I., Jansen, M., Chase, A., Cotton, E. and Lewis, C. **2018**. "Energy Revolution : A Global Outlook Headline Messages." Drax: Selby, 1–39. https://www.drax.com/wp-content/uploads/2018/12/Energy-Revolution-Global-Outlook-Report-Final-Dec-2018-COP24.pdf.

Sun, Y., Jiang, E., Xu, X., Wang, J. and Li Z. **2018**. "Supplied Oxygen Properties of $NiO/NiAl_2O_4$ in Chemical Looping Re-Forming of Biomass Pyrolysis Gas: The Influence of Synthesis Method." ACS Sustainable Chemistry & Engineering 6 (11): 14660–68.

Team, ESRL. 2019. "ESRL Global Monitoring Division - Global Greenhouse Gas Reference Network." 2019. https://www.esrl.noaa.gov/gmd/ccgg/trends/global.html.

UNEP. **2018**. The Emissions Gap Report 2018. Nairobi: United Nations Environment Programme.

UNFCCC. **2015**. "Paris Agreement." UNFCCC. https://doi.org/FCCC/CP/2015/L.9.

Vangkilde-Pedersen, T., Anthonsen, K. L., Smith, N., Kirk, K., Neele, F., van der Meer, B., Le Gallo, Y., et al. **2009**. "Assessing European Capacity for Geological Storage of Carbon Dioxide–the EU GeoCapacity Project." Energy Procedia (1): 2663–70.

Virginie, M., Adánez, J., Courson, C., de Diego, L. F., García-Labiano, F., Niznansky, D., Kiennemann, A., Gayán, P. and Abad, A. **2012**. "Effect of Fe–

REFERENCES

Olivine on the Tar Content during Biomass Gasification in a Dual Fluidized Bed." Applied Catalysis B: Environmental 121–122 (June): 214–22.

Visser, E., de Hendriks, C., Barrio, M., Mølnvik, M. J., de Koeijer, G., Liljemark, S. and Le Gallo, Y. **2008**. "Dynamis CO_2 Quality Recommendations." International Journal of Greenhouse Gas Control 2 (4): 478–84.

Werther, J., Saenger, M., Hartge, E. U., Ogada, T. and Siagi, Z. **2000**. "Combustion of Agricultural Residues." Progress in Energy and Combustion Science 26 (1): 1–27.

Wiesenthal, T., Mourelatou, A., Petersen, J. E. and Taylor P. **2006**. "How Much Bioenergy Can Europe Produce without Harming the Environment?" Eea No. 7 (7): 1–72. http://reports.eea.europa.eu/eea_report_2006_7/en.

Williams, A., Jones, J.M., Ma, L. and Pourkashanian M. **2012**. "Pollutants from the Combustion of Solid Biomass Fuels." Progress in Energy and Combustion Science 38 (2): 113–37.

Belotskaia E. D., Galkin I. V., Galkina A. A., Geller E. I., Gimadi V. I., Grigoriev L. M., et al. **2016**. "Global and Russian Energy Outlook 2016." Edited by The Analytical Center for the Government of the Russian Federation, November 2016, Moscow, 1-198

Yan, J., Shen, L., Jiang, S., Wu, J., Shen, T., and Song, T. **2017**. "Combustion Performance of Sewage Sludge in a Novel CLC System with a Two-Stage Fuel Reactor." Energy & Fuels 31 (11): 12570–81.

Zapatero, M. A., Reyes, J. L., Martínez, R., Suárez, I., Arenillas, A. and Perucha, M. A. **2008**. "Estudio Preliminar de Las Formaciones Favorables Para El Almacenamiento Subterráneo de CO_2 En España." Instituto Geológico y Minero de España, 1-135.

Zevenhoven, M., Sevonius, C., Salminen, P., Lindberg, D., Brink, A., Yrjas, P. and Hupa, L. **2018**. "Defluidization of the Oxygen Carrier Ilmenite – Laboratory Experiments with Potassium Salts." Energy 148 (April): 930–40.

156

APPENDIX - PAPERS

PAPER I

CrossMark
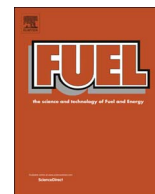
Full Length Article

Chemical Looping Combustion of different types of biomass in a 0.5 kW$_{th}$ unit

T. Mendiara*, A. Pérez-Astray, M.T. Izquierdo, A. Abad, L.F. de Diego, F. García-Labiano, P. Gayán, J. Adánez

Department of Energy and Environment, Instituto de Carboquímica-ICB-CSIC. Miguel Luesma Castán 4, 50018 Zaragoza, Spain

ABSTRACT

Chemical Looping Combustion (CLC) using renewable solid fuels appears as an important option to reach negative carbon emissions. In this work, three types of forest and agricultural residues (pine sawdust, olive stone and almond shell) were tested between 900–980 °C in a 0.5 kW$_{th}$ unit with an iron ore as oxygen carrier (Tierga ore) working under *In situ* Gasification-Chemical Looping Combustion (*i*G-CLC) mode. Specific solids inventories lower than 1000 kg/MW$_{th}$ were tested as they were consider more representative of what can be used in a larger CLC unit. CO_2 represented about 70% in the fuel reactor outlet gas stream, followed by unburnt compounds: H_2, CO and CH_4. CO_2 capture efficiencies increased with the fuel reactor temperature achieving almost 100% of capture with the three biomasses at temperatures above 950 °C. In contrast, no clear trend with the fuel reactor temperature was observed for the total oxygen demand, achieving values about 25%. The major contribution to this value comes from the unburned volatiles with a small contribution coming from tar ($\approx 1\%$). Regarding tar, naphthalene was the major compound found at the different operating conditions. The present results support the consideration of the CLC process with biomass (bio-CLC) as a promising Bio-Energy with Carbon Capture (BECCS) technology.

1. Introduction

Sustainability is becoming one of the most important challenges of present societies. One of the threats to the sustainability of our planet is climate change. In order to mitigate the effects of the changes in climate, different actions should be taken to restrict anthropogenic greenhouse gas (GHG) emissions. Based on the findings presented in the 5th Assessment Report of the International Panel on Climate Change (IPCC) [1], the Paris Agreement in 2015 set the objective of limiting the global average temperature increase to 2 °C by reducing the GHG emissions and within them, CO_2 emissions [2]. To reach this goal it becomes necessary to develop not only neutral but also negative carbon emission technologies (NETs) during the present century [3]. NETs comprise different types of technologies which actually reduce carbon concentration in the atmosphere, such as afforestation, agricultural land management, bio-char soil sequestration, ocean liming, enhanced weathering, ocean fertilization and Bio-Energy with Carbon Capture and Storage (BECCS) [4].

BECCS technologies are drawing increasing attention in the last years. They match both biomass combustion and Carbon Capture and Storage (CCS) and this combination reinforces their potential to

generate heat and/or power, while removing CO_2 from the atmosphere [4]. Biomass carbon emissions are considered neutral because of their short life cycle. Moreover, biomass accessibility, simply sustainable management as well as relatively homogeneous world distribution must be considered as important characteristics of biomass compared to other fuels. In this way, including biomass technologies, the energy mix self-sufficiency and environmental protection in energy supply would be ensured [5,6]. The bio-energy concept associated with BECCS includes both biomass fuelled biochemical and thermochemical processes easily combinable with CCS [7]. An almost pure CO_2 stream should be produced during fuel conversion to make feasible its transportation and storage. Simply pre-treated biomass or even biomass derived liquid and gas fuels can be used.

CCS technologies allow CO_2 emission reduction from stationary point sources in energy production. In this context, chemical looping combustion (CLC) processes have demonstrated to be one of the most suitable alternatives for CCS because of the low cost of carbon capture and energy penalty [8]. This technology allows fuel combustion in nitrogen-free atmosphere. A solid oxygen carrier (OC) provides the oxygen needed for fuel oxidation via redox reaction while circulating between the so-called fuel and air reactors. CLC combustion of solid

Nomenclature

C_nH_m	general formula for tar compounds
$F_{i,FR}$	i species molar flow in the fuel reactor outlet stream (mol/h)
$F_{CO2,AR}$	CO_2 molar flow in the air reactor (mol/h)
$F_{C,vol}$	carbon flow coming from the volatile matter (mol/h)
M_O	oxygen atomic weight (g/mol)
$\dot{m}_{OC}$	solid circulation rate (kg/h)
$\dot{m}_{SF}$	biomass mass flow (kg/h)
R_{OC}	oxygen transport capacity

X_{char}	char conversion (–)

Greek symbols:

η_{CC}	CO_2 capture efficiency (%)
Ω_{SF}	amount of oxygen to burn the solid fuel (kg oxygen/kg biomass)
ϕ	oxygen carrier to fuel ratio
Ω_T	total oxygen demand (%)
Ω_{tar}	oxygen demanded by the tar at the fuel reactor outlet (%)

fuels has reached an important development in the last decade [9]. Most of the knowledge has been gained using coal as fuel in prototypes in the range 0.5 kW$_{th}$ to 3 MW$_{th}$. The majority of the CLC units operated under the *In Situ* Gasification-Chemical Looping Combustion (*i*G-CLC) mode. Fig. 1 shows the scheme of a typical *i*G-CLC unit for solid fuels. In this process, the solid fuel is gasified in the fuel reactor using steam as gasifying agent. Both the volatile compounds and the gasification products generated react with the oxygen carrier to produce CO_2 and H_2O. The possible unburnt compounds at the outlet of the fuel reactor would be further oxidised in an oxygen polishing step. This stream can be easily dried to obtain a CO_2 stream ready to be transported and stored. Finally, the oxygen carrier is re-oxidized in the air reactor.

Based on this experience, the biomass fuelled CLC became feasible as a BECCS technology. First results using biomass (pine sawdust) and iron ore as oxygen carrier were obtained by Shen et al. [10] in a 10 kW$_{th}$ unit. They evaluated the influence of the fuel reactor temperature on the gas product composition. Pine sawdust was also used in the experiments performed at Instituto de Carboquímica by Mendiara et al. [11] with a Fe-based iron ore (Tierga ore) as oxygen carrier. The influence of the fuel reactor temperature on the CO_2 capture and combustion efficiency was assessed. Tar measurements were also performed. Moreover, no interaction of biomass ashes with the oxygen carrier was observed after 78 h of continuous operation. Several manganese ores were used as oxygen carriers by Schmitz et al. [12] for wood char combustion in a continuous 10 kW$_{th}$ CLC unit at Chalmers University of Technology. Some of them presented low oxygen demands and high carbon capture efficiencies. Wood char was also used by Linderholm et al. [13] in a 100 kW$_{th}$ CLC plant also located at Chalmers University of Technology. In this case, Tierga ore was used as oxygen carrier. The highest combustion efficiency observed in these experiments was 93%. It should be mentioned that high specific solids inventories (> 1000 kg/MW$_{th}$) were used in the previously described studies. According to the experience gained in experiments with coal in different continuous CLC units, the optimum value of this parameter would be lower to avoid high pressure drop in the fuel reactor [14]. This could affect the combustion efficiency reached. Recently, a new 10–50 kW$_{th}$ scale CLC plant for biomass combustion was built at VTT Technical Research Centre in Finland an operated by Pikkarainen et al. [15]. They found high oxygen demands during the combustion of wood

pellets due in this case to an insufficient bed temperature of the fuel reactor, as the unit was originally designed for gasification.

A big step in the scale-up of the biomass CLC process was recently presented by Berdugo-Vilches et al. [16]. Several experimental campaigns were carried out in a semi-commercial dual fluidized bed (DFB) unit at Chalmers University consisting of a 12 MW$_{th}$ boiler coupled to a 2–4 MW$_{th}$ bubbling bed gasifier. The gasifier can be assimilated to a fuel reactor of a conventional CLC unit and the boiler to the air reactor. More than 1000 hours of combustion were reported using commercial wood pellets as fuel and ilmenite and a manganese ore as oxygen carriers. Combustion efficiencies up to 60% were achieved although the temperature in the gasifier was not high, about 830 °C. Although this plant represents a non-optimized reactor design for CLC applications, these results highlight the strong potential of the CLC technology for biomass combustion and reinforce its possibilities as BECCS technology.

In this line, the present work aims at further contributing to the knowledge of biomass CLC. Commonly, pine or spruce tree pellets have been used as fuels. The objective of this work is to extend the study to other types of biomass (agricultural residues such as olive stones and almond shells) in order to identify possible differences during combustion. Besides, operation with specific solids inventories lower than 1000 kg/MW$_{th}$will be assessed. Experiments are performed in a continuous 0.5 kW$_{th}$ unit operating under *i*G-CLC mode. The influence of the fuel reactor temperature on the results obtained is evaluated using specific solids inventories realistic for industrial CLC units.

2. Experimental

2.1. Oxygen carrier and biomass

Tierga ore was used as oxygen carrier in the present experiments. In a comparative study among Fe-based oxygen carriers, Tierga ore showed the highest reactivity in the combustion of coal [17,18] as well as stability and durability combined with its low cost. Thus, it was also selected to perform biomass combustion experiments. After receiving it from an hematite mine in Tierga (Zaragoza, Spain), the ore was crushed to 100–300 μm size particle and calcined at 950 °C during 12 hours for increasing its mechanical strength. The main properties of Tierga ore are summarized in Table 1. A detailed description of the techniques
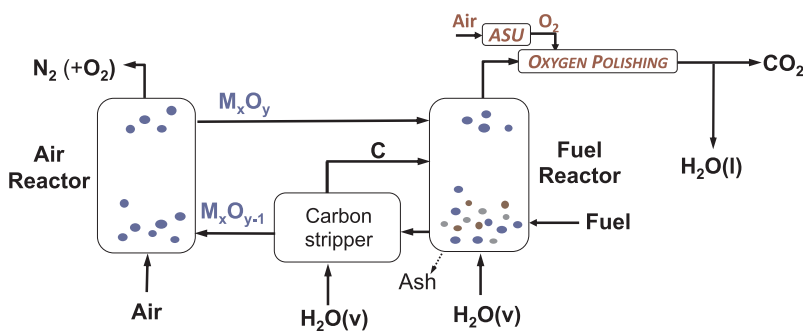
Fig. 1. Scheme of the *i*G-CLC process.

Table 1
Main characteristics of the calcined Tierga ore used as oxygen carrier.

Fe$_2$O$_3$	wt%	76.5
XRD main phases		Fe$_2$O$_3$, SiO$_2$, Al$_2$O$_3$, CaO, MgO
Crushing strength	N	5.8
Oxygen transport capacity, R$_{OC}$	%	2.5
Porosity	%	26.3
Skeletal density	kg/m^3	4216
Specific surface area, BET	(m^2/g)	1.4

used in the characterization of the sample can be found elsewhere [17].

Three Spanish biomass residues were selected as fuels. One forest residue, pine sawdust (*Pinus sylvestris*) from Spain, was chosen as a reference material. Besides, olive stones (*Olea europaea*) and almond shell (*Prunus dulcis*) were selected as they are agricultural residues with high annual production. In 2014, world olive oil production reached 3.2 million tons and almond production 1.1 million tons [19,20]. Raw materials were dried and sieved to adequate their size to a particle distribution between 0.5 and 2 mm. Proximate and ultimate analyses of each biomass are presented on Table 2. In this Table, the low heating value and the value of the oxygen demand of the solid fuel, Ω_{SF}, were also included. The latter parameter represents the stoichiometric amount of oxygen to burn the solid fuel.

2.2. Experimental setup and procedure

The ICB-CSIC-s1 experimental unit showed in Fig. 2 consists of the fuel (1) and the air (3) reactors, both fluidized type. The biomass is fed into the fuel reactor (50 mm ID) at the bottom of the bubbling fluidized bed with a series of two screw feeders. Steam used as gasifying agent was produced by heating up in an evaporator the corresponding water flow supplied by a peristaltic pump. There is no carbon stripper between fuel and air reactors. This facilitated the analysis of the influence on biomass combustion of different variables affecting the fuel reactor. The fuel reactor is connected to the air reactor by a U-shaped fluidized bed reactor (30 mm ID) placed as loop seal (2) to prevent the mixture of the gases between them. The loop seal was fluidized with nitrogen. Previous tests demonstrated that approximately 50% of the loop seal fluidizing agent reached the fuel reactor. The reduced oxygen carrier was transferred to the air reactor which is also a bubbling fluidized bed (80 mm ID). Once re-oxidized it was sent up the air reactor through a riser (4) helped by a secondary air entrance, collected by a cyclone (5) and sent to a deposit (7) that keeps both reactor atmospheres separated. A diverting solid valve (6) was used to measure the solid circulation rate during the experiment. The flow of oxygen carrier fed to the fuel reactor from this deposit was controlled by a solids valve (8).

Main combustion and gasification product concentrations at the fuel reactor outlet (CO, CO$_2$, H$_2$ and CH$_4$) and air reactor (CO, CO$_2$ and O$_2$) were recorded by on-line analyzers. Gas samples were taken in order to detect gaseous C$_2$-C$_4$ hydrocarbons at the fuel reactor outlet with an HP 5890 gas chromatograph (GC) coupled with a Thermal Conductivity Detector (TCD). Tar compounds at the fuel reactor outlet were collected in impingers following the standard tar protocol [21]. The quantitative determination of the concentrations of the different tar compounds in the samples was done by a GC (Agilent 7890A) fitted with a capillary column (HP-5) and a Flame Ionization Detector (FID). Furthermore, the GC was coupled with a mass spectrometer (Agilent 5975C). Naphthalene and phenanthrene were selected for the external calibration procedure. The quantitative values were obtained assuming a similar response factor to naphthalene for tar compounds of 1–2 rings and similar to phenanthrene for 3-rings compounds [22].

Combustion conditions were maintained near to stoichiometric conditions during all the performed experiments. For this purpose, the oxygen carrier to fuel ratio (ϕ) compares the oxygen that could be supplied by the circulating oxygen carrier with the oxygen needed for the complete combustion of the fed fuel.

$$\phi = \frac{\dot{m}_{OC} \cdot R_{OC}}{\dot{m}_{SF} \cdot \Omega_{SF}} \quad (1)$$

The oxygen carrier inventory in the unit was about 3.5 kg and the solids circulation rate of oxygen carrier was about 8 kg/h. The fuel reactor steam flow was set to achieve a velocity of 0.08 m/s at 900 °C. The velocity in the air reactor was 0.5 m/s at 900 °C. Table 3 shows the experimental conditions and results of the experiments performed. A total of 60 h of hot operation were accomplished, 40 of which corresponds to biomass combustion.

2.3. Data evaluation

In order to evaluate the performance of the *i*G-CLC process with biomass, three parameters were considered, i.e. CO$_2$ capture efficiency, char conversion and total oxygen demand. The CO$_2$ capture efficiency (η_{CC}) was defined as the fraction of the carbon introduced which was converted to gas in the fuel reactor. The carbon converted was calculated from the CH$_4$, CO and CO$_2$ concentrations exiting the fuel reactor. Considering the low amounts of C$_2$-C$_4$ detected in the tests, the amount of hydrocarbons heavier than CH$_4$ were considered negligible for the calculations.

$$\eta_{CC} = \frac{\left[F_{CO_2,FR} + F_{CO,FR} + F_{CH_4,FR}\right]_{out}}{\left[F_{CO_2,FR} + F_{CO,FR} + F_{CH_4,FR} + F_{CO_2,AR}\right]_{out}} \quad (2)$$

The CO$_2$ capture efficiency calculated according Eq. (2) depended on the fraction of char that was gasified in the fuel reactor. The char conversion (X_{char}) was defined as the fraction of carbon in the char formed in the fuel reactor which was released to the fuel reactor exhaust gas stream:

$$X_{char} = \frac{\left[F_{CO_2,FR} + F_{CO,FR} + F_{CH_4,FR} - F_{C,vol}\right]_{out}}{\left[F_{CO_2,FR} + F_{CO,FR} + F_{CH_4,FR} + F_{CO_2,AR} - F_{C,vol}\right]_{out}} \quad (3)$$

$F_{C,vol}$ was calculated from the biomass analyses as the difference between the total carbon in the biomass and the fixed carbon.

The total oxygen demand (Ω_T) was calculated as the quotient between the oxygen required in order to reach complete combustion of the unconverted gases (CH$_4$, CO and H$_2$) and the oxygen needed for complete combustion of the biomass fed.

$$\Omega_T = \frac{4 \cdot F_{CH_4,FR} + F_{CO,FR} + F_{H_2,FR}}{\frac{1000}{M_O} \cdot \dot{m}_{SF} \cdot \Omega_{SF}} \quad (4)$$

Two more parameters were calculated in order to better understand the combustion of biomass in our CLC unit. The results were also included in Table 3. First, the volatile conversion was estimated. For its calculation, it was considered that methane is the compound at the fuel reactor outlet coming exclusively from volatile release. Both the CO and

Table 2
Analyses of the biomasses.

	Pine sawdust	Olive stone	Almond shell
Proximate analysis (wt%)			
Moisture	4.2	9.4	2.3
Ash	0.4	0.8	1.1
Volatile matter	81.0	72.5	76.6
Fixed carbon	14.4	17.3	20.0
Ultimate analysis (wt%)			
C	51.3	46.5	50.2
H	6.0	4.8	5.7
N	0.3	0.2	0.2
S	0.0	0.0	0.0
O	37.8	38.3	40.5
LHV (kJ/kg)	19158	16807	18071
Ω_{SF} (kg oxygen/kg fuel)	1.5	1.2	1.4

Fig. 2. Experimental unit ICB-CSIC-s1.

H_2 found could also come from char gasification. Therefore methane was used as volatile reference compound to calculate volatile conversion. Thus, the flow of methane at the fuel reactor outlet was compared to that predicted by an empirical model [23] at the corresponding fuel reactor temperature. Additionally, based on tar composition, the oxygen required to completely burn tar (C_nH_m) to CO_2 and H_2O was calculated and compared to the oxygen needed to completely burn the fuel. This ratio has been defined as the tar oxygen demand (Ω_{tar}).

$$\Omega_{tar} = \frac{(n + m/4) \cdot F_{C_nH_{m,FR}}}{\frac{1000}{M_O} \cdot \dot{m}_{SF} \cdot \Omega_{SF}} \tag{5}$$

3. Results and discussion

3.1. Gas composition at the fuel reactor outlet

Fig. 3 presents the temporal evolution of the main gaseous products obtained in both fuel and air reactors for a typical experiment. Data correspond to pine sawdust combustion although similar profiles were obtained for the other biomasses. Air and nitrogen were used as fluidizing agents during the heating period. After reaching the desired temperatures, the fluidizing agent in the fuel reactor was switched to steam and biomass was fed. After the stabilization period, steady state was reached and maintained for about 1 hour. The operation was generally smooth regarding fuel feeding and solids circulation. The average concentrations so obtained both for the fuel and air reactors were considered as representative of those corresponding to the operating conditions.

Fig. 4 presents the concentration of the main gaseous products at the fuel reactor outlet obtained for the different temperatures and biomasses. No clear differences were detected among biomasses. CO_2 appeared as the major compound, with about 70% in all cases, followed by unburnt compounds: H_2 (10–15 vol%), CO (10–12 vol%) and CH_4 (6–8 vol%). The amount of other light hydrocarbons, C_2-C_4, was

negligible.

The high content of volatiles in biomass (between 72.5 and 81% according to Table 2) would explain these concentrations of unburnt products at the outlet of the fuel reactor. Previous works using coal as fuel performed in the same unit at ICB-CSIC already indicated that the contact between volatiles and the oxygen carrier bed was not sufficient to ensure a good volatile conversion as volatiles were released in a plume [9].

3.2. Tar measurement

In the combustion experiments with the three biomasses, tar compounds from the fuel reactor were collected and further analysed using the tar protocol. Fig. 5 shows the tar compounds identified in experiments at 950 and 980 °C. In all cases, naphthalene was the major compound identified at any temperature followed by acenaphthylene and phenanthrene. These compounds account for approximately 80% of all the tar mass detected in any case.

No important differences in tar composition were observed for the different types of biomass. The high temperatures at which biomass gasification proceeds in the fuel reactor favours the formation of tertiary tars (mainly methyl derivatives of aromatics and PAHS without substituents) and this may soften possible differences in tar composition depending on the biomass used as fuel.

Recently, result data from operation in the boiler/gasifier loop (12 and 2–4 MW_{th}, respectively) at Chalmers University of Technology using low-cost oxygen carriers and biomass were reported by Berdugo-Vilches et al. [16]. Commercial wood pellets from spruce trees were used as biomass fuel and the operating temperature in the gasifier was about 830 °C. Tar samples were collected using a high accuracy method based on Solid Phase Adsorption (SPA). Under these conditions, they also identified benzene, phenolic species and 1-ring compounds as tar compounds at the fuel reactor outlet. In our work, the experimental methodology used would allow detecting benzene in case it was present. Despite following the standard tar protocol, negligible amounts of

Table 3
Operating conditions and experimental results of the tests with the biomasses (PN = pine sawdust, OS = olive stone, AS = almond shell).

Biomass	PN	PN	PN	PN	OS	OS	OS	AS	AS	AS
Time of combustion (h)	3.3	5.7	2.6	2.2	8.1	3.0	2.3	3.7	3.3	3.8
Time hot fluidization (h)	6.5	8.2	4.1	3.1	9.4	4.5	3.0	6.3	9.3	6.4
Temperatures (°C)										
Fuel reactor	895	910	950	985	905	955	980	905	955	985
Air reactor	950	950	950	950	950	950	950	950	950	950
Operating conditions										
Biomass flow (g/h)	152	113	98	98	164	141	141	190	102	88
OC circulation rate (kg/h)	10.1	9.2	6.7	6.7	8.8	7.6	7.6	13	7	5.9
Oxygen carrier to fuel ratio, ϕ	1.1	1.3	1.1	1.1	1.0	1.0	1.0	1.2	1.2	1.2
Specific solids inventory (kg/MW$_{th}$)	475	750	785	780	600	600	590	370	550	890
Gas composition										
Fuel reactor (vol%, N$_2$ free, dry basis)										
CO	11.0	9.5	10.1	11.7	10.3	12.7	12.5	10.4	10.6	9.8
CO_2	69.2	71.1	72.1	65.2	70.0	66.2	65.0	70.8	65.0	72.9
H_2	11.1	12.3	11.4	15.4	11.3	13.1	14.5	10.4	16.2	11.3
CH_4	8.7	7.1	6.4	7.7	8.4	8.0	8.0	8.4	8.2	6.0
CH_4 conversion (%)	–	73.5	–	–	65.1	–	–	71.0	–	–
Air reactor (vol%)										
O_2	17.5	18.4	19.4	19.3	17.8	18.6	19.2	17.2	19.4	19.3
CO_2	0.2	0.1	0.0	0.0	0.5	0.1	0.0	0.5	0.0	0.0
Tar analysis										
H_2O content (vol%)	–	–	12.0	8.8	–	9.4	8.5	–	10.6	12.8
Total tar (g/Nm^3 dry)	–	–	4.30	2.48	–	3.59	3.72	–	2.98	2.64
Total tar (g/kg daf fuel)	–	–	2.76	1.59	–	1.70	1.77	–	1.82	1.84
Tar oxygen demand, Ω_{tar} (%)	–	–	1.4	0.9	–	1.2	1.3	–	1.0	1.0
Tar composition (g/Nm^3 dry)										
Styrene	–	–	0.21	0.08	–	0.26	0.14	–	0.16	0.11
Indene	–	–	0.13	0.05	–	0.14	0.11	–	0.10	0.07
Naphthalene	–	–	2.64	1.77	–	2.11	2.47	–	1.98	1.73
Naphthalene 2-methyl	–	–	0.03	0.02	–	0.03	0.02	–	0.02	0.02
Naphthalene 1-methyl	–	–	0.02	0.01	–	0.02	0.01	–	0.02	0.01
Biphenil	–	–	0.09	0.05	–	0.09	0.07	–	0.07	0.07
Acenaphthylene	–	–	0.38	0.16	–	0.29	0.26	–	0.24	0.22
Fluorene	–	–	0.03	0.01	–	0.03	0.02	–	0.02	0.02
Phenanthrene	–	–	0.39	0.16	–	0.32	0.28	–	0.18	0.19
Anthracene	–	–	0.08	0.04	–	0.07	0.06	–	0.04	0.04
Naphthalene 2-phenyl	–	–	0.02	0.01	–	0.02	0.02	–	0.01	0.01
Fluoranthene	–	–	0.15	0.07	–	0.12	0.13	–	0.07	0.06
Pyrene	–	–	0.12	0.06	–	0.10	0.12	–	0.06	0.05
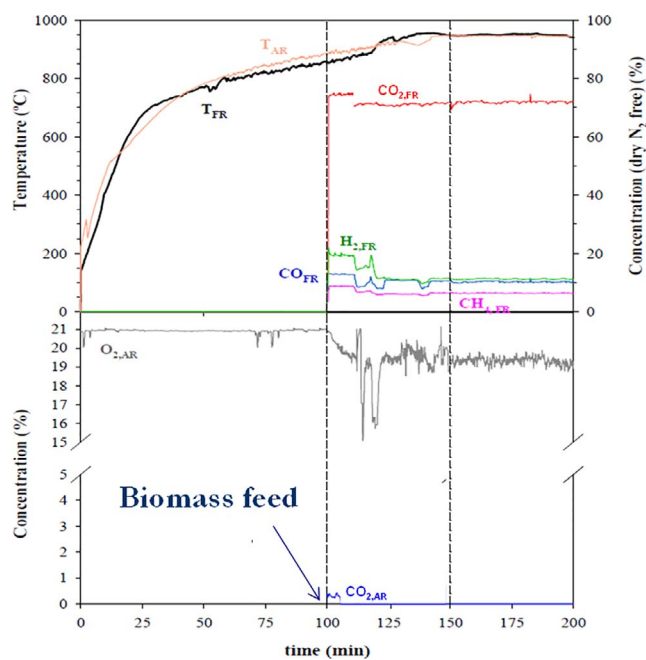
Fig. 3. Example of data evolution in a typical test. Biomass: pine sawdust. ϕ = 1.1. T_{FR} = 950 °C.

benzene were detected.

The results corresponding to pine sawdust in the present work can be compared to those previously obtained operating at lower temperatures (880–915 °C) in the same experimental unit [11]. In that study, naphthalene was also detected as the major compound in tar, but only indene and styrene were detected at the same time. The fact that in the present experiments more 3-ring compounds were also present in the tar mixture can be attributed to the lower solids inventory present in the fuel reactor during the current tests (750–785 kg/MW$_{th}$ compared to 1550 kg/MW$_{th}$ in experiments in [11]).

According to Table 3, the increase of temperature in the fuel reactor produces a decrease in the tar concentration measured in the experiments with pine sawdust and almond shell. At the highest temperature tested (980 °C), the total tar concentration was 2.48, 3.72 and 2.60 g/Nm^3 for pine sawdust, olive stone and almond shell, respectively. In the experiments performed at Chalmers University [16], 21–22 g tar per kg dry-ash-free fuel was measured for ilmenite and a manganese ore as oxygen carriers. As it is shown in Table 3, the values in the present work are 8–13 times lower than those reported. Besides the different methodology employed in the tar collection and analysis, the differences can be also attributed to the higher temperatures used in the fuel reactor during gasification.

The tar concentration values found in the present work are higher than those considered adequate to avoid operational problems derived from tar condensation and subsequent polymerization leading to
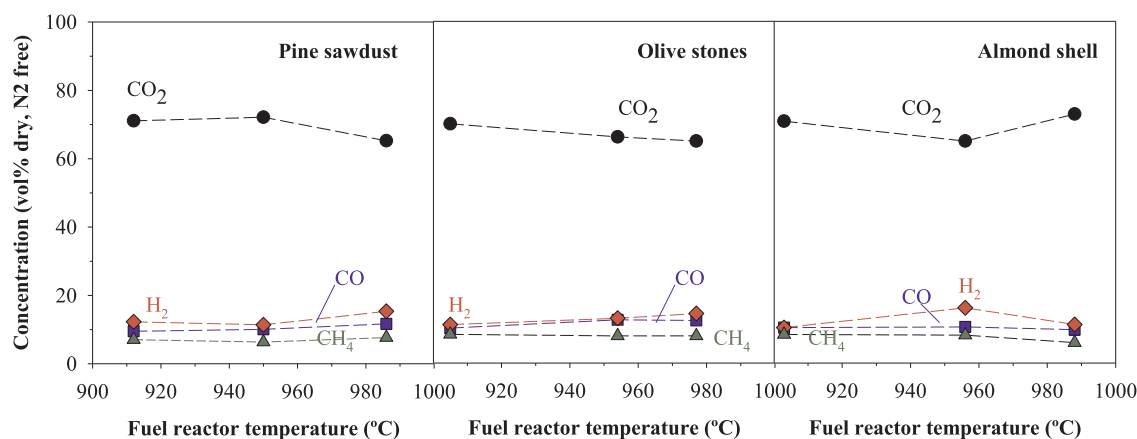
Fig. 4. Effect of fuel reactor temperature on the gas product composition obtained with different biomasses. φ ≈ 1.1.
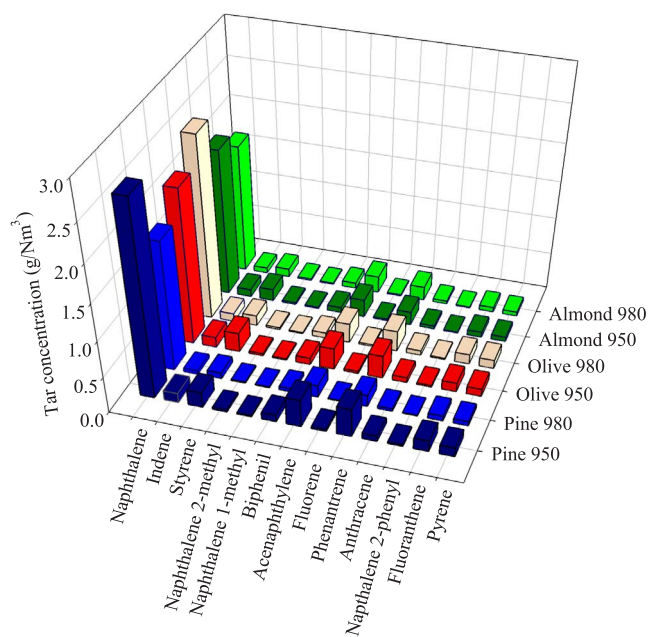
Fig. 5. Tar composition for the three biomasses tested at different fuel reactor temperatures.

fouling. Reed et al. [24] limited to the range 0.05–0.5 g/Nm³ the tar content for compressing and piping any distance a biomass gasification gas. Nevertheless, no fouling problems downstream due to the tar presence can be anticipated in CLC. In an industrial CLC unit it would be expected that tar compounds were burned in the oxygen polishing
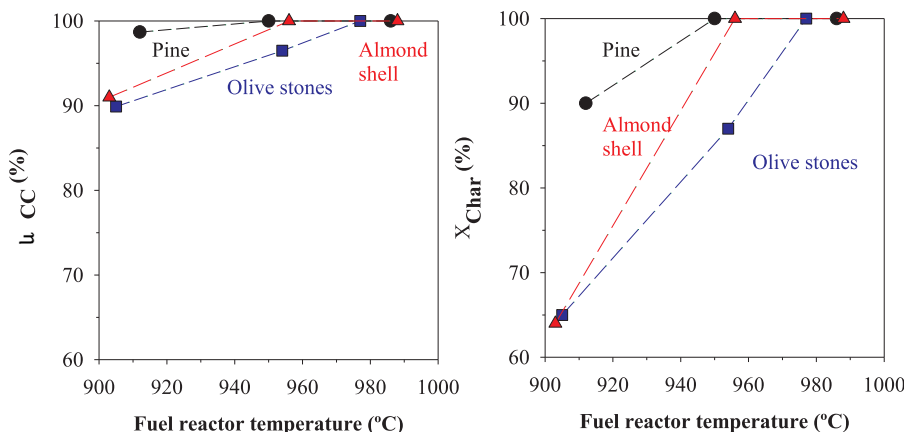
step downstream the fuel reactor. From the tar composition showed in Table 3 for the three biomasses at 950 and 980 °C, the tar oxygen demand (Ω_{tar}) was calculated (see Table 3). According to the results obtained, the oxygen demanded by the tar would be about 1% of that needed to burn the fuel. Tar contribution to the oxygen demand should then be considered in the design of the oxygen polishing step. Nevertheless, it would not represent a problem since the oxygen demanded by the other gaseous unburned compounds (CO, H_2 and CH_4) would be significantly higher as it would be shown in the following sections.

3.3. Combustion parameters

The fuel and air reactor gas outlet concentrations were used to evaluate the combustion of the three different types of biomass in the *i*G-CLC process. Fig. 6 presents the obtained values for the CO_2 capture efficiency and the char conversion.

Both parameters increased with the fuel reactor temperature reaching values of almost 100% from 950 °C in the case of pine sawdust and almond shell. This could be due to their higher volatile content compared to olive stone. It is interesting to highlight that 100% CO_2 capture was achieved with the three biomasses at 980 °C even in the absence of a carbon stripper between fuel and air reactors in this experimental unit. In fact, lower CO_2 capture efficiencies were reached in previous experiments with the same oxygen carrier and different types of coal. At temperatures in 900–930 °C range and specific solids inventories (1500–2000 kg/MW$_{th}$), Mendiara et al. [18] reported CO_2 capture efficiency values of 30–45% for anthracite, 50–57% for a bituminous Colombian coal and 85–94% for lignite. Therefore, it can be concluded that the higher volatile content of biomass and higher reactivity of biomass char compared to coal makes that the use of a

Fig. 6. Effect of fuel reactor temperature on the CO_2 capture efficiency (η_{CC}) and the char conversion (X_{char}) for the different biomasses.

carbon stripper is not as decisive as in the combustion of coal.

Fig. 7 presents the total oxygen demand at different fuel reactor temperatures. No clear trend was observed with the fuel reactor temperature. In general, the total oxygen demand for the three biomasses was similar and about 20–30%. The high carbon capture efficiencies obtained in most cases indicates that char is completely gasified in the fuel reactor. Char gasification products are known to be almost completely consumed by the oxygen carrier in the fuel reactor in this continuous unit [9]. Therefore it is realistic to assume that most of the oxygen demand is generated by the volatiles that escape the fuel reactor bed without interacting with the oxygen carrier particles.

In order to estimate how much is the volatile conversion in the present experiments, an empirical model by Neves et al. [23] for the prediction of biomass pyrolysis products was used. The amount of volatiles that could be released could be then calculated and afterwards compared to the results in the present experiments. The model does not consider the physical-chemical processes occurring within the biomass particles. It is based on mass balances to the overall pyrolysis processes and experimentally-based closing parameters obtained after the compilation of a significant amount of experimental data for different types of biomass and pyrolysis conditions. It should be pointed out that only mass balances to carbon, hydrogen and oxygen are considered. Those corresponding to nitrogen, sulphur and chlorine were not included in the original model.

The input data required by the model used were the CHO composition of the parent fuel (dry-ash-free) and the temperature of pyrolysis in °C. As output, the model calculates the dry-ash-free composition of resulting tar, C_xH_y, CH_4, CO, CO_2, H_2O and H_2. An extra assumption was herein made in order to adapt this composition to the reacting conditions existing in the CLC process. It must be remarked that steam is used as gasifying agent in the fuel reactor in order to convert the char produced during biomass pyrolysis to CO and H_2. The presence of steam would facilitate the conversion of most of the tar and C_xH_y formed during biomass pyrolysis to CH_4 and carbon. Considering this, the amounts of the different species resulting from biomass pyrolysis predicted by the model were here recalculated.

Table 3 shows the volatile conversion in the 0.5 kW$_{th}$ unit according to the assumptions detailed in section 2.3. Volatile conversion was estimated at 900 °C for the three biomasses tested. An average volatile conversion about 70% was estimated for the three biomasses. These values are in line with the oxygen demand about 25–30% showed in Fig. 7. It has to be remarked that the fuel reactor in this CLC unit is a bubbling fluidized bed. Previous studies in this unit indicated that under these conditions, all the gasification products are burned by the oxygen carrier [25]. Thus, the oxygen demand of the volatiles would correspond to the total oxygen demand. In order to improve volatile conversion, changes in both the design of the fuel reactor and in the reactivity of the oxygen carrier would be needed. In this respect, highly reactive carriers would favour volatile conversion but more significant improvements in volatile conversion would be expected if a circulating fluidized bed was used as fuel reactor.

Results corresponding to pine sawdust experiments in the present work complement those previously published by Mendiara et al. [11] were higher specific solids inventories were used. Using higher but less realistic solids inventories in the fuel reactor allowed reaching lower values of oxygen demand in the temperature range 880–915 °C under similar experimental conditions. The influence of the solids inventory in the fuel reactor on the oxygen demand value is assessed in several experiments performed in this work with Tierga ore and pine sawdust and shown in Fig. 8.

In fact, lower total oxygen demand values could be reached with higher solids inventories because of the increasing oxygen availability to oxidize the volatiles and char gasification products generated in the fuel reactor. However, in theoretical studies dedicated to CLC scale-up [14,26], specific solids inventories larger than 1000 kg/MW$_{th}$ are not recommended. These studies showed that higher inventories would

only slightly improve combustion efficiency while the resulting high pressure drop in the fuel reactor would be too much increased. Nevertheless, a compromise should be reached between enlarging reactors to allow higher solids inventories and the reduction of the oxygen demand. Additional actions for unburned compounds minimization should be also taken. Although an oxygen polishing step contributes to this point, different low energy penalty options were recently proposed. A system for a better volatile distribution in the fuel reactor bed has already been presented by Lyngfelt and Leckner [8]. The so-called "volatile distributor" is basically a downwards-opening box inserted at the bottom of the fuel reactor bed with holes in the sides. The design has been already patented but construction details are still not clear. This device is expected to be optimized using cold-flow or fluid-dynamic models. Gayán et al. [27] recently outlined several design solutions for reducing the total oxygen demand. Some of the most promising are the use of a secondary fuel reactor or the changes in the fuel feeding point to the CLC system. The incorporation of a secondary fuel reactor after the main fuel reactor would facilitate the combustion of unburned compounds with a low increase in the total specific solids inventory. This would not compromise the economics of the process, especially if a low-cost oxygen carrier is used. However, the operation of this second fluidized bed connected to the main fuel reactor should be also optimized in order to guarantee a correct solid flow. First operational results using two bubbling fluidized beds as fuel reactor were recently reported in experiments using coal as fuel [28]. On the other hand, feeding the solid fuel to the carbon stripper has also been proposed to minimize the unburned compounds generated. Under this configuration, the carbon stripper would act as the primary fuel reactor. In the carbon stripper, only a small fraction of the char generated would be gasified before being separated from the oxygen carrier particles and sent to the fuel reactor, which would then act as a secondary fuel reactor. In this second fuel reactor, char gasification would proceed in a higher extent and the volatiles already released in the carbon stripper would be better burned.

3.4. Effect of the biomass ashes on biomass combustion

It is already known that the presence of alkali (mainly Na and K) in biomass ashes can be the cause of different problems during biomass combustion (i.e ash melting, defluidization and corrosion). The major element in the biomasses tested in this work was potassium. The values of K_2O found were 8.9, 29.5 and 12.6 wt% for pine sawdust, olive stone and almond shell, respectively. Nevertheless, no operational problems (fluidization, melting) were observed during the present experiments which accumulated 40 h of biomass combustion. The reactivity of the
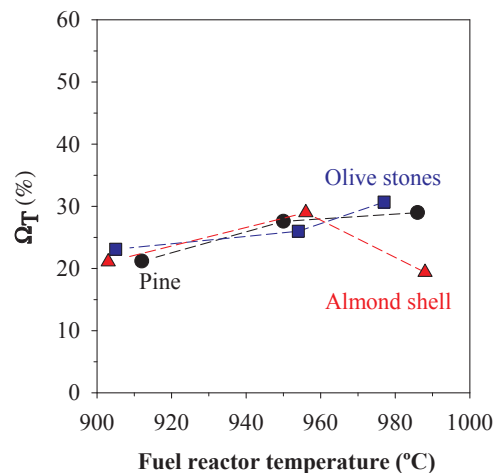
Fig. 7. Total oxygen demand (Ω_T) for the three biomasses at different fuel reactor temperatures.
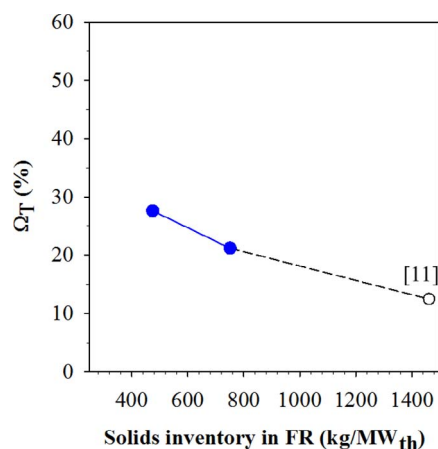
Fig. 8. Effect of the specific solids inventory on the total oxygen demand (Ω_T). T_{FR} = 900 °C. Biomass = pine sawdust, $\phi \approx 1.1$.

oxygen carrier was also not affected. However, longer combustion times operating with the different biomasses would be needed in order to assess the effect of the alkali content of biomass ashes on biomass combustion in CLC. This would be the focus of future research.

4. Conclusions

Three biomasses (pine sawdust, olive stone and almond shell) were tested under iG-CLC mode in a 0.5 kW$_{th}$ unit. 40 hours of biomass combustion were achieved using a low-cost cost oxygen carrier (Tierga ore) at temperatures in the range 900–980 °C. Specific solids inventories lower than 1000 kg/MW$_{th}$ were used as these were considered realistic to operate in a larger CLC unit.

No differences in the combustion behaviour were observed among the biomasses. CO_2 capture of almost 100% can be achieved during biomass fuelled CLC without the use of any carbon stripper. However, the high volatile content of biomass led to high values of total oxygen demand, with values about 25–30%. Using methane as volatile reference compound, the volatile conversion in these experiments was estimated to be about 70%. Naphthalene was the major compound detected in the tar for all biomasses and temperatures. The presence of tar at the outlet of the fuel reactor increases about 1% the value of the total oxygen demand.

Acknowledgments

References

[1] IPCC Climate Change 2014: Synthesis Report. Contribution of working groups I, II and III to the fifth assessment report of the intergovernmental panel on climate change; Geneva (Switzerland); 2014; p 151.

[2] United Nations Framework Convention for Climate Change. The Paris Agreement. http://unfccc.int/paris_agreement/items/9485.php. In 2015.

[3] Williamson P. Emissions reduction: scrutinize CO_2 removal methods. Nature 2016;530:153–5.

[4] Hetland J, Yowargana P, Leduc S, Kraxner F. Carbon-negative emissions: systemic impacts of biomass conversion. A case study on CO_2 capture and storage options. Int J Greenhouse Gas Con 2016;49:330–42.

[5] Kemper J. Biomass and carbon dioxide capture and storage: a review. Int J Greenhouse Gas Con 2015;40:401–30.

[6] Canadell JG, Schulze ED. Global potential of biospheric carbon management for climate mitigation. Nat Commun 2014(5).

[7] Williams RH, Liu G, Kreutz TG, Larson ED. Coal and biomass to fuels and power. Ann Rev Chem Biomol Eng 2011;2:529–53.

[8] Lyngfelt A, Leckner B. A 1000 MW$_{th}$ boiler for chemical-looping combustion of solid fuels – discussion of design and costs. Appl Energy 2015;157:475–87.

[9] Adánez J, Abad A, Mendiara T, Gayán P, De Diego LF, García-Labiano F. Review and assessment of experimental results from chemical looping combustion units burning solid fuels. Prog Energy Combust Sci 2017. http://dx.doi.org/10.1016/j.pecs.2017.07.005.

[10] Shen L, Wu J, Xiao J, Song Q, Xiao R. Chemical-looping combustion of biomass in a 10 kW$_{th}$ reactor with iron oxide as an oxygen carrier. Energy Fuels 2009;23:2498–505.

[11] Mendiara T, Abad A, de Diego LF, García-Labiano F, Gayán P, Adánez J. Biomass combustion in a CLC system using an iron ore as an oxygen carrier. Int J Greenhouse Gas Con 2013;19:322–30.

[12] Schmitz M, Linderholm C, Hallberg P, Sundqvist S, Lyngfelt A. Chemical-looping combustion of solid fuels using manganese ores as oxygen carriers. Energy Fuels 2016;30:1204–16.

[13] Linderholm C, Schmitz M. Chemical-looping combustion of solid fuels in a 100 kW dual circulating fluidized bed system using iron ore as oxygen carrier. J Environ Chem Eng 2016;4:1029–39.

[14] Abad A, Adánez J, Gayán P, de Diego LF, García-Labiano F, Sprachmann G. Conceptual design of a 100 MW$_{th}$ CLC unit for solid fuel combustion. Appl Energy 2015;157:462–74.

[15] Pikkarainen T, Hiltunen I, Teir S. In: Piloting of bio-CLC for BECCS, 4th International Conference on Chemical Looping, Nanjing (China); 2016. Nanjing (China).

[16] Berdugo Vilches T, Lind F, Rydén M, Thunman H. Experience of more than 1000 h of operation with oxygen carriers and solid biomass at large scale. Appl Energy 2017;190:1174–83.

[17] Mendiara T, Pérez R, Abad A, De Diego LF, García-Labiano F, Gayán P, et al. Low-cost Fe-based oxygen carrier materials for the iG-CLC process with coal. 1. Ind Eng Chem Res 2012;51:16216–29.

[18] Mendiara T, De Diego LF, García-Labiano F, Gayán P, Abad A, Adánez J. On the use of a highly reactive iron ore in Chemical Looping Combustion of different coals. Fuel 2014;126:239–49.

[19] International Olive Oil Council. http://www.internationaloliveoil.org; 2017 [accessed 16.03.2017].

[20] International Nut & Dried Fruit. http://www.nutfruit.org; 2017 [accessed 16.03.2017].

[21] Simell P, Ståhlberg P, Kurkela E, Albrecht J, Deutsch S, Sjöström K. Provisional protocol for the sampling and analysis of tar and particulates in the gas from large-scale biomass gasifiers. Version 1998. Biomass Bioenergy 2000;18:19–38.

[22] Virginie M, Adánez J, Courson C, De Diego LF, García-Labiano F, Niznansky D, et al. Effect of Fe-olivine on the tar content during biomass gasification in a dual fluidized bed. Appl Catal B 2012;121–122:214–22.

[23] Neves D, Thunman H, Matos A, Tarelho L, Gómez-Barea A. Characterization and prediction of biomass pyrolysis products. Prog Energy Combust Sci 2011;37:611–30.

[24] Reed TB, Levie B, Graboski MS. Tar conversion. Fundamentals, Development and Scaleup of the Air-Oxygen Stratified Downdraft Gasifier. Solar Energy Research Institute; 1987. SERI/PR-234-2571.

[25] Cuadrat A, Abad A, García-Labiano F, Gayán P, de Diego LF, Adánez J. The use of ilmenite as oxygen-carrier in a 500 W$_{th}$ chemical-looping coal combustion unit. Int J Greenhouse Gas Con 2011;5:1630–42.

[26] Cuadrat A, Abad A, Gayán P, De Diego LF, García-Labiano F, Adánez J. Theoretical approach on the CLC performance with solid fuels: Optimizing the solids inventory. Fuel 2012;97:536–51.

[27] Gayán P, Abad A, de Diego LF, García-Labiano F, Adánez J. Assessment of technological solutions for improving chemical looping combustion of solid fuels with CO_2 capture. Chem Eng J 2013;233:56–69.

[28] Thon A, Kramp M, Hartge EU, Heinrich S, Werther J. Operational experience with a system of coupled fluidized beds for chemical looping combustion of solid fuels using ilmenite as oxygen carrier. Appl Energy 2014;118:309–17.

PAPER II

Manuscript Details

Manuscript number	FUPROC_2019_1949
Title	Manganese ores as low-cost oxygen carriers for biomass chemical looping combustion in a 0.5 kWth unit
Article type	Research Paper

Abstract

Negative Emission Technologies (NETs) should be implemented to reach the objectives set by the Paris Agreement to limit the average temperature increment to 2 °C. One of the options is the development of bioenergy with Carbon Capture and Storage (BECCS) technologies. In this sense, Chemical Looping Combustion (CLC) is one of the most efficient CO_2 Capture technologies both from economical and energy points of view. In CLC, a solid oxygen carrier is used to transfer the oxygen from air to the fuel. In this work two manganese-based ores were used as oxygen carriers to burn three different types of biomass (pine sawdust and two Spanish agricultural residues) in a 0.5 kWth CLC continuous unit. Operational conditions were varied to evaluate their effect on the CO_2 capture efficiency and the total oxygen demand of the process. Almost 100% of CO_2 capture efficiency was reached working with pine sawdust as well as with almond shells. However, high values of total oxygen demand were found, which led to consider further technological solutions to increase the combustion efficiency. In this respect, fuel reactor outlet recycling was evaluated as an operational solution to reduce the oxygen demand with good results.

Keywords	NETs, BECCS; Chemical Looping Combustion (CLC); biomass; manganese ores; oxygen carrier
Taxonomy	Greenhouse Gas Emission, Biomass Technology
Corresponding Author	Luis de Diego
Corresponding Author's Institution	Instituto de Carboquímica (ICB-CSIC)
Order of Authors	Antón Pérez-Astray, Teresa Mendiara, Luis de Diego, Alberto Abad, Francisco García-Labiano, Maria Teresa Izquierdo, Juan adanez
Suggested reviewers	Matthias Schmitz, Marcus Hedberg, Malin Hanning, Johannes Haus, Huijun Ge

Submission Files Included in this PDF

File Name [File Type]

Perez-Astray et al_Cover letter.doc [Cover Letter]

Perez-Astray et al_Highlights.doc [Highlights]

Perez-Astray et al_Manuscript.docx [Manuscript File]

To view all the submission files, including those not included in the PDF, click on the manuscript title on your EVISE Homepage, then click 'Download zip file'.

Dr. Luis F. de Diego
Instituto de Carboquímica (ICB-CSIC)
Miguel Luesma Castán, 4
E-50018 Zaragoza (Spain)
Phone: +34 976 733 977
email: ldediego@icb.csic.es

22th October 2019

Dear editor,

Please find enclosed the file of the manuscript:

" Manganese ores as low-cost oxygen carriers for biomass chemical looping combustion in a 0.5 kW$_{th}$ unit" by Antón Pérez-Astray, Teresa Mendiara, Luis F. de Diego, Alberto Abad, Francisco García-Labiano, María Teresa Izquierdo y Juan Adánez

to be considered for publication in Fuel Processing Technology.

Bio-Energy with Carbon Capture and Storage (BECCS) technologies are crucial to reach the objective set by the Paris Agreement. They allow to actually remove CO_2 previously emitted to the atmosphere, which is commonly known as negative CO_2 emissions. One of the BECCS is Chemical Looping Combustion (CLC) of biomass. CLC was recognized by the International Panel on Climate Change (IPCC) as one of the most promising CCS technologies since it allows 100% CO_2 capture with the lowest energy penalty and cost when compared with operating CCS technologies. In CLC, the oxygen needed for combustion is supplied by a solid oxygen carrier. Thus, oxygen carrier development is one of the cornerstones of this technology. In biomass CLC, it is especially important that these oxygen carriers are as low-cost and environmentally friendly as possible.

The present work analyses the potential as oxygen carriers for biomass CLC of two manganese ores. Results were obtained in a continuous CLC pilot unit (0.5 kW$_{th}$), which adds value to the present work, since limited information of continuous operation can be found in literature. Almost 100% CO_2 capture efficiencies were obtained with these manganese ores as well as better combustion efficiency than oxygen carriers tested up to date. Moreover, the fate of nitrogen in biomass was studied and NO_x emissions in the CLC system evaluated.

This paper is original and all the co-authors agree to the publication in this journal. Moreover, this manuscript has not been previously published, is not currently submitted for review to any other journal, and will not be submitted elsewhere before a decision is made by this journal.

Yours sincerely,

Luis F. de Diego

Papers listed in the reference section of the present paper that have been published within the past 18 months in Fuel Processing Technology and other journals:

[5] J. Adánez, A. Abad, T. Mendiara, P. Gayán, L.F. de Diego, F. García-Labiano, Chemical looping combustion of solid fuels, Prog. Energy Combust. Sci., 65 (**2018**) 6-66.

[6] J. Adánez, A. Abad, Chemical-looping combustion: Status and research needs, Proceedings of the Combustion Institute, 37 (**2019**) 4303-4317.

[11] A. Abad, P. Gayán, T. Mendiara, J.A. Bueno, F. García-Labiano, L.F. de Diego, J. Adánez, Assessment of the improvement of chemical looping combustion of coal by using a manganese ore as oxygen carrier, **Fuel Process. Technol.,** 176 (**2018**) 107-118.

[12] M. Schmitz, C. Linderholm, Chemical looping combustion of biomass in 10- and 100-kW pilots - Analysis of conversion and lifetime using a sintered manganese ore, Fuel, 231 (**2018**) 73-84.

[15] T. Mendiara, A. Pérez-Astray, M.T. Izquierdo, A. Abad, L.F. de Diego, F. García-Labiano, P. Gayán, J. Adánez, Chemical Looping Combustion of different types of biomass in a 0.5 kWth unit, Fuel, 211 (**2018**) 868-875.

[18] C. Kajnäs, M. Hedberg, H. Leion, The Effect of Iron- and Manganese-Based Oxygen Carriers as Bed Materials in Oxygen Carrier Aided Combustion, Energy Technology, 7 (**2019**).

[21] M. Hanning, A. Corcoran, F. Lind, M. Rydén, Biomass ash interactions with a manganese ore used as oxygen-carrying bed material in a 12 MWth CFB boiler, Biomass Bioenergy, 119 (**2018**) 179-190.

[22] F. Hildor, T. Mattisson, H. Leion, C. Linderholm, M. Rydén, Steel converter slag as an oxygen carrier in a 12 MWth CFB boiler – Ash interaction and material evolution, Int. J. Greenh. Gas Con., 88 (**2019**) 321-331.

[32] J. Haus, Y. Feng, E.U. Hartge, S. Heinrich, J. Werther, High volatiles conversion in a dual stage fuel reactor system for Chemical Looping Combustion of wood biomass, in: International Conference on Negative CO_2 emissions, Göteborg (Sweden), **2018**.

[34] S. Jiang, L. Shen, J. Yan, H. Ge, T. Song, Performance in Coupled Fluidized Beds for Chemical Looping Combustion of CO and Biomass Using Hematite as an Oxygen Carrier, Energy Fuels, 32 (**2018**) 12721-12729.

Highlights

- Manganese ores tested as low-cost oxygen carriers for biomass CLC

- Almost 100 % CO_2 capture efficiency was obtained with all manganese ores

- With MnGBHNE oxygen demand values >20% were obtained, similarly to Tierga ore

- MnSA reduced the oxygen demand values to about 10%

- Oxygen demand reduction of 30% recirculating 50% of the fuel reactor outlet flow

1 **Manganese ores as low-cost oxygen carriers for biomass chemical**

2 **looping combustion in a 0.5 kW$_{th}$ unit**

3 A. Pérez-Astray, T. Mendiara, L. F. de Diego*, A. Abad, F. García-Labiano, M. T. Izquierdo,

4 J. Adánez

5 Department of Energy and Environment, Instituto de Carboquímica-ICB-CSIC

6 Miguel Luesma Castán 4, 50018, Zaragoza, Spain

7 ldediego@icb.csic.es

8

9

10

11

12

13

14

15

16

17

18   * Corresponding author:

19   Phone: + 34 976 733 977;

20   Fax: +34 976 733 318

21 **Abstract**

22 Negative Emission Technologies (NETs) should be implemented to reach the objectives set

23 by the Paris Agreement to limit the average temperature increment to 2 ºC. One of the options

24 is the development of bioenergy with Carbon Capture and Storage (BECCS) technologies. In

25 this sense, Chemical Looping Combustion (CLC) is one of the most efficient CO_2 Capture

26 technologies both from economical and energy points of view. In CLC, a solid oxygen carrier

27 is used to transfer the oxygen from air to the fuel.

28 In this work two manganese-based ores were used as oxygen carriers to burn three different

29 types of biomass (pine sawdust and two Spanish agricultural residues) in a 0.5 kW_{th} CLC

30 continuous unit. Operational conditions were varied to evaluate their effect on the CO_2

31 capture efficiency and the total oxygen demand of the process. Almost 100% of CO_2 capture

32 efficiency was reached working with pine sawdust as well as with almond shells. However,

33 high values of total oxygen demand were found, which led to consider further technological

34 solutions to increase the combustion efficiency. In this respect, fuel reactor outlet recycling

35 was evaluated as an operational solution to reduce the oxygen demand with good results.

36

37

38 **Keywords;** NETs, BECCS, Chemical Looping Combustion (CLC), biomass, manganese ores,

39 oxygen carrier

1 Introduction

40

41 The anthropogenic CO_2 emissions associated to the use of fossil fuels for energy production

42 has altered the CO_2 concentration in the atmosphere increasing the natural greenhouse effect.

43 Based on this evidence, the Intergovernmental Panel on Climate Change (IPCC) alerted about

44 the dramatic consequences of increasing the Greenhouse Gases (GHG) emissions. This was

45 already reflected in the Paris Agreement, signed by most of the countries in the world in 2015.

46 The agreement pursues to limit the global average temperature increase in less than 2 ºC at the

47 end of the present century [1].

48 The energy sector is responsible for an important part of the CO_2 emitted to the atmosphere.

49 Only in 2018, about 33.1 Gt_{CO2} were released [2]. In this context, fossil fuels represented

50 about 80% of the primary energy demand in the world. Thus, in order to follow the

51 recommendations in the Paris Agreement actions should be taken in the energy sector to

52 reduce the dependence on fossil fuels. These actions are mostly based on energy efficiency

53 improvement, deployment of renewable energy and implementation of Carbon Capture and

54 Storage technologies (CCS). In this context, the European Union (UE) aimed to increase

55 about 40 % the biomass power contribution in 2020 [3], guaranteeing the almost null CO_2

56 balance and the sustainability of power generation in the lifecycle analysis. Bio Energy with

57 Carbon Capture and Storage (BECCS) combines the use of renewable biofuels, such as

58 biomass, with CCS. The deployment of BECCS technologies would contribute to achieve a

59 negative-CO_2-emission energy sector in the last decades of the present century, and to meet

60 the objectives of the Paris Agreement by removing 22.5 Gt_{CO2} from the atmosphere [4].

61 Different studies have pointed to the Chemical Looping Combustion (CLC) technology as one

62 of the most efficient CCS technologies from both energy and economical points of view [3,

63 5]. The CLC process allows the fuel thermal conversion producing a concentrated CO_2 outlet

64 stream, suitable for a long-term storage in safe locations. Figure 1 shows a scheme of the CLC

65   processes. In CLC, a solid oxygen carrier is used to transfer the oxygen from the air to the

66   fuel using two interconnected reactors, most commonly fluidized beds. In one of the reactors

67   (fuel reactor), the oxygen carrier is reduced while the fuel is oxidized to CO_2 and H_2O. In the

68   other reactor (air reactor), the oxygen carrier is oxidized again in air. A CO_2 concentrated

69   stream at the fuel reactor outlet is thus generated after steam condensation. One of the

70   mechanisms for solid fuel conversion in CLC system is the so–called *In situ* Gasification

71   Chemical Looping Combustion (*i*G-CLC). In *i*G-CLC, the solid fuel enters into the fuel

72   reactor and it is devolatilized. A fluidization agent, namely H_2O or CO_2, is used as a gasifying

73   agent for the char produced during devolatilization. The oxygen carrier interacts then with the

74   gaseous biomass decomposition products .Its lattice reacts with them producing H_2O and

75   CO_2.
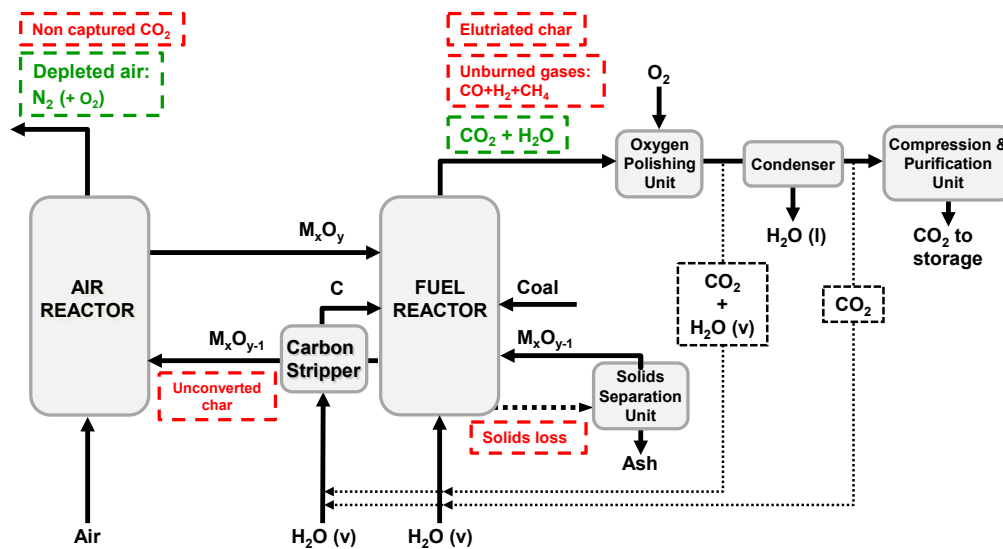
76

77   Figure 1. General scheme of a CLC process for solid fuels

78   The development and testing of potential oxygen carriers is the cornerstone of the CLC

79   technology. Most of the materials developed to date as oxygen carriers are based on nickel,

80   copper, iron and manganese oxides [5], although the use of nickel oxide has been recently

81   disregarded due to its toxicity. Besides, in the case of the combustion of solid fuels, it is

82   especially important to consider the cost of the oxygen carrier to be used in the process since

83   some oxygen carrier losses are expected in the periodic drainage of the solid fuel ashes from

84   the CLC system [6]. In this sense, both iron and manganese oxides would be preferred, due to

85   their large availability, low cost and non-toxic properties. In recent years, intensive research

86   has been conducted to identify both synthetic materials and minerals based on iron and

87   manganese oxides as potential oxygen carriers for the CLC combustion of solid fuels [5]. In

88   the case of the iG-CLC process, research has specifically focused on minerals or industrial

89   residues since they require minimal pretreatment/conditioning and have low production costs

90   [7]. Different iron ores were firstly investigated in the combustion of coal. Many of the

91   research works used ilmenite ($FeTiO_3$) as oxygen carrier. Its good reactivity and mechanical

92   properties converted it in the reference material for solid fuel combustion [5]. Nevertheless,

93   there are other hematite-based minerals with promising characteristics like that denoted as

94   Tierga ore. Experiments with coal in continuous CLC units demonstrated that it was possible

95   to achieve better combustion efficiencies in the iG-CLC process using Tierga ore when

96   compared under similar conditions to the values obtained with ilmenite [8, 9]. Manganese

97   ores have also attracted attention as oxygen carriers for the iG-CLC process in recent years.

98   They showed better performance than ilmenite in the combustion of coal [10-12] but in many

99   cases lower mechanical properties (soft and prone to attrition) [13].

100   Focusing on the specific case of biomass combustion, most of the experience up to date has

101   been obtained operating under iG-CLC mode. High values of carbon capture efficiency were

102   obtained using hematite-based minerals or ilmenite in experimental campaigns in continuous

103   iG-CLC units using different types of biomass. Niu et al. [14] reported almost 100% CO_2

104   capture in 1 kW_{th} continuous unit burning sewage sludge with this type of oxygen carriers.

105   Mendiara et al. also reported CO_2 capture efficiencies between 90-100% in the combustion of

106   pine sawdust and two agricultural residues (olive stones and almond shells) with Tierga ore as

107   oxygen carrier in a 0.5 kW_{th} unit [15] and in a 50 kW_{th} unit [16]. Similar results with Tierga

108   ore were reached by Linderholm and Schmitz [9] burning wood char. However, in many of

109   these works, low values of combustion efficiencies were reached, which represented a total

110   oxygen demand of 20-30 % [3].

111   Manganese ores from different origins and different characteristics have been also studied in

112   recent years as oxygen carriers for biomass combustion at various laboratory scales due to its

113   high reactivity compared to Fe-based ores. Schmitz et al. [10, 12] tested different manganese

114   ores in a 10 and 100 kW_{th} units using biochar and black wood pellets reaching up to 93.5%

115   combustion efficiency. Pikkarainen and Hiltunen [17] used wood pellets, black pellets and

116   wood char in different tests in a 50 kW_{th} unit with braunite as oxygen carrier. Total oxygen

117   demands between 27 and 31% were obtained for the wood pellets. Recently, manganese ores

118   have been tested one step closer to industrial CLC application through the process known as

119   Oxygen Carrier Aided Combustion (OCAC) [18, 19]. In the OCAC process, an oxygen carrier

120   is used as bed material (alone or mixed with sand) in fluidized bed boilers. The OCAC

121   process allow to test the material over longer periods of time than those reported in pilot units

122   and in a more realistic conditions [20]. For example, the effect of biomass ash on the oxygen

123   carrier performance could be better evaluated in OCAC experiments [21, 22].

124   The authors of the present paper perfomed a previous screening study in a batch fluidized bed

125   reactor with various manganese oxygen carriers including manganese ores from South Africa,

126   Gabon and Brazil [23, 24]. They identified two promising materials, i.e. a manganese ore

127   from South Africa which (MnSA) showed high reactivity to CO and one manganese ore from

128   Gabon (MnGBHNE) with good reactivity to H_2, CO and CH_4 as well as long lifetime [23].

129   Working with the manganese ore in a continuous 0.5 kW_{th} unit and with coal as fuel, Abad et

130   al. [11] found remarkable values of CO2 capture efficiency attributed to the high char

131   gasification rate presented by this mineral and an improvement in the combustion efficiency

132   reached when compared to the reference oxygen carrier ilmenite.

133   Thus, the main objective of the present work was to assess the potential of the manganese ores

134   from South Africa and Gabon in the CLC of biomass in order to improve the combustion

135   efficiency of the process and therefore reduce the oxygen demand values previously reported

136   for Fe-based oxygen carriers. To reach this objective, the influence of different operating

137   variables, such as the fuel reactor temperature or the specific solids inventory on the

138   performance of the process was evaluated. Different types of biomass were used as fuel,

139   including pine sawdust and two Spanish agricultural residues (olive stones and almond

140   shells). Besides the evaluation of more reactive oxygen carriers, the reduction of the total

141   oxygen demand in CLC of biomass will be addressed considering other technological options

142   such as recirculation of the outlet stream from the fuel reactor.

143 **2   Material and methods**

144 **2.1   Materials**

145   Two manganese-based ores were used during the experimental campaign as oxygen carriers.

146   One came from Gabon (hereafter named MnGBHNE) and another one from South Africa

147   (hereafter named MnSA), both supplied by Hidro Nitro Española S.A. The natural ores were

148   crushed and sieved to 100–300 μm. Then, a thermal treatment was carried out in air at 800 °C

149   during 2 h to complete the oxidation of the particles and to increase the crushing strength of

150   these materials. Table 1 presents the main properties of both manganese oxygen carriers.

151   More information about the oxygen carriers can be found elsewhere [23]. The reactivity of

152   these materials were evaluated in a TGA, considering the Mn_3O_4-MnO and the Fe_2O_3-Fe_3O_4

153   redox pairs [23]. A Spanish pine wood biomass (*Pinus sylvestris*) together with two Spanish

154   agricultural residues, olive stones (*Olea europaea*) and almond shells (*Prunus dulcis*), were

155   selected as fuels because of their high availability [25, 26]. The raw materials were ground

156   and sieved to +500–2000 μm. The main characteristics of these fuels are presented in Table 2.

157 <div align="center">Table 1: Main characteristics of the manganese ores oxygen carriers.</div>

		MnGBHNE	MnSA
Crushing strength (N)		1.8	4.6
Air Jet Index (%)		14.4	5.5
Oxygen transport capacity, R_{OC} (%)		5.1	4.7
Porosity (%)		38.7	12.3
Skeletal density (kg/m^3)		2800	3510
BET surface area (m^2/g)		12.3	0.6
XRD main crystalline phases(wt.%)	**Mn_2O_3**	68.2	46.2
	Fe_2O_3	10.6[a]	4.4[a]

158 <div align="center">[a] Determined by XRD and quantified by thermogravimetric analysis.</div>

159 2.2 Experimental set up

160 A 0.5 kW$_{th}$ continuous CLC unit placed at the ICB-CSIC (Spain) was used during all the

161 experimental campaign. Figure 2 presents a scheme of the CLC unit. A detailed description of

162 the unit can be found elsehwere and only a brief description will be included here [15]. The

163 unit is based in two bubbling bed reactors connected by the loop seals that avoid the mixture

164 of the gases. The upper loop seal also acts as solids reservoir at the fuel reactor entrance. A

165 conical solids valve is used in the unit for the solids circulation rate control. Besides a

166 diverting valve is used for the solids circulation rate measurement. Various highly efficient

167 cyclones collect the solids materials exiting the reactors. The unit is equipped with different

168 temperature and pressure drop sensors connected to a computer where data are registered. A

169 double screw feeder is used to control the solid fuel fed at the botton part of the fuel reactor.

170 Electric furnaces allow the temperature control in each reactor. The experimental campaign

171 involved more than 160 h of hot fluidization with more than 63 h of biomass *i*G-CLC

172 operation. Carbon balances closed about 99%.

173

174　　　　　　　　　　　　Table 2: Main characteristics of the different tyoes of biomas.

	Pine sawdust	Almond shells	Olive stones
Proximate Analysis (wt%)			
Moisture	4.2[a]	2.3[a]	9.4[a]
Volatile matter	81.0	76.6	72.5
Fixed carbon	14.4	20.0	17.3
Ash	0.4	1.1	0.8
Ultimate Analysis (wt%)			
C	51.3	50.2	46.5
H	6.0	5.7	4.8
N	0.3	0.2	0.2
S	0.0	0.0	0.0
O	37.8[b]	40.5[b]	38.3[b]
LHV (kJ/kg)	19158	18071	17807
Ω_{sf} (kg O_2/kg biomass)	1.5	1.4	1.2

175　　　　　　　　　　[a] Stabilized by exposure to the atmosphere. [b] By difference.

176　The flows of the fluidizing gas at the fuel reactor and air reactor entrance were kept constant

177　at 130 and 1200 L/h (STP), respectively, during all the experimental campaign. These flows

178　corresponded to fluidization velocities of about 0.1 m/s for the fuel reactor and 0.5 m/s for the

179　air reactor. The fuel reactor temperature range was varied between 850 and 966 ºC. The

180　temperature in the air reactor was always 950 ºC. The solids inventory was about 2.3 kg for

181　the MnGBHNE and about 2.0 kg for the MnSA. Tar collection at the fuel reactor outlet was

182　carried out according to the standard protocol [27] and a gas chromatograph coupled to a mass

183　spectrometer was used in the analysis, being naphthalene and phenanthrene chosen for the

184　external calibration procedure [28].

185

1.- Fuel Reactor	7.- Solid reservoir
2.- Loop Seal	8.- Solids control valve
3.- Air Reactor	9.- Fuel feeding system
4.- Riser	10.- Evaporator
5.- Cyclone	11.- Furnace
6.- Diverting solids valve	12.- Filter
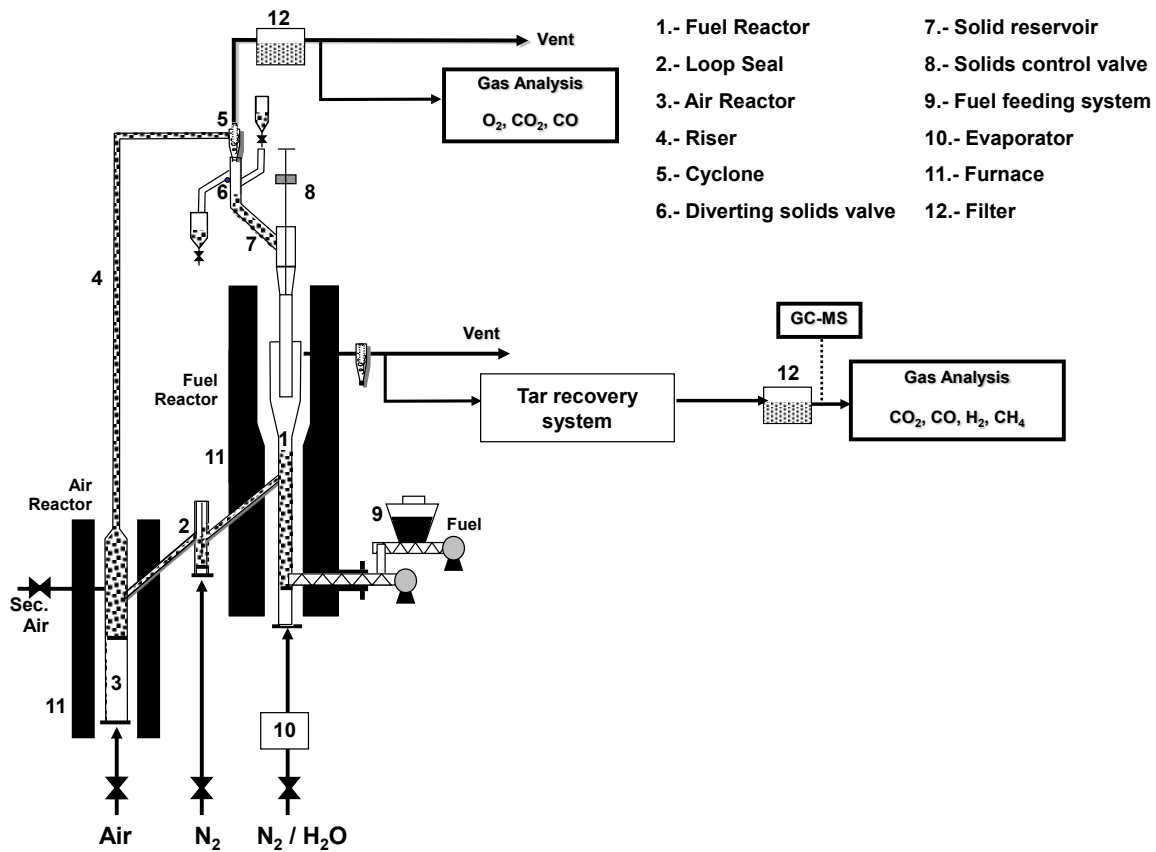
186

187   Figure 2. Experimental unit ICB-CSIC-s1

188   Table 3 presents the experimental series with the main operating conditions in the

189   experimental campaign performed. A total of 17 tests at steady state operating conditions were

190   carried out with MnGBHNE and 4 with MnSA as oxygen carriers in the 0.5 kW$_{th}$ CLC unit for

191   solid fuels previously presented. Previous experiments with different types of biomass

192   performed with the Fe-based oxygen carrier named as Tierga ore were also considered for

193   comparison [15]. Tierga ore has been previously identified as one of the most reactive Fe-

194   based oxygen carriers.

195   **2.3   Data evaluation**

196   To analyze the effect of different operating variables on the performance of both manganese

197   minerals as oxygen carriers and compare them, the CO_2 capture efficiency (η_{CC}) and the total

198   oxygen demand (Ω_T) have been selected as the key parameters.

Table 3: Operating conditions in the experimental campaign with MnGBHNE and MnSA

Test	F.A (-)	Biomass	T_{FR} (ºC)	ϕ (-)	$\dot{m}_{OC}$ (kg/h)	$\dot{m}_{sf}$ (kg/h)	P (W$_{th}$)	$\dot{m}_{FR}^{*}$ kg/MW	norm. $\dot{m}_{oc}$ (kg/s)/MW$_{th}$
					MnGBHNE				
GB1	H_2O	Pine	935	2,0	7,2	0,12	639	605	3,1
GB2	H_2O	Pine	900	2,0	7,2	0,12	639	625	3,1
GB3	H_2O	Pine	855	2,0	7,2	0,12	639	590	3,1
GB4	H_2O	Pine	890	1,8	7,2	0,135	718	555	2,8
GB5	H_2O	Olive	900	1,9	6,2	0,132	610	700	2,8
GB6	H_2O	Almond	905	1,9	6,5	0,124	617	675	2,9
GB7	H_2O	Almond	940	1,5	5,0	0,124	617	650	2,3
GB8	CO_2	Pine	910	2,9	9,8	-	612	775	4,5
GB9	CO_2	Pine	915	2,7	9,8	0,123	655	715	4,2
GB10	CO_2	Pine	900	2,9	9,7	-	612	665	4,4
GB11	CO_2	Pine	950	3,3	12,4	0,128	681	520	5,0
GB12	H_2O	Pine	935	1,0	3,8	0,128	681	700	**1,6**
GB13	H_2O	Pine	920	3,5	12,0	0,12	639	685	**5,4**
GB14	H_2O	Pine	925	3,5	12,0	0,117	623	675	**5,4**
GB15	H_2O	Pine	950	1,0	3,8	0,117	623	650	**1,6**
GB16	H_2O	Pine	945	3,5	12,0	0,128	681	670	**5,4**
GB17	H_2O	Pine	965	0,7	2,8	0,117	623	530	**1,2**
					MnSA				
SA1	CO_2	Pine	910	2,5	9,2	0,116	615	**770**	4,4
SA2	CO_2	Pine	930	2,7	9,6	0,116	615	**730**	4,0
SA3	CO_2	Pine	900	1,9	7,2	0,12	639	**970**	3,1
SA4	CO_2	Pine	890	2,2	8,4	0,12	639	**970**	3,7

200

201   The CO_2 capture efficiency evaluates the CO_2 already captured as a fraction of the produced

202   carbon gases.

203 $$\eta_{CC} = 1 - \frac{F_{CO_2,outAR}}{F_{CO_2,outFR} + F_{CH_4,outFR} + F_{CO,outFR} + F_{CO_2,outAR}} \qquad (1)$$

204 The total oxygen demand is the fraction of oxygen needed for the combustion of all the

205 unburned compounds produced and the oxygen needed for the complete combustion of the

206 introduced solid fuel.

207 $$\Omega_T = \frac{4F_{CH_4,outFR} + F_{CO,outFR} + F_{H_2,outFR}}{\frac{1}{M_0}\Omega_{sf}\dot{m}_{sf}} \qquad (2)$$

208 The oxygen to fuel ratio (ϕ) relates oxygen transferred from the air reactor to the fuel into the

209 fuel reactor with the oxygen needed for the fuel complete combustion.

210 $$\phi = \frac{\dot{m}_{OC} \cdot R_{OC}}{\dot{m}_{sf} \cdot \Omega_{sf}} \qquad (3)$$

211 Another parameter related the oxygen carrier to fuel ratio (ϕ) is the solids circulation rate,

212 normalized per MW_{th} (m_{FR}^*).

3 Results and discussion

3.1 Evaluation of MnGBHNE as oxygen carrier

215 3.1.1 Influence of the fuel reactor temperature and the gasifying agent

216 The first series of experiments (GB1-GB17) in Table 3 evaluated the performance of

217 MnGBHNE oxygen carrier in a range of specific solids inventories of 520-775 kg/MW_{th}.

218 Figure 3 presents the results corresponding to the evaluation of the effect of the fuel reactor

219 temperature (tests GB1 to GB7) on both the CO_2 capture efficiency (η_{CC}) and the total oxygen

220 demand (Ω_T) using the different types of biomass (pine, olive stone and almond shell). These

221 experiments were done using steam as fluidizing agent and values of normalized solids

222 circulation rates ($norm.\dot{m}_{oc}$) close to 3 $kg/(s \cdot MW_{th})$. Also previous experimental results

223　obtained with the Tierga ore were here presented (open symbols) to facilitate the comparison

224　between both oxygen carriers.

225
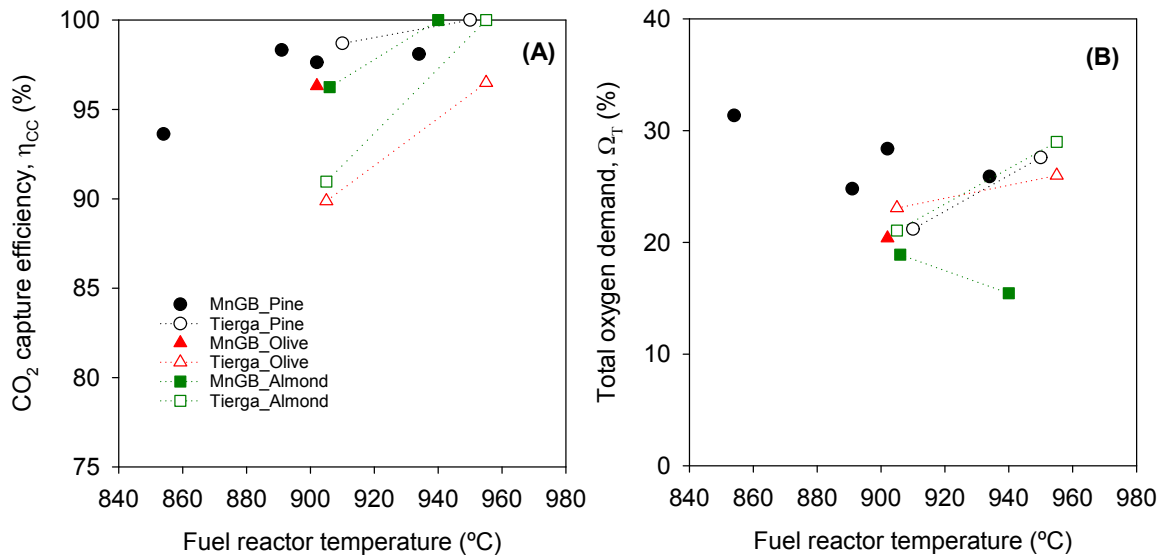
Figure 3. CO_2 capture efficiency and total oxygen demand at different fuel reactor temperatures using

227　MnGBHNE as oxygen carrier with different types of biomass

228　As it was the case in the experiments with Tierga ore, the CO_2 capture efficiencies reached

229　with the MnGBHNE oxygen carrier increased with the fuel reactor temperature and were

230　higher than 90% regardless the biomass used. It should be here reminded that these results

231　were obtained in the absence of a carbon stripper in the 0.5 kW_{th} unit where the experiments

232　with both oxygen carriers were performed. Nevertheless, differences can be observed in

233　Figure 3(A) between oxygen carriers and type of biomass. In the experiments with

234　MnGBHNE carried out in the temperature range between 855 and 935 ºC, the values of CO_2

235　capture efficiencies were larger than 95 % for pine, olive stone and almond shells. However,

236　in the experiments with Tierga ore, lower CO_2 capture efficiencies have been reached in the

237　experiments with olive stones and almond shells when compared to pine. This different

238　behaviour would indicate that the conversion of biomass char would be more favoured when

239　MnGBHNE is used as oxygen carrier, as it has been previously reported using coal as fuel

240　[11]. Figure 3(B) shows the values obtained for the total oxygen demand with the different

13

241   types of biomass. Results corresponding to MnGBHNE showed a clear tendency of the total

242   oxygen demand to decrease with the increase in the fuel reactor temperature. Nevertheless,

243   the oxygen demand values reached were in line to those previously reported for Tierga ore

244   working under similar conditions [15]. Higher oxygen demand values were determined for

245   the experiments with pine compared to those obtained for olive stone and almond shell, which

246   may be attributed to the different composition of the volatiles/gasification products depending

247   on the biomass considered.

248   Figure 4 shows the contribution to the total oxygen demand value of the different unburnt

249   compounds measured at the fuel reactor exit (H_2, CO and CH_4) for the experiments performed

250   with pine and the two oxygen carriers under similar operating conditions.
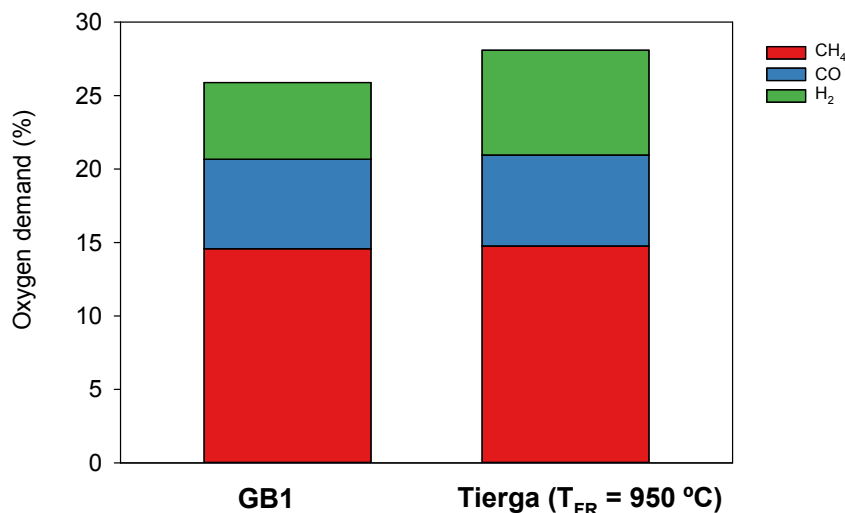
251

252   Figure 4. Comparison of partial oxygen demand for H_2, CO and CH_4 at similar conditions using Tierga ore and

253   MnGBHNE as oxygen carriers in experiments with pine

254   As it can be seen in Figure 4, the partial oxygen demands for CO and CH_4 were similar at

255   comparable specific solids circulation rates, 3.1-3.6 kg/(s·MW$_{th}$, for MnGBHNE and Tierga

256   ores in experiments using H_2O as gasifying agent and pine sawdust as biomass. However, a

257   reduced contribution to the total oxygen demand of the H_2 partial demand is observed in the

258   experiments with MnGBHNE in comparison to Tierga.

259　All the experiments in Figure 3 used steam as gasifying agent. The influence of the gasifying

260　agent on the results obtained (G8-G11) was also assessed with MnGBHNE oxygen carrier and

261　shown in Figure 5. The figure compares the values of CO_2 capture efficiency and total oxygen

262　demand in experiments with pine at different fuel reactor temperatures and a normalized

263　solids circulation rate of 3-4 kg/(s·MW$_{th}$). Similar trends were obtained in both cases when

264　steam or CO_2 were used as gasifying agents. In Figure 5(A) CO_2 capture efficiencies close to

265　100% are obtained in all the experiments with CO_2, regardless the temperature in the fuel

266　reactor. In the case of the total oxygen demand values in Figure 5(B), the values obtained with

267　H_2O and CO_2 as gasifying agents follow the same decreasing trend with the fuel reactor

268　temperature, reaching a value of 16.9% at 950ºC. If results with CO_2 and steam as gasifying

269　agents are similar, the use of CO_2 would be preferred for further experiments with the

270　MnGBHNE material since in the operation at higher scale recirculated CO_2 from the fuel

271　reactor outlet could be used as gasifyig agent, with the corresponding energy saving

272　associated to steam generation.
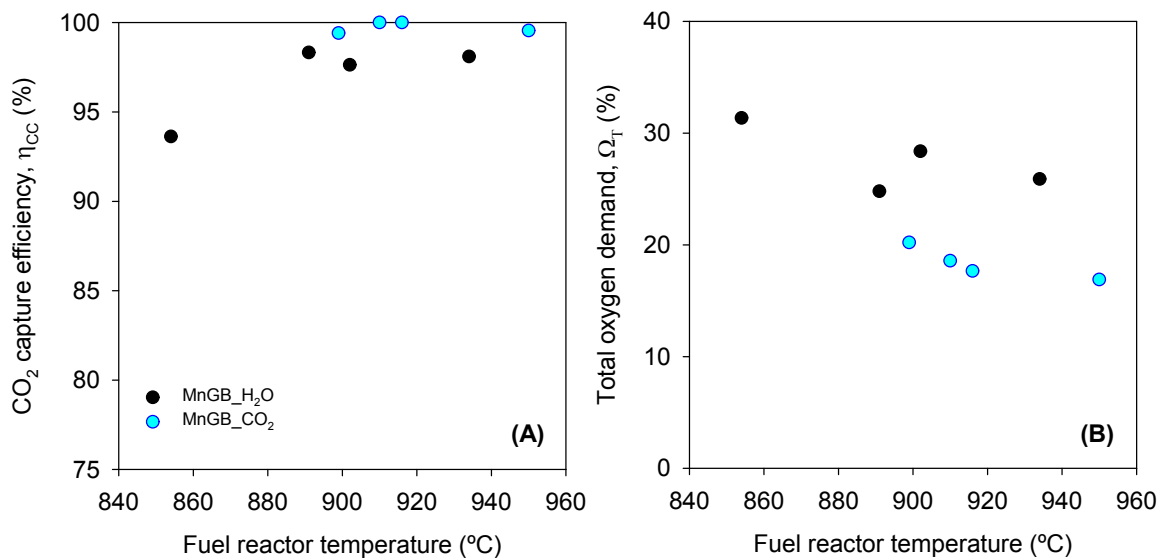
273

274　Figure 5. CO_2 capture efficiency and total oxygen demand at different fuel reactor temperatures using

275　MnGBHNE as oxygen carrier with pine and H_2O or CO_2 as gasifying agents

276

277   3.1.2 Influence of the normalized solids circulation rate (m_{FR}^*)

278   As mentioned before, the solids circulation rate, normalized per MW_{th} (m_{FR}^*) is related to the

279   amount of oxygen the oxygen carrier to fuel ratio (ϕ). In this section, the influence of the

280   variation of this parameter on the results obtained with the MnGBHNE oxygen carrier is

281   addressed (G12-G17). Figure 6 shows the CO_2 capture efficiency and the total oxygen

282   demand at various normalized solids circulation rates for the MnGBHNE burning pine

283   sawdust and using H_2O as gasifying agent at a temperature in the fuel reactor of 940 ºC.
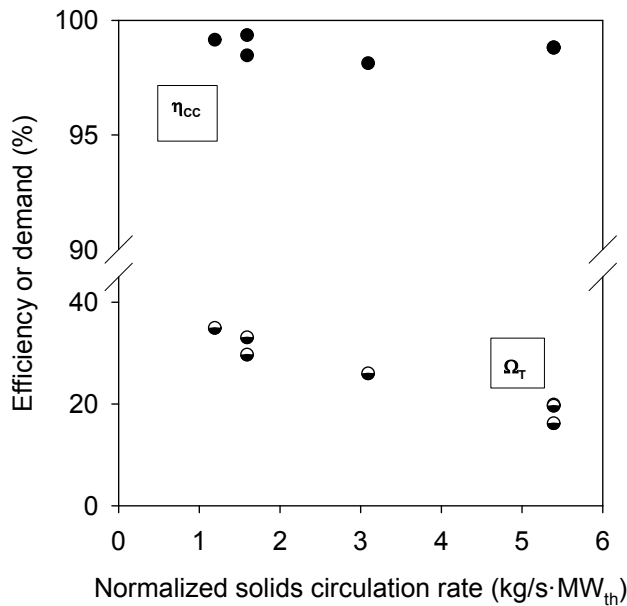
284

285   Figure 6 .CO_2 capture efficiency and total oxygen demand for different normalized solids circulation rates at a

286   fuel reactor temperature of 940ºC burning pine sawdust and using H_2O as gasifying agent

287   Although the increase in the solids circulation rate implies a decrease in the average residence

288   time in the fuel reactor, the CO_2 capture efficiency seems to be not affected by the normalized

289   solids circulation rate in these experiments since very high values (>98%) were obtained at

290   any of the conditions tested. The high reactivity of the biomass char may compensate the

291   decrease in the residence time. However, the total oxygen demand for MnGBHNE decreases

292   when the normalized solids circulation rate increases, reaching a value about 19.6% with 5.4

293   kg/(s·MW_{th}), corresponding to $\phi = 3.5$. A higher solids circulation rate implies higher oxygen

294   supply in the fuel reactor. This may be the reason for the decrease in the total oxygen demand.

295   From the evaluation made in the experimental campaign involving MnGBHNE and the

296   subsequent comparison performed with previous results obtained with Tierga ore under

297   similar conditions, it can be said that both carriers performed similarly in CLC of biomass and

298   no clear advantage of one carrier over the other was found. This was the reason to evaluate

299   another of the pre-selected manganese minerals, i.e. MnSA, which has been previously found

300   by the authors as especially reactive to CO. Moreover, it presented adequate fluidization

301   properties and lifetime [23]. The results obtained in CLC of biomass with MnSA will be

302   presented next and compared to MnGBHNE.

303   **3.2   Evaluation of MnSA as oxygen carrier**

304   As it is shown in Table 3, experiments were conducted using MnSA as oxygen carrier and

305   pine as fuel at different fuel reactor temperatures (SA1-SA4). In this case, CO_2 was used as

306   gasifying agent, as it was the case in the experiments with MnGBHNE. Figure 7 presents the

307   CO_2 capture efficiencies and the total oxygen demands obtained with both MnGBHNE and

308   MnSA for the various fuel reactor temperatures analyzed and using specific solids inventories

309   about 700 kg/MW_{th} with both of them.

310   Regarding the CO_2 capture efficiency values in Figure 7(A), no differences can be found

311   between oxygen carriers. Regardless the fuel reactor temperature both carriers reached values

312   of CO_2 capture efficiency higher than 99% in this CLC unit without a carbon stripper. Figure

313   7(B) shows the total oxygen demand for different fuel reactor temperatures for both oxygen

314   carriers. The values of the oxygen demand decrease with temperature for both materials. In

315   the comparison between MnGBHNE and MnSA it was observed that the oxygen demands

316   obtained with MnSA were clearly lower than those corresponding to MnGBHNE, reaching a

317   value as low as 10.2% at 928 ºC. Moreover, to obtain oxygen demand values about 10 %

318   working with Tierga ore it was necessary to increase the solids inventory to about 1400

17

319 kg/MW$_{th}$ and decrease the normalized solids circulation rate [29]. Therefore, MnSA improved

320 the performance of the other two minerals and can be considered a better alternative for

321 biomass CLC.
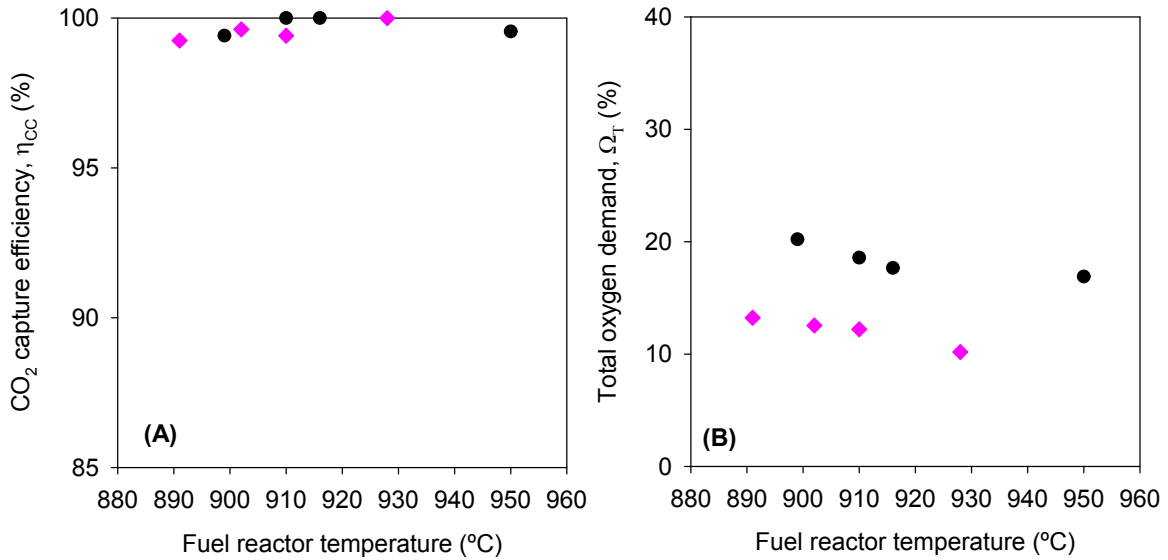
322

323 Figure 7 .CO$_2$ capture efficiency and total oxygen demand for MnGBHNE and MnSA for different fuel reactor

324 temperatures burning pine sawdust and using CO$_2$ as gasifying agent (normalized solids circulation rate = 3.5-4.5

325 kg/MW$_{th}$·s)

326 It is possible to compare the partial contributions to the total oxygen demand made by each of

327 the unburnt gases in the experiments with both MnGBHNE and MnSA. This was made in

328 Figure 8 for fuel reactor temperature of 910 ºC (GB8 and SA1) and averaged 925 ºC (GB9

329 and SA2) and normalized solids circulation rate about 4 (kg/s)/MW$_{th}$. For both oxygen

330 carriers, the major contribution to the oxygen demand is that coming from unburned methane.

331 However, the contribution of H$_2$ and CO in the case of MnSA is clearly diminished compared

332 to that found for MnGBHNE since MnSA seems to be more reactive to these gases than

333 MnGBHNE. It should be hihghlighted that complete H$_2$ combustion at a fuel reactor

334 temperature as low as 910 ºC was reached with the MnSA
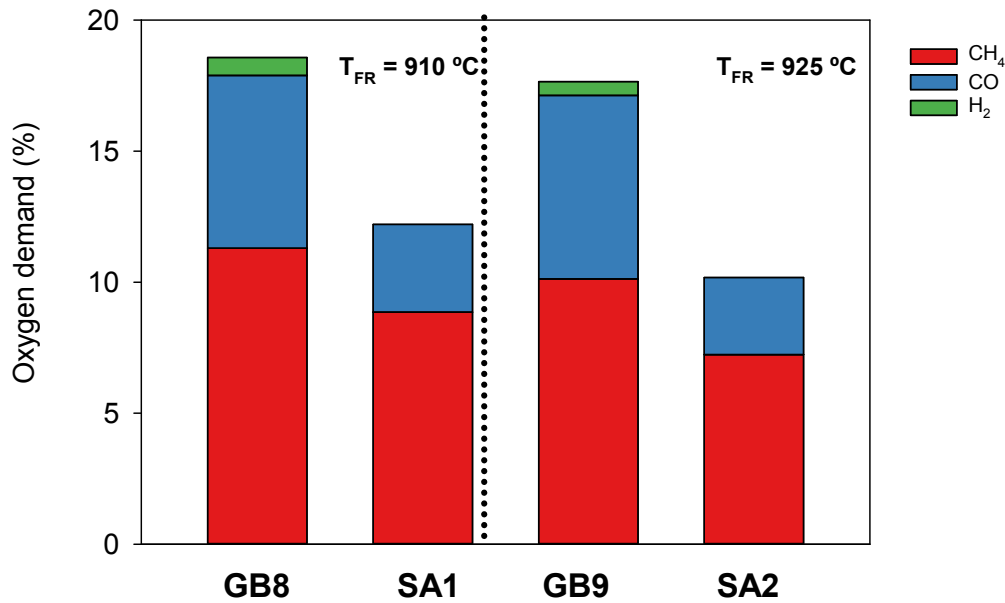
Figure 8. Partial oxygen demand for H_2, CO and CH_4 using MnGBHNE and MnSA as oxygen carriers in experiments with pine at fuel reactor temperatures between 910 and 925 ºC and normalized solids circulation rate about 4 (kg/s)/MW_{th}

3.3 Measures to decrease the oxygen demand in biomass CLC

As it has been also observed in the present work, one of the main problems found in the performance of CLC of biomass is the high values obtained for the total oxygen demand [3]. These high values are associated to the high volatile content of biomass when compared to other fuels such as coal. The existence of an elevated amount of unburned products at the fuel reactor outlet makes necessary the incorporation of a polishing step to complete the combustion. This oxygen polishing represents an important energy penalization for the CLC process and therefore it should be either minimized or even avoided [5]. Several strategies have been proposed in literature to avoid this oxygen polishing step [30]. One of them is the use of highly reactive oxygen carriers. A higher reactivity of the oxygen carrier would facilitate the combustion of H_2, CO and CH_4 in the fuel reactor and decrease the total oxygen demand. This strategy has been already considered in section 3.2 of the present work, with the testing of MnSA searching for an improvement of the results obtained with MnGBHNE.

352   However, it is already known that not only the reactivity of the oxygen carrier can make the

353   difference in the final value of the oxygen demand. There are other factors associated to the

354   contact between unburned gases and oxygen carrier particles that would also significantly

355   contribute to the oxygen demand decrease [31]. Gayán et al. recently proposed different

356   technological solutions for the decrease in the oxygen demand [30], such as the use of a

357   second fuel reactor, the feed of the solid fuel to the carbon stripper or the recirculation of part

358   of the fuel reactor outlet stream. In line with the first of these options (second fuel reactor),

359   some technological alternatives have been already tested and results published in literature. At

360   Hamburg University of Technology, a two-stage bubbling bed fuel reactor system in a 25

361   kW$_{th}$ CLC unit was commissioned and tested [32]. The two stages were separated by a gas

362   distributor placed between the two beds. German hard wood biomass was used as fuel and a

363   copper-based metal oxide, CuO/Al_2O_3, as oxygen carrier. The biomass was fed to the lower

364   stage of the fuel reactor and was gasified there. The gaseous gasification products (H_2, CO

365   and CH_4) rose to the second stage and reacted with freshly oxidized oxygen carrier particles,

366   thus facilitating their combustion. Almost complete combustion of biomass gasification

367   products was achieved in the experiments since the oxygen demand values reported were as

368   low as 1.6%. The effect on the oxygen demand of splitting the fuel reactor into several

369   fluidized beds consecutively placed was also considered in another two 1-2 kW$_{th}$ continuous

370   CLC units [33, 34]. Yan et al. [33] tested a two-step fuel reactor consisting of two spout-

371   fluidized bed using hematite as oxygen carrier. The fuel (sewage sludge) was fed in the bed at

372   the bottom and then gasified. The combustible gases released reacted afterwards in the second

373   bed with oxidized oxygen carrier particles returning from the air reactor. To evaluate the

374   effect of the second bed, the authors defined the combustion compensation efficiency

375   ($\eta_{(G),FR}$), which calculated the degree of conversion of the combustible gases in the second

376   step of the fuel reactor. They found that this value increased with temperature, reaching

377   values of 50% at 900ºC, the highest temperature tested. Recently, Jiang et al. [34] built a fuel

378   reactor with four gas distributors that divided the reaction chamber into five chambers which

379   were bubbling fluidized beds. In this case, the oxygen carrier particles (Australian hematite)

380   went up with the fuel (sawdust/rice husk) through gas distributors. The conversion of

381   gasification products was significantly improved and no hydrogen was found at the fuel

382   reactor flue gas.

383   In the present work, another of the technological options for oxygen demand reduction has

384   been considered. We evaluated the effect of the gas recirculation to the fuel reactor of the fuel

385   reactor outlet stream. The methodology used for this purpose was to simulate a recycled

386   stream and to analyze the behavior of the different unburned compounds (i.e H_2, CO and

387   CH_4). For that, tests identified in Table 3 as GB8 and SA1 were selected and individual flows

388   of each unburned compound corresponding to gas concentrations from 0-10% in the inlet

389   stream were introduced while the total flow at the fuel reactor inlet was kept constant at 130

390   l_N/h. Knowing the amount of gas introduced and the gas concentrations before and after the

391   gas introduction, it was estimated the degree of conversion (χ) in the fuel reactor for each of

392   the introduced gases in Table 4. Hydrogen was completely converted regardless the molar

393   flow introduced to the fuel reactor. In the case of CO and CH_4, about 80% and 70%

394   conversion, respectively, were reached for the different molar flows of each compound that

395   were tested.

396   Table 4. Conversion χ (%) for each gasification gas in the fuel reactor bed at 900 ºC

Unburned gas	MnGBHNE	MnSA
H_2	100	100
CO	81	78
CH_4	67	70

397

398   After the experimental tests, it was simulated the behavior of a CLC unit with different gas

399   recirculation (R), see Figure 9.
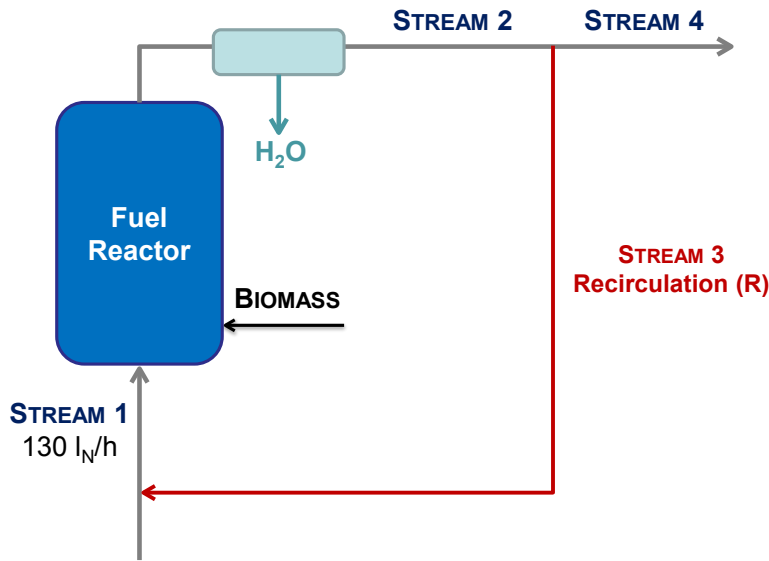
400

401   Figure 9. Fuel reactor outlet recycling scheme

402   Dry recycle (stream 3) was assumed in the calculations. The recirculation (R) is defined as the

403   percentage of the outlet stream (stream 2) being recycled to the fuel reactor (stream 3). For the

404   simulation, the iterative scheme shown in Figure 10 was used. The iterative process started

405   considering the composition of stream 3 which is the same as that of stream 2 when

406   recirculation is R = 0 %. Then, a value of R is assumed and the molar flows of each

407   component calculated. The value of χ in Table 4 for each gaseous compound was considered

408   in order to recalculate the composition in the new stream 2. These values are compared to

409   those calculated in the previous iteration. If the molar flows are similar, then the iterative

410   process is stopped and the total oxygen demand at the fuel reactor outlet calculated based on

411   these molar flows. If they are not similar, the process is repeated.

412
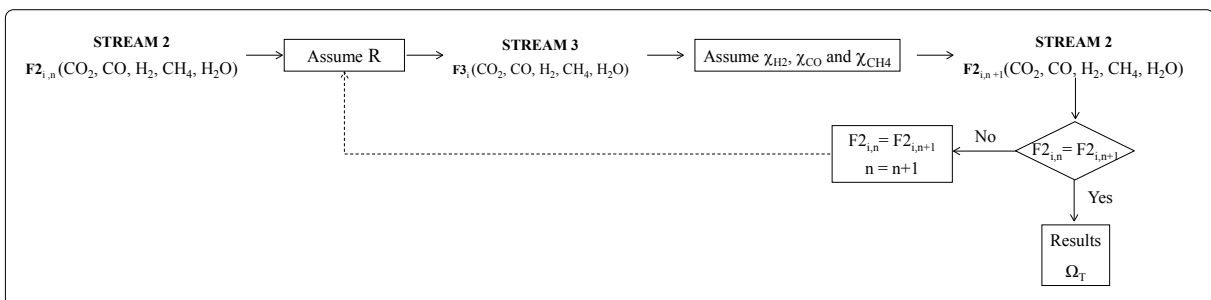
413   Figure 10. Scheme for the iterative process followed to simulate the recirculation of the fuel reactor outlet stream

22

414 The simulation was carried out with a molar $CO_2/C_{biomass}$ ratio ~ 1.2, similar to the ratio in the

415 experiments GB8 and SA1 and assuming in the first iteration the composition of those tests.

416 Figure 11 represents the total oxygen demand values obtained through the application of the

417 iterative simulation as a function of the recirculation for both MnGBHNE and MnSA oxygen

418 carriers in the combustion of pine sawdust. As it can be observed, the total oxygen demand is

419 reduced when the gas recirculation is increased. In the limit case, that is, when the fuel reactor

420 is fluidized with only recirculated gas (R~50%), values close to 30% of total oxygen demand

421 reduction were observed for both oxygen carriers, pointing to the promising possibilities of

422 this technical improvement.
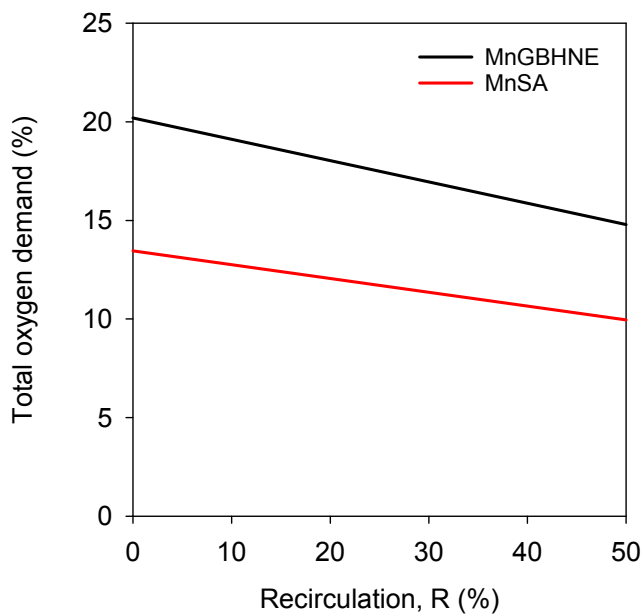
423

424 Figure 11. Effect of fuel reactor outlet gas recycling

425 **3.4   NO$_x$ and tar emissions during biomass combustion**

426 Previous studies with biomass fueled CLC using the Tierga ore as oxygen carrier

427 demonstrated the lower formation of NO$_x$ compared with the conventional biomass

428 combustion. In experiments with Tierga ore, most of the fuel-N appeared as N$_2$ at the fuel

429 reactor outlet with only little presence of NO at the air reactor [35]. Similar conclusions were

430 obtained in the present work with both MnGBHNE and MnSA oxygen carriers. The high CO$_2$

23

431   capture efficiencies reached shown in Figures 3 to 7 revealed a high char conversion in the

432   fuel reactor and therefore, almost no unconverted char reached the air reactor. Thus, no NO

433   emissions from the air reactor were detected during the present experimental campaign.

434   Regarding the amount of NO present in the fuel reactor outlet stream the value of the NO_x/C

435   molar ratio as it was done in the experiments with Tierga ore in order to determine whether

436   this ratio was lower than that recommended for CO_2 concentrated streams to be transported

437   and stored [36]. The limit of the ratio was 280 ppm. In all of the cases in the experiments

438   with MnGBHNE and MnSA, the ratio was well below this value as it can be seen in Table 5.

439   In the table, similar results for the NO_x/C were obtained for pine sawdust and olive stones and

440   slightly lower for almond shells under similar experimental conditions (GB3, GB5 and GB6).

441   The value of ϕ seems to also influence the final NO_x/C molar ratio. Comparing results for

442   GB16 and GB17, higher values of ϕ decreased the amount of NO_x formed. Comparing the

443   results obtained with both MnGBHNE and MnSA under similar conditions, i.e. GB9 and

444   SA2, it can be concluded that no differences were observed between both oxygen carriers.

445   Table 5. Comparison of the NO_x/C ratio obtained under different experimental conditions

	Gasifying agent	Biomass	T_{FR} (ºC)	ϕ	NO_x/C
GB3	H_2O	Pine sawdust	854	2.0	218
GB5	H_2O	Olive stones	902	1.9	213
GB6	H_2O	Almond shells	906	1.9	160
GB9	CO_2	Pine sawdust	916	2.7	78
GB16	H_2O	Pine sawdust	946	3.5	67
GB17	H_2O	Pine sawdust	966	0.7	142
SA2	CO_2	Pine sawdust	928	2.7	123
SA4	CO_2	Pine sawdust	891	2.2	97

446

447   Another of the emissions from biomass combustion systems is tar. The tar presence in

448   biomass gasification units should be minimized in order to avoid the problems caused by

449   fouling. Previous studies of tar in a 0.5 kW_{th} *i*G-CLC plant with the Tierga ore as oxygen

450   carrier identified naphthalene as the major compound in the tar measured at different

451   operating conditions with pine sawdust. The authors reported a total tar amount of 4.29 g/Nm^3

452   at 950 ºC and 785 kg/MW$_{th}$ [35]. Similar results were obtained in the experiments with

453   MnGBHNE and MnSA as oxygen carriers. In both cases it was also naphthalene the major

454   compound. A total concentration of 2.42 g/Nm^3 of tar was obtained in the present work for

455   the MnGBHNE at comparable conditions (950 ºC and 722 kg/MW$_{th}$) to those used in the

456   experiments with Tierga ore. The rest of the compounds present in tar for the experiments

457   with MnGBHNE is shown in Figure 12.
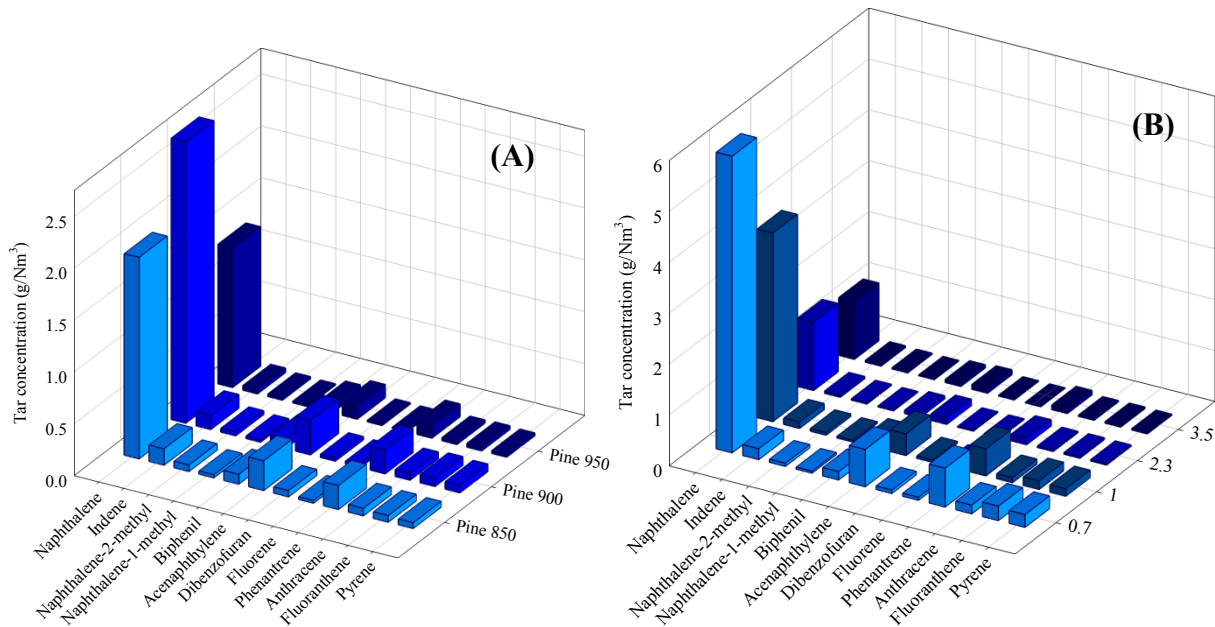
458

459   Figure 12. Tar composition depending on (a) fuel reactor temperature (b) the oxygen to fuel ratio (ϕ) in the

460   experiments with MnGBHNE experiments burning pine sawdust.

461   In the figure, tar composition is expressed as (dry basis). Two different graphics can be found

462   in Figure 12. In Figure 12(A) the tar composition is shown as a function of the fuel reactor

463   temperature. The fuel reactor temperature increase diminishes the tar amount collected In

464   Figure 12(B), the increase of the oxygen to carrier ratio, ϕ, and therefore, the oxygen

465   availability into the fuel reactor, decreased the tar concentration especially for ratios higher

466 than the stoichiometric (1.0). A minimum tar concentration of 1.558 g/Nm^3 was reached at

467 950 ºC and ϕ =3.5.

4 Conclusions

469 The use of low-cost materials in the combustion of solid fuels is recommended since the costs

470 associated to oxygen carrier loss due to ash drainage are minimized. Up to date many Fe-

471 based materials (minerals, industrial wastes) have been used as oxygen carriers in the

472 combustion of biomass. However, manganese ores can be an alternative considering their

473 reactivity. In this work, two manganese ores (MnGBHNE and MnSA) were used as oxygen

474 carriers in a 0.5 kW$_{th}$ experimental plant burning three different types of biomass, a pine

475 sawdust from Spain and also two Spanish agricultural residues largely produced, olive stones

476 and almond shells. First, it should be noted that values about 100% of CO_2 Capture efficiency

477 were obtained with both oxygen carriers. Under the same experimental conditions,

478 MnGBHNE perfomed similarly to Tierga ore, a highly reactive Fe-based mineral previously

479 tested with both coal and biomass as fuels. High oxygen demand values (>20%) were

480 obtained. However, MnSA reduced the oxygen demand values reached to about 10%, which

481 is a significant improvement. Thus, this newly identified manganese mineral can be thought

482 as an interesting oxygen carrier for further scale up.

483 For further oxygen demand decrease, simulation of the recycling of the fuel reactor outlet was

484 done. Results indicate a possibility for oxygen demand reduction of 30% working with any of

485 the manganese ores and pine sawdust as fuel at 900 ºC and recirculating about 50% of the fuel

486 reactor outlet flow.

487

488

Nomenclature

F_i	flow of compound i (mol/s)
M_i	Atomic or molecular weight of i element or compound (kg/mol)
$\dot{m}_{OC}$	solids circulation flow rate (kg/s)
$\dot{m}_{sf}$	mass flow of solid fuel fed (kg/s)
m_{FR}^*	specific solids inventory in the fuel reactor (kg/MW$_{th}$)
R_{OC}	Oxygen carrier oxygen transport capacity (-)
P	thermal power
R_{OC}	oxygen transport capacity (kg oxygen per kg oxygen carrier)

Greek symbols

ϕ	oxygen carrier-to-fuel ratio (-)
η_{CC}	CO_2 capture efficiency (%)
Ω_{sf}	oxygen demand of the solid fuel (kg oxygen per kg solid fuel)
Ω_T	total oxygen demand (%)

5 References

[1] ONU, United Nations Framework Convention for Climate Change. The Paris Agreement. http://unfccc.int/paris_agreement/items/9485.php, in, 2015.

[2] IEA, Global Energy and CO2 Status report, in, Paris (France), 2019.

[3] T. Mendiara, F. García-Labiano, A. Abad, P. Gayán, L.F. de Diego, M.T. Izquierdo, J. Adánez, Negative CO_2 emissions through chemical looping technology, Appl. Energ., 232 (2018) 657-684.

[4] M. Fajardy, A. Koeberle, N. Mac Dowell, BECCS deployment: a reality check, Grantham Inst. Brief Pap. 28. Imp. Coll. London, (2019) 1-13.

[5] J. Adánez, A. Abad, T. Mendiara, P. Gayán, L.F. de Diego, F. García-Labiano, Chemical looping combustion of solid fuels, Prog. Energy Combust. Sci., 65 (2018) 6-66.

[6] J. Adánez, A. Abad, Chemical-looping combustion: Status and research needs, Proceedings of the Combustion Institute, 37 (2019) 4303-4317.

[7] M. Matzen, J. Pinkerton, X. Wang, Y. Demirel, Use of natural ores as oxygen carriers in chemical looping combustion: A review, Int. J. Greenh. Gas Con., 65 (2017) 1-14.

[8] T. Mendiara, L.F. De Diego, F. García-Labiano, P. Gayán, A. Abad, J. Adánez, On the use of a highly reactive iron ore in Chemical Looping Combustion of different coals, Fuel, 126 (2014) 239-249.

[9] C. Linderholm, M. Schmitz, Chemical-looping combustion of solid fuels in a 100 kW dual circulating fluidized bed system using iron ore as oxygen carrier, J Environ Chem Eng, 4 (2016) 1029-1039.

[10] M. Schmitz, C. Linderholm, P. Hallberg, S. Sundqvist, A. Lyngfelt, Chemical-Looping Combustion of Solid Fuels Using Manganese Ores as Oxygen Carriers, Energy Fuels, 30 (2016) 1204-1216.

[11] A. Abad, P. Gayán, T. Mendiara, J.A. Bueno, F. García-Labiano, L.F. de Diego, J. Adánez, Assessment of the improvement of chemical looping combustion of coal by using a manganese ore as oxygen carrier, Fuel Process. Technol., 176 (2018) 107-118.

[12] M. Schmitz, C. Linderholm, Chemical looping combustion of biomass in 10- and 100-kW pilots - Analysis of conversion and lifetime using a sintered manganese ore, Fuel, 231 (2018) 73-84.

[13] S. Sundqvist, N. Khalilian, H. Leion, T. Mattisson, A. Lyngfelt, Manganese ores as oxygen carriers for chemical-looping combustion (CLC) and chemical-looping with oxygen uncoupling (CLOU), Journal of Environmental Chemical Engineering, 5 (2017) 2552-2563.

[14] X. Niu, L. Shen, H. Gu, S. Jiang, J. Xiao, Characteristics of hematite and fly ash during chemical looping combustion of sewage sludge, Chem. Eng. J., 268 (2015) 236-244.

[15] T. Mendiara, A. Pérez-Astray, M.T. Izquierdo, A. Abad, L.F. de Diego, F. García-Labiano, P. Gayán, J. Adánez, Chemical Looping Combustion of different types of biomass in a 0.5 kW_{th} unit, Fuel, 211 (2018) 868-875.

[16] F. García-Labiano, R. Pérez-Vega, A. Pérez-Astray, T. Mendiara, L.F. de Diego, M.T. Izquierdo, Chemical Looping Combustion of biomass in a 50 kWth unit, in: 5th International Conference on Chemical Looping, Utah (EEUU), 2018.

540 [17] T. Pikkarainen, I. Hiltunen, Chemical looping combustion of solid biomass -
541 Performance of ilmenite and braunite as oxygen carrier materials, in: Eur. Biomass Conf.
542 Exhib. Proc. , Stockholm, Sweden, 2017, pp. 1837-1844.

543 [18] C. Kajnäs, M. Hedberg, H. Leion, The Effect of Iron- and Manganese-Based Oxygen
544 Carriers as Bed Materials in Oxygen Carrier Aided Combustion, Energy Technology, 7
545 (2019).

546 [19] T. Berdugo Vilches, F. Lind, M. Rydén, H. Thunman, Experience of more than 1000 h of
547 operation with oxygen carriers and solid biomass at large scale, Appl. Energ., 190 (2017)
548 1174-1183.

549 [20] M. Rydén, M. Hanning, A. Corcoran, F. Lind, Oxygen Carrier Aided Combustion
550 (OCAC) of Wood Chips in a Semi-Commercial Circulating Fluidized Bed Boiler Using
551 Manganese Ore as Bed Material, Applied Science 6(2016) 347.

552 [21] M. Hanning, A. Corcoran, F. Lind, M. Rydén, Biomass ash interactions with a
553 manganese ore used as oxygen-carrying bed material in a 12 MWth CFB boiler, Biomass
554 Bioenergy, 119 (2018) 179-190.

555 [22] F. Hildor, T. Mattisson, H. Leion, C. Linderholm, M. Rydén, Steel converter slag as an
556 oxygen carrier in a 12 MWth CFB boiler − Ash interaction and material evolution, Int. J.
557 Greenh. Gas Con., 88 (2019) 321-331.

558 [23] D. Mei, T. Mendiara, A. Abad, L.F. De Diego, F. García-Labiano, P. Gayán, J. Adánez,
559 H. Zhao, Evaluation of Manganese Minerals for Chemical Looping Combustion, Energy
560 Fuels, 29 (2015) 6605-6615.

561 [24] D. Mei, T. Mendiara, A. Abad, L.F. De Diego, F. García-Labiano, P. Gayán, J. Adánez,
562 H. Zhao, Manganese Minerals as Oxygen Carriers for Chemical Looping Combustion of
563 Coal, Ind. Eng. Chem. Res., 55 (2016) 6539-6546.

564 [25] International Olive Oil Council, http://www.internationaloliveoil.org, in, 2019.

565 [26] International Nut and dried Fruit. http://www.nutfruit.org in, 2019.

566 [27] P. Simell, P. Ståhlberg, E. Kurkela, J. Albrecht, S. Deutsch, K. Sjöström, Provisional
567 protocol for the sampling and anlaysis of tar and particulates in the gas from large-scale
568 biomass gasifiers. Version 1998, Biomass Bioenergy, 18 (2000) 19-38.

569 [28] M. Virginie, J. Adánez, C. Courson, L.F. De Diego, F. García-Labiano, D. Niznansky, A.
570 Kiennemann, P. Gayán, A. Abad, Effect of Fe-olivine on the tar content during biomass
571 gasification in a dual fluidized bed, Appl. Catal. B: Environ., 121-122 (2012) 214-222.

572 [29] T. Mendiara, A. Abad, L.F. de Diego, F. García-Labiano, P. Gayán, J. Adánez, Biomass
573 combustion in a CLC system using an iron ore as an oxygen carrier, Int. J. Greenh. Gas Con.,
574 19 (2013) 322-330.

575 [30] P. Gayán, A. Abad, L.F. de Diego, F. García-Labiano, J. Adánez, Assessment of
576 technological solutions for improving chemical looping combustion of solid fuels with CO_2
577 capture, Chem. Eng. J., 233 (2013) 56-69.

578 [31] A. Cuadrat, A. Abad, P. Gayán, L.F. De Diego, F. García-Labiano, J. Adánez,
579 Theoretical approach on the CLC performance with solid fuels: Optimizing the solids
580 inventory, Fuel, 97 (2012) 536-551.

581 [32] J. Haus, Y. Feng, E.U. Hartge, S. Heinrich, J. Werther, High volatiles conversion in a
582 dual stage fuel reactor system for Chemical Looping Combustion of wood biomass, in:
583 International Conference on Negative CO_2 emissions, Göteborg (Sweden), 2018.

584   [33] J. Yan, L. Shen, S. Jiang, J. Wu, T. Shen, T. Song, Combustion Performance of Sewage
585   Sludge in a Novel CLC System with a Two-Stage Fuel Reactor, Energy Fuels, 31 (2017)
586   12570-12581.

587   [34] S. Jiang, L. Shen, J. Yan, H. Ge, T. Song, Performance in Coupled Fluidized Beds for
588   Chemical Looping Combustion of CO and Biomass Using Hematite as an Oxygen Carrier,
589   Energy Fuels, 32 (2018) 12721-12729.

590   [35] A. Pérez-Astray, I. Adánez-Rubio, T. Mendiara, M.T. Izquierdo, A. Abad, P. Gayán, L.F.
591   de Diego, F. García-Labiano, J. Adánez, Comparative study of fuel-N and tar evolution in
592   chemical looping combustion of biomass under both iG-CLC and CLOU modes, Fuel, 236
593   (2019) 598-607.

594   [36] E. de Visser, C. Hendriks, M. Barrio, M.J. Mølnvik, G. de Koeijer, S. Liljemark, Y. Le
595   Gallo, Dynamis CO_2 quality recommendations, Int. J. Greenh. Gas Con., 2 (2008) 478-484.

596

PAPER III

Manuscript Details

Manuscript number   SEPPUR_2019_4790

Title   CLC of biomass as a BECCS technology using a manganese-iron mixed oxide doped with titanium

Article type   Full Length Article

Abstract

Chemical Looping Combustion (CLC) of biofuels is a Bio-Energy with Carbon Capture and Storage (BECCS) technology with inherent CO_2 capture, which allows to obtain concentrated CO_2 streams. Thus, CLC with biofuels allow to separate CO_2 previously emitted to the atmosphere with one of the lowest energy penalties. This paper presents the results of pine sawdust CLC in a 0.5 kWth CLC unit using a manganese-iron mixed oxide doped with titanium as oxygen carrier, able to release molecular oxygen. The effect on the CO_2 capture efficiency and on the total oxygen demand of different operational variables, especially the specific solids inventory (600 - 2000 kg/MWth), the air excess (1.1 to 1.9) and the air reactor temperature (880-930 ºC), was analyzed. CO_2 Capture efficiencies close to 100% were obtained with fuel reactor temperatures between 885-965 ºC. Total oxygen demands as low as 5 % were achieved optimizing conditions. These results reinforce the promising possibilities of biomass CLC as a BECCS technology.

Keywords   NETs; BECCS; Chemical Looping Combustion (CLC); biomass; manganese-iron mixed oxide

Manuscript category   Application areas include CO_2 capture and removal from gas streams, air separation

Corresponding Author   Teresa Mendiara

Corresponding Author's Institution   Instituto de Carboquímica (ICB-CSIC)

Order of Authors   Antón Pérez-Astray, Teresa Mendiara, Luis de Diego, Alberto Abad, Francisco García-Labiano, Maria Teresa Izquierdo, Juan adanez

Suggested reviewers   Yngve Larring, Toni Pikkarainen, Daofeng Mei

Submission Files Included in this PDF

File Name [File Type]

Perez-Astray et al_Cover letter.doc [Cover Letter]

Perez-Astray et al_Highlights.doc [Highlights]

Perez-Astray et al_Manuscript.docx [Manuscript File]

Perez-Astray et al_declaration-of-competing-interests.docx [e-Component]

Submission Files Not Included in this PDF

File Name [File Type]

Perez-Astray et al_Reviewers.txt [e-Component]

To view all the submission files, including those not included in the PDF, click on the manuscript title on your EVISE Homepage, then click 'Download zip file'.

Dr. Teresa Mendiara
Instituto de Carboquímica (ICB-CSIC)
Miguel Luesma Castán, 4
E-50018 Zaragoza (Spain)
Phone: +34 976 733 977
email: tmendiara@icb.csic.es

4th November 2019

Dear editor,

Please find enclosed the file of the manuscript:

"CLC of biomass as a BECCS technology using a manganese-iron mixed oxide doped with titanium" by Antón Pérez-Astray, Teresa Mendiara, Luis F. de Diego, Alberto Abad, Francisco García-Labiano, María Teresa Izquierdo y Juan Adánez

to be considered for publication in *Separation and Purification Technology.*

We were recently informed by the editor of the publication *Chemical Engineering Journal* about his decision that this manuscript was not suitable for the abovementioned journal. However, he did think it could be considered by *Separation and Purification Technology*. Thus, we were offered the option of taking advantage of the article transfer service and transferred it to *Separation and Purification Technology*.

We considered that the topic of our research will fit into the scope of this journal since this manuscript focuses on separation processes in emerging technologies in the fields of biotechnology-biobased feedstocks/products. In order to limit the increase in global temperature to 2 ºC (or less) urged by the Paris Agreement, technologies that separate carbon dioxide from the atmosphere must be developed. They are the Negative Emission Technologies (NETs). Among the different NETs, the only capable of producing energy while CO_2 is separated are the Bio-Energy with Carbon Capture and Storage (BECCS) technologies. The present work focuses on one of these BECCS technologies: the Chemical Looping Combustion (CLC) when combined with biofuels (in our case, biomass). The International Panel on Climate Change (IPCC) pointed CLC as one of the most promising CCS technologies since it allows 100% CO_2 capture with the lowest energy penalty and cost when compared with currently operating CCS technologies.

We consider that this work could appear attractive for potential readers of *Separation and Purification Technology* for several reasons that we summarize below:

• The results obtained in this work contribute to assess the viability of CLC with biomass (bio-CLC) as a technology allowing the separation of CO_2 from the rest of gases present in the atmosphere. To date, limited information is available in literature about the bio-CLC process. Moreover, results presented were obtained in a continuous CLC pilot unit (0.5 kW_{th}), which allowed to identify the problems that may be encountered in a future scale-up of the process.

• Novel oxygen carriers were used in the combustion of biomass, which allowed to obtain a better combustion efficiency of the process when compared with that attained by reference oxygen carriers tested up to date.

• Besides, this is one of the first studies to evaluate NO_x emissions during biomass CLC. According to the results in this work, lower emissions than in conventional combustions systems can be expected.

This paper is original and all the co-authors agree to the publication in this journal. Moreover, this manuscript has not been previously published, is not currently submitted for review to any other journal, and will not be submitted elsewhere before a decision is made by this journal.

Yours sincerely,

Teresa Mendiara

Highlights

- CLC of biomass assessed as BECCS technology able to separate atmospheric CO_2

- Using a Mn-Fe-Ti mixed oxide almost 100 % CO_2 capture efficiency was obtained

- Bixbyite regeneration in AR influenced oxygen release in FR and thus oxygen demand

- 1.8-1.9 air excess and AR temperature of 880 ºC optimized bixbyite regeneration

- No NO_x emissions were found in AR and in FR were below the recommended

CLC of biomass as a BECCS technology using a manganese-iron mixed oxide doped with titanium

A. Pérez-Astray, T. Mendiara*, L.F. de Diego, A. Abad, F. García-Labiano, M.T. Izquierdo, J. Adánez

Department of Energy and Environment, Instituto de Carboquímica-ICB-CSIC

Miguel Luesma Castán 4, 50018, Zaragoza, Spain

tmendiara@icb.csic.es

* Corresponding author:

Phone: + 34 976 733 977;

Fax: +34 976 733 318

Abstract

Chemical Looping Combustion (CLC) of biofuels is a Bio-Energy with Carbon Capture and Storage (BECCS) technology with inherent CO_2 capture, which allows to obtain concentrated CO_2 streams. Thus, CLC with biofuels allow to separate CO_2 previously emitted to the atmosphere with one of the lowest energy penalties. This paper presents the results of pine sawdust CLC in a 0.5 kW_{th} CLC unit using a manganese-iron mixed oxide doped with titanium as oxygen carrier, able to release molecular oxygen.

The effect on the CO_2 capture efficiency and on the total oxygen demand of different operational variables, especially the specific solids inventory (600 - 2000 kg/MW_{th}), the air excess (1.1 to 1.9) and the air reactor temperature (880-930 ºC), was analyzed. CO_2 Capture efficiencies close to 100% were obtained with fuel reactor temperatures between 885-965 ºC. Total oxygen demands as low as 5 % were achieved optimizing conditions. These results reinforce the promising possibilities of biomass CLC as a BECCS technology.

1. Introduction

Sustainability has become a big concern nowadays. The increase of CO_2 emissions since the beginning of the industrial revolution, mainly because of fossil fuel combustion, has been changing its atmosphere concentration [1]. In the 24th Conference of the Parties to the United Nations Framework Convention on Climate Change (UNFCCC), 200 member States arranged an agreement to make special efforts on mitigation and adaptation to the Climate Change, following the evidences shown by the 5th Assessment Report of the Intergovernmental Panel on Climate Change (IPCC) [1] and the objective set in the Paris Agreement [2]. The Paris Agreement tries to limit the increase in the global average temperature to less than 2 ºC at the end of the century with respect to preindustrial values. For this purpose, it is not only necessary to increase the energy efficiency and to reduce the Greenhouse Gas (GHG) emissions [2, 3], but also to develop Negative Emission Technologies (NETs) within the next decades [4, 5]. NETs are able to separate CO_2 previously emitted from the rest of the gases in the atmosphere. There are several NETs technologies: afforestation, biochar and soil sequestration, Direct Air CO_2 Capture and Storage (DACCS), enhanced weathering, ocean fertilization and Bio-Energy with Carbon Capture and Storage (BECCS). The potential carbon reduction and cost of each technology has been evaluated by Fuss et al [6]. Among them, BECCS stands out because it can produce heat and/or power while separating CO_2 from the atmosphere.

Chemical Looping Combustion (CLC) is gaining attention to restrict anthropogenic greenhouse gas emissions because of its BECCS potential. CLC technology has been studied during last decades as a CO_2 capture technology without gas separation steps. It allows inherent CO_2 capture with one of the lowest energy penalties and, consequently, cost [7]. The use of sustainable-managed biomass fuels with this technology can offer

3

new opportunities as a NET. In a general CLC process burning solid fuels (Figure 1) an oxygen carrier circulates between two different reactors in a redox reaction cycle. Without gas mixing between reactors, the oxidized oxygen carrier (M_xO_y) reaches the fuel reactor where it reacts with the fuel yielding CO_2 and H_2O. In this reaction the oxygen carrier is reduced (M_xO_{y-1}). The reduced oxygen carrier circulates again to the air reactor to be regenerated in air and prepared for a new cycle.
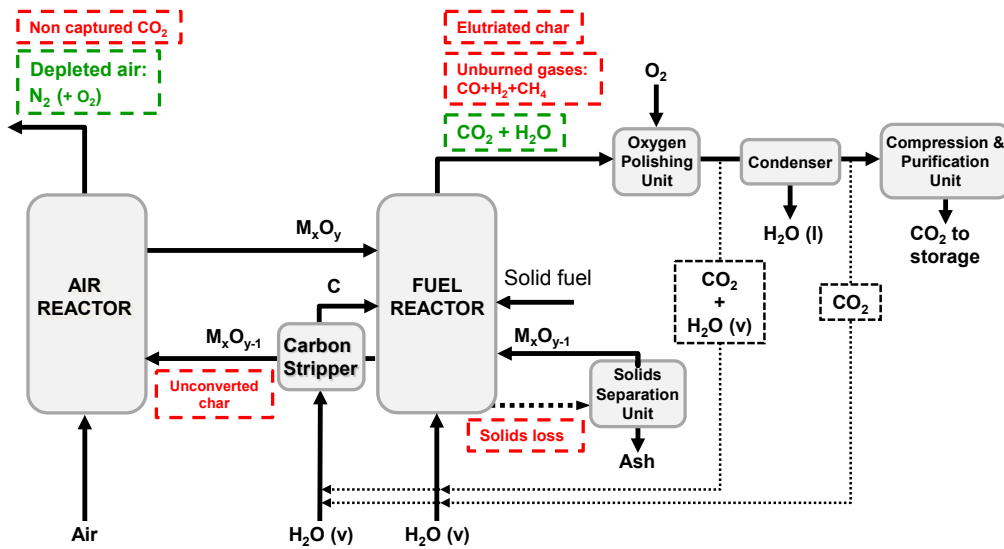
Figure 1. General scheme of a CLC process

There are two different reaction mechanisms for CLC combustion of solid fuels, i.e. *in-situ* Gasification CLC (*i*G-CLC) and CLC with Oxygen Uncoupling (CLOU). Figure 2 depicts the main differences and characteristics of both processes. Under *i*G-CLC, a gasifying agent is introduced to convert the char in the solid fuel to CO and H_2. Then, the oxygen carrier reacts with the devolatilization and gasification products to produce CO_2 and H_2O [7]. Under the CLOU mode, the oxygen carrier releases molecular oxygen (O_2) that is able to easily react with the biomass char and devolatilization products in a similar way than in a conventional combustion [8]. Most of the experience gained in solids fuel CLC in recent years has been acquired by testing different types of coal. Nevertheless, there are important differences between coal and biomass that may affect

the combustion process. Biomass contents more volatile matter and generates a more reactive char. At the same time, biomass has lower content and different composition of ashes, although tar formation is larger [9].
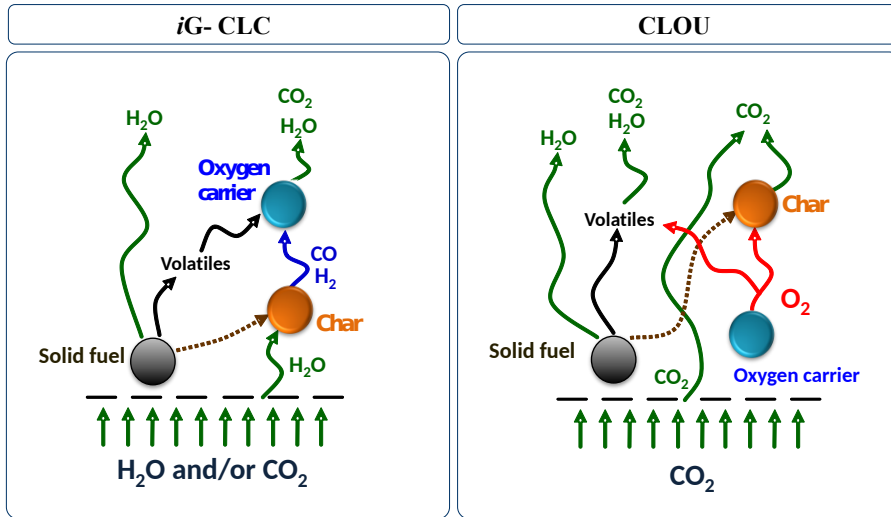
Figure 2. In-situ Gasification CLC (iG-CLC) and Chemical Looping Combustion with Oxygen Uncoupling (CLOU) reaction schemes.

Most of the biomass fueled CLC studies to date have used mineral or industrial residues oxygen carriers for iG-CLC in experimental campaigns at prototype scales from 0.5 kW_{th} to 4 MW_{th} [10-31]. The origin of this type of materials, typically iron or manganese oxides, confer them a low cost. Results reported in literature regarding CO_2 capture efficiency show high values for this parameter, close to 100% in many cases, both in the operation with iron and manganese ores or residues. However different values were reported for combustion efficiency. Studies analyzing manganese ores from different origins found higher combustion efficiencies than ilmenite, an iron based mineral considered as a reference for the iG-CLC process [19, 23, 32]. In any case, the values of combustion efficiency are higher burning biomass than burning coal under similar experimental conditions. During the last years, different solid biofuels have been tested in continuous CLC units. Pine sawdust is the most commonly used fuel due to its large world production and distribution and therefore it is usually used as a reference

material [10, 15-17, 19, 23, 24, 28, 30]. Another used fuel is biochar [20, 22] from different types of biomass. Moreover, recent studies have used different solid biofuels, such as agricultural residues, namely almond shells and olive stones [17] or rice husk [15, 33], or even solid wastes, namely sewage sludge [12, 14]. Other options, such as co-combustion of coal and biomass are also being explored [11, 13, 31] and results indicate that co-combustion has a positive effect on the CO_2 capture efficiency.

Biomass combustion under the CLOU mode has been reported to significantly reduce the total oxygen demand of the biomass combustion process compared to results under iG-CLC [34]. Cooper oxides have shown a good performance as oxygen carriers for the CLOU process. First tests with biomass in a continuous CLC unit were addressed with and oxygen carrier based on CuO supported on $MgAl_2O_4$ and using pine sawdust as oxygen carrier [35]. Combustion efficiencies close to 100% were reached as well as high CO_2 capture efficiencies with low oxygen carrier inventories. More recently, the same authors [8] tested agricultural residues using a synthetic Cu-Mn based oxygen carrier. Combustion efficiencies close to 100% were again reached even at lower temperatures (775-850ºC) than in the previous study. Besides copper-based oxygen carriers, synthetic calcium manganate materials showing CLOU properties were tested in the combustion of biochar and black wood pellets [25, 36]. High combustion efficiencies between 95-97.9% and CO_2 capture efficiencies higher than 80% have been reported in continuous units of 10 and 100 kW_{th}. Similar results were obtained with a synthetic CLOU oxygen carrier based on manganese-silicon and titanium [37].

Recently, manganese-iron mixed oxides have received attention because of their relatively low cost and high reactivity [38-42]. Although they can operate under iG-CLC mode, these oxygen carriers are also able to release oxygen during their reduction under specific operational conditions [41]. This ability has been named Chemical

Looping assisted by Oxygen Uncoupling (CLaOU) and allows to obtain better results in the oxygen demand without expensive scheme modifications, such as using distributor plates at the bottom part of the fuel reactor for a better volatile distribution [43] or a second fuel reactor to convert the unburnt matter at the exit of the first fuel reactor [44, 45].

Reactions (R1) to (R4) describe the reduction reactions of the iron-mangaese based mixed oxides in CLC. The bixbyite phase, $(Mn_xFe_{1-x})_2O_3$, decomposes in a spinel phase, $(Mn_xFe_{1-x})_3O_4$, and molecular oxygen at specific operational condicions (R1). In addition to the molecular oxygen release, the spinel phase oxidizes the biomass gasification products according to (R2) to (R4).

$$3(Mn_xFe_{1-x})_2O_3 \leftrightarrow 2(Mn_xFe_{1-x})_3O_4 + 0.5O_2 \qquad \text{(R1)}$$

$$(Mn_xFe_{1-x})_3O_4 + H_2 \rightarrow 3(Mn_xFe_{1-x})O + H_2O \qquad \text{(R2)}$$

$$(Mn_xFe_{1-x})_3O_4 + CO \rightarrow 3(Mn_xFe_{1-x})O + CO_2 \qquad \text{(R3)}$$

$$4(Mn_xFe_{1-x})_3O_4 + CH_4 \rightarrow 12(Mn_xFe_{1-x})O + CO_2 + 2H_2O \qquad \text{(R4)}$$
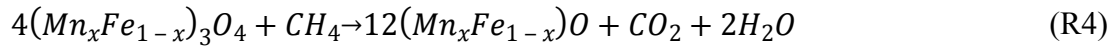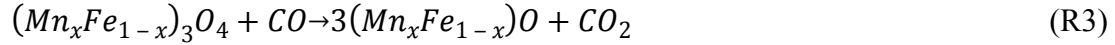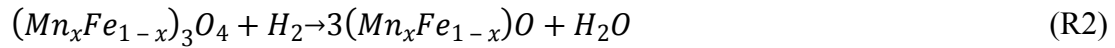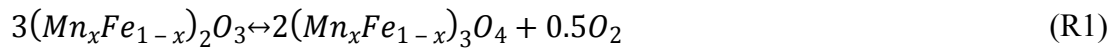
Good results were previously obtained using a manganese-iron mixed oxide doped with titanium as oxygen carrier in a 0.5 kW$_{th}$ CLC unit burning coal. In this case, operational conditions were optimized in order to enhance the the oxygen uncoupling mechanism and almost full coal combustion was achieved setting the air reactor temperature about 880 ºC as well as using an air excess of 1.8 at 925 ºC into the fuel reactor [42]. Therefore, the testing of this type of oxygen carriers with biomass as fuel seems to be profitable in order to reduce the high total oxygen demand values typically achieved working under iG-CLC mode with the advantage of not being highly expensive materials.

The present work analyses the performance of a mixed manganese-iron oxide doped with titanium as oxygen carrier in a 0.5 kW_{th} CLC unit using pine sawdust as biomass fuel. The experimental campaign was designed to analyze the effect of the capability of this material to release molecular oxygen on the total oxygen demand of the biomass combustion process. For that purpose, several operating variables were evaluated. The CO_2 capture and the total oxygen demand were evaluated.

2. Materials and methods

A synthetic oxygen carrier, named Mn66FeTi7, based on manganese and iron oxides with TiO_2 addition was prepared by spray granulation in a spouted bed system at the ICB-CSIC using 60 wt% of Mn_3O_4 (Elkem), 33 wt% of Fe_2O_3 (Chemlab) and a 7 wt% of TiO_2 (Panreac). The oxygen carrier was thermally processed in air atmosphere during 2 h at 1050 ºC. After that, the particles were sieved to the particle distribution from 0.1 to 0.3 mm. The stoichiometric formula of the particles was $(Mn_{0.66}Fe_{0.34})_2O_3 \cdot (TiO_2)_{0.15}$. The reactivity of this oxygen carrier was evaluated in a thermogravimetric analyzer (TGA) in a previous work. The oxygen carrier showed high reactivity with H_2, CO and CH_4 [41]. In addition, it was observed in the TGA that the molecular oxygen released by the oxygen carrier in the reduction of the bixbyite to spinel (R1) solid phase was highly influenced by the temperature, in the range 850-900ºC, and the oxygen concentration used during the oxygen carrier oxidation. The contribution of the oxygen release mechanism of this oxygen carrier is clearly affected by kinetics and thermodynamics [40]. Table 1 shows the main properties and characteristics of Mn66FeTi7 oxygen carrier. Identification of crystalline chemical species was done using powder X–ray diffractometer Bruker AXS D8ADVANCE (XRD). A FGN-5X force gauge (Shimpo) was used for the particle crushing strength determination. The

presented value was calculated as the average of the crushing strength of 20 oxygen carrier particles. The porosity of the particles was determined by Hg intrusion in a Quantachrome PoreMaster 33 and their real density was measured with a Micromeritics AccuPycc II 1340 helium pycnometer. Also a ATTRI-AS (Materials Technologies Snc.) was used to determine the Air Jet Index (AJI) of the different samples [46].

Table 1. Main characteristics of the Mn66FeTi7oxygen carrier

XRD main phases (wt%)	
$(Mn_xFe_{1-x})_2O_3$	81.0
$(Mn_xFe_{1-x})_3O_4$	13.4
TiO_2	5.6
Crushing strength (N)	2.0
Oxygen transport capacity, R_{OC} (%)	9.4
Porosity (%)	9.5
Skeletal density (kg/m^3)	4630

[a] Determined by thermogravimetric analysis.

Pine sawdust was chosen as biofuel because of its large production and extended use for energy production. The biofuel was crushed and sieved to a size distribution from 0.5 to 2 mm. Table 2 shows the proximate and ultimate analyses and the low heating value of the pine sawdust. The oxygen demand for the stoichiometric complete combustion of the biomass fuel (Ω_{sf}) was calculated and also included in the table.

An experimental campaign was performed in a 0.5 kW$_{th}$ CLC unit for solid fuels at the ICB-CSIC. A layout of the CLC unit is shown in Figure 3. This CLC unit is based on two fluidized bed reactors (fuel and air reactors) connected by a loop seal. A screw feeder system was used to feed the biomass into the bottom part of the fuel reactor, where the biomass reacted with the oxygen carrier reducing it. The partially reduced oxygen carrier reached the air reactor through the loop seal that prevents the mixture of the different reactor atmospheres. The oxygen carrier was oxidized again in the air reactor and sent through the riser to a reservoir deposit which isolated the different

reactor atmospheres. A solids valve allowed controlling the amount of solids returned to the fuel reactor.

Table 2. Main characteristics of the pine used as fuel.

Proximate analysis (wt%)	
Moisture[a]	4.2
Ash(wt%)	0.4
Volatile matter (wt%)	81.0
Fixed carbon (wt%)	14.4
Ultimate analysis (wt%)	
C (wt%)	51.3
H	6.0
N	0.3
S	0.0
O[b]	37.8
LHV (kJ/kg)	19158
Ω_{sf} (kg O/kg fuel)	1.5

[a] Stabilized by exposure to the atmosphere. [b] By difference.

1.- Fuel Reactor	7.- Solid reservoir
2.- Loop Seal	8.- Solids control valve
3.- Air Reactor	9.- Fuel feeding system
4.- Riser	10.- Evaporator
5.- Cyclone	11.- Furnace
6.- Diverting solids valve	12.- Filter
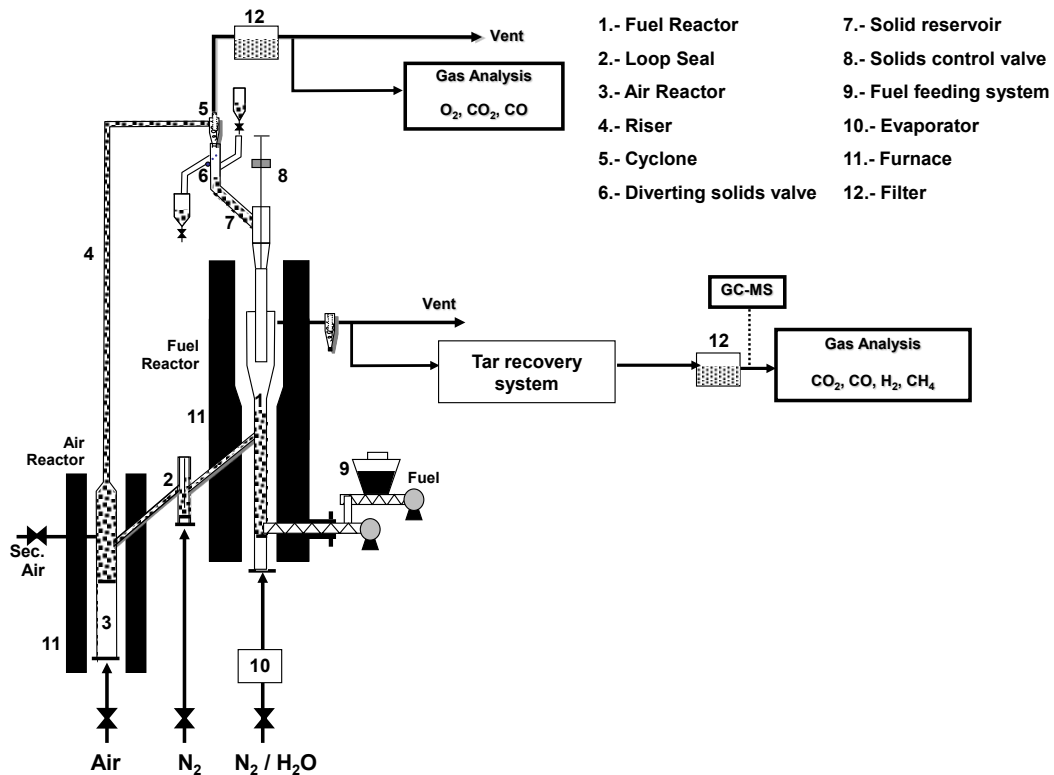
Figure 3. Experimental unit ICB-CSIC-s1

Specific mass flow controllers were used for feeding different gases while a peristaltic pump followed by an evaporator was used for the water steam feeding into the fuel reactor. CO_2 or steam could be supplied to fluidize the fuel reactor. Different N_2-air mixtures could be introduced into the air reactor in order to control de oxygen concentration during oxidation. N_2 was normally used for the loop seal fluidization but CO_2 was used in the tests in which NO_x was measured.The gas outlet composition of both reactors was measured and recorded. A non-dispersive infrared analyzer (Siemens Ultramat 23) was used for the CO_2, CO and CH_4 online analysis and a thermal conductivity detector (Siemens Calomat 6) for the H_2. The O_2 concentration was measured with a paramagnetic analyzer (Siemens Ultramat 23 and Oxymat 6). A non-dispersive infrared analyzer Siemens Ultramat 23 was used in selected experiments for NO_x determination. The reactor temperatures were independently controlled thanks to the electric furnaces and the temperature and pressure drops in the reactors were recorded during all the experiments. More detailed information about the design and operation of the unit can be found elsewhere [17].

Different operating conditions were analyzed to optimize the performance of Mn66FeTi7 in CLC of biomass. The operating conditions were varied to further analyze the effect of the molecular oxygen release of the Mn66FeTi7 oxygen carrier on the total oxygen demand reduction in biomass CLC experiments. In this sense, previous results using coal as fuel concluded that the oxygen release in the fuel reactor depends on the air excess ratio and the temperature in the air reactor since both variables affect the oxidation from spinel to the bixbyite phase which is responsible for the oxygen release [40]. The air excess ratio, λ^*, was calculated as:

$$\lambda^* = \frac{1 - y_{O_2, ARout}}{1 - \frac{y_{O_2, ARout}}{0.21}} \qquad (1)$$

A wide range from 1.1 to 1.9 of air excess was used during the experiments while the air reactor temperature was kept constant at 880 ºC or 930 ºC. Fluidization velocities were maintained constant during the experimental campaign to 0.08 m/s in the fuel reactor and 0.5 m/s in the air reactor, both calculated at 900 ºC.

Table 3 summarizes the operating conditions used in the experiments performed at the CLC unit during about 180 hours of hot fluidization, of which 41 h corresponded to biomass combustion. A total of 16 tests at steady state operating conditions were performed in order to compare and to analyze the effect of different operating variables on the CO_2 capture and the total oxygen demand.

Table 3. Operating conditions in the experimental campaign with Mn66FeTi7 oxygen carrier

Test	F.A. (-)	T_{FR} (ºC)	T_{AR} (ºC)	λ^* (-)	ϕ (-)	$\dot{m}_{OC}$ (kg/h)	$\dot{m}_{sf}$ (kg/h)	P (W)	$\dot{m}_{FR}^*$ (kg/MW$_{th}$)	$norm.\,\dot{m}_{oc}$ ((kg/s)/MW$_{th}$)
P01	CO_2	930	880	**1.2**	2.6	5.3	0.13	692	**600**	2.1
P02	CO_2	925	880	**1.1**	3.5	3.5	0.063	335	**1420**	2.9
P03	CO_2	935	880	**1.2**	6	4.3	0.06	245	**1870**	4.9
P04	CO_2	900	880	**1.4**	1.8	1.7	0.059	314	1575	1.5
P05	CO_2	950	880	**1.4**	5	4.7	0.059	314	1515	4.1
P06	CO_2	900	880	**1.8**	2.9	3	0.065	346	1330	2.4
P07	CO_2	930	880	**1.9**	3.1	3	0.062	330	1400	2.5
P08	CO_2	890	880	1.6	2.1	2.6	0.086	458	**1110**	2.1
P09	CO_2	905	880	1.6	2.1	2.6	0.086	458	**1075**	2.1
P10	CO_2	900	880	1.9	2.9	2.9	0.048	255	**1855**	3.1
P11	CO_2	930	880	1.9	3.5	3.5	0.048	255	**1890**	3.8
P12	CO_2	935	**930**	1.2	3.8	3.6	0.046	319	1310	3.1
P13	CO_2	905	**930**	1.8	3	3.7	0.066	351	1240	3
P14	CO_2	960	**930**	1.8	3.1	3.9	0.066	351	1240	3.1
P15	CO_2	925	**930**	1.8	4	4	0.064	341	1485	3.3
P16	CO_2	940	**930**	1.8	4	4	0.064	341	1385	3.3

Different experimental series were planned to analyze the influence of different variables. In the first series (P01-P03), conditions in the air reactor were set to 880 ºC

and low air excess ratio while the solid inventory in the fuel reactor was changed. In the second series (P04-P07) and the third series (P08-P11), the solids inventory in the fuel reactor was maintained constant and then the air excess ratio in the air reactor was changed while temperature remained at 880 ºC. Finally, the fourth series (P12-P16) set the values of air excess ratio and solids inventory and increased the temperature in the air reactor to 930 ºC.

The evaluation of a CLC system with solid fuels usually implies the analysis of two parameters: the CO_2 capture efficiency and the total oxygen demand. More information about these parameters was reported by Adánez et al. [47].

The CO_2 capture efficiency (η_{CC}) evaluates the gaseous carbon exiting the fuel reactor as a fraction of the total gaseous carbon products produced.

$$\eta_{CC} = 1 - \frac{F_{CO_2,outAR}}{F_{CO_2,outFR} + F_{CH_4,outFR} + F_{CO,outFR} + F_{CO_2,outAR}} \tag{2}$$

The total oxygen demand (Ω_T) evaluates the oxygen needed for the full conversion of the unburnt products as a fraction of the oxygen needed for the biomass total conversion.

$$\Omega_T = \frac{4F_{CH_4,outFR} + F_{CO,outFR} + F_{H_2,outFR}}{\frac{1}{M_0}\Omega_{sf}\dot{m}_{sf}} \tag{3}$$

These parameters depend on the oxygen carrier to fuel ratio, ϕ, which is the fraction of oxygen supplied by the oxygen carrier assuming its complete regeneration in the air reactor divided by the oxygen demanded by the fuel ($\phi = 1$ correspond to stoichiometric conditions).

$$\phi = \frac{\dot{m}_{OC} \cdot R_{OC}}{\dot{m}_{sf} \cdot \Omega_{sf}} \tag{4}$$

3. Results and Discussion

During the experimental campaign performed the Mn66FeTi7 oxygen carrier showed good fluid dynamic performance and no agglomeration problems were observed during the experiments. When operating conditions were modified, steady state was usually reached after 20 min and maintained at least during 60 min. The gas concentrations measured at the outlet of fuel and air reactors during each experiment and under steady state conditions were averaged. These averaged values were used to calculate the CO_2 capture efficiency and the total oxygen demand by equations (2) and (3). For each experiment, the carbon mass balance was checked. The calculated deviations found were below 5% in all cases.

3.1 CO_2 Capture efficiency

The influence of different operating variables on the CO_2 capture efficiency has been previously assessed for the Mn66FeTi oxygen carrier in experiments with coal [42]. In that study, carbon dioxide capture was mainly affected by the solids residence time in the fuel reactor. However in the experiments with biomass, the values of CO_2 capture efficiency under the different conditions in Table 3 were so close to 100 % that no influence of the operating conditions could be found. The high values of CO_2 capture efficiency reached were attributed to the almost full char conversion in the fuel reactor since almost no CO_2 was measured at the outlet of the air reactor.

3.2 Total oxygen demand

Effect of the solids inventory: The high volatile content of biomass compared to coal has been pointed as the reason for the high oxygen demand values reached in previous experimental campaigns of biomass CLC using low cost oxygen carriers [17]. Therefore, the use of highly reactive materials such as Mn66FeTi7, could contribute to significantly reduce those values of total oxygen demand. The experimental campaign

in the present work started testing the Mn66FeTi7 material under similar conditions to those already used by the authors with a highly reactive iron-based material (Tierga ore) [17]. Figure 4 shows the results obtained with the Mn66FeTi7 oxygen carrier working under similar conditions of low air excess and solids inventory (600 kg/MW$_{th}$) (P01) to those used with Tierga iron ore. In this case, the temperature in the air reactor was maintained at 880 ºC.
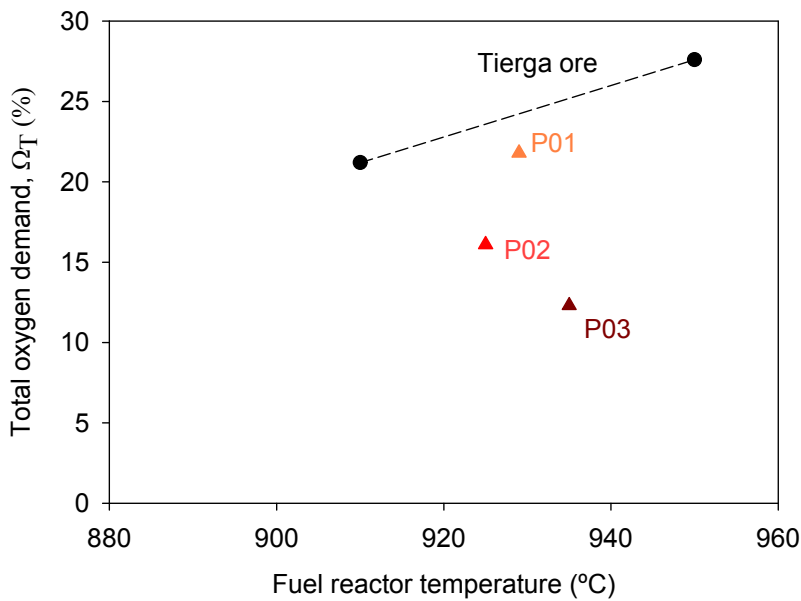
Figure 4. Total oxygen demand (Ω_T) values for Tierga ore [17] and Mn66FeTi7 (P01-P03)

Under similar operating conditions (P01), the Mn66FeTi7 oxygen carrier performed similarly to Tierga ore also yielding high values of oxygen demand (21.8%). Increasing the solids inventory in the fuel reactor and keeping constant the rest of operating conditions a further reduction in the oxygen demand value was reached, as it is shown in Figure 4 with points P02 and P03. Working with 1870 kg/MW$_{th}$ in the fuel reactor, an oxygen demand of 12.3 % was obtained. Thus, the increase in the solids inventory in the fuel reactor can be used as a measure for oxygen demand reduction. However, high solids inventories (> 1000 kg/MW$_{th}$) could represent an operational problem due to the excessive size of the fuel reactor needed [48].

Effect of the air excess ratio: In the second and third series of experiments in Table 3 several operating conditions affecting Mn66FeTi7 regeneration in the air reactor were analyzed. In the second series (P04-P07), the air excess in the air reactor was increased from 1.1 (P02) to 1.9 (P07) while maintaining the temperature in the air reactor at 880 ºC and an average solids inventory of 1455 kg/MW$_{th}$. The results in Figure 5 show that the increase in the air excess ratio makes the oxygen demand values to decrease.
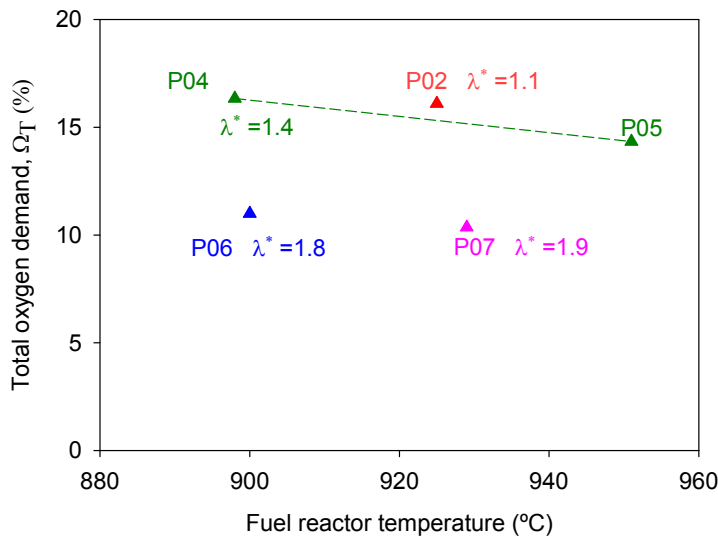
Figure 5. Total oxygen demand values (Ω_T) for Mn66FeTi7 and different values of air excess (λ^*) (P04-P07). T$_{AR}$ = 880 ºC; average solids inventory 1455 kg/MW$_{th}$

The largest reductions in the oxygen demand were observed for $\lambda^* = 1.8\text{-}1.9$. Under these conditions, oxygen demand values of 10.4 % (P07) were reached, which represents reductions of 35% with respect to the reference value with $\lambda^* = 1.1$ (P02). The effect of the excess air ratio has been also assessed in the third series of the experimental campaign (P08-P11). The results are shown in Figure 6 and correspond to experiments performed under similar conditions to those shown in Figure 5 but with two different averaged solids inventories, i.e. 1095 kg/MW$_{th}$ and 1875 kg/MW$_{th}$. When P04-P05 are compared to P08-P09 it can be observed that lower values of oxygen demand were obtained for P08 and P09 ($\lambda^* = 1.6$) than for P04 and P05 ($\lambda^* = 1.4$) even

with lower solids inventory available at the fuel reactor (1095 kg/MW$_{th}$). It can be also observed in Figure 6 that the combination of high air excess ratios ($\lambda^* = 1.9$) and high solids inventories (1875 kg/MW$_{th}$) in P10-P11 tests led to values of the oxygen demand as low as 4.6 % at 930 ºC (P11).
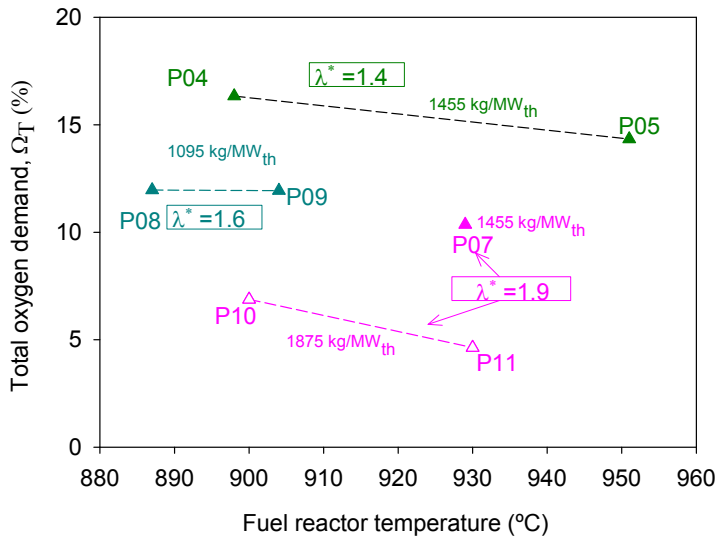
Figure 6. Total oxygen demand values (Ω_T) for Mn66FeTi7 and different values of air excess (λ^*) (P08-P11). T$_{AR}$ = 880 ºC

Effect of the air reactor temperature: The third parameter affecting the regeneration of the Mn66FeTi7 oxygen carrier and therefore its capacity to release oxygen in the fuel reactor is the temperature in the air reactor. This parameter was evaluated. All the experimental results shown in Figures 4 to 6 were obtained maintaining a temperature in the air reactor of approximately 880 ºC. The fourth series of experiments in Table 3 was carried out increasing the temperature of the air reactor to 930 ºC. Under this conditions, two different air excess rations were tested, i.e. 1.1-1.2 and 1.8-1.9. Results are shown in Figure 7. Tests corresponding to P02 and P12 were performed with a low air excess ratio ($\lambda^* = 1.1-1.2$) and an averaged solids inventory 1365 kg/MW$_{th}$. In this case a slightly lower oxygen demand value was attributed to the experiment at 880 ºC in the air reactor. A similar comparison can be performed at higher air excess ratio, namely (λ^*

= 1.8-1.9) and similar solids inventories for the tests identified as P06-P07 (1455 kg/MW$_{th}$), P13-P14 (1240 kg/MW$_{th}$) and P15-P16 (1435 kg/MW$_{th}$) in Table 3. Working at 930 ºC in the air reactor, a decrease in the oxygen demand values was observed from P13-P14 to P15-P16 when the solids inventory in the fuel reactor was slightly increased. Nevertheless, the lowest oxygen demand value was again obtained when the air reactor operated at 880 ºC (P06-P07).
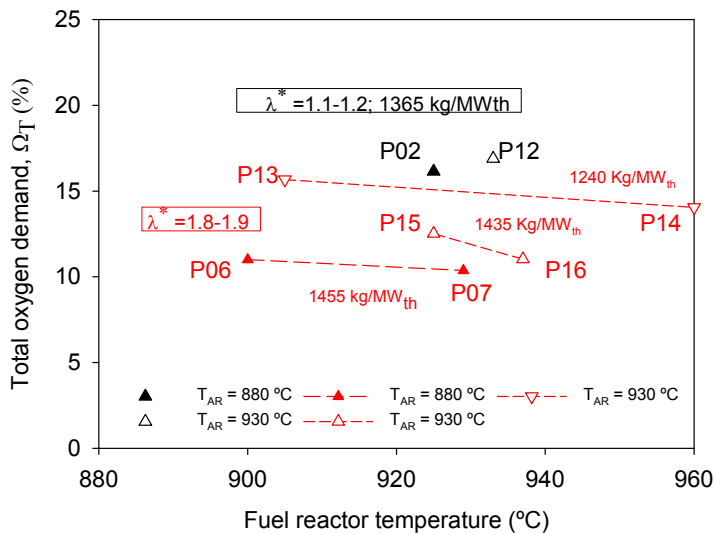
Figure 7. Total oxygen demand values (Ω_T) for Mn66FeTi7 and different temperatures in the air reactor

Effect of the operating conditions on partial oxygen demands: A further analysis of the oxygen demand values is shown in Figure 8. The figure represents the oxygen demand attributed to each of the unburned compounds found at the fuel reactor exit, i.e. CH_4, CO and H_2, in the different experimental tests in Table 3. In Series I, the main contribution to the total oxygen demand value came from methane followed by CO regardless the solids inventory in the fuel reactor. In Series II and III, when the air excess ratio increased, methane was better burned and its contribution to the total oxygen demand decreased and became similar to that of CO or even lower (see P07, P10 and P11). These results demonstrated how the increased presence of molecular oxygen in the fuel reactor improved the oxygen demand by improving methane

18

combustion. Comparing Series I and Series IV it can be seen that the increase in the solids inventory in the fuel reactor decreased the contribution of methane to the total oxygen demand.
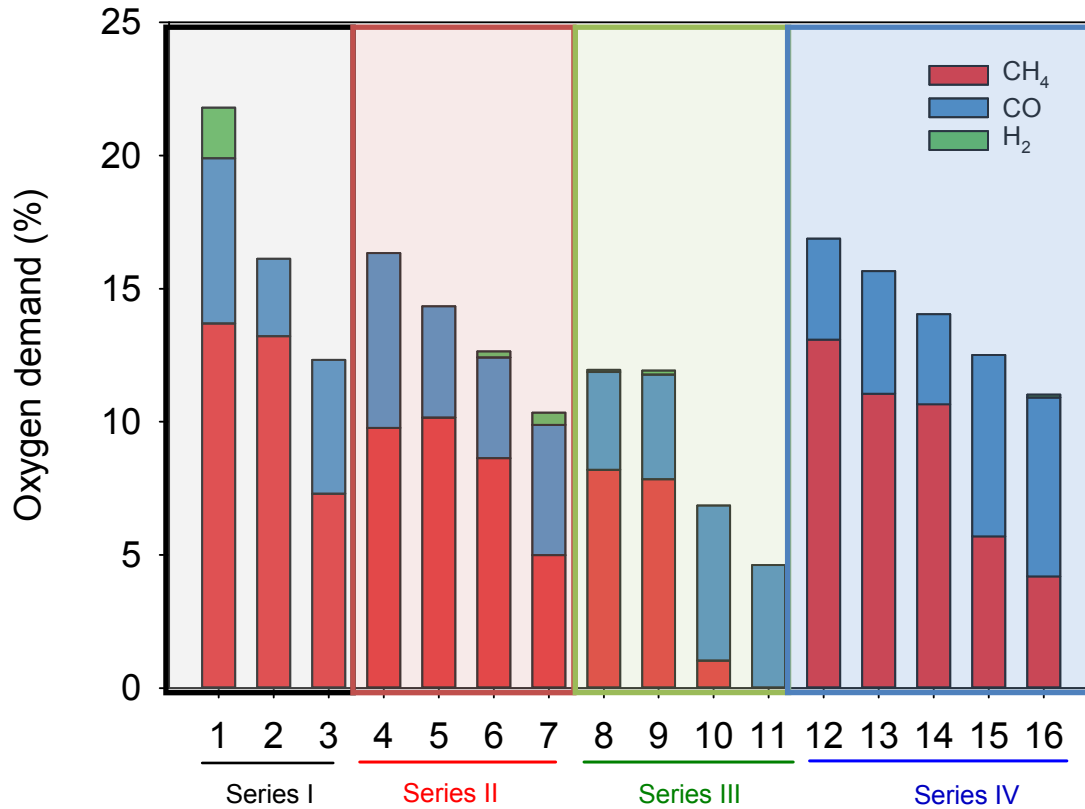
Figure 8. Oxygen demand attributed to each of the unburned compounds found at the fuel reactor exit in the different experimental tests in Table 3

3.3 NO_x emissions in biomass combustion with Mn66FeTi7

One of the advantages of the CLC technology compared to other conventional combustion processes is the reduction in thermal NO_x emission [49]. This is due to the fact that temperatures at which the air reactor operates are lower than those considered threshold for thermal NO_x formation. Therefore, NO_x emissions from a CLC system are limited to those associated with the non-reacted char being oxidized in the air reactor [50, 51]. As it was mentioned before in section 3.1, the conversion of the pine sawdust char in the fuel reactor was almost complete and no char reached the air reactor.

Accordingly, neither CO_2 nor NO_x emissions were recorded at the outlet of the air reactor during the experimental campaign.

In the experiments performed in the present work, the nitrogen contained in the biomass was released in the fuel reactor. The major nitrogen species found in the fuel reactor was nitrogen (N_2). No N_2O was detected in the experiments since the temperature in the fuel reactor was always too high for N_2O to be present. Regarding NO_x formation, the species detected was NO. Although there is at present no legal limit indicating the maximum NO_x content in a CO_2 stream to be transported and stored underground, there are some recommendations about the quality of the CO_2 captured and intended for storage [52]. According to these recommendations, the maximum NO_x/C molar ratio at the fuel reactor outlet stream would be 280 (expressed as ppm, i.e. mol NO_x/(mol C·10^{-6})). Table 4 shows the NO_x/C molar ratio values obtained for experiments in Figure 5 with different air excess ratios at 880 ºC in the air reactor and an average solids inventory in the fuel reactor of 1455 kg/MW$_{th}$.

Table 4. NO_x/C molar ratio values obtained for experiments in Figure 5 with different air excess ratios in the air reactor (T_{AR}= 880 ºC; 1455 kg/MW$_{th}$)

	λ^*	NO_x/C
Recommended limit [52]	–	**280**
P02	1.1	421
P04	1.4	480
P05	1.4	458
P06	1.8	228
P07	1.9	202

According to these results, the NO_x/C molar ratio decreased when the air excess ratio increased. Results are below the recommended limit for the highest values of λ^*, which are also the most favorable conditions previously determined to obtain low oxygen

demand values in the biomass combustion process. Thus, it can be concluded that under the optimum operation conditions for the Mn66FeTi7 oxygen carrier the CO_2 stream captured at the fuel reactor exit complies with the recommended limit for further transport and storage regarding the presence of nitrogen compounds.

3.4 Characterization of the oxygen carrier after biomass combustion

The successive redox cycles suffered by the Mn66FeTi7 oxygen carrier during biomass combustion in the CLC continuous unit may affect the oxygen carrier physical and mechanical properties. The oxygen carrier was characterized by several techniques at the end of the experimental campaign. First, the Air Jet Index (AJI) and mechanical strength of fresh and used particles were compared. As it can be seen from the values gathered in Table 5, a slight increase in these parameters was observed.

Table 5. Main properties of the fresh and used Mn66FeTi7 particles after biomass experiments

	Fresh	Used	
Air Jet Index (AJI) (%)	5.1	7.5	
Mechanical strength (N)	1.9	2.1	
Relative magnetic permeability, μ_r (-)		FR	AR
P01	1.0	7.5	5.5
P16		8.4	5.2

The reactivity of the oxygen carrier after its use in biomass combustion was also assessed in a TGA apparatus described elsewhere [53]. Experiments at 950 ºC using 15% CH_4 and 20 % H_2O were performed with the fresh and used oxygen carrier. Figure 9 shows the conversion versus times curves obtained in each case and no significant changes in reactivity could be observed. Another interesting characteristic of the Mn66FeTi7 oxygen carrier regarding its use in CLC of solid fuels is its magnetic behavior which can be attributed to the presence of the spinel phase ((Mn_xFe_{1-x})$_3O_4$). Spinel has magnetic properties which can facilitate the separation of oxygen carrier

particles from the fuel ashes generated in the combustion process [41]. To quantify the magnetic behavior of the particles, the relative permeability, μ_r, of samples exiting from the air and fuel reactors was obtained by measuring magnetic susceptibility following the procedure described elsewhere [39]. The results are included in Table 5. A sample is considered to present magnetic properties when the value of relative permeability is higher than 1. According to this, fresh particles cannot be considered as magnetic but magnetism exists in the used particles. The magnetism of two different samples has been evaluated, corresponding to points P01 and P12 in Table 3. Samples extracted from the fuel and air reactors were evaluated separately since the presence of spinel phase in each reactor maybe different and hence the magnetism. In both samples, the highest values of the magnetic susceptibility are found in the samples extracted from the fuel reactor compared to those extracted from the air reactor. This indicated that the amount of spinel is larger in the samples from the fuel reactor which was expected since bixbyite reduction to spinel takes place in this reactor.
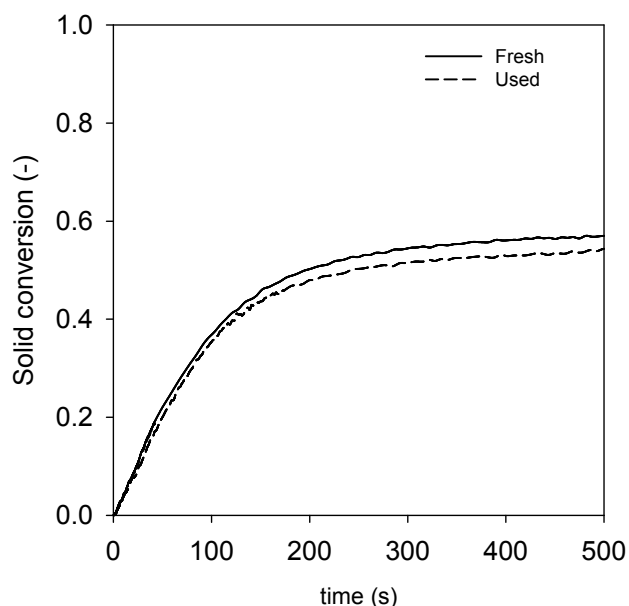
Figure 9. Conversion versus times curves obtained in a TGA for fresh and used Mn66FeTi7 particles (T = 950 ºC; 15% CH$_4$ + 20 % H$_2$O)

4. Conclusions

Almost 100 % CO_2 capture efficiency was always obtained in pine sawdust combustion with the Mn66FeTi7 oxygen carrier. Operating parameters were optimized to maximize bixbyite regeneration in the air reactor and thus oxygen release in the fuel reactor. Air excess ratio was the most influencing variable. Values of 1.8-1.9 were recommended together with relatively low temperature in the air reactor (880 ºC). Under these optimal conditions and with adequate solids inventory in the fuel reactor, total oxygen demand values below 5% were reached. No NO_x emissions were found in the air reactor. In the fuel reactor, NO_x values under optimal conditions were below those recommended for CO_2 transportation.

Nomenclature

F_i flow of compound i (mol/s)

M_i molecular or atomic mass of i (kg/mol)

$\dot{m}_{OC}$ solids circulation flow rate (kg/s)

$\dot{m}_{sf}$ mass flow of solid fuel fed (kg/s)

m_{FR}^* specific solids inventory in the fuel reactor (kg/MW$_{th}$)

P thermal power

R_{OC} oxygen transport capacity (kg oxygen per kg oxygen carrier)

y_{O_2} oxygen molar fraction (-)

Greek symbols

ϕ oxygen carrier-to-fuel ratio (-)

η_{CC} CO_2 capture efficiency (-)

λ^* air excess ratio supplied to the air reactor (-)

Ω_{sf} oxygen demand of the solid fuel (kg oxygen per kg solid fuel)

Ω_T total oxygen demand (%)

Acronyms

BECCS   Bioenergy with Carbon dioxide Capture and Storage

CCS   Carbon dioxide Capture and Storage

CLC   Chemical Looping Combustion

CL*a*OU Chemical Looping *assisted by* Oxygen Uncoupling

CLOU   Chemical Looping with Oxygen Uncoupling

*i*G-CLC *in-situ* Gasification Chemical Looping Combustion

IPCC   Intergovernmental Panel on Climate Change

LHV   Lower Heating Value (kJ/kg of coal)

NET   Negative emission technologies

TGA   Thermogravimetric Analyzer

XRD   X-Ray Diffraction

Subscripts

AR   air reactor

FR   fuel reactor

in   inlet

out   outlet

References

[1] IPCC, Climate Change 2014: Synthesis Report. Contribution of Working Groups I, II and III to the Fifth Assessment Report of the Intergovernmental Panel on Climate Change, in: R.K.P.a.L.A.M. Core Writing Team (Ed.)Geneva (Switzerland). 2014, pp. 151.

[2] ONU, United Nations Framework Convention for Climate Change. The Paris Agreement. http://unfccc.int/paris_agreement/items/9485.php, 2015.

[3] J. Hetland, P. Yowargana, S. Leduc, F. Kraxner, Carbon-negative emissions: Systemic impacts of biomass conversion. A case study on CO_2 capture and storage options, Int. J. Greenh. Gas Con. 49 (2016) 330-342.

[4] EASAC, European Academies – Science Advisory Council. Negative emission technologies: What role in meeting Paris Agreement Targets? , in: T.C.P. Ltd (Ed.)Teutschenthal, Germany, 2018.

[5] IEA, Energy Technology Perspectives. Towards Sustainable Urban Energy Systems, 2016.

[6] S. Fuss, W.F. Lamb, M.W. Callaghan, J. Hilaire, F. Creutzig, T. Amann, T. Beringer, W. De Oliveira Garcia, J. Hartmann, T. Khanna, G. Luderer, G.F. Nemet, J. Rogelj, P. Smith, J.V. Vicente, J. Wilcox, M. Del Mar Zamora Dominguez, J.C. Minx, Negative emissions - Part 2: Costs, potentials and side effects, Environmental Research Letters 13 (2018).

[7] J. Adanez, A. Abad, F. Garcia-Labiano, P. Gayan, L.F. De Diego, Progress in chemical-looping combustion and reforming technologies, Prog. Energy Combust. Sci. 38 (2012) 215-282.

[8] I. Adánez-Rubio, A. Pérez-Astray, T. Mendiara, M.T. Izquierdo, A. Abad, P. Gayán, L.F. de Diego, F. García-Labiano, J. Adánez, Chemical looping combustion of biomass: CLOU experiments with a Cu-Mn mixed oxide, Fuel Process. Technol. 172 (2018) 179-186.

[9] A. Salimben, C. Beal, Biomass chemical looping combustion: Advanced combustion technology for low cost CO_2 storage and NO_x free bioenergy generation, 23rd European Biomass Conference and Exhibition. , 2015, pp. 1802-1808.

[10] L. Shen, J. Wu, J. Xiao, Q. Song, R. Xiao, Chemical-looping combustion of biomass in a 10 kW_{th} reactor with iron oxide as an oxygen carrier, Energy Fuels 23 (2009) 2498-2505.

[11] H. Gu, L. Shen, J. Xiao, S. Zhang, T. Song, Chemical looping combustion of biomass/coal with natural iron ore as oxygen carrier in a continuous reactor, Energy Fuels 25 (2011) 446-455.

[12] X. Niu, L. Shen, H. Gu, S. Jiang, J. Xiao, Characteristics of hematite and fly ash during chemical looping combustion of sewage sludge, Chem. Eng. J. 268 (2015) 236-244.

[13] S. Jiang, L. Shen, X. Niu, H. Ge, H. Gu, Chemical Looping Co-combustion of Sewage Sludge and Zhundong Coal with Natural Hematite as the Oxygen Carrier, Energy Fuels 30 (2016) 1720-1729.

[14] J. Yan, L. Shen, S. Jiang, J. Wu, T. Shen, T. Song, Combustion Performance of Sewage Sludge in a Novel CLC System with a Two-Stage Fuel Reactor, Energy Fuels 31 (2017) 12570-12581.

[15] S. Jiang, L. Shen, J. Yan, H. Ge, T. Song, Performance in Coupled Fluidized Beds for Chemical Looping Combustion of CO and Biomass Using Hematite as an Oxygen Carrier, Energy Fuels 32 (2018) 12721-12729.

[16] T. Mendiara, A. Abad, L.F. de Diego, F. García-Labiano, P. Gayán, J. Adánez, Biomass combustion in a CLC system using an iron ore as an oxygen carrier, Int. J. Greenh. Gas Con. 19 (2013) 322-330.

[17] T. Mendiara, A. Pérez-Astray, M.T. Izquierdo, A. Abad, L.F. de Diego, F. García-Labiano, P. Gayán, J. Adánez, Chemical Looping Combustion of different types of biomass in a 0.5 kW$_{th}$ unit, Fuel 211 (2018) 868-875.

[18] A. Abad, R. Pérez-Vega, A. Pérez-Astray, T. Mendiara, L.F. De Diego, F. García-Labiano, P. Gayán, M.T. Izquierdo, J. Adánez, Biomass Combustion with CO_2 Capture by Chemical Looping: Experimental results in a 50 kWth Pilot plant, International Conference on Negative CO_2 EmissionsGothemburg (Sweden), 2018.

[19] A. Pérez-Astray, T. Mendiara, A. Abad, F. García-Labiano, L.F. de Diego, M.T. Izquierdo, J. Adánez, Manganese ores as low-cost oxygen carriers for biomass chemical looping combustion in a 0.5 kWth unit, Fuel Process. Technol. (2019).

[20] C. Linderholm, M. Schmitz, P. Knutsson, M. Källén, A. Lyngfelt, Use of low-volatile solid fuels in a 100 kW chemical-looping combustor, Energy Fuels 28 (2014) 5942-5952.

[21] M. Schmitz, C. Linderholm, P. Hallberg, S. Sundqvist, A. Lyngfelt, Chemical-Looping Combustion of Solid Fuels Using Manganese Ores as Oxygen Carriers, Energy Fuels 30 (2016) 1204-1216.

[22] C. Linderholm, M. Schmitz, Chemical-looping combustion of solid fuels in a 100 kW dual circulating fluidized bed system using iron ore as oxygen carrier, J Environ Chem Eng 4 (2016) 1029-1039.

[23] M. Schmitz, C. Linderholm, Chemical looping combustion of biomass in 10- and 100-kW pilots - Analysis of conversion and lifetime using a sintered manganese ore, Fuel 231 (2018) 73-84.

[24] P. Moldenhauer, C. Linderholm, M. Rydén, A. Lyngfelt, Avoiding CO_2 capture effort and cost for negative CO_2 emissions using industrial waste in chemical-looping

combustion/gasification of biomass, Mitigation and Adaptation Strategies for Global Change (2019).

[25] I. Gogolev, C. Linderholm, D. Gall, M. Schmitz, T. Mattisson, J.B.C. Pettersson, A. Lyngfelt, Chemical-looping combustion in a 100 kW unit using a mixture of synthetic and natural oxygen carriers – Operational results and fate of biomass fuel alkali, Int. J. Greenh. Gas Con. 88 (2019) 371-382.

[26] T. Berdugo Vilches, F. Lind, M. Rydén, H. Thunman, Experience of more than 1000 h of operation with oxygen carriers and solid biomass at large scale, Appl. Energ. 190 (2017) 1174-1183.

[27] T. Pikkarainen, I. Hiltunen, S. Teir, Piloting of bio-CLC for BECCS, 4th International Conference on Chemical LoopingNanjing (China). 2016.

[28] T. Pikkarainen, I. Hiltunen, Chemical looping combustion of solid biomass - Performance of ilmenite and braunite as oxygen carrier materials, Eur. Biomass Conf. Exhib. Proc. Stockholm, Sweden, 2017, pp. 1837-1844.

[29] J. Haus, Y. Feng, E.U. Hartge, S. Heinrich, J. Werther, High volatiles conversion in a dual stage fuel reactor system for Chemical Looping Combustion of wood biomass, International Conference on Negative CO_2 emissionsGöteborg (Sweden), 2018.

[30] Ø. Langørgen, I. Saanum, Chemical Looping Combustion of wood pellets in a 150 kW_{th} CLC reactor, International Conference on Negative CO_2 emissions Göteborg (Sweden), 2018.

[31] P. Ohlemüller, J. Ströhle, B. Epple, Chemical looping combustion of hard coal and torrefied biomass in a 1 MW_{th} pilot plant, Int. J. Greenh. Gas Con. 65 (2017) 149-159.

[32] C. Linderholm, M. Schmitz, M. Biermann, M. Hanning, A. Lyngfelt, Chemical-looping combustion of solid fuel in a 100 kW unit using sintered manganese ore as oxygen carrier, Int. J. Greenh. Gas Con. 65 (2017) 170-181.

[33] H.C. Wu, Y. Ku, H.H. Tsai, Y.L. Kuo, Y.H. Tseng, Rice husk as solid fuel for chemical looping combustion in an annular dual-tube moving bed reactor, Chem. Eng. J. 280 (2015) 82-89.

[34] T. Mendiara, F. García-Labiano, A. Abad, P. Gayán, L.F. de Diego, M.T. Izquierdo, J. Adánez, Negative CO_2 emissions through chemical looping technology, Appl. Energ. 232 (2018) 657-684.

[35] I. Adánez-Rubio, A. Abad, P. Gayán, L.F. De Diego, F. García-Labiano, J. Adánez, Biomass combustion with CO_2 capture by chemical looping with oxygen uncoupling (CLOU), Fuel Process. Technol. 124 (2014) 104-114.

[36] M. Schmitz, C.J. Linderholm, Performance of calcium manganate as oxygen carrier in chemical looping combustion of biochar in a 10 kW pilot, Appl. Energ. 169 (2016) 729-737.

[37] M. Schmitz, C.J. Linderholm, A. Lyngfelt, Chemical looping combustion of four different solid fuels using a manganese-silicon-titanium oxygen carrier, Int. J. Greenh. Gas Con. 70 (2018) 88-96.

[38] R. Pérez-Vega, A. Abad, P. Gayán, L.F. de Diego, F. García-Labiano, J. Adánez, Development of $(Mn_{0.77}Fe_{0.23})_2O_3$ particles as an oxygen carrier for coal combustion with CO_2 capture via in-situ gasification chemical looping combustion (iG-CLC) aided by oxygen uncoupling (CLOU), Fuel Process. Technol. 164 (2017) 69-79.

[39] R. Pérez-Vega, A. Abad, F. García-Labiano, P. Gayán, L.F. de Diego, M.T. Izquierdo, J. Adánez, Chemical Looping Combustion of gaseous and solid fuels with manganese-iron mixed oxide as oxygen carrier, Energy Convers. Manage. 159 (2018) 221-231.

[40] A. Abad, R. Pérez-Vega, L.F. de Diego, P. Gayán, M.T. Izquierdo, F. García-Labiano, J. Adánez, Thermochemical assessment of chemical looping assisted by oxygen uncoupling with a MnFe-based oxygen carrier, Appl. Energ. 251 (2019).

[41] R. Pérez-Vega, A. Abad, M.T. Izquierdo, P. Gayán, L.F. de Diego, J. Adánez, Evaluation of Mn-Fe mixed oxide doped with TiO_2 for the combustion with CO_2 capture by Chemical Looping assisted by Oxygen Uncoupling, Appl. Energ. 237 (2019) 822-835.

[42] R. Pérez-Vega, A. Abad, P. Gayán, F. García-Labiano, M.T. Izquierdo, L.F. de Diego, J. Adánez, Coal combustion via Chemical Looping assisted by Oxygen Uncoupling with a manganese‑iron mixed oxide doped with titanium, Fuel Process. Technol. 197 (2020).

[43] A. Lyngfelt, B. Leckner, A 1000 MW_{th} boiler for chemical-looping combustion of solid fuels - Discussion of design and costs, Appl. Energ. 157 (2015) 475-487.

[44] P. Gayán, A. Abad, L.F. de Diego, F. García-Labiano, J. Adánez, Assessment of technological solutions for improving chemical looping combustion of solid fuels with CO_2 capture, Chem. Eng. J. 233 (2013) 56-69.

[45] H. Gu, L. Shen, S. Zhang, M. Niu, R. Sun, S. Jiang, Enhanced fuel conversion by staging oxidization in a continuous chemical looping reactor based on iron ore oxygen carrier, Chem. Eng. J. 334 (2018) 829-836.

[46] A. Cabello, P. Gayán, F. García-Labiano, L.F. De Diego, A. Abad, J. Adánez, On the attrition evaluation of oxygen carriers in Chemical Looping Combustion, Fuel Process. Technol. 148 (2016) 188-197.

[47] J. Adánez, A. Abad, T. Mendiara, P. Gayán, L.F. de Diego, F. García-Labiano, Chemical looping combustion of solid fuels, Prog. Energy Combust. Sci. 65 (2018) 6-66.

[48] A. Abad, J. Adánez, P. Gayán, L.F. de Diego, F. García-Labiano, G. Sprachmann, Conceptual design of a 100 MW_{th} CLC unit for solid fuel combustion, Appl. Energ. 157 (2015) 462-474.

[49] M. Ishida, H. Jin, A novel chemical-looping combustor without NO_x formation, Ind. Eng. Chem. Res. 35 (1996) 2469-2472.

[50] T. Mendiara, M.T. Izquierdo, A. Abad, L.F. de Diego, F. García-Labiano, P. Gayán, J. Adánez, Release of pollutant components in CLC of lignite, Int. J. Greenh. Gas Con. 22 (2014) 15-24.

[51] A. Pérez-Astray, I. Adánez-Rubio, T. Mendiara, M.T. Izquierdo, A. Abad, P. Gayán, L.F. de Diego, F. García-Labiano, J. Adánez, Comparative study of fuel-N and tar evolution in chemical looping combustion of biomass under both iG-CLC and CLOU modes, Fuel 236 (2019) 598-607.

[52] E. de Visser, C. Hendriks, M. Barrio, M.J. Mølnvik, G. de Koeijer, S. Liljemark, Y. Le Gallo, Dynamis CO_2 quality recommendations, Int. J. Greenh. Gas Con. 2 (2008) 478-484.

[53] J. Adánez, L.F. De Diego, F. García-Labiano, P. Gayán, A. Abad, J.M. Palacios, Selection of oxygen carriers for chemical-looping combustion, Energy Fuels 18 (2004) 371-377.

Declaration of interests

☒ The authors declare that they have no known competing financial interests or personal relationships that could have appeared to influence the work reported in this paper.

☐The authors declare the following financial interests/personal relationships which may be considered as potential competing interests:

PAPER IV

Research article

Chemical looping combustion of biomass: CLOU experiments with a Cu-Mn mixed oxide

Iñaki Adánez-Rubio[a,b], Antón Pérez-Astray[a], Teresa Mendiara[a,*], María Teresa Izquierdo[a], Alberto Abad[a], Pilar Gayán[a], Luis F. de Diego[a], Francisco García-Labiano[a], Juan Adánez[a]

[a] Instituto de Carboquímica (ICB-CSIC), Dept. of Energy & Environment, Miguel Luesma Castán 4, 50018 Zaragoza, Spain
[b] Aragón Institute of Engineering Research (I3A), Dept. of Chemical and Environmental Engineering, University of Zaragoza, Zaragoza 50018, Spain

ABSTRACT

Chemical looping combustion (CLC) is a low-cost CO_2 capture technology with a low energy penalty. Bio-energy with CO_2 capture and storage (BECCS) opens up the possibility for negative CO_2 emissions involving the removal of CO_2 already emitted into the atmosphere. The oxygen needed for combustion in CLC processes is supplied by a solid oxygen carrier circulating between the fuel reactor and the air reactor. In this work, the combustion of different types of biomass, such as pine sawdust, olive stones and almond shells, was studied in a continuous 1.5 kW_{th} CLC unit. A mixed Cu-Mn oxide was used as the oxygen carrier. This material releases gaseous oxygen when reduced, resulting in Chemical looping combustion with oxygen uncoupling (CLOU). The released oxygen reacts with both the volatiles and char generated inside the fuel reactor when biomass is fed into it. The oxygen carrier is reoxidized in air inside the air reactor. High CO_2 capture and 100% combustion efficiencies were achieved with this Cu-Mn oxygen carrier. The oxygen concentration inside the air reactor did not affect CO_2 capture efficiency under the studied conditions.

1. Introduction

Anthropogenic carbon dioxide (CO_2) is the leading contributor to global warming, as a result of the large amounts of this gas emitted from fossil fuel combustion processes and its long residence time into the atmosphere. In order to limit the effects of global warming, the Paris Agreement (2015) [1] established a commitment to limit the global temperature increase to 2 °C or less over the next century. The agreement implies the need to decreasing CO_2 emissions into the atmosphere and even achieving negative CO_2 emissions during the present century. Recent data indicate that CO_2 Capture and Storage (CCS) technologies can contribute about 12% of cumulative emissions reductions needed by around mid-century [2–4]. However, in order to reduce the CO_2 concentration in the atmosphere and not only to reduce CO_2 emissions, efforts should be made in the development of negative emissions technologies (NET). Among these, bioenergy with CO_2 capture and storage (BECCS) technologies allow CO_2 to be removed from the atmosphere because of the intrinsic neutral CO_2 balance of biomass and the combination of CCS techniques [5].

The chemical looping combustion (CLC) process is a CCS technology with a reduced energy penalty and low cost associated with CO_2 capture [6]. The oxygen needed for fuel combustion in CLC is supplied by a

solid oxygen carrier, thereby preventing air and fuel mixing. The oxygen carrier, typically a metal oxide, circulates between two interconnected reactors, the fuel reactor and air reactor. The fuel in the fuel reactor is burnt to CO_2 and H_2O, while the oxygen carrier is reduced. The reduced oxygen carrier is then transferred to the air reactor, where it is re-oxidized with air [6,7]. The combination of CLC with biomass as fuel can be considered a promising BECCS technology currently under development [8]. The feasibility of CLC with biomass has mostly been demonstrated in the in-situ gasification chemical looping combustion (iG-CLC) mode. In the iG-CLC mode, a gasifying agent is needed as a fluidizing gas to facilitate reactions between the fuel gasification products and the solid oxygen carrier. Experiments in continuous CLC units with different types of biomass showed that it was possible to reach 100% CO_2 capture efficiency [8,9]. However, significant amounts of unburnt products, in the range of 10–30%, were detected at the fuel reactor outlet, showing that the combustion efficiency of the process is not optimum. Berdugo Vilches et al. [10] studied the combustion of commercial wood pellets in a boiler/gasifier loop (with power inputs of 12 MW_{th} and 2–4 MW_{th}, respectively) using two oxygen carriers, ilmenite and a manganese ore. They found combustion efficiencies of around 60% at 830 °C and char conversion of around 0.4. An improvement in the combustion efficiency might be expected working in

the so-called chemical looping with oxygen uncoupling (CLOU) mode.

The CLOU process uses an oxygen carrier that releases gaseous oxygen under operation conditions, which presents better combustion kinetics for both char and volatile matter from the solid fuel resulting from gas-gas reactions [11], see reactions (1)–(4).
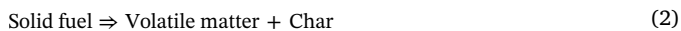
$$2M_XO_Y \Longleftrightarrow 2M_XO_{Y-1} + O_2 \qquad (1)$$

$$\text{Solid fuel} \Rightarrow \text{Volatile matter} + \text{Char} \qquad (2)$$

$$\text{Volatile matter} + O_2 \Rightarrow CO_2 + H_2O \qquad (3)$$

$$\text{Char} + O_2 \Rightarrow CO_2 + \text{Ash} \qquad (4)$$

Few metal oxides present adequate partial pressure of oxygen at conditions relevant for combustion processes (CuO/Cu_2O, Mn_2O_3/Mn_3O_4 and Co_3O_4/CoO) [12]. Among these, Cu-based materials have been the focus of research as their oxygen release is faster than that of Mn-based oxides, and their temperature window for oxygen release is higher than in the case of Mn and Co-based oxides [6]. In order to improve the thermodynamic restrictions associated with manganese, mixed oxides (Mn-Si, Mn-Mg, Mn-Fe, Mn-Cu) have been proposed. Adding another metal to manganese oxide enables oxidation of the material to be performed at higher temperatures [13–21]. More specifically, the mixed oxide based on Cu-Mn has shown high oxygen uncoupling capability [17]. A synthetic Cu-Mn mixed oxide material was recently developed by Adánez-Rubio et al. [22] and tested in a 1.5 kW$_{th}$ continuous unit using coal as fuel [23,24]. It showed 100% combustion efficiency, which qualified this oxygen carrier as a potential material for testing in experiments with biomass.

Current experience in biomass combustion in CLOU mode is quite limited. Adánez-Rubio et al. [25] demonstrated the feasibility of CLOU with biomass using a Cu-based oxygen carrier in a 1.5 kW$_{th}$ continuous unit. In that work, 100% CO_2 capture and combustion efficiencies were achieved at 935 °C. Schmitz and Linderholm [26] tested a perovskite ($CaMn_{0.9}Mg_{0.1}O_{3-\delta}$) using a biochar with a very low sulphur content in a 10 kW$_{th}$ unit. High combustion efficiencies and CO_2 capture efficiencies of up to 98% were reached in this case. At lab scale, Wang et al. [27] analysed the behaviour of a Cu-based oxygen carrier supported on olivine (38 wt% CuO) in a batch fluidized bed reactor while burning batches of pine sawdust. Fuel conversion of 99.3% was achieved at 950 °C, together with unburnt products at the outlet gas stream. Hanning et al. [28] studied the combustion of wood char in a batch fluidized with a Mn-Si mixed oxide and Mn-Si-Ti oxygen carriers. They found the CLC reaction to be more important than CLOU with these oxygen carriers.

The aim of this present work was to further analyse the CLC of biomass in CLOU mode with this new Cu-Mn-based oxygen carrier. For this purpose, three different types of biomass were considered and several operating parameters were evaluated in a 1.5 kW$_{th}$ continuous unit.

2. Materials and methods

2.1. Oxygen carrier

A Cu-Mn mixed oxide was used as oxygen carrier for the CLOU process. The oxygen carrier was prepared by spray granulation in a spouted bed system at ICB-CSIC using CuO (CHEM-LAB) and Mn_3O_4 (Micromax ®, ELKEM). This oxygen carrier was given the name Cu34Mn66-GR. The particles contained 34 wt% CuO and 66 wt% Mn_3O_4. They were calcined for 2 h at 1125 °C. The active phase in the mixed oxide was $Cu_{1.5}Mn_{1.5}O_4$. The excess Mn_3O_4 in the particles acted as an inert [22]. Reaction (5) describes the release of gaseous oxygen by the oxygen carrier.

$$2Cu_{1.5}Mn_{1.5}O_4 \Longleftrightarrow 3CuMnO_2 + O_2 \qquad (5)$$

Table 1 shows the main properties of the oxygen carrier. The

Table 1
Properties of the oxygen carrier used in this work.

XRD main phases	$Cu_{1.5}Mn_{1.5}O_4$, Mn_3O_4
Composition	72 wt% $Cu_{1.5}Mn_{1.5}O_4$
	28 wt% Mn_3O_4
Oxygen transport capacity for CLOU, R_{OC} (wt%)	4.0
Crushing strength (N)	1.9
Skeletal density of particles (kg/m^3)	4100
Air jet index, AJI (%)	3.0
Porosity (%)	12.1
Specific surface area, BET (m^2/g)	< 0.5

particle size used was + 100–300 μm.

Chemical and physical properties of the oxygen carrier particles (crushing strength, skeletal density, BET surface area, pore volumes, crystalline chemical species) were analysed using different methods. For more information on the characterization techniques used, see Adánez-Rubio et al. [23].

2.2. Solid fuels

Three different biomasses were tested during the combustion experimental campaign with the oxygen carrier. Pine (*Pinus sylvestris*) sawdust is commonly used as a reference biomass because of its wide use and distribution. Two different agricultural waste products were also used and compared with the pine sawdust: almond (*Prunus dulcis*) shells and olive (*Olea europaea*) stones. They were selected by taking into consideration their high annual production in Spain [29,30]. The raw materials were dried and sieved to + 500–2000 μm. Properties of the three biomasses are shown in Table 2.

2.3. Experimental set-up

Fig. 1 is a diagram of the ICB-CSIC-s1 unit. The fuel and the air reactors in this facility are bubbling fluidized beds interconnected by means of another fluidized bed that acts as a loop seal. The fuel is continuously fed through a screw feeder into the fuel reactor bed. Once reduced, the oxygen carrier is transferred from the fuel to the air reactor where it is re-oxidized. Oxygen carrier particles at the air reactor outlet are recovered by a cyclone and sent to a deposit. A solids valve provides control of the solids flow sent from this reservoir back to the fuel reactor. The solids circulation rate can be measured by a solids diverter valve. More details concerning the configuration of ICB-CSIC-s1 unit can be found elsewhere [8].

The oxygen carrier inventory into the facility was kept steady at about 3 kg. N_2 was used in the fuel reactor as the fluidizing gas instead of CO_2 in order to improve the accuracy for calculation of the carbon

Table 2
Properties of the biomasses used in this work.

	Pine sawdust	Almond shells	Olive stones
Proximate analysis (wt%)			
Moisture	4.2	2.3	9.4
Volatile matter	81.0	76.6	72.5
Fixed carbon	14.4	20.0	17.3
Ash	0.4	1.1	0.8
Ultimate analysis (wt%)			
C	51.3	50.2	46.5
H	6.0	5.7	4.8
N	0.3	0.2	0.2
S[a]	0.0	0.0	0.0
O[a]	37.8	40.5	38.3
LHV (kJ/kg)	19,158	18,071	17,807
Ω_{sf} (kg O_2/kg biomass)	1.5	1.4	1.2

[a] Calculated by difference.

Fig. 1. Scheme of the ICB-CSIC-s1 unit.

reactor, CO_2 capture efficiency and char conversion in the fuel reactor [6].

Combustion efficiency in the fuel reactor is defined as the fraction of oxygen required by the fuel that is supplied by the oxygen carrier in the fuel reactor:

$$\eta_{comb,FR} = 1 - \frac{4F_{CH_4,outFR} + F_{CO,outFR} + F_{H_2,outFR}}{\frac{1}{M_{O_2}} \cdot 2\Omega_{sf} \cdot \dot{m}_{sf} - 2F_{CO_2,outAR}} \tag{6}$$

where M_{O_2} represents the molecular weight of O_2 (kg/mol); Ω_{sf} is the stoichiometric mass of O_2 to convert 1 kg of biomass (kg/kg); and m_{sf} is the biomass rate fed into the fuel reactor (kg/s).

CO_2 capture efficiency (η_{CC}) is defined as the fraction of carbon actually captured at the outlet of the fuel reactor in relation to the total carbon in gases exiting from the chemical looping unit:

$$\eta_{CC} = 1 - \frac{F_{CO_2,outAR}}{F_{CO_2,outFR} + F_{CO,outFR} + F_{CH_4,outFR} + F_{CO_2,outAR}} \tag{7}$$

Char conversion in the fuel reactor ($X_{char,FR}$) shows the ratio between the char converted inside the fuel reactor and the char generated in the fuel reactor when biomass was fed and devolatilized (mainly composed of fixed carbon). Carbon in elutriated char is considered negligible.

$$X_{char,FR} = \frac{f_{CFix} \cdot \dot{m}_{sf} - M_C \cdot F_{CO_2,outAR}}{f_{CFix} \cdot \dot{m}_{sf}} \tag{8}$$

where $f_{C,fix}$ represents the mass fraction of fixed carbon in biomass and M_C is the atomic weigh of carbon (kg/mol).

It is also possible to calculate the char conversion rate, $(-r_{Char})$, by knowing the char conversion in the fuel reactor and the mean residence time of particles of char in the fuel reactor, τ_{char}.

$$(-r_{char}) = \frac{X_{char,FR}}{\tau_{char}} \tag{9}$$

$$\tau_{char} = \tau_{FR} \cdot (1 - X_{char,FR}) \tag{10}$$

The air reactor temperature was kept steady at around 800 °C for the entire experimental campaign, and the effect of the oxygen carrier-to-fuel ratio was analysed first. Eq. (11) defines the oxygen carrier-to-fuel ratio, ϕ, as the quotient between the oxygen available in the oxygen carrier and the oxygen required for the complete combustion of the fuel. In order to study this, the solids circulation rate was varied between 8.7 and 27.2 kg/h, and a low feed of solid fuel was maintained at 0.082 kg/h of biomass (P01–P04).
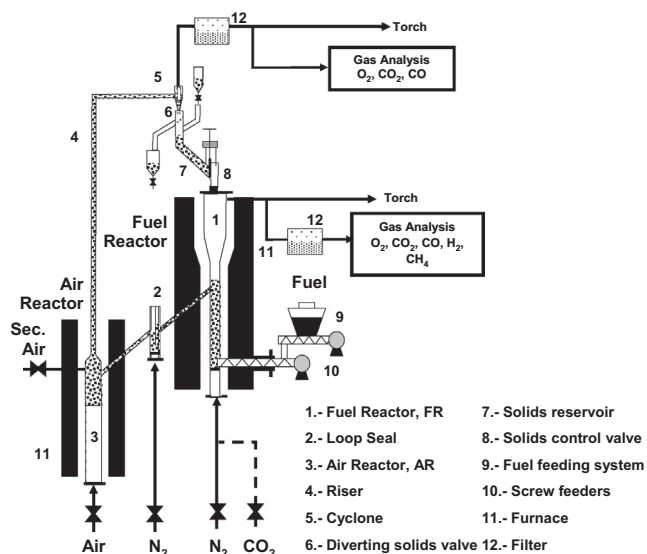
burnt in the fuel reactor. In a previous work, it had been determined that the fluidization agent did not have any influence on the oxygen carrier behaviour [31,32]. CO, CO_2, H_2, CH_4 and O_2 gas concentrations were measured and recorded at the fuel reactor outlet, as well as those of CO, CO_2 and O_2 at the air reactor outlet. A non-dispersive infrared (NDIR) analyser (Siemens Ultramat 23) was used for CH_4, CO and CO_2; a paramagnetic analyser (Siemens Ultramat 23 and Oxymat 6) was used for O_2 concentration measurement; and a thermal conductivity detector (Siemens Calomat 6) was used for H_2.

2.4. Experimental planning

Table 3 shows a compilation of the main variables set and measured in each test. The same batch of oxygen carrier particles was maintained during 65 h of hot fluidization conditions, 40 h of which included biomass combustion.

Mass balances were checked and closing values of about 95% were found for the carbon and oxygen balances. Thus, carbon present in fly ash was of low relevance. The performance of the CLC system was evaluated based on three parameters: combustion efficiency in the fuel

Table 3
Main data for experimental tests in the CLOU prototype.

Test	T_{FR} (°C)	T_{AR} (°C)	$[O_2]_{inAR}$ (%)	ϕ	$\dot{m}_s$ (kg/h)	$\dot{m}_{sf}$ (kg/h)	Power (W)	m_{FR}^* (kg/MW$_{th}$)
P01	850	800	21	**7.6**	**27.2**	0.082	435	2200
P02	850	800	21	**5.3**	**19.3**	0.082	435	2200
P03	850	800	21	**4.7**	**16.8**	0.082	435	2200
P04	850	800	21	**2.3**	**8.7**	0.082	435	2200
P05	**775**	800	21	3.9	22.5	0.14	740	1200
P06	**800**	800	21	3.9	22.5	0.14	740	1200
P07	**825**	800	21	3.9	22.5	0.14	740	1200
P08	**850**	800	21	3.9	22.5	0.14	740	1200
P09	800	800	10	3.9	22.5	**0.14**	740	1200
P10	800	800	10	3.4	28.5	**0.19**	1000	900
P11	800	800	10	2.6	28.5	**0.25**	1330	715
A01	**775**	800	21	3.0	20.3	0.173	860	1150
A02	**800**	800	21	3.0	20.3	0.173	860	1150
A03	**825**	800	21	3.0	20.3	0.173	860	1150
A04	**850**	800	21	3.0	20.3	0.173	860	1150
O01	**775**	800	21	3.3	22.5	0.225	1040	760
O02	**800**	800	21	3.3	22.5	0.225	1040	760
O03	**825**	800	21	3.3	22.5	0.225	1040	760
O04	**850**	800	21	3.3	22.5	0.225	1040	760

Data in bold represent the operating variables analysed.

$$\phi = \frac{\text{Oxygen available in the oxygen carrier}}{\text{Oxygen required for complete solid fuel combustion}} \qquad (11)$$

The power input was also analysed, with a pine sawdust feeding rate of between 0.140 and 0.250 kg/h corresponding to a power input range of between 740 and 1330 W_{th} (P09–P11), and the solids circulation rate maintained at about 28.5 kg/h. In addition, the influence of the oxygen available to regenerate the oxygen carrier in the air reactor was analysed by decreasing the oxygen concentration from 21 vol% (P01–P08) to 10 vol% (P09–P11).

3. Results and discussion

The effect of the temperature in the fuel reactor was analysed and compared among the three biomasses. For this purpose, the fuel reactor temperature was varied between 775 °C and 850 °C for the pine sawdust fuel (P05–P08), almond shells (A01–A04) and olive stones (O01–O04). During the experiments with pine sawdust, the solids circulation rate ($\dot{m}_s$) was 22.5 kg/h, with a solid fuel feed of 0.140 kg/h. The solids circulations rate was of 20.3 kg/h for the almond shells and 22.5 kg/h for the olive stones, with a solid fuel feed of between 0.173 and 0.225 kg/h.

3.1. Pine sawdust combustion

Biomass combustion by CLOU process was investigated by means of several tests involving the burning of three different biomasses: pine sawdust, almond shells and olive stones. In the case of pine sawdust, three different parameters were analysed: the oxygen carrier-to-fuel ratio, fuel reactor temperature and power input. A total of 20 h of pine sawdust biomass combustion was carried out with the Cu34Mn66-GR oxygen carrier, without problems of agglomeration.

Fig. 2 shows the gas concentration (dry basis) as a function of the operation time in the pine sawdust experiments, where the effect of the fuel reactor temperature was analysed (P05–P08). The fuel reactor temperature varied between 775 °C and 850 °C, and each temperature was maintained at a steady state for around 60 min. It can be seen that when the fuel reactor temperature was varied, a transition period of around 20 min appear before the new steady state was reached. During the steady state, the temperature and the gas concentration were practically maintained as constants. No unburnt products (CH$_4$, CO or H$_2$) were detected in the outlet gases, even at the lower temperature
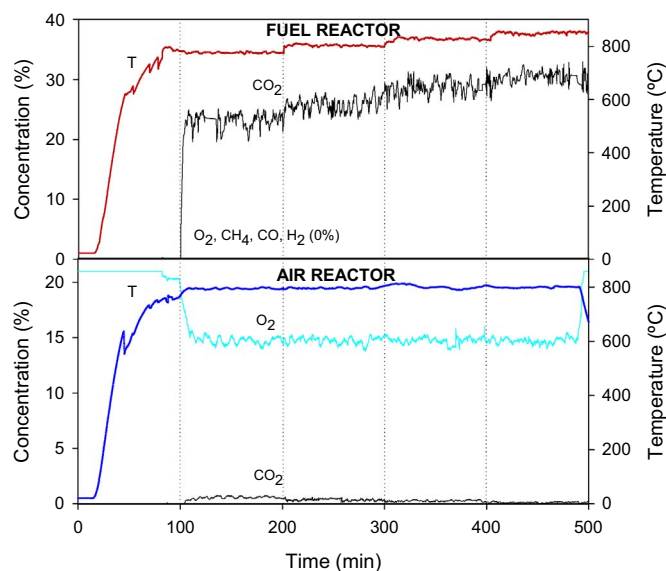

Fig. 2. Evolution of gas composition in the air and fuel reactors as fuel reactor temperature was varied. Experimental tests P05–P08. $\dot{m}_S$ = 22.5 kg/h; $\dot{m}_{SF}$ = 0.140 kg/h.

(775 °C). Therefore, complete combustion of the biomass to CO_2 and H_2O was achieved in the fuel reactor, and all the volatiles were completely converted inside the fuel reactor by the molecular oxygen released by the oxygen carrier.

It can be seen that an increase in the fuel reactor temperature resulted in an increase in the CO_2 concentration in the fuel reactor outlet gas stream. This was caused by the increase in char conversion inside the fuel reactor that decreased the CO_2 concentration at the air reactor outlet. Also worthy of note is the fact that no gaseous oxygen was measured at the fuel reactor outlet, contrary to experience in a previous work burning biomass with a Cu-based oxygen carrier [25]. This could be associated with the low fuel reactor temperature, together with the large proportion of volatiles in the biomass composition. However, using this oxygen carrier, CO_2 and H_2O were the only gases detected in the fuel reactor outlet stream, together with a fraction of the N_2 used as fluidizing agent. Moreover, some small amounts of NO_X at ppm level were detected coming from the nitrogen inherent to the biomass. However, evaluation of the nitrogen species was outside the scope of this work.

Fig. 3 shows the effect of the oxygen carrier-to-fuel ratio, ϕ, on the combustion and CO_2 capture efficiencies, and on char conversion (P01–P04). In order to achieve high oxygen carrier-to-fuel ratio values, a biomass feed rate of 0.082 g/h (435 W_{th}) was set and the solids circulation rate was varied between 8.7 and 27.8 kg/h. Complete combustion to CO_2 and H_2O was always obtained, as measured at the fuel reactor outlet. Therefore, the oxygen carrier under these conditions was able to generate enough oxygen to fully convert the fed-in biomass. CO_2 capture efficiencies of around 100% were achieved. It was necessary to reach ϕ values of 7 for the CO_2 capture efficiency to be reduced from 100% to 99.6%. This was due to the high reactivity of the biomass char, which was similar to that of Spanish lignite previously evaluated [24].

With regard to char conversion in the fuel reactor, Fig. 3 shows that with ϕ values lower than 5, all the char fed into the continuous unit was converted inside the fuel reactor. With ϕ values higher than 5, the effect of the decrease in the residence time of char and oxygen carrier in the fuel reactor started to become more significant owing to the increase in the solids circulation rate, see Table 3. Moreover, similar behaviour had previously been observed for Spanish lignite; in those experiments it was also necessary to strongly increase the oxygen carrier-to-fuel ratio in order to see a reduction in CO_2 capture efficiency. This change in trend shows the high ϕ values needed to counter the effect of the excess of oxygen generated in the fuel reactor with the increased char entering the air reactor from the fuel reactor [24].

In order to study the effect of the fuel reactor temperature on the biomass combustion by means of the CLOU process, the biomass feed rate was increased from those used in previous tests to 0.140 kg/h (740 W_{th}) and the circulation rate was fixed at 22.5 kg/h, see Table 3. Fig. 4 shows combustion and CO_2 capture efficiencies, as well as the char conversion as a function of the fuel reactor temperature (P05–P08). In a similar way to experiments (P01–P04), complete combustion of the biomass to CO_2 and H_2O was achieved for all the temperatures analysed. It is remarkable that complete combustion was even obtained at such a low fuel reactor temperature as 775 °C. The pine sawdust used contained 81% volatile matter; therefore, even with this high volatile matter content, the results showed full combustion of the biomass in all the tests. In contrast, unburnt compounds were always present at the fuel reactor outlet in the iG-CLC process, even if highly reactive materials or high solids inventories were used [8]. Note that incomplete combustion was observed at fuel reactor temperatures lower than 900 °C, with a high amount of CO, in previous experiments with pine using a Cu-based CLOU oxygen carrier [25]. This difference is a result of the low O_2 equilibrium concentration under 900 °C for CuO oxygen carriers without Mn in their composition (at 850 °C, 0.4 vol% for CuO [32] and 2 vol% for $Cu_{1.5}Mn_{1.5}O_4$ [22]). Interestingly, the present work shows that a Cu-Mn-based oxygen carrier is able to achieve complete combustion of the pine biomass even at 775 °C.
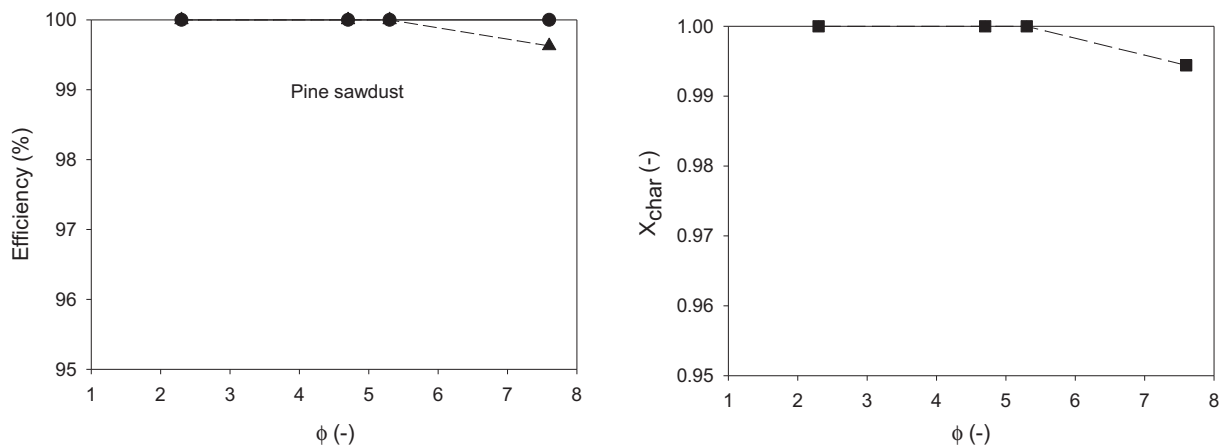
Fig. 3. Combustion (–●–) and CO_2 capture (–▲–) efficiencies, and char conversion (–■–) at different oxygen carrier-to-fuel ratio, φ, values (P01–P04).

CO_2 capture efficiency depends on how much unburnt char is transferred to the air reactor, where it is burnt emitting CO_2 into the atmosphere. It can be seen that high CO_2 capture efficiency was obtained in all cases at temperatures higher than 800 °C in the fuel reactor with pine. CO_2 capture efficiencies were higher than 90%, reaching 97.8% at 850 °C. Also, Fig. 4 demonstrates the positive effect on CO_2 capture efficiency of fuel reactor temperature. CO_2 capture efficiency increased from 86% to 95% with a 50 °C increase in the fuel reactor temperature. When the fuel reactor temperature reached 850 °C, the value of CO_2 capture efficiency increased to 97.8%. Under these conditions, CO_2 capture efficiency showed a value as high as 97.8%, without the use of a carbon separation system, i.e., avoiding the need for a carbon stripper.

Remarkably high CO_2 capture efficiency values were obtained at the relatively low fuel reactor temperatures. Compared to previous experiments carried out in the same continuous unit using a Cu-based oxygen carrier and burning pine sawdust, fuel reactor temperatures higher than 920 °C were necessary in order to achieve similar values of CO_2 capture efficiency [25]. These high CO_2 capture efficiencies at temperatures between 775 °C and 850 °C are due to the fact that the Cu-Mn oxygen carrier is able to generate high concentrations of gaseous oxygen within this window of operation, which improves combustion of the biomass. Therefore, the absence of unburnt products together with the high CO_2 capture efficiency highlights the high reactivity of the oxygen carrier for solid fuels combustion [23,24]. The high CO_2 capture efficiency is associated with fast char conversion by direct combustion with the oxygen released by the oxygen carrier in the fuel reactor. Fig. 4

also shows the char conversion as a function of the fuel reactor temperature. It can be seen that char conversion increased with the fuel reactor temperature. This effect appeared because by increasing the temperature, the char conversion rate in the fuel reactor was also increased, thus the amount of unburnt char transferred to the air reactor was reduced, increasing the CO_2 capture efficiency.

Finally, the effect of the biomass feeding rate (power) was analysed for the pine sawdust. Fig. 5 shows the effect of the power on the combustion and CO_2 capture efficiencies, and also on char conversion at 800 °C. It can be seen that the effect of power on CLOU performance was lower than that of fuel reactor temperature (P05–P08). However, an influence on CO_2 capture efficiency can be appreciated that is directly related to char conversion in the fuel reactor, see Fig. 5. However, when the biomass feeding rate was increased, CO_2 capture efficiency decreased as a result of the reduction in char conversion in the fuel reactor. Under these conditions, when the biomass feeding rate increases, the φ value and the oxygen carrier inventory decreases; see Table 3. A decrease in the oxygen carrier-to-fuel ratio value increases oxygen carrier conversion in the fuel reactor, decreasing the rate at which O_2 is released by the Cu-Mn mixed oxide. Thus char conversion depends on oxygen carrier conversion [17]. It is important to highlight that even with a power input of 1330 W_{th} and fuel reactor temperature as low as 800 °C, there was complete combustion of the biomass in the fuel reactor. Higher CO_2 capture efficiencies can be obtained by increasing the temperature to 850 °C, which is an optimum temperature at which to operate the fuel reactor when using the Cu34Mn66-GR oxygen carrier [23].

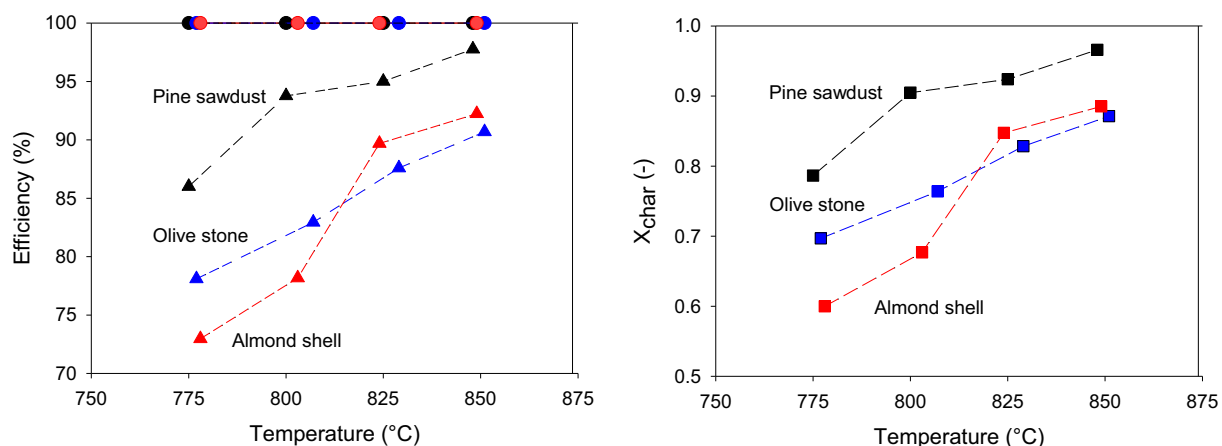Fig. 4. Combustion (–●–) and CO_2 capture (–▲–) efficiencies, and char conversion (–■–) at different fuel reactor temperatures for the three different biomasses studied: pine sawdust (P05–P08), almond shells (A01–A04) and olive stones (O01–O04).
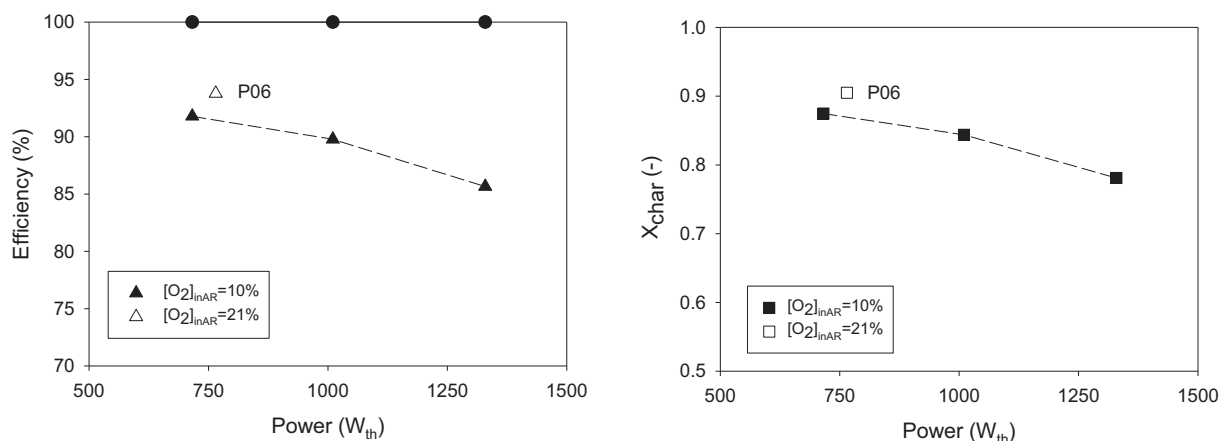
Fig. 5. Combustion (–●–) and CO$_2$ capture (–▲–) efficiencies, and char conversion (–■–) at different power inputs and oxygen concentrations in the air reactor (P06, P09–P011). T = 800 °C.

Moreover, the effect of the oxygen concentration available to regenerate the oxygen in the air reactor on CO$_2$ capture efficiency and char conversion was analysed during tests P09–P11. When comparing experiments P06 and P09, it can be seen that with 10 vol% of O$_2$ at the air reactor inlet flow (air excess ratio of 2), CO$_2$ capture efficiency and char conversion were both stable at around 92% and 0.89, respectively. It can be concluded that oxidization is possible in the air reactor with an air excess ratio of 2, as it was found previously when burning coal with the Cu34Mn66-GR oxygen carrier [23,24].

3.2. Combustion of other biomasses: almond shells and olive stones

Once the main parameters of pine sawdust combustion by the CLOU process were analysed, the combustion of two additional biomasses, almond shells and olive stones, was studied. Both biomasses showed different properties, as seen in Table 2, and it was necessary to know how they would behave in the continuous CLOU unit. This is the first time in the bibliography that biomasses other than pine sawdust have been used as solid fuel in the CLOU process. A total of 20 h of biomass combustion (10 h of combustion with each biomass) were carried out with the Cu34Mn66-GR oxygen carrier, without problems of agglomeration.

For both biomasses the effect on combustion and CO$_2$ capture efficiency, and char conversion as a function of the fuel reactor temperature was studied. For this purpose, the fuel reactor temperature was varied between 775 °C and 850 °C, see Table 3. The results can be seen in Fig. 4. It is remarkable that for both biomasses, as with the pine sawdust experiments, no unburnt gases were found in the fuel reactor outlet, even at the relatively low fuel reactor temperature of 775 °C. This may be associated with the higher oxygen equilibrium concentration at lower temperatures of the Cu-Mn-based oxygen carrier, together with the possible presence of a gas-solid reaction between the oxygen carrier and the volatile matter of biomass, as it was previously analysed by Adánez-Rubio et al. by burning coal in a batch fluidized bed reactor [17,22].

Focusing on CO$_2$ capture efficiency, Fig. 4 shows that the CO$_2$ capture efficiency for both biomasses, the almond shells and olive stones, was lower than that achieved for the pine sawdust in the entire fuel reactor temperature interval studied. For both biomasses, as well as in the case of the pine biomass, CO$_2$ capture efficiency increased with fuel reactor temperature, reaching values higher than 90% at 850 °C. This was because CO$_2$ capture efficiency is directly related to char conversion and its reactivity: the higher the rate of char conversion in the fuel reactor, the lower the amount of unburnt char transferred to the air reactor and released into the atmosphere. As can be seen in Fig. 4, char conversion was lower for almond shells and olive stones in

the entire fuel reactor interval temperature studied. Table 2 shows that almond shells and olive stones have a larger proportion of fixed carbon in their compositions (therefore, a larger amount of char is produced in the fuel reactor) and that more power was fed into the fuel reactor for both biomasses, see Table 3. As Fig. 5 shows, the power input has less effect on CO$_2$ capture efficiency than fuel reactor temperature. Consequently, the difference in char conversion for the different biomasses would be related with the difference in their char reactivity. Also, it can be seen that char conversion is lower for almonds shell than it is for olive stones in the interval 775 °C–800 °C; however, char conversions were similar for both almond shells and olive stones at temperatures higher than 800 °C, with similar CO$_2$ capture efficiencies achieved for both biomasses. Therefore, for biomasses with lower reactivity than that of pine sawdust, it would be necessary to increase the fuel reactor temperature or to install a carbon stripper to reduce the amount of unburnt char transferred to the air reactor, and thus to increase char combustion reactivity and to increase CO$_2$ capture efficiency to over 95%.

The char conversion rate was analysed to compare the reactivity of the three different biomasses studied. With the experimental data obtained in the continuous unit, it was possible to calculate the char conversion rate using the Eq. (9). Fig. 6 shows the char conversion rate as a function of the fuel reactor temperature for the three biomasses studied in this work. Pine sawdust char was the most reactive, as can
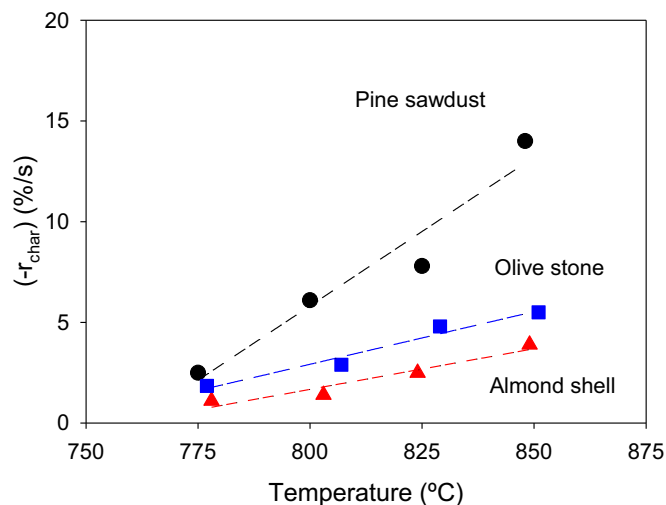

Fig. 6. Char conversion rate for the different biomasses studied as a function of fuel reactor temperature: pine sawdust (●), almond shells (▲), olive stones (■). ϕ = 3.0–3.9.

also be observed in Fig. 4 with higher CO_2 capture efficiency values. Moreover, it can be seen that the char conversion rate for the three biomasses increased with fuel reactor temperature. The increase in char conversion was almost linear for almond shells, olive stones and pine sawdust. This enabled CO_2 capture efficiency to reach a value of 98% for the pine biomass, while maximum values of 92.3% and 90.5%, respectively, were obtained for almond shells and olive stones at 850 °C under the selected conditions used.

It is possible to compare the results obtained by the CLOU process when burning three different biomasses with the results obtained with the *i*G-CLC process. Mendiara et al. [8] performed experiments in this same unit for the *i*G-CLC process by burning the same three biomasses at temperatures between 900 °C and 990 °C. They found that at temperatures ~900 °C, CO_2 capture efficiency was around 90% for almond shells and olive stones and 96% for pine sawdust, similar to those obtained in the CLOU process at 850 °C, see Fig. 4. In the same study, 100% CO_2 capture efficiency was obtained at 950 °C for all biomasses. However, when considering combustion efficiency in the fuel reactor, in the case of the *i*G-CLC process at all temperatures, oxygen demand (which is directly related with the combustion efficiency in the fuel reactor) was around 10–30% for the interval of temperatures studied. On the contrary, no gaseous unburnt products were found in the gas exit stream of the CLOU process experiments.

4. Conclusions

The operation with three different biomasses was carried out in a 1.5 kW$_{th}$ CLOU system for 65 h (40 h of combustion) using a Cu-Mn mixed oxide as an oxygen carrier (Cu34Mn66-GR). Gaseous unburnt compounds were not present in the fuel reactor outlet, even at the lowest temperature studied (775 °C), with CO_2 and H_2O being the only reaction products for the three biomasses studied in this work. When using pine sawdust as fuel, CO_2 capture efficiency was higher than 95% in most of the cases at operating temperatures in the fuel reactor as low as 850 °C.

Throughout the experimental campaign, no unburnt gaseous compounds appeared at the fuel reactor outlet, thus showing that combustion efficiency in the fuel reactor was always 100%. In experiments where the effect of the oxygen carrier-to-fuel ratio, ϕ, was studied, the oxygen carrier was able to generate enough oxygen to release excess into the fuel reactor stream and to fully convert the fed-in biomass. CO_2 capture efficiencies achieved values of around 100%.

Char combustion was improved at higher temperatures, reaching a char conversion of 96.6% at 850 °C with pine. At this condition, CO_2 capture efficiency showed a value as high as 98%, which therefore meant that the presence of a carbon separation system, i.e. a carbon stripper, could be avoided. The oxygen carrier-to-fuel ratio (ϕ) was found to be a fundamental parameter in order to obtain high CO_2 capture efficiencies. Higher ϕ values led to higher char conversion rates in the fuel reactor. This was due to the fact that the oxygen generation rate of this oxygen carrier depends on its reduction conversion. The lower the reduction conversion, the higher oxygen the generation rate, producing higher char conversion rates and also higher CO_2 capture efficiencies.

The effect of the oxygen available to regenerate the oxygen carrier in the air reactor was also investigated, with O_2 concentrations of 21% and 10 vol% at the air reactor inlet. CO_2 capture did not show a significant decrease. It can be concluded that it is possible to oxidize the oxygen carrier in the air reactor with an oxygen concentration of 10 vol % at the inlet (4 vol% at the outlet) and obtain high CO_2 capture efficiencies.

Complete combustion was also obtained for almond shells and olive stones, and CO_2 capture efficiency increased with fuel reactor temperature, reaching values higher than 90% at 850 °C. As a function of the results obtained, for biomasses with lower reactivity than pine sawdust, it would be necessary to increase the fuel reactor temperature

or to install a carbon stripper to reduce the amount of unburnt char transferred to the air reactor, and thereby to increase CO_2 capture efficiency. Finally, char conversion rate was analysed to compare the reactivity of the three biomasses studied. The increase in char conversion was almost linear for almond shells, olive stones and pine sawdust. This enabled CO_2 capture efficiency, in the case of the pine biomass, to achieve a value of 98%, while the maximum value obtained for almond shells and olive stones at 850 °C was 92.3% and 90.7%, respectively.

Notation

Symbols

f_i	mass fraction of element or compound i ($-$) in biomass
F_i	molar flow of compound i (mol/s)
M_i	atomic or molecular mass of i elements or compound (kg/mol)
$\dot{m}_{sf}$	mass flow rate of biomass fed into the fuel reactor (kg/h)
m_{FR}^*	specific solids inventory (kg/MW$_{th}$)
$\dot{m}_s$	solids circulation rate (kg/h)
$(-r_{char})$	char conversion rate (s^{-1})
R_{OC}	oxygen transport capability (kg oxygen per kg oxygen carrier)
X_{char}	char conversion ($-$)

Greek letters

ϕ	oxygen carrier-to-fuel ratio ($-$)
η_{CC}	CO_2 capture efficiency ($-$)
$\eta_{comb, FR}$	combustion efficiency in the fuel reactor ($-$)
τ_{char}	mean residence time of char particles in the fuel reactor (s)
τ_{FR}	mean residence time of solids in the fuel reactor (s)
Ω_{sf}	stoichiometric mass of O_2 to convert 1 kg of biomass (kg/kg)

Subscripts

inAR	inlet stream to the air reactor
inFR	inlet stream to the fuel reactor
outAR	outlet stream from air reactor
outFR	outlet stream from fuel reactor

References

[1] N. United, United Nations Framework Convention for Climate Change, The Paris Agreement (2015).
[2] IEA, Energy Technology Perspectives 2016, International Energy Agency, Paris, France, 2016.
[3] R. Global CCS Institute, Global CCS Institute, (2017).
[4] IPCC, Special Report on Renewable Energy Sources and Climate Change, Mitigation Technical Support Unit Working Group III, Potsdam Institute for Climate Impact Research (PIK), (2012).
[5] N.R. McGlashan, M.H.W. Workman, B. Caldecott, N. Shah, Negative Emissions Technologies, Imperial College London Grantham Institute for Climate Change, 2012.
[6] J. Adánez, A. Abad, T. Mendiara, P. Gayán, L.F. de Diego, F. García-Labiano, Chemical looping combustion of solid fuels, Prog. Energy Combust. Sci. 65 (2018) 6–66.
[7] A. Lyngfelt, B. Leckner, A 1000 MW$_{th}$ boiler for chemical-looping combustion of

solid fuels – discussion of design and costs, Appl. Energy 157 (2015) 475–487.

[8] T. Mendiara, A. Pérez-Astray, M.T. Izquierdo, A. Abad, L.F. de Diego, F. García-Labiano, P. Gayán, J. Adánez, Chemical looping combustion of different types of biomass in a 0.5 kW$_{th}$ unit, Fuel 211 (2018) 868–875.

[9] T. Mendiara, A. Abad, L.F. de Diego, F. García-Labiano, P. Gayán, J. Adánez, Biomass combustion in a CLC system using an iron ore as an oxygen carrier, Int. J. Greenhouse Gas Control 19 (2013) 322–330.

[10] T. Berdugo Vilches, F. Lind, M. Rydén, H. Thunman, Experience of more than 1000 h of operation with oxygen carriers and solid biomass at large scale, Appl. Energy 190 (2017) 1174–1183.

[11] A. Abad, I. Adánez-Rubio, P. Gayán, F. García-Labiano, L. de Diego, J. Adánez, Demonstration of chemical-looping with oxygen uncoupling (CLOU) process in a 1.5 kW$_{th}$ continuously operating unit using a Cu-based oxygen-carrier, Int. J. Greenhouse Gas Control 6 (2012) 189–200.

[12] T. Mattisson, A. Lyngfelt, H. Leion, Chemical-looping with oxygen uncoupling for combustion of solid fuels, Int. J. Greenhouse Gas Control 3 (2009) 11–19.

[13] A. Shulman, E. Cleverstam, T. Mattisson, A. Lyngfelt, Manganese/iron, manganese/nickel, and manganese/silicon oxides used in chemical-looping with oxygen uncoupling (CLOU) for combustion of methane, Energy Fuel 23 (2009) 5269–5275.

[14] A. Shulman, E. Cleverstam, T. Mattisson, A. Lyngfelt, Chemical – looping with oxygen uncoupling using Mn/Mg-based oxygen carriers – oxygen release and reactivity with methane, Fuel 90 (2011) 941–950.

[15] N. Pour, H. Leion, M. Rydén, T. Mattisson, Combined Cu/Mn oxides as an oxygen carrier in chemical looping with oxygen uncoupling (CLOU), Energy Fuel 27 (2013) 6031–6039.

[16] H. Leion, Y. Larring, E. Bakken, R. Bredesen, T. Mattisson, A. Lyngfelt, Use of CaMn$_{0.875}$Ti$_{0.125}$O$_3$ as oxygen carrier in chemical-looping with oxygen uncoupling, Energy Fuel 23 (2009) 76–83.

[17] I. Adánez-Rubio, A. Abad, P. Gayán, I. Adánez, L.F. De Diego, F. García-Labiano, J. Adánez, Use of hopcalite-derived Cu-Mn mixed oxide as oxygen carrier for chemical looping with oxygen uncoupling process, Energy Fuel 30 (2016) 5953–5963.

[18] D. Hosseini, Q. Imtiaz, P.M. Abdala, S. Yoon, A.M. Kierzkowska, A. Weidenkaff, C.R. Müller, CuO promoted Mn$_2$O$_3$-based materials for solid fuel combustion with inherent CO$_2$ capture, J. Mater. Chem. A 3 (2015) 10545–10550.

[19] M. Rydén, H. Leion, T. Mattisson, A. Lyngfelt, Combined oxides as oxygen-carrier material for chemical-looping with oxygen uncoupling, Appl. Energy 113 (2014)

1924–1932.

[20] A.-M. Azad, A. Hedayati, M. Rydén, H. Leion, T. Mattisson, Examining the Cu–Mn–O spinel system as an oxygen carrier in chemical looping combustion, energy, Technology 1 (2013) 59–69.

[21] S. Sajen, S.K. Singh, P. Mungse, S. Rayalu, K. Watanabe, G. Saravanan, N. Labhasetwar, Mechanically stable mixed metal oxide of Cu and Mn as oxygen carrier for chemical looping syngas combustion, Energy Fuel 30 (2016) 7596–7603.

[22] I. Adánez-Rubio, M.T. Izquierdo, A. Abad, P. Gayan, L.F. De Diego, J. Adánez, Spray granulated Cu-Mn oxygen carrier for chemical looping with oxygen uncoupling (CLOU) process, Int. J. Greenhouse Gas Control 65 (2017) 76–85.

[23] I. Adánez-Rubio, P. Gayan, A. Abad, L.F. De Diego, F. García-Labiano, J. Adánez, Coal combustion by a spray granulated Cu-Mn mixed oxide for CLOU process, Appl. Energy 208 (2017) 561–570.

[24] I. Adánez-Rubio, A. Abad, P. Gayan, L.F. De Diego, J. Adánez, CLOU process performance with a Cu-Mn oxygen carrier in the combustion of different types of coal with CO$_2$ capture, Fuel 212 (2018) 605–612.

[25] I. Adánez-Rubio, A. Abad, P. Gayán, L.F. de Diego, F. García-Labiano, J. Adánez, Biomass combustion with CO$_2$ capture by chemical looping with oxygen uncoupling (CLOU), Fuel Process. Technol. 124 (2014) 104–114.

[26] M. Schmitz, C.J. Linderholm, Performance of calcium manganate as oxygen carrier in chemical looping combustion of biochar in a 10 kW pilot, Appl. Energy 169 (2016) 729–737.

[27] X. Wang, T. Xu, X. Jin, Z. Hu, S. Liu, B. Xiao, Z. Chen, M. Hu, CuO supported on olivine as an oxygen carrier in chemical looping processes with pine sawdust used as fuel, Chem. Eng. J. 330 (2017) 480–490.

[28] M. Hanning, V. Frick, T. Mattisson, M. Rydén, A. Lyngfelt, Performance of combined manganese-silicon oxygen carriers and effects of including titanium, Energy Fuel 30 (2016) 1171–1182.

[29] I.O.O. Council, http://www.internationaloliveoil.org, (2017).

[30] I.N.D. Fruit, http://www.nutfruit.org, (2017).

[31] P. Gayán, I. Adánez-Rubio, A. Abad, L.F. de diego, F. García Labiano, J. Adánez, Development of Cu-based oxygen carriers for chemical-looping with oxygen uncoupling (CLOU) process, Fuel 96 (2012) 226–238.

[32] I. Adánez-Rubio, P. Gayán, A. Abad, L.F. de diego, F. García Labiano, J. Adánez, Evaluation of a spray-dried CuO/MgAl$_2$O$_4$oxygen carrier for the chemical looping with oxygen uncoupling process, Energy Fuel 26 (2012) 3069–3081.

PAPER V

ORIGINAL ARTICLE

CrossMark

Chemical looping with oxygen uncoupling: an advanced biomass combustion technology to avoid CO_2 emissions

Iñaki Adánez-Rubio [1,2] · Antón Pérez-Astray [1] · Alberto Abad [1] · Pilar Gayán [1] · Luis F. De Diego [1] · Juan Adánez [1]

Abstract

Bioenergy with carbon dioxide (CO_2) capture and storage (BECCS) technologies represent an interesting option to reach negative carbon emissions, which implies the removal of CO_2 already emitted to the atmosphere. Chemical looping combustion (CLC) with biomass can be considered as a promising BECCS technology since CLC has low cost and energy penalty. In CLC, the oxygen needed for combustion is supplied by a solid oxygen carrier circulating between the fuel and air reactors. In the fuel reactor, the fuel is oxidized producing a CO_2-concentrated stream while the oxygen carrier is reduced. In the air reactor, the oxygen carrier is regenerated with air. Chemical looping with oxygen uncoupling (CLOU) is a CLC technology that allows the combustion of solid fuels as in common combustion with air by means of an oxygen carrier that release gaseous oxygen in the fuel reactor. In the last years, several Cu-based, Mn-based, and mixed oxide oxygen (O_2) carriers have been tested showing good CLOU properties. Among them, copper (Cu)-based and Cu-Manganese (Mn) mixed oxides showed high reactivity, O_2 release rate, and high O_2 equilibrium concentration. The aim of this work is to study the viability of biomass combustion by CLOU process. The combustion of three types of biomass (pine sawdust, olive stone, and almond shell) were studied in a continuous 1.5 kW_{th} CLC unit. Two O_2 carriers were tested: a Cu-based oxygen carrier with Magnesium, Aluminum, Oxgen ($MgAl_2O_4$) as an inert prepared by spray drying (Cu60MgAl) and a mixed Cu-Mn oxide prepared by spray granulation (Cu34Mn66). These materials are capable of releasing gaseous oxygen when they are reduced in a different range of temperatures. CO_2 capture and combustion efficiency were evaluated. Two fuel reactor operation temperatures were used: 775–850 °C for Cu34Mn66 and 900–935 °C for Cu60MgAl. High CO_2 capture efficiencies and 100% combustion efficiency were reached with both oxygen carriers and with all the biomasses tested. Therefore, the CLOU technology with the Cu- and Cu-Mn-based oxygen carriers allowed avoiding CO_2 emissions maintaining high combustion efficiencies. Results obtained demonstrate that this innovative biomass combustion technology combined with carbon storage lets an efficient BECCS process implementation.

Keywords Biomass combustion · CO_2 capture · CLOU · Chemical looping · Oxygen carrier · BECCS

✉ Pilar Gayán
pgayan@icb.csic.es

Extended author information available on the last page of the article

🖄 Springer

1 Introduction

According to the United Nations Framework Convention on Climate Change 21st Conference of the Parties, Paris 2015 (IPCC 2014), it is necessary to decrease carbon dioxide (CO_2) emissions to the atmosphere and even to reach negative CO_2 emissions during this century in order to limit the global temperature increase to 2 °C or less. Carbon capture and storage (CCS) technologies allow CO_2 capture from large stationary combustion sources. If waste biomass is used as fuel in these processes, then these technologies can be considered as bioenergy with carbon capture and storage (BECCS) technologies. Biomass is a CO_2 neutral fuel. Therefore, BECCS technologies would actually allow removing CO_2 from the atmosphere making the negative CO_2 emissions concept possible.

One of the CCS technologies with lower energy penalty and cost associated to CO_2 capture is chemical looping combustion (CLC). The basic principle behind CLC is the avoidance of contact between fuel and air during the combustion process. Therefore, inherent CO_2 capture in the process is obtained. In CLC, the oxygen (O_2) needed for combustion is supplied by a solid oxygen carrier, normally a metal oxide, circulating between two interconnected reactors: the fuel and air reactors. In the fuel reactor, the fuel is burned to CO_2 and water H_2O while the oxygen carrier is reduced. The reduced O_2 carrier is then transferred to the air reactor where it is reoxidized in air before a new cycle begins. Figure 1 shows a scheme of the CLC process for solid fuels. When solid fuels are used in CLC, it is possible that part of unconverted char is transferred to the air reactor with the reduced O_2 carrier, decreasing the CO_2 capture process. To avoid this, it could be necessary to use a carbon (C) stripper that allows the separation of the unconverted char from the O_2 carrier and its recirculation to the fuel reactor. Moreover, if the fuel is not fully burned to CO_2 and H_2O in the fuel reactor, it would be necessary to convert those gases at the fuel reactor outlet completely to not decrease the combustion efficiency. In that case, an O_2 polishing step downstream the fuel reactor should be incorporated in the CLC scheme. Certain carriers are able to release gaseous oxygen while they are reduced. This is known as chemical looping with oxygen uncoupling (CLOU). The gaseous O_2 is able to burn the volatiles and the char generated once the solid fuel has been introduced into the fuel reactor.
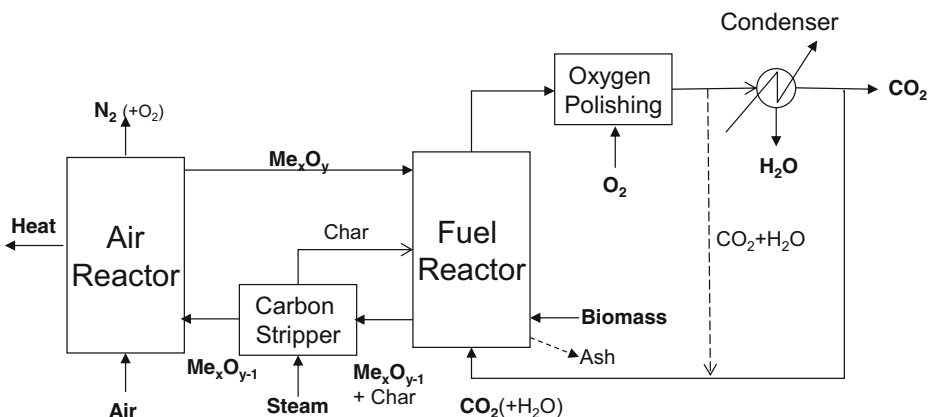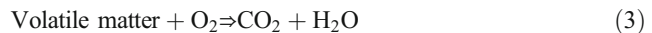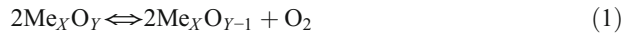

Fig. 1 Scheme of the chemical looping combustion (CLC) process for solid fuels

One of the main differences between CLOU and CLC processes is the oxygen carrier, which is able to generate O_2 (g) at the operating conditions for CLOU process. This gaseous oxygen improves the kinetic of combustion of volatile matter and char from the solid fuel by gas-gas and gas-solid reactions (Abad et al. 2012); see reactions (1)–(4).

$$2Me_XO_Y \Longleftrightarrow 2Me_XO_{Y-1} + O_2 \tag{1}$$

$$Solid\ fuel \Rightarrow Volattile\ matter + Char \tag{2}$$

$$Volatile\ matter + O_2 \Rightarrow CO_2 + H_2O \tag{3}$$

$$Char + O_2 \Rightarrow CO_2 + Ash \tag{4}$$

Only a few oxides have the adequate characteristic to be used in CLOU process involving copper, Manganese, and other elements (CuO/Cu_2O, Mn_2O_3/Mn_3O_4, and Co_3O_4/CoO) (Mattisson et al. 2009). Cu-based oxygen carriers have faster oxygen release than Mn-based oxides, and the operational temperature is higher than that for Mn and Co-based oxides.

The feasibility of CLC of biomass under CLOU mode was already demonstrated by Adánez-Rubio et al. (2014a, 2018b) (Mendiara et al. 2016) using Cu-based or Cu-Mn mixed oxide oxygen carriers. In those works, high CO_2 capture and combustion efficiencies were reached. A perovskite-type oxygen carrier ($CaMn_{0.9}Mg_{0.1}O_{3-\delta}$) was used by Schmitz and Linderholm, using a very low sulfur biochar as fuel in a 10 kW_{th} unit (Schmitz and Linderholm 2016). They observed high combustion efficiencies and CO_2 capture efficiencies higher than 98%. Moreover, Wang et al. (2017) used a Cu supported on olivine oxygen carrier (38 wt% of CuO) burning batches of pine sawdust in a batch fluidized bed reactor. They obtained a 99.3% of CO_2 capture efficiency at 950 °C, together with unburnt products in the gas stream. In this context, the aim of this work is to compare the behavior of two oxygen carriers, a Cu-based and a Cu-Mn mixed oxide, in the combustion of different kind of biomasses. Both oxygen carriers have been previously tested with different solid fuels, mainly coals. In the case of the Cu-based oxygen carrier, it was tested with coal and its char in a batch fluidized bed reactor (Adánez-Rubio et al. 2012a) and with coals of different ranks in a continuous CLOU unit (Abad et al. 2012; Adánez-Rubio et al. 2013; Adánez-Rubio et al. 2014b). On the other hand, the Cu-Mn mixed oxide was also tested with coal and its char in a batch fluidized bed reactor (Adánez-Rubio et al. 2017b) and with different rank coals in a continuous CLOU unit (Adánez-Rubio et al. 2018a; Adánez-Rubio et al. 2017a).

2 Experimental

2.1 Materials

Two oxygen carriers have been studied for the biomass combustion by the CLOU process. The Cu-based oxygen carrier prepared by spray drying was manufactured by VITO (Flemish Institute for Technological Research, Belgium) using $MgAl_2O_4$ as inert material. The CuO content was 60 wt%. Particles were calcined for 24 h at 1100 °C. This oxygen carrier was labelled Cu60MgAl. Reaction (5) describes the release of gaseous oxygen by this oxygen

carrier. The Cu-Mn mixed oxide oxygen carrier was prepared by spray granulation in a spouted fluidized bed system in our installations. The CuO content of Cu-Mn mixed oxide oxygen carrier was 34 wt%. The particles were calcined 2 h at 1125 °C. This oxygen carrier was labelled Cu34Mn66. The active phase in the mixed oxide was $Cu_{1.5}Mn_{1.5}O_4$. Reaction (6) describes the release of gaseous oxygen by Cu34Mn66 oxygen carrier.

$$2 \, CuO \leftrightarrow Cu_2O + {}^1/_2 \, O_2 \tag{5}$$

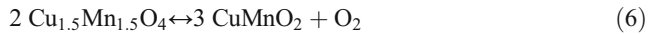$$2 \, Cu_{1.5}Mn_{1.5}O_4 \leftrightarrow 3 \, CuMnO_2 + O_2 \tag{6}$$

Table 1 shows the main properties of both oxygen carriers. The particle size used was + 100–300 μm.

Three different biomasses were combusted during the experimental campaign with the oxygen carrier. Pine sawdust (*Pinus sylvestris*) is commonly used as a reference biomass because of its large use and distribution. Two different agricultural residues were also used and compared with the pine sawdust: almond shell (*Prunus dulcis*) and olive stone (*Olea europaea*). They were selected considering their annual production (Council 2017; Fruit 2017). Raw materials were dried and sieved to + 500–2000 μm. Properties of the three biomasses are shown in Table 2.

2.2 Experimental setup

A schematic view of the experimental setup is shown in Fig. 2. The setup was basically composed of two interconnected fluidized bed reactors—the air and fuel reactors—joined by a loop seal, a riser for solid transport from the air reactor to the fuel reactor, a cyclone, and a solid valve to control the solid circulation flow rate in the system. A diverting solid valve located below the cyclone allowed the measurement of the solid circulation flow rates at any time. Therefore, this design allowed the solid circulation flow rate between both reactors' control and measurement.

The fuel reactor consisted of a bubbling fluidized bed with 5 cm of inner diameter and 20-cm bed height. The fuel reactor was fluidized with N_2 for an accurate analysis of the results. The gas flow was 250 L_N/h, corresponding to a gas velocity of ~ 0.15 m/s at 900 °C. Biomass was fed by a screw feeder at the bottom of the bed just above the fuel reactor distributor plate in order to maximize the time that the fuel and volatile matter are in contact with the bed material. A small N_2 flow (24 L_N/h) was introduced in the initial part of the screw feeder to avoid any possible reverse gas flow. The oxygen carrier was reduced, and the fuel was burned

Table 1 Properties of the oxygen carriers used in this work

	Cu60MgAl	Cu34Mn66
Experimental oxygen transport capacity, R_{OC} (wt%)	6.0	4.0
Crushing strength (N)	2.4	1.9
Skeletal density (kg/m³)	4600	4100
Porosity (%)	16.1	12.0
Specific surface area (m²/g)	< 0.5	< 0.5
X-ray diffraction main phases	CuO, $MgAl_2O_4$	$Cu_{1.5}Mn_{1.5}O_4$, Mn_3O_4

Table 2 Properties of the biomasses used in this work

	Pine sawdust	Almond shell	Olive stone
Proximate analysis (wt%)			
Moisture	4.2	2.3	9.4
Volatile matter	81.0	76.6	72.5
Fixed carbon	14.4	20.0	17.3
Ash	0.4	1.1	0.8
Ultimate analysis (wt%)			
C	51.3	50.2	46.5
H	6.0	5.7	4.8
N	0.3	0.2	0.2
S	0.0	0.0	0.0
O*	37.8	40.5	38.3
Low heating value (kJ/kg)	19,158	18,071	17,807
Ω_{SF} (kg O_2/kg biomass)	1.5	1.4	1.2

*Calculated by difference

in the fuel reactor. Reduced oxygen carrier particles overflowed into the air reactor through a U-shaped fluidized bed loop seal with 3 cm of inner diameter, to avoid gas mixing between fuel and air. A N_2 flow of 90 L_N/h was introduced in the loop seal.

The oxidation of the carrier took place in the air reactor, consisting of a bubbling fluidized bed with 8 cm of inner diameter and 10-cm bed height, and followed by a riser. The air flow was 2100 L_N/h. In addition, a secondary air flow (600 L_N/h) was introduced at the top of the bubbling bed to help particle entrainment. N_2 and unreacted O_2 left the air reactor passing
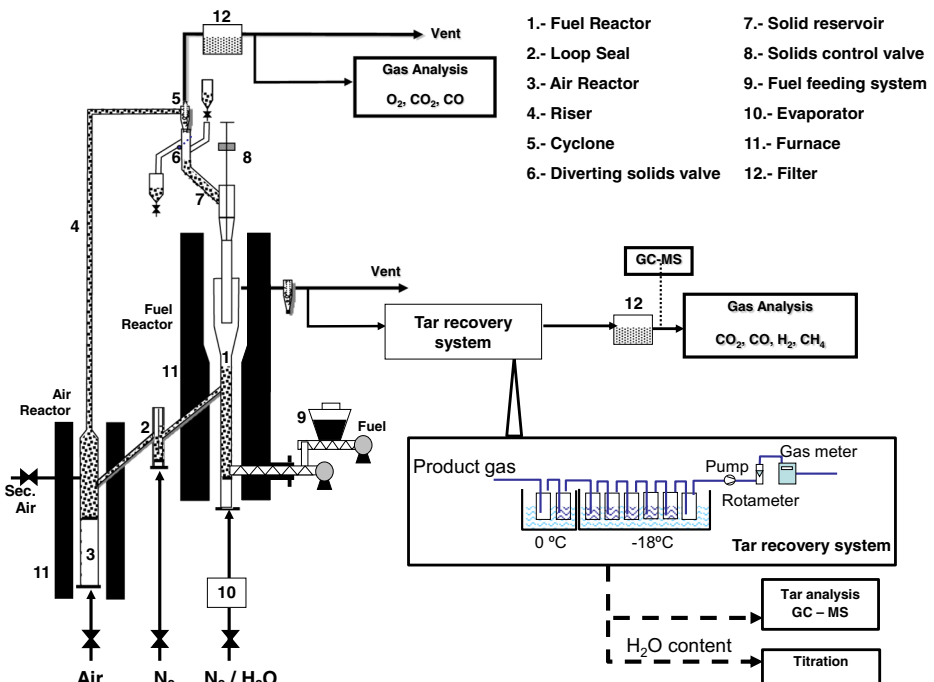
Fig. 2 Schematic view of the CLOU unit used in the experiments

through a high-efficiency cyclone and a filter before the stack. The oxidized solid particles recovered by the cyclone were sent to a solid reservoir, setting the oxygen carrier ready to start a new cycle. In addition, these particles act as a loop seal avoiding the leakage of gas between the fuel reactor and the riser. The regenerated oxygen carrier particles returned to the fuel reactor by gravity from the solid reservoir through a solid valve, which controlled the flow rate of solids entering the fuel reactor.

The total oxygen carrier inventory in the system was 3 kg, being about 1 kg in the fuel reactor. CO, CO_2, H_2, CH_4, and O_2 concentration in the fuel reactor outlet and also CO, CO_2, and O_2 from the air reactor were continuously recorded. For CH_4, CO, and CO_2, a nondispersive infrared (NDIR) analyzer (Siemens Ultramat 23) was used; a paramagnetic analyzer (Siemens Ultramat 23 and Oxymat 6) was used for O_2 concentration measurement, and a thermal conductivity detector (Siemens Calomat 6) was used for H_2. The collection of tar at the fuel reactor outlet was done according to the standard tar protocol (Simell et al. 2000).

2.3 Experimental planning

Table 3 shows a compilation of the main variables used in each test. With the oxygen carrier Cu60MgAl, a total of 10 h of operation were carried out without agglomeration. With the Cu34Mn66 oxygen carrier, a total of 65 h of hot fluidization operation from which 40 h correspond to biomass combustion using the same batch of oxygen carrier particles were carried out.

The oxygen carrier to fuel ratio, ϕ, is defined as the quotient between the oxygen supplied by the oxygen carrier and the oxygen demanded for the complete fuel combustion. The oxygen carrier to fuel ratio (ϕ) was calculated by the following equation:

$$\phi = \frac{\text{Oxygen supply by the oxygen carrier}}{\text{Oxygen demanded by the fuel for full combustion}} \tag{7}$$

Table 3 Main data for experimental tests in the CLOU unit

Test	T_{FR} (°C)	T_{AR} (°C)	$[O_2]_{inAR}$ (%)	ϕ	$\dot{m}_s$ (kg/h)	$\dot{m}_{SF}$ (kg/h)	Power (W)	m_{FR}^* (kg/MW$_{th}$)
Cu60MgAl								
P01	900	900	21	1.2	4.1	0.22	1200	565
P02	920	900	21	1.2	4.1	0.22	1200	565
P03	935	900	21	1.2	4.1	0.22	1200	565
Cu34Mn66								
P04	775	800	21	3.9	22.5	0.14	740	1200
P05	800	800	21	3.9	22.5	0.14	740	1200
P06	825	800	21	3.9	22.5	0.14	740	1200
P07	850	800	21	3.9	22.5	0.14	740	1200
A01	775	800	21	3.0	20.3	0.173	860	1150
A02	800	800	21	3.0	20.3	0.173	860	1150
A03	825	800	21	3.0	20.3	0.173	860	1150
A04	850	800	21	3.0	20.3	0.173	860	1150
O01	775	800	21	3.3	22.5	0.225	1040	760
O02	800	800	21	3.3	22.5	0.225	1040	760
O03	825	800	21	3.3	22.5	0.225	1040	760
O04	850	800	21	3.3	22.5	0.225	1040	760

To analyze the performance of the CLOU process, the combustion efficiency in the fuel reactor and the CO_2 capture efficiency were calculated. Calculations were based on the molar flow of every gas analyzed, F_i, which was determined from the measured concentrations. Mass balances were checked, and a closing about 95% for the carbon balance was found.

The combustion efficiency in the fuel reactor was calculated through the ratio between the oxygen required to fully burn unconverted gases (CH_4, CO, and H_2) at the fuel reactor exit and the oxygen demanded by the biomass converted in the fuel reactor. Thus, the oxygen demanded by the carbon bypassed to the air reactor, $F_{CO_2,AR}$, is subtracted to the oxygen demanded by biomass in the denominator. Therefore, the combustion efficiency in the fuel reactor was calculated as

$$\eta_{comb,FR} = 1 - \frac{4F_{CH_4,outFR} + F_{CO,outFR} + F_{H_2,outFR}}{\frac{1}{M_{O_2}} 2\Omega_{SF}\dot{m}_{SF} - 2F_{CO_2,outAR}} \tag{8}$$

where Ω_{SF} is the stoichiometric mass of O_2 to convert 1 kg of biomass (kg/kg), m_{SF} is the mass-based flow of biomass fed-in to the fuel reactor (kg/s), and M_{O_2} is the molecular weight of O_2 (kg/mol).

The CO_2 capture efficiency, η_{CC}, was defined as the fraction of carbon initially present in the biomass fed which is actually at the outlet of fuel reactor as CO_2. This is the actual CO_2 captured in the CLOU system; the rest is exiting together with nitrogen at the air reactor outlet.

$$\eta_{CC} = 1 - \frac{F_{CO_2,outAR}}{F_{CO_2,outFR} + F_{CO,outFR} + F_{CH_4,outFR} + F_{CO_2,outAR}} \tag{9}$$

The char conversion ($X_{char,FR}$) was defined as the fraction of carbon in the char formed in the fuel reactor which is released to the fuel reactor exhaust gas stream (Adánez et al. 2018; Mendiara et al. 2018):

$$X_{Char,FR} = \frac{\left[F_{CO_2,FR} + F_{CO,FR} + F_{CH_4,FR} - F_{C,vol} \right]_{out}}{\left[F_{CO_2,FR} + F_{CO,FR} + F_{CH_4,FR} + F_{CO_2,AR} - F_{C,vol} \right]_{out}} \tag{10}$$

where $F_{C,vol}$ is the carbon flow coming from the volatile matter.

3 Results

The effect of the temperature in the fuel reactor was analyzed and compared for both oxygen carriers and among the three biomasses. For this purpose, the fuel reactor temperature was varied from 900 to 935 °C with Cu60MgAl oxygen carrier burning pine sawdust (P01–P03). For Cu34Mn66, the fuel reactor temperature was varied from 775 to 850 °C for the pine sawdust fuel (P04–P07), the almond shell (A01–A04), and the olive stone (O01–O04). Note that the fuel reactor temperature is usually higher than the temperature in the air reactor. This fact would be possible due to that the global conversion process happening in the fuel reactor is exothermic. For example, in the case of a Cu-based oxygen carrier, the temperature increase in the fuel reactor could be as high as 90 °C (Mattisson 2013).

The gases that exit the fuel and the air reactors were continuously analyzed. As an example, Fig. 3 shows the gas concentration (dry basis) as a function of the operation time for the pine sawdust experiments with Cu34Mn66 oxygen carrier (P04–P07). The fuel reactor temperature
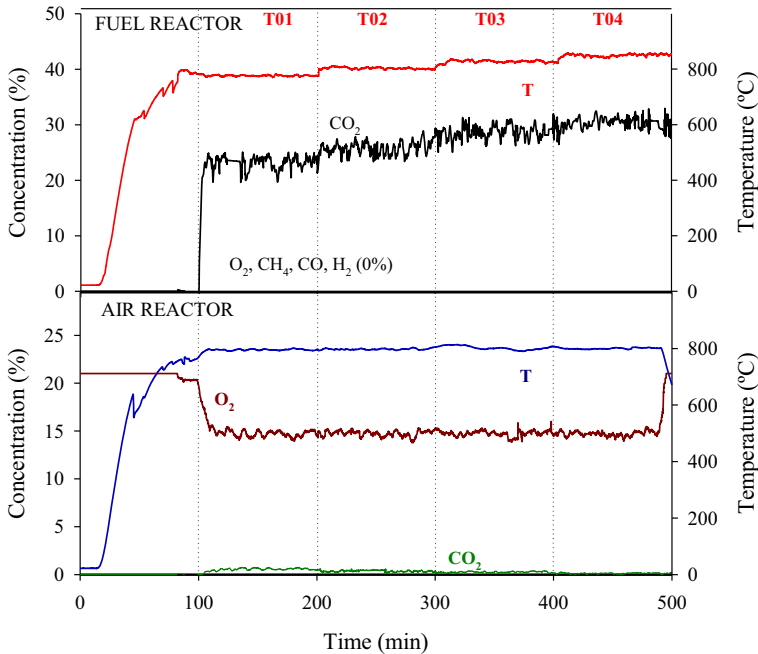
Fig. 3 Evolution of the gas composition in the air and fuel reactor as temperature in the fuel reactor was varied. Experimental tests P04–P07. ($\dot{m}_S$) = 22.5 kg/h; ($\dot{m}_{SF}$) = 0.140 kg/h

varied from 775 to 850 °C, and each temperature was maintained at steady state around 60 min. It can be seen that it was needed a period around 20 min as a transition period when the fuel reactor temperature was varied to reach a new steady-state period. During the steady state, the temperature and the gas concentration were maintained almost constant. No unburnt products (CH_4, CO, or H_2) were detected at the outlet gases not even at the lower temperature (775 °C) used. So, complete combustion of the biomass in the fuel reactor to CO_2 and H_2O was obtained, and all the volatiles were completely converted in the fuel reactor by the molecular oxygen released by the oxygen carrier. Insignificant tar amounts were found using tar protocol (Simell et al. 2000) for both oxygen carriers.

It can be seen that an increase in the fuel reactor temperature results in an increase of the CO_2 concentration in the fuel reactor outlet gas stream. This is because of the increase of char conversion in the fuel reactor that decreased the CO_2 concentration at the air reactor outlet. In addition, it can be appreciated that no gaseous oxygen was measured at the exit of the fuel reactor. This was different of what happened in a previous work burning biomass with a Cu-based oxygen carrier (Adánez-Rubio et al. 2014a). This fact could be related with the low fuel reactor temperature together with the high amount of volatiles in the biomass composition. Volatiles in the fuel reactor would consume the oxygen released by the oxygen carrier. This issue is highly relevant with biomass due to its high volatile content. Therefore, the oxygen concentration in the fuel reactor outlet could decrease to 0, especially with a material with a lower oxygen uncoupling capability as is the case of Cu34Mn66 compared to Cu60MgAl. However with the Cu34Mn66 oxygen carrier, CO_2 was the only gas detected in the fuel reactor outlet stream, together with a fraction of the N_2 used as fluidizing agent. Here, it is relevant to say that N_2 was used as fluidizing agent during the experimental campaign in order to allow an

accurate calculation of the combustion efficiency and CO_2 capture parameters. However, the fuel reactor would be fluidized by recirculated CO_2 instead of N_2 at an industrial scale. Thus, CO_2 would not be diluted in N_2, being the CO_2 capture intrinsic to the CLC process. During the biomass combustion it is possible that part of the volatiles generated by the devolatilization of the biomass react directly with the oxygen carrier by CLC reaction. However, most of oxygen would be transferred via oxygen uncoupling because: (1) complete combustion is achieved, which was not possible via gas-solid reaction with solid fuels (Adánez et al. 2018); and (2) the char is highly converted even in the absence of a gasification agent in the fluidizing medium (Adánez-Rubio et al. 2012a), being O_2 from the oxygen carrier the gasifying agent. In fact, it was determined that the oxygen uncoupling mechanism prevailed over the gas-solid reaction with materials with this capability, as was the case of a CaMn perovskite-type oxygen carrier (Abad et al. 2018).

Respect to the air to fuel ratio in CLOU experiments and considering the design of the experimental CLOU unit, the required air excess is high and, as a consequence, the oxygen concentration at the air reactor outlet was about 15%; see Fig. 3. However, no restrictions on the oxygen carrier regeneration have been observed for the Cu60MgAl material (Adánez-Rubio et al. 2014c), while a slight decrease in the regeneration capability was observed for the Cu34Mn66 material (Adánez-Rubio et al. 2017b). Anyway, the effect of the air excess with the Cu34Mn66 material was evaluated in a previous work. It was observed that a decrease in the air excess did not affect negatively to the combustion efficiency, and only a slight decrease in the char conversion was verified (Adánez-Rubio et al. 2018b).

3.1 Combustion efficiency

Taking into account the experiments carried out with Cu60MgAl oxygen carrier, Fig. 4 shows the combustion efficiency obtained in the experimental unit as a function of the fuel reactor temperature. Complete combustion of biomass to CO_2 and H_2O was found in the fuel reactor at temperatures higher than 900 °C. The solid inventory in the fuel reactor was 565 kg/MW$_{th}$ in all tests. Nevertheless, complete combustion can be expected with a lower solids inventory.

In Fig. 4, it can also be seen the combustion efficiency as a function of the fuel reactor temperature using Cu34Mn66 oxygen carrier for the three biomasses. Complete combustion of all biomasses to CO_2 and H_2O was obtained for all the temperatures analyzed. It is remarkable

Fig. 4 Combustion efficiency in the fuel reactor as a function of the fuel reactor temperature for the experiments carried out with Cu60MgAl and Cu34Mn66 oxygen carriers and three different biomasses: pine sawdust (filled circles, empty circles), almond shell (squares), and olive stone (triangles). Points superimposed
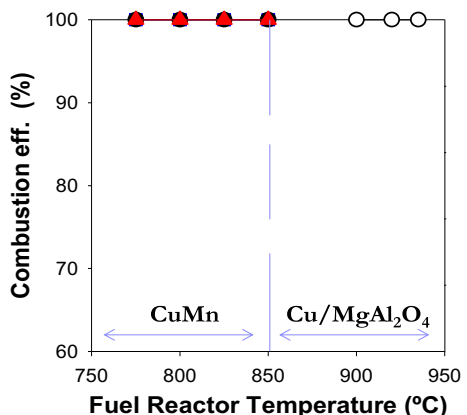
that complete combustion was even obtained at a fuel reactor temperature as low as 775 °C. So, the present work shows that the Cu34Mn66 oxygen carrier is able to obtain complete combustion of the pine biomass even at 775 °C. This high combustion efficiency at low fuel reactor temperatures was due to the higher O_2 equilibrium concentration of the Cu-Mn mixed oxide ($Cu_{1.5}Mn_{1.5}O_4$) under 900 °C (at 850 °C 2 vol% for $Cu_{1.5}Mn_{1.5}O_4$ (Adánez-Rubio et al. 2017b) and 0.4 vol% for CuO (Adánez-Rubio et al. 2012b)).

Figure 5 shows the equilibrium concentration of O_2 as a function of the temperature for the systems CuO/Cu_2O and Mn_2O_3/Mn_3O_4 together the O_2 concentrations measured in batch fluidized bed reactor tests (Adánez-Rubio et al. 2017b), because thermodynamic information on $Cu_{1.5}Mn_{1.5}O_4$ was not available. As for other mixed oxides, O_2 concentration is intermediate between those corresponding to the pure metal oxides. Experimental points plotted correspond to the measurement in a zone of nearly constant concentration.

Note that biomass has high volatile matter content, e.g., pine sawdust contains 81% volatile matter. Therefore, the results showed full combustion of the biomasses in all tests in CLOU mode with Cu and Cu-Mn materials even with these high volatile matter contents. Note also that unburnt compounds are always present at the outlet of the fuel reactor for materials without oxygen uncoupling properties, even if highly reactive materials or a high solids inventory were used (Garcia Labiano et al. 2013; Gayán et al. 2013). For example, the combustion efficiency of biomass using an iron-based oxygen carrier was about $\eta_{comb,FR} = 80\%$ with a solid inventory of 1550 kg/MW$_{th}$. This fact highlights the relevance of the oxygen uncoupling process with both Cu60MgAl and Cu34Mn66 mixed oxide oxygen carriers in order to achieve complete combustion of the fuel by the CLOU process with a low amount of solids.

Complete combustion was obtained at the respective oxygen carrier operating temperature window: 775–850 °C for Cu34Mn66 and 900–935 °C for Cu60MgAl when the CLOU effect is high enough. Therefore, the need of an oxygen polishing step would be avoided (see Fig. 1), which is required using materials without oxygen uncoupling capability (Adánez et al. 2018).

3.2 CO$_2$ capture efficiency

The CO_2 capture efficiency depends on the unburnt char transferred to the air reactor, where this char is burnt emitting CO_2 to the atmosphere. Figure 6 shows (a) the CO_2 capture efficiency and (b) the char conversion in the experiments carried out with Cu60MgAl and

Fig. 5 O_2 concentration at equilibrium as a function of the temperature for the systems: CuO/Cu_2O (line), Mn_2O_3/Mn_3O_4 (dash line), and experimental points obtained for $Cu_{1.5}Mn_{1.5}O_4/CuMnO_2$ (circles) (Adánez-Rubio et al. 2017b)
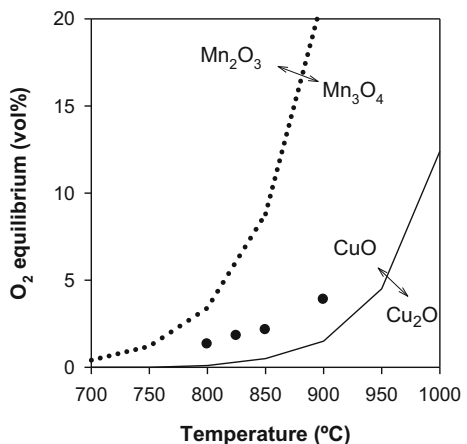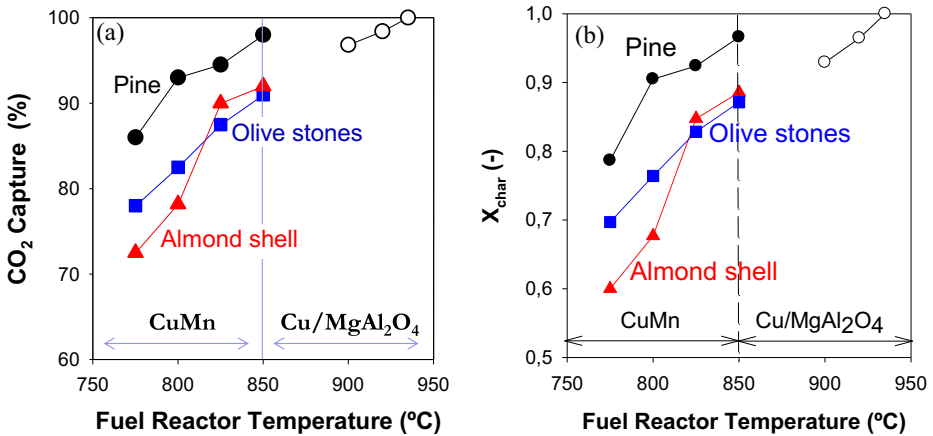
Fig. 6 **a** CO_2 capture efficiency and **b** char conversion, as a function of the fuel reactor temperature for the experiments carried out with Cu60MgAl and Cu34Mn66 oxygen carriers and three different biomasses: pine sawdust (filled circles, empty circles), almond shell (squares), and olive stone (triangles)

Cu34Mn66 oxygen carriers. For pine sawdust, Fig. 6a shows that high CO_2 capture efficiency was obtained in all cases. With temperatures higher than 800 °C in the fuel reactor, the CO_2 capture efficiencies were higher than 90%. Also, it can be seen the positive effect of the fuel reactor temperature on the CO_2 capture efficiency, reaching a value of 98% at 850 °C with Cu34Mn66 and 100% of capture with Cu60MgAl at 935 °C. This fact can be explained in terms of the direct relationship between CO_2 capture efficiency and char conversion and its reactivity; see Fig. 6b. The higher the char conversion in the fuel reactor, the lower amount of unburnt char is transferred to the air reactor and thus the lower CO_2 released to the atmosphere (Adánez-Rubio et al. 2018b).

More in detail, the CO_2 capture efficiency increased from 86 to 95% with an increase of 50 °C in the fuel reactor temperature with Cu33Mn66 and pine sawdust. When the fuel reactor temperature reached 850 °C, the value of the CO_2 capture efficiency increased to 98%. The CO_2 capture efficiency when using almond shell and olive stone was lower than that obtained for the pine sawdust along the entire fuel reactor temperature interval studied. On the other hand, the CO_2 capture efficiency increased with the fuel reactor temperature, reaching values higher than 90% for the three biomasses. The difference between char conversion for the different biomasses would be related with their char reactivity differences (Adánez-Rubio et al. 2018b). In addition, it can be seen that almond shell and olive stone have a larger content of fixed carbon; see Table 2. Therefore, a larger amount of char would be produced in the fuel reactor, which must be burned. Thus, it would be necessary to either increase the fuel reactor temperature or install a carbon stripper (see Fig. 1) to reduce the amount of unburnt char transferred to the air reactor in order to increase the CO_2 capture efficiency over 95% for biomasses with lower reactivity than the pine sawdust. However, the use of a carbon stripper could be avoided with pine sawdust as high CO_2 capture values were achieved without the need of using a carbon separation system.

Figure 6 shows that CO_2 capture efficiency increases with the fuel reactor temperature for both oxygen carriers. Thus, high CO_2 capture efficiencies were found at fuel reactor temperatures higher than 900 °C, reaching 100% efficiency at 935 °C with the pine sawdust. As the temperature increases, the oxygen uncoupling effect increases. Thus, the O_2 equilibrium at

900 °C is 1.5 vol%. But what is more relevant is the high oxygen generation rate that the oxygen carrier showed at temperatures higher than 900 °C (Adánez-Rubio et al. 2012a). As a consequence, when the fuel reactor temperature increased, the rate of char combustion was directly increased, increasing the CO_2 capture efficiency (Adánez-Rubio et al. 2014a).

Comparing the results obtained for both oxygen carriers burning pine sawdust biomass, it can be seen in Fig. 6 that the fuel reactor temperature is a key parameter to obtain high CO_2 capture efficiencies. With Cu60MgAl, a 100% CO_2 capture efficiency was reached at 935 °C. In the case of Cu34Mn66, it would predictable to reach a 100% of CO_2 capture around 865–875 °C. So, it can be concluded that the Mn introduced in a Cu-based oxygen carrier reduces the operating temperature window in the fuel reactor maintaining the complete fuel combustion to CO_2 and H_2O. In addition, high CO_2 capture efficiency was achieved for high reactive biomass without the need of a carbon separation system; i.e., the carbon stripper could be avoided. However, for biomasses less reactive than pine sawdust, e.g., almond shell and olive stone, it would be necessary either to increase the fuel reactor temperature over 875 °C or to install a carbon stripper.

It is possible to compare the results obtained by CLOU process burning three different biomasses with the results obtained with a iG-CLC process. Mendiara et al. (2017) carried out experiments in a 0.5 kW$_{th}$ unit for iG-CLC process burning three different biomasses between 900 and 990 °C. They found that at 900 °C, the CO_2 capture efficiency was around 90% for almond shell and olive stone and 96% for pine sawdust (920 °C), like in CLOU process at 850 °C. In the same study, 100% CO_2 capture efficiency was obtained at 950 °C for all biomasses. However, looking for the combustion efficiency in the fuel reactor, in the case of the iG-CLC process, the oxygen demand (which it is directly related with the combustion efficiency in the fuel reactor) was around 10–30% for the interval of temperatures studied. On the contrary, no gaseous unburnt products were found in the gas outlet stream of the CLOU process experiments.

4 Conclusions

The operation with three different biomasses and two different CLOU oxygen carriers was carried out in a 1.5 kW$_{th}$ CLOU system during 10 h using a Cu-based oxygen carrier (Cu60MgAl) and 65 h (40 h of combustion) using a Cu-Mn mixed oxide as oxygen carrier (Cu34Mn66). Gaseous unburnt compounds were not present in the fuel reactor outlet even at the lowest temperature studied (775 °C) in the fuel reactor, being CO_2, H_2O, and O_2 the only products of reaction for the three biomasses studied in this work.

The relation between oxygen release and temperature for Cu60MgAl and Cu34Mn66 is different, and therefore, different operating windows for the biomass combustion were determined. Thus, the CO_2 capture efficiency for pine sawdust reached 98% at 850 °C for Cu34Mn66 and 100% at 935 °C for Cu60MgAl. For biomasses with lower reactivity than pine sawdust, that is almond shells and olive stones, it would be necessary to increase the fuel reactor temperature or to install a carbon stripper to increase the CO_2 capture efficiency over 95%.

In summary, the CLOU technology with the Cu- and Cu-Mn-based oxygen carriers would allow avoiding CO_2 emissions maintaining high combustion efficiencies. Results obtained demonstrate that this innovative biomass combustion technology combined with carbon storage would let an efficient BECCS process implementation.

Abbreviations: F_i, Molar flow of compound i (mol/s); M_i, Atomic or molecular mass of i elements or compound (kg/mol); $\dot{m}_{SF}$, Mass flow rate of biomass fed in to the fuel reactor (kg/h); m_{FR}^*, Specific solid inventory (kg/MW_{th}); $\dot{m}_S$, Solids circulation rate (kg/h); R_{OC}, Oxygen transport capability (kg oxygen per kg of oxygen carrier); T, Temperature (°C); $X_{char,FR}$, Char conversion (−);

Greek letters ϕ, Oxygen carrier to fuel ratio (−); η_{CC}, CO_2 capture efficiency (−); $\eta_{comb,\ FR}$, Combustion efficiency in the fuel reactor (−); Ω_{SF}, Stoichiometric mass of O_2 to convert 1 kg of biomass (kg/kg);

Subscripts $outAR$, Outlet stream from air reactor; $outFR$, Outlet stream from fuel reactor

Publisher's note Springer Nature remains neutral with regard to jurisdictional claims in published maps and institutional affiliations.

References

Abad A, Adánez-Rubio I, Gayán P, García-Labiano F, de Diego L, Adánez J (2012) Demonstration of chemical-looping with oxygen uncoupling (CLOU) process in a 1.5 kW_{th} continuously operating unit using a Cu-based oxygen-carrier. Int J Greenhouse Gas Control 6:189–200

Abad A, Gayán P, de Diego LF, García-Labiano F, Adánez J (2018) Modelling chemical-looping assisted by oxygen uncoupling (CLaOU): assessment of natural gas combustion with calcium manganite as oxygen carrier. Proc Combust Inst. https://doi.org/10.1016/j.proci.2018.09.037

Adánez J, Abad A, Mendiara T, Gayán P, de Diego LF, García-Labiano F (2018) Chemical looping combustion of solid fuels. Prog Energy Combust Sci 65:6–66. https://doi.org/10.1016/j.pecs.2017.07.005

Adánez-Rubio I, Abad A, Gayán P, de Diego LF, García-Labiano F, Adánez J (2012a) Identification of operational regions in the chemical-looping with oxygen uncoupling (CLOU) process with a Cu-based oxygen carrier. Fuel 102:634–645

Adánez-Rubio I, Gayán P, Abad A, de Diego LF, García-Labiano F, Adánez J (2012b) Evaluation of a spray-dried CuO/MgAl₂O₄Oxygen carrier for the chemical looping with oxygen uncoupling process. Energy Fuel 26:3069–3081

Adánez-Rubio I, Abad A, Gayán P, de Diego LF, García-Labiano F, Adánez J (2013) Performance of CLOU process in the combustion of different types of coal with CO_2 capture. Int J Greenhouse Gas Control 12:430–440

Adánez-Rubio I, Abad A, Gayán P, de Diego LF, García-Labiano F, Adánez J (2014a) Biomass combustion with CO_2 capture by chemical looping with oxygen uncoupling (CLOU). Fuel Process Technol 124:104–114. https://doi.org/10.1016/j.fuproc.2014.02.019

Adánez-Rubio I, Abad A, Gayán P, García-Labiano F, de Diego LF, Adánez J (2014b) The fate of sulphur in the Cu-based chemical looping with oxygen uncoupling (CLOU). Process. Appl Energy 113:1855–1862

Adánez-Rubio I, Gayán P, Abad A, García-Labiano F, de Diego LF, Adánez J (2014c) Kinetic analysis of a Cu-based oxygen carrier: relevance of temperature and oxygen partial pressure on reduction and oxidation reactions rates in chemical looping with oxygen uncoupling (CLOU). Chem Eng J 256:69–84. https://doi.org/10.1016/j.cej.2014.06.102

Adánez-Rubio I, Gayan P, Abad A, de Diego LF, García-Labiano F, Adánez J (2017a) Coal combustion by a spray granulated Cu-Mn mixed oxide for CLOU process. Appl Energy 208:561–570. https://doi.org/10.1016/j.apenergy.2017.09.098

Adánez-Rubio I, Izquierdo MT, Abad A, Gayan P, de Diego LF, Adánez J (2017b) Spray granulated Cu-Mn oxygen carrier for chemical looping with oxygen uncoupling (CLOU) process. Int J Greenhouse Gas Control 65:76–85. https://doi.org/10.1016/j.ijggc.2017.08.021

Adánez-Rubio I, Abad A, Gayan P, de Diego LF, Adánez J (2018a) CLOU process performance with a Cu-Mn oxygen carrier in the combustion of different types of coal with CO_2 capture. Fuel 212:605–612

Adánez-Rubio I, Pérez-Astray A, Mendiara T, Izquierdo MT, Abad A, Gayán P, de Diego LF, García-Labiano F, Adánez J (2018b) Chemical looping combustion of biomass: CLOU experiments with a Cu-Mn mixed oxide. Fuel Process Technol 172:179–186. https://doi.org/10.1016/j.fuproc.2017.12.010

Council IOO (2017) http://www.internationaloliveoil.org Acessed 5 November 2017

Fruit IND (2017) http://www.nutfruit.org

Garcia Labiano F, García Labiano F, de Diego L, Gayán P, Abad A, Adánez J (2013) Fuel reactor modelling in chemical-looping combustion of coal: 2—simulation and optimization. Chem Eng Sci 87:173–182

Gayán P, Abad A, de Diego LF, García-Labiano F, Adánez J (2013) Assessment of technological solutions for improving chemical looping combustion of solid fuels with CO_2 capture. Chem Eng J 233:56–69. https://doi.org/10.1016/j.cej.2013.08.004

IPCC (2014) Climate Change 2014: Synthesis Report. Contribution of Working Groups I, II and III to the Fifth Assessment Report of the Intergovernmental Panel on Climate Change; Geneva (Switzerland):151

Mattisson T, Lyngfelt A, Leion H (2009) Chemical-looping with oxygen uncoupling for combustion of solid fuels. Int J Greenhouse Gas Control 3:11–19

Mendiara T, Adánez-Rubio I, Gayán P, Abad A, de Diego LF, García-Labiano F, Adánez J (2016) Process comparison for biomass combustion: in situ gasification-chemical looping combustion (iG-CLC) versus chemical looping with oxygen uncoupling (CLOU). Energy Technol 4:1130–1136. https://doi.org/10.1002/ente.201500458

Mendiara T et al (2017) Chemical looping combustion of different types of biomass in a 0.5 kW_{th} unit. Fuel 211: 868–875

Mendiara T, García-Labiano F, Abad A, Gayán P, de Diego LF, Izquierdo MT, Adánez J (2018) Negative CO_2 emissions through the use of biofuels in chemical looping technology: a review. Appl Energy 232:657–684. https://doi.org/10.1016/j.apenergy.2018.09.201

Schmitz M, Linderholm CJ (2016) Performance of calcium manganate as oxygen carrier in chemical looping combustion of biochar in a 10 kW pilot. Appl Energy 169:729–737. https://doi.org/10.1016/j.apenergy.2016.02.088

Simell P, Ståhlberg P, Kurkela E, Albrecht J, Deutsch S, Sjöström K (2000) Provisional protocol for the sampling and anlaysis of tar and particulates in the gas from large-scale biomass gasifiers. Version 1998. Biomass Bioenergy 18:19–38

Wang X, Xu T, Jin X, Hu Z, Liu S, Xiao B, Chen Z, Hu M (2017) CuO supported on olivine as an oxygen carrier in chemical looping processes with pine sawdust used as fuel. Chem Eng J 330:480–490. https://doi.org/10.1016/j.cej.2017.07.175

Affiliations

Iñaki Adánez-Rubio[1,2] · Antón Pérez-Astray[1] · Alberto Abad[1] · Pilar Gayán[1] · Luis F. De Diego[1] · Juan Adánez[1]

[1] Instituto de Carboquímica (ICB-CSIC), Miguel Luesma Castán 4, 50018 Zaragoza, Spain

[2] Aragón Institute of Engineering Research (I3A), Dept. of Chemical and Environmental Engineering, University of Zaragoza, 50018 Zaragoza, Spain

PAPER VI

Full Length Article

Comparative study of fuel-N and tar evolution in chemical looping combustion of biomass under both *i*G-CLC and CLOU modes

A. Pérez-Astray[a], I. Adánez-Rubio[a,b], T. Mendiara[a,*], M.T. Izquierdo[a], A. Abad[a], P. Gayán[a], L.F. de Diego[a], F. García-Labiano[a], J. Adánez[a]

[a] Department of Energy and Environment, Instituto de Carboquímica (ICB-CSIC), Miguel Luesma Castán 4, 50018 Zaragoza, Spain
[b] Aragón Institute of Engineering Research (I3A), Dept. of Chemical and Environmental Engineering, University of Zaragoza, 50018 Zaragoza, Spain

ARTICLE INFO

ABSTRACT

Chemical looping combustion (CLC) processes combined with CO_2 sequestration and sustainable management of biomass represent a promising BioEnergy with Carbon Capture and Storage (BECCS) technology. One of the aspects to be considered in the combustion of biomass is the formation of NO_x and the possible existence of tar in the gaseous product stream. The advantage of the CLC technology compared to other CO_2 capture technologies is that only fuel-N contributes to nitrogen oxides formation. Moreover, scarce information is available about tar formation in CLC. Thus, this work focuses on these two aspects and compares the results obtained when two different chemical looping combustion modes are used, namely *In Situ* Gasification Chemical Looping Combustion (*i*G-CLC) and Chemical Looping with Oxygen Uncoupling (CLOU). Important differences were observed depending on the combustion mode. In both cases most of the fuel-N appeared as N_2 in the fuel reactor. However, in *i*G-CLC more than 94% of the nitrogen measured in the fuel reactor was N_2 independently of the biomass used. These percentages under the CLOU mode were lower. In this case, low amounts of N_2O were also detected, although it decreased to almost zero at 850 °C. In the air reactor, NO was found and its concentration remained below the legal limit for NO_x emissions in power installations with all the types of biomass tested and operating modes. Tar species and concentrations found at the fuel reactor outlet stream were different under the two combustion modes. About 2.5–3.7 g/Nm^3 total tar could be found at 980 °C burning under *i*G-CLC mode, mostly naphthalene. On the contrary, insignificant tar amounts were found in CLOU.

1. Introduction

The last report from the Intergovernmental Panel on Climate Change (IPCC) outlined the average increase of the global temperature that could be expected depending on the CO_2 emission trends in the present century [1]. Considering this report and in order to restrict the impact of climate change, the Paris Agreement established a commitment to limit the global temperature increase to 2 °C or less [2]. To reach this milestone it becomes necessary to decrease CO_2 emissions to the atmosphere and even to reach negative CO_2 emissions at the end of this century. If a safe CO_2 storage is guaranteed, Biomass Energy with Carbon Capture and Storage (BECCS) can be considered as Negative Emission Technologies (NETs) [3]. Some studies anticipate that BECCS technologies could contribute to about 12% of the global CO_2 emission reduction needed in 2060 to mitigate the climate change [1]. Excluding emission from biomass transport and pretreatment, biomass combustion emits the same quantity of CO_2 as that previously removed from

the atmosphere (neutral CO_2 emitter). Moreover, CCS technologies have reached an important level of development in recent years [4,5]. CCS technologies allow generating a concentrated CO_2 stream from stationary combustion sources and storing it, mainly in geological formations.

Among CCS technologies, Chemical Looping Combustion (CLC) is one of the most promising due to its low energy penalty associated to CO_2 capture [6]. In CLC, combustion takes place in two separate reactors so that there is no mixture between fuels and air (see Fig. 1). In one of the reactors, noted as fuel reactor in the figure, the fuel is burned with the oxygen supplied by a solid oxygen carrier (M_xO_y), which circulates between the fuel reactor and the air reactor. CO_2 and steam are obtained in the combustion and once the steam is condensed, a highly-concentrated CO_2 stream is obtained, which can be easily transported and stored. In the fuel reactor, the oxygen carrier is reduced. Afterwards, it is regenerated in air once it reaches the air reactor. Then it is ready for a new redox cycle and continuous combustion of the fuel is
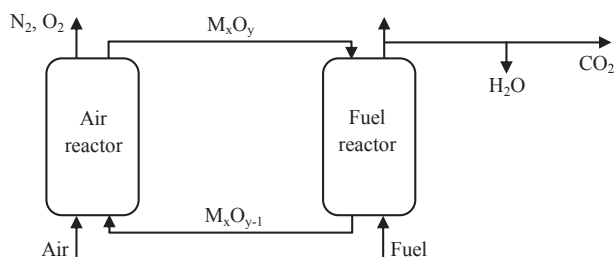

Fig. 1. Scheme of the CLC process.

maintained.

When solid fuels such as biomass are considered, CLC has developed two possible combustion processes [7]. One of them is the *In Situ* Gasification Chemical Looping Combustion (*i*G-CLC). In this process, steam or carbon dioxide should be fed to the fuel reactor as fluidizing/gasifying agents. Once the solid fuel is introduced in the fuel reactor, the volatiles are released and the char is gasified. Then, volatiles and char gasification products (H_2/CO) react with the oxygen carrier forming CO_2 and H_2O. The other option for solid fuel CLC is known as Chemical Looping with Oxygen Uncoupling (CLOU). In this case, the oxygen carrier is capable of releasing gaseous oxygen (O_2) that reacts with volatiles and char as in conventional combustion. Both processes have advantages and disadvantages. In the *i*G-CLC process, the main limiting step is the slow gasification rate of the char generated but cheap oxygen carriers can be used in the process [7]. In order to enhance char gasification, the use of a carbon stripper between fuel and air reactors has been proposed [8,9]. In the carbon stripper, unconverted char is separated and returned to the fuel reactor for further gasification. Another drawback in the *i*G-CLC process, is the existence of unburnt compounds (both volatile and char gasification products) at the fuel reactor outlet [7]. This makes the incorporation of an oxygen polishing step downstream the fuel reactor necessary to complete the combustion. The CLOU process facilitates volatile and char combustion compared to the *i*G-CLC mode, as the gaseous oxygen released by the oxygen carrier is able to react directly with the gases and char produced. The oxygen carrier must have adequate oxygen equilibrium partial pressure at temperatures of interest for combustion (800–1200 °C) and also withstands long periods of continuous redox cycles. Up to date, only few materials have demonstrated their adequacy for the CLOU process [10–12], mostly based on copper oxides or perovskites. Thus, they are also expensive oxygen carriers when compared to those for *i*G-CLC.

Although most of the works on CLC of solid fuels have been performed using different types of coal as fuel, in the recent years, some experience has also been gained in biomass combustion, named Bio-CLC [13]. Many of those works correspond to operation in continuous units under *i*G-CLC mode in the range of 0.5 kW$_{th}$ to 4 MW$_{th}$. These works used different oxygen carriers, mainly based on iron oxides and manganese oxides [14–21]. They demonstrated that working under optimized conditions it is possible to reach almost 100% CO_2 capture [15,22]. Some tar was detected in the gas stream at the fuel reactor outlet and no problems related with the ash present in biomass have been found. However, high values of unburnt compounds at the fuel reactor outlet have been reported, which requires the incorporation of an oxygen polishing step after the fuel reactor. Only few works addressed biomass combustion under CLOU mode in continuous units ranging from 1.5 to 10 kW$_{th}$ [23–26]. However, the challenge of finding CLOU materials with longer lifetime still remains.

One of the advantages of CLC over conventional combustion is the reduction in NO$_x$ [27] and tar formation [14]. In CLC there is no mixing between fuel and air and combustion temperatures are lower, therefore, the contribution to NO$_x$ formation of thermal NO is avoided and the main source for NO$_x$ formation is the nitrogen contained in the biomass. There is some information in literature about the fate of fuel-N in CLC

processes, mainly referred to coal as fuel [7]. The majority of the *i*G-CLC studies carried out conclude that most of fuel-N is released in the fuel reactor as N_2 and only low amounts of NO$_x$ can be found [28–30]. In the air reactor, the fuel-N in the unconverted char that may reach the air reactor is released as NO. The oxidizing atmosphere existing in the fuel reactor in the CLOU process influences NO$_x$ formation compared to what occurs in *i*G-CLC. Although most of the fuel-N is again released in the fuel reactor as N_2, there are larger amounts of NO$_x$ [31]. Besides, tar formation in the fuel reactor in *i*G-CLC can be reduced since tar can be either burned by the oxygen carrier particles or even reformed with steam/CO_2 aided by the oxygen carrier that would then act as a catalyst. Regarding tar formation, previous *i*G-CLC studies with different types of biomass showed tar contents of about 2.5–4.5 g/Nm^3 at temperatures between 950 and 980 °C with the major contribution of naphthalene. This would represent an increase of about 1% in the total oxygen demand from unburnt compounds at the fuel reactor outlet [15]. On the other hand, no tar was detected in any of the experiments performed under CLOU mode with a Cu-based oxygen carrier operating in the 900–950 °C range [23,32]. Considering that the information about both NO$_x$ and tar formation in CLC is still scarce if biomass is considered as fuel, the aim of the present paper is to further contribute to the understanding of these aspects and therefore contribute to the advance of the Bio-CLC as a BECCS technology. Experiments both under *i*G-CLC and CLOU modes will be performed using different types of biomass as fuel and later compared.

2. Experimental

2.1. Oxygen carrier and biomass

Fe-based minerals are commonly used as cheap materials in CLC processes [14,15,18,21,22,33]. In the present work, a Fe-based ore obtained in a hematite mine from Tierga (Zaragoza, Spain) was used as oxygen carrier for *i*G-CLC. A Cu-Mn mixed oxide, named as Cu34Mn66-GR, was used as oxygen carrier under CLOU operation. In both cases, the oxygen carrier was sieved to a particle size of 100–300 μm. Table 1 shows the main properties of both oxygen carriers. Further information about properties of both materials can be found elsewhere [15,24]. In this work, three Spanish biomass wastes were used as fuels. Pine sawdust (*Pinus sylvestris*) was chosen as the reference material because of its wide use and distribution. Also two different types of biomass wastes used for energetic purposes were chosen, namely, olive stone (*Olea europaea*) and almond shell (*Prunus dulcis*). Raw biomass was dried and sieved to 0.5–2 mm. Table 2 comprises proximate and ultimate analyses of each biomass including the low heating value and the value of the oxygen demand of the solid fuel (Ω_{sf}), which represents the amount of oxygen needed to burn the biomass.

2.2. Experimental setup and procedure

Fig. 2 shows the experimental unit at ICB-CSIC-s1 used in the experiments both under *i*G-CLC and CLOU modes. Detailed information

Table 1
Properties of the oxygen carriers used in this work.

	Tierga ore	Cu$_{34}$Mn$_{66}$-GR
Composition	Fe_2O_3, SiO_2, Al_2O_3, CaO, MgO	$Cu_{1.5}Mn_{1.5}O_4$, Mn_3O_4
XRD active phases, Me$_x$O$_y$ (wt%)	76.5 (Fe_2O_3)	72.0 ($Cu_{1.5}Mn_{1.5}O_4$)
Crushing strength (N)	5.8	1.9
Oxygen transport capacity, R_{OC} (wt%)	2.5	4.0
Porosity (%)	26.3	12.1
Skeletal density of particles (kg/m^3)	4216	4100
Specific surface area, BET (m^2/g)	1.4	< 0.5

Table 2
Proximate and ultimate analyses of the types of biomass.

	Pine sawdust	Olive stone	Almond shell
Proximate analysis (wt%)			
Moisture	4.2	9.4	2.3
Ash	0.4	0.8	1.1
Volatile matter	81.0	72.5	76.6
Fixed carbon	14.4	17.3	20.0
Ultimate analysis (wt%)			
C	51.3	46.5	50.2
H	6.0	4.8	5.7
N	0.3	0.2	0.2
S	0.0	0.0	0.0
O	37.8	38.3	40.5
LHV (kJ/kg)	19,158	16,807	18,071
Ω_{sf} (kg oxygen/kg fuel)	1.5	1.2	1.4

about the design and operation of the unit can be found elsewhere [10] and only its main features will be mentioned here. The ICB-CSIC-s1 unit consists of two interconnected fluidized bed reactors, acting as fuel and air reactors, respectively. To prevent the mixing of atmospheres, a third fluidized bed reactor is placed as a loop seal between the fuel and the air reactors. The biomass is fed into the fuel reactor at the bottom of the bubbling fluidized bed with a series of two screw feeders. The ICB-CSIC-s1 unit allows operation between 0.5 (*i*G-CLC) and 1.5 kW_th (CLOU) nominal power. There is no carbon stripper between fuel and air reactors and an important feature of this unit is the possibility of measuring and controlling the solids flow circulating between the fuel and the air reactors.

During this experimental campaign where nitrogen emissions were evaluated, CO_2 was used to fluidize the fuel reactor and the loop seal. However, tar measurements were performed using steam as gasifying

agent in the *i*G-CLC experiments and nitrogen as fluidizing agent in CLOU.

CO, CO_2, H_2, CH_4 and O_2 concentrations in the fuel reactor exit as well as CO, CO_2 and O_2 concentrations at the exit of the air reactor were measured and recorded. For CH_4, CO and CO_2 a nondispersive infrared (NDIR) analyzer (Siemens Ultramat 23) was used; a paramagnetic analyzer (Siemens Ultramat 23 and Oxymat 6) was used for O_2 concentration measurement and a thermal conductivity detector (Siemens Calomat 6) was used for H_2.

NH_3, HCN, N_2, NO, N_2O and NO_2 were measured with a quadrupole mass spectrometer from Pfeiffer. NO in fuel and air reactor was also measured using a nondispersive infrared (NDIR) analyzer (Siemens Ultramat 23). The collection of tar at the fuel reactor outlet was done according to the standard tar protocol [34]. The concentrations of the different tar compounds in the samples was measured by a GC (Agilent 7890A) fitted with a capillary column (HP-5) and a Flame Ionization Detector (FID). Furthermore, the GC was coupled with a mass spectrometer (Agilent 5975C). Naphthalene and phenanthrene were selected for the external calibration procedure. The quantitative values were obtained assuming a similar response factor to naphthalene for tar compounds of 1–2 rings and similar to phenanthrene for 3-rings compounds [35]. A standard solution with several lineal hydrocarbons was used as the external calibration in some of the compounds detected under CLOU mode.

The total oxygen carrier inventory in the ICB-CSIC-s1 unit was about 3.5 kg in the *i*G-CLC experiments and about 3 kg during CLOU operation. In *i*G-CLC, a total of 60 h of hot operation were accomplished, 40 h of which with biomass combustion. In CLOU, 45 h were reached in hot operation with 25 h of those with biomass combustion. Tables 3 and 4 shows the experimental conditions of the experiments performed [15,24]. In the tables, the value of the parameter oxygen carrier to fuel ratio (ϕ) was included. This parameter compares the available oxygen

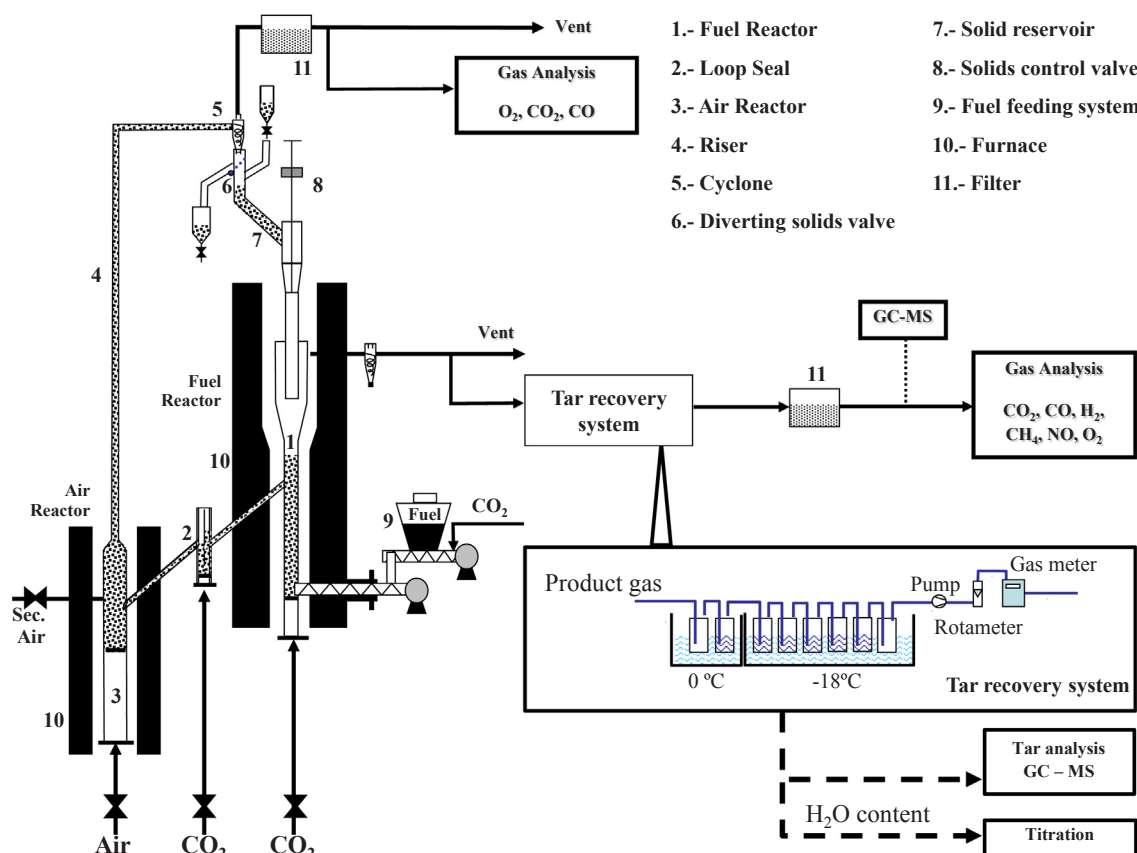
1.- Fuel Reactor
2.- Loop Seal
3.- Air Reactor
4.- Riser
5.- Cyclone
6.- Diverting solids valve
7.- Solid reservoir
8.- Solids control valve
9.- Fuel feeding system
10.- Furnace
11.- Filter

Fig. 2. Experimental unit ICB-CSIC-s1.

Table 3

Operating conditions of the *i*G-CLC tests with the different types of biomass (PN = pine sawdust; OS = olive stone; AS = almond shell).

Biomass	PN_1	PN_2	PN_3	OS_1	OS_2	OS_3	AS_1	AS_2	AS_3
Time of combustion (h)	5.7	2.6	2.2	8.1	3.0	2.3	3.7	3.3	3.8
Time of hot fluidization (h)	8.2	4.1	3.1	9.4	4.5	3.0	6.3	9.3	6.4
Temperatures (°C)									
Fuel reactor	910	950	985	905	955	980	905	955	985
Air reactor	950	950	950	950	950	950	950	950	950
Operating conditions									
Biomass flow (g/h)	113	98	98	164	141	141	190	102	88
OC circulation rate (kg/h)	9.2	6.7	6.7	8.8	7.6	7.6	13.0	7.0	5.9
Oxygen carrier to fuel ratio, ϕ	1.3	1.1	1.1	1.0	1.0	1.0	1.2	1.2	1.2
Specific solids inventory in fuel reactor (kg/MW$_{th}$)	750	785	780	600	600	590	370	550	890

in the circulating oxygen carrier with the oxygen needed for the complete combustion of the fed fuel.

$$\phi = \frac{\dot{m}_{OC} R_{OC}}{\dot{m}_{sf} \Omega_{sf}} \tag{1}$$

3. Results and discussion

3.1. Analysis of the performance of the CLC unit

Before analyzing NO$_x$ and tar formation in the biomass experiments under both *i*G-CLC and CLOU modes, the performance of the system should be evaluated. First of all, the conversion of the solid fuel was checked and an average value about 95% was found. In order to analyze the performance of the CLC system three parameters were considered, i.e. the combustion efficiency in the fuel reactor, the CO$_2$ capture efficiency and the char conversion in the fuel reactor. The combustion efficiency in the fuel reactor ($\eta_{comb,FR}$) is a measure of the gas conversion in the fuel reactor. It is defined as the fraction of oxygen demanded by the volatile matter and gasification products supplied by the oxygen carrier in the fuel reactor [7].

$$\eta_{comb,FR} = \frac{\text{oxygen transferred in fuel reactor}}{\text{oxygen demanded by solid fuel converted in fuel reactor}} \tag{2}$$

The CO$_2$ capture efficiency (η_{CC}) specifies how much of the carbon introduced with the solid fuel is captured in gaseous form at the fuel reactor outlet [7]

$$\eta_{cc} = \frac{\text{carbon in gases from fuel reactor}}{\text{carbon in gases from fuel reactor and air reactor}} \tag{3}$$

Carbon in gases exiting the fuel reactor comes from carbon contained in the volatiles and the carbon in the gasified char. As a result, all

this carbon will be converted to captured CO$_2$. The CO$_2$ capture efficiency depends on the fraction of char gasified in the fuel reactor, which is noted as char conversion in the fuel reactor ($X_{char,FR}$). This char conversion can be also considered as an indicator of the gasification efficiency.

$$X_{char,FR} = \frac{\text{fixed carbon converted in fuel reactor}}{\text{fixed carbon in solid fuel−carbon in elutriated char}} \tag{4}$$

Performance results from the experiments under both *i*G-CLC and CLOU modes were discussed in detail in Fig. 3 in order to be afterwards correlated to the results obtained in the analysis of pollutant emissions. Note that although all the experiments in this work were done using CO$_2$ as gasifying agent in the fuel reactor, Fig. 3 shows performance results obtained in similar operating conditions using steam/nitrogen as gasifying agents [15,24] as they could be calculated more accurately.

The first consideration about *i*G-CLC and CLOU results is the different temperature range in the fuel reactor within which they were obtained. The experiments with the two oxygen carriers were done under previously optimized operating conditions for each of them. The different temperature interval is justified by the reactivity of the material used as oxygen carrier [36]. The experiments under *i*G-CLC mode operated between 900 and 980 °C while in the CLOU mode lower temperatures were used (775–850 °C). In the case of *i*G-CLC, it was observed that the reactivity of the Tierga ore notably increases at temperatures above 950 °C [37]. However, in the case of CLOU experiments, the suitable operating conditions are found at those lower temperatures [36,38]. Previous studies indicated that it was possible to reach adequate O$_2$ equilibrium concentrations (up to 2% at 850 °C) to achieve complete combustion of the fuel with the Cu-Mn oxygen carrier used in this work [38]. The different temperature interval considered for each operating mode is important as it can affect the nitrogen chemistry and tar formation occurring in the fuel reactor. As it can be

Table 4

Operating conditions of the CLOU tests with the different types of biomass (PN = pine sawdust; OS = olive stone; AS = almond shell).

| Biomass	PN_4	PN_5	PN_6	PN_7	OS_4	OS_5	OS_6	OS_7	AS_4	AS_5	AS_6	AS_7
Time of combustion (h)	2.2	2.0	2.1	1.9	1.9	2.1	1.8	2.1	2.3	2.1	2.2	2.1
Time of hot fluidization (h)	3.4	3.2	3.3	3.5	3.7	3.6	3.2	3.6	3.3	3.6	3.9	3.8
Temperatures (°C)												
Fuel reactor	775	800	825	850	775	800	825	850	775	800	825	850
Air reactor	800	800	800	800	800	800	800	800	800	800	800	800
Operating conditions												
Biomass flow (g/h)	140	140	140	140	225	225	225	225	173	173	173	173
OC circulation rate (kg/h)	22.5	22.5	22.5	22.5	22.5	22.5	22.5	22.5	20.3	20.3	20.3	20.3
Oxygen carrier to fuel ratio, ϕ	3.9	3.9	3.9	3.9	3.3	3.3	3.3	3.3	3.0	3.0	3.0	3.0
Specific solids inventory in fuel reactor (kg/MW$_{th}$)	1200	1200	1200	1200	760	760	760	760	1150	1150	1150	1150
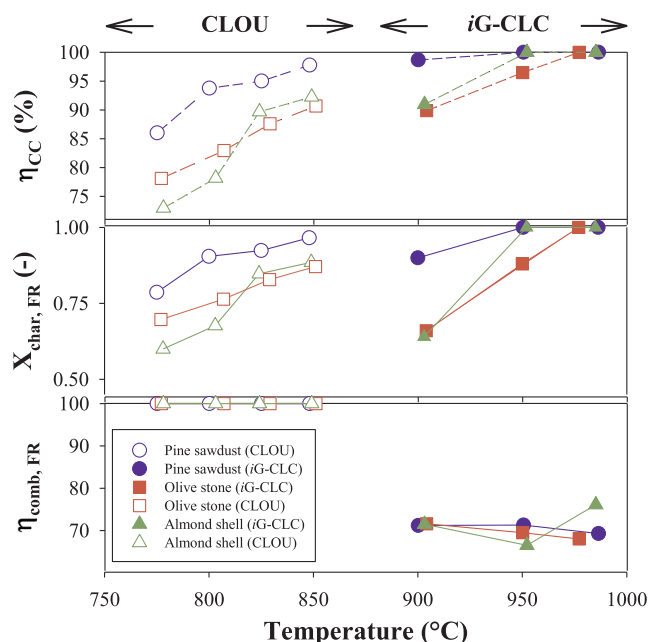
Fig. 3. Combustion efficiency ($\eta_{comb,FR}$), char conversion in the fuel reactor ($X_{char,\ FR}$) and CO_2 capture efficiency (η_{CC}) for iG-CLC (filled symbols) and CLOU (open symbols) burning pine sawdust, olive stone and almond shell.

seen in Fig. 3, under the iG-CLC mode high values of CO_2 capture efficiencies were obtained with all the types of biomass. The values increase with the fuel reactor temperature reaching almost 100% at 980 °C. These values for CO_2 capture efficiencies are correlated to those calculated for the char conversion in the fuel reactor, which also increase with the fuel reactor temperature from 0.7 to 0.8 to almost 1. In iG-CLC, low combustion efficiencies (about 70%) were found for all the types of biomass tested mainly due to the fraction of volatiles released by the biomass that are not burnt by the oxygen carrier. In the CLOU experiments also shown in Fig. 3, the CO_2 capture efficiencies increased with temperature because more char was converted at higher temperatures in the fuel reactor and therefore, less unconverted char reached the air reactor. With this Cu-Mn based oxygen carrier values of CO_2 capture efficiencies about 95% at 850 °C were obtained. In order to increase the values of these CO_2 capture efficiencies a carbon stripper would be needed. The combustion efficiencies for CLOU experiments in Fig. 3 were always close to 100% even at the lowest temperature (775 °C), due to the release of gaseous oxygen in the fuel reactor.

3.2. Fate of fuel-N

3.2.1. Fuel-N distribution between fuel and air reactors

As it was mentioned before, one of the advantages of CLC is that the contribution of thermal NO_x to the NO_x formation in combustion is avoided [27]. Therefore, the main contribution to NO_x formation comes from fuel-N. According to the composition of the different types of biomass in Table 2, the highest nitrogen content is observed for pine sawdust (0.3 wt%), while olive stone and almond shell are reported 0.2 wt%. Fuel-N in biomass is released during biomass devolatilization. The dominant nitrogenous volatile species are NH_3 and HCN [39]. Both can evolve to either N_2 or NO, depending on the combustion conditions. On the other hand, char-bound nitrogen can evolve to NO, N_2O or N_2. However, at temperatures higher than 900 °C N_2O decomposes to N_2 [40]. In these experiments performed under both iG-CLC and CLOU modes, different atmospheres can be found in the fuel reactor when biomass devolatilization takes place. In the experiments CO_2 was supplied to the fuel reactor as gasifying/fluidizing agent. Therefore, in iG-CLC a reducing environment is generated due to the presence of

gasification products, i.e. H_2 and CO. However, oxygen is present in the reacting atmosphere under CLOU operation. In both processes, N_2 from air is not present, which is an important difference compared to the conventional combustion in air.

Fig. 4 presents fuel-N distribution between fuel and air reactors in the experiments under iG-CLC and CLOU modes summarized in Tables 3 and 4. Results from three types of biomass tested are shown. As a general conclusion shown in Fig. 4, it can be said that for both operating modes, the most of the nitrogen in the fuel is released in the fuel reactor, in line with the results previously reported in literature for CLC using coal as fuel [7]. This is a consequence of the high CO_2 capture efficiencies reached and shown in Fig. 3. The percentage of fuel-N released in the fuel reactor slightly increases with temperature. The fuel-N released in the air reactor comes from the little amounts of unconverted char that reaches this reactor and is burned there. The trend in the percentage of fuel-N released in the air reactor is the opposite of that observed for char conversion in the fuel reactor in Fig. 3. Larger values of char conversion imply little bypass of unconverted char to the air reactor and therefore, less fuel-N reaching the air reactor.

However, there are differences between both operating modes that can be observed in Figs. 3 and 4, especially in the case of the experiments with pine sawdust. In Fig. 3 similar CO_2 capture efficiencies were observed at 850 °C under CLOU mode and 900 °C under iG-CLC conditions. However, lower amounts of fuel-N were found in the fuel reactor in Fig. 4 under the CLOU mode despite the high char conversions reached in both CLC modes. This reveals the different nitrogen chemistry behind the two processes. Under similar operating conditions, fuel-N conversion in the fuel reactor seems to be favoured under iG-CLC mode.

3.2.2. Evolution of nitrogen species in the fuel reactor

Neither under iG-CLC nor under CLOU mode the presence of NH_3 or HCN was detected at the fuel reactor outlet. As it is shown in Table 5, only N_2, NO_x and N_2O were identified depending on the conditions. This indicated that all the nitrogen released as NH_3 or HCN in the devolatilization was converted via homogenous or heterogeneous reactions.

Both in iG-CLC and CLOU, the major nitrogen species found in the fuel reactor was N_2, followed by NO_x and by certain amounts of N_2O, the later only in the case of CLOU experiments. The presence of N_2O can be attributed to the temperature range of operation (775–850 °C) and the release of molecular oxygen in the fuel reactor atmosphere [40]. In iG-CLC, 97.2, 96.7 and 94.6% of the nitrogen measured in the fuel reactor was N_2 in the experiments at 980 °C with pine sawdust, olive stone and almond shell, respectively. The corresponding percentages under the CLOU mode operating at 850 °C were 97.3, 92.0 and 81.5%.

Fig. 5(A) shows the different trends in the evolution of the molar ratio NO_x/C (expressed in ppm) with the fuel reactor temperature for both iG-CLC and CLOU. The NO_x/C ratio increased with temperature in CLOU since more oxygen was released by the oxygen carrier with the increase of the fuel reactor temperature [38]. However, this molar ratio slightly varied with the fuel reactor temperature under iG-CLC. Besides higher values of the NO_x/C ratio were found in CLOU. This was expected since the presence of gaseous oxygen in the fuel reactor atmosphere favours fuel-N oxidation to NO [41].

Focusing on the CLOU experiments for the three types of biomass, higher values of NO_x/C ratio were obtained for almond shell followed by olive stone and pine sawdust. This order was the opposite of that found for the corresponding char conversion in Fig. 3, where the higher char conversion values were obtained for pine sawdust then followed by olive stone and almond shell. Therefore, although pine char was converted in a larger extent, the conversion of fuel-N to NO was less favoured than in the rest of the biomass types considered. This effect becomes clearly shown at the highest temperature tested in CLOU (850 °C). Once formed, NO can react with biomass char to be reduced to N_2 following reaction (R1) [40]:
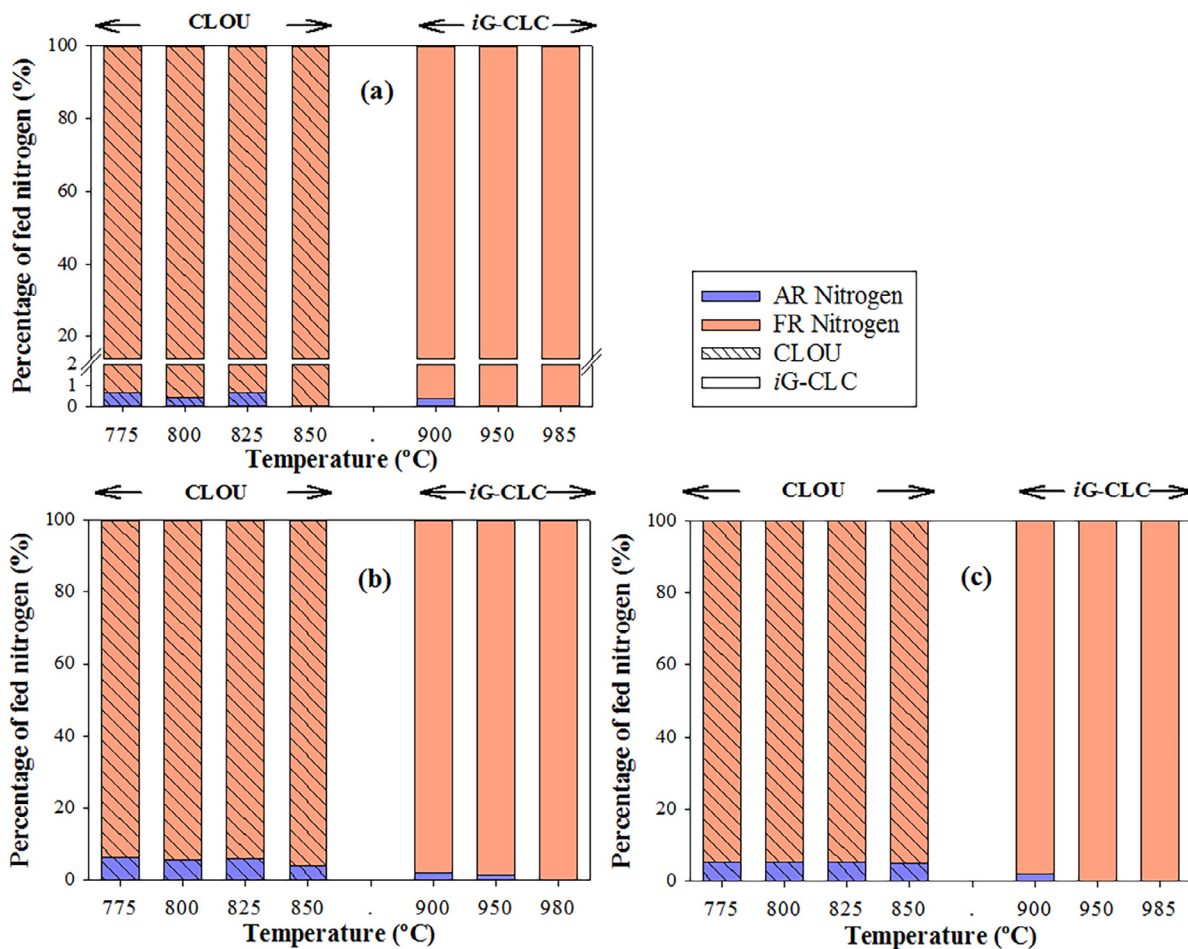
Fig. 4. Fuel-N distribution between fuel and air reactors for *i*G-CLC and CLOU processes burning the three different types of biomass: (a) pine sawdust, (b) olive stone and (c) almond shell at different fuel reactor temperatures.

Table 5
Nitrogen species found at the fuel reactor outlet in the *i*G-CLC and CLOU experiments.

*i*G-CLC	N_2, NO_x
CLOU	N_2, NO_x, N_2O

$$C(char) + NO \rightarrow CO + 1/2N_2 \tag{R1}$$

The differences in char reactivity to NO could contribute to the different NO_x/C molar ratios obtained in Fig. 5(A) with the different types of biomass. If the pine sawdust char were more reactive to NO than the rest of the chars in the temperature interval considered (775–850 °C), it could react with the NO in the atmosphere to produce N_2, therefore decreasing the NO_x/C molar ratio. Different results were
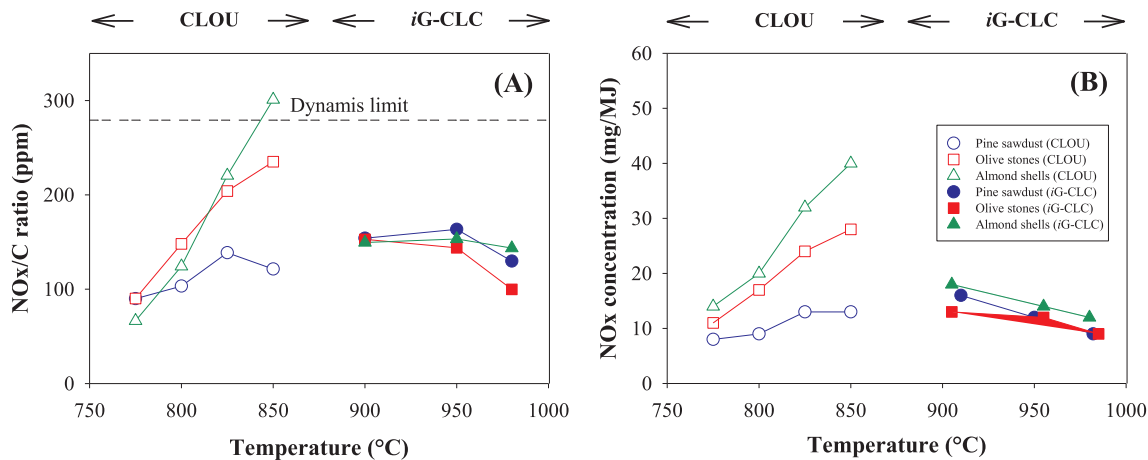

Fig. 5. (A) Molar ratio NO_x/C and (B) NO_x concentration per MJ at the fuel reactor outlet for CLOU (open symbols) and *i*G-CLC (filled symbols) processes at different fuel reactor temperatures.
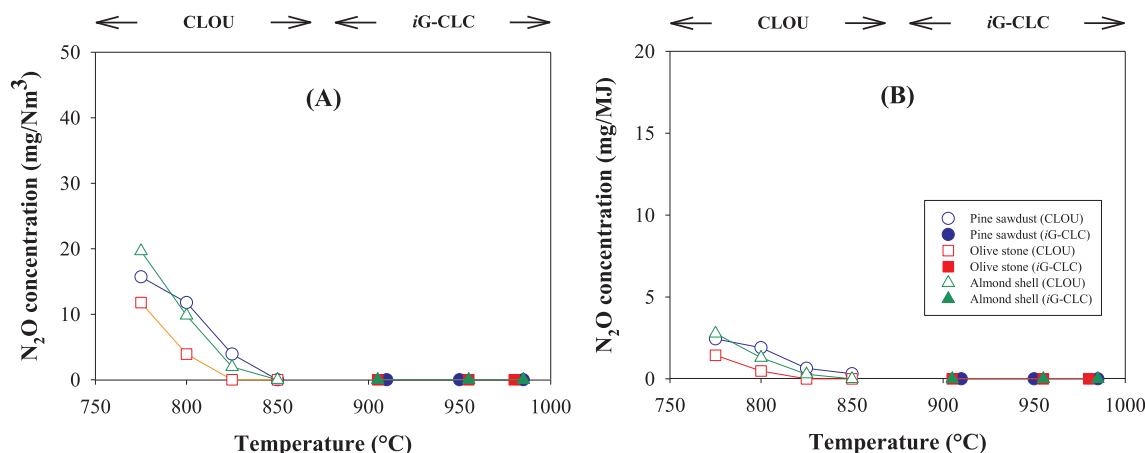
Fig. 6. N_2O concentrations (A) in mg/Nm^3 and (B) in mg/MJ at the fuel reactor outlet for CLOU (open symbols) and iG-CLC (filled symbols) processes at different fuel reactor temperatures.

found for the iG-CLC experiments, where no significant differences in NO_x/C ratio were found in the fuel reactor temperature range studied. In this case, the fuel reactor temperature is higher than in CLOU and it would notably enhance the heterogeneous reaction between char and NO (R1). Thus, the possible differences in char reactivity would be hindered or softened.

The quality of the CO_2 to be captured can be affected by the presence of different compounds in the outlet stream from the fuel reactor. Steam, N_2, O_2, CO, H_2, CH_4 and other hydrocarbons, SO_2, particles and also NO_x levels should be controlled in order to ensure that the captured CO_2 stream can be transported and safely stored. To date, no legal requirements exist and only recommendations have been outlined for the quality of CO_2 [42]. The limit marked by this recommendations regarding NO_x content in the CO_2 stream is indicated in Fig. 5(A). The experiments under iG-CLC would fulfil the requirements, as well as almost all of those performed under CLOU mode. Fig. 5(B) normalizes the emissions registered per MJ of fuel fed. According to Fig. 5(B), the trends previously observed in Fig. 5(A) are mostly maintained.

N_2O is a greenhouse gas with a long atmospheric lifetime and important radiative forcing compared to CO_2. Moreover, N_2O also plays an important role in the depletion of the ozone layer. The temperatures used in conventional fluidized bed combustion (800–900 °C) facilitate N_2O appearance [40]. Thus, its presence in CLC was assessed. Fig. 6(A) presents the evolution of N_2O concentration (expressed in mg/Nm^3) with the fuel reactor temperature for both iG-CLC and CLOU.

As it can be seen in Fig. 6(A), only in the experiments under CLOU mode N_2O was observed. The concentration of N_2O in the fuel reactor

outlet stream decreased with temperature to values close to zero at 850 °C. This was observed for the three types of biomass tested. The maximum concentration reached at the lowest temperature did not exceed 20 mg/Nm^3; see Fig. 6(A). The reduction of N_2O with the increase in temperature has already been reported in literature in the case of conventional combustion in fluidized bed [43]. Under iG-CLC mode, no N_2O was detected at the outlet of the fuel reactor, since temperatures were always higher than 900 °C. Fig. 6(B) shows the same results normalized per MJ of fuel fed.

3.2.3. Evolution of nitrogen species in the air reactor

Both during iG-CLC and CLOU operation, the main nitrogen species besides N_2 found at the air reactor outlet was NO. In this case, no N_2O was detected. This NO is originated in the oxidation of the fuel-N present in the unconverted char that reaches the air reactor. Fig. 7(A) and (B) shows the evolution of the NO concentration (both in mg/Nm^3 and mg/MJ) with the fuel reactor temperature, respectively. The NO concentrations have been normalized to 6% O_2 in the stream, as it is indicated in the legal emission limit.

In Fig. 7(A), the trends for both operating modes, iG-CLC and CLOU, are the same for all the types of biomass tested. The NO emissions decrease when the fuel reactor temperature increases. The reason for this trend is that an increase in the fuel reactor temperature enhances char gasification. If more char is converted, less unconverted char is transferred to the air reactor. Thus, the fuel-N released in the air reactor is decreased. Some differences can be appreciated among types of biomass. In all cases, higher NO concentrations in the air reactor were
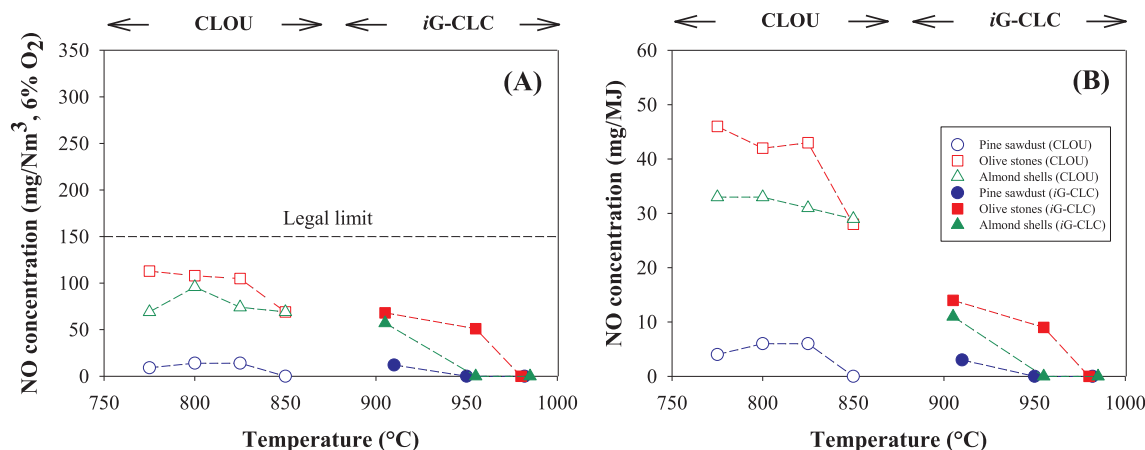

Fig. 7. NO_x concentrations (A) in mg/Nm^3 (6% O_2) and (B) in mg/MJ at the air reactor outlet for CLOU (open symbols) and iG-CLC (filled symbols) processes at different fuel reactor temperatures burning the three different types of biomass: pine sawdust, olive stone and almond shell.
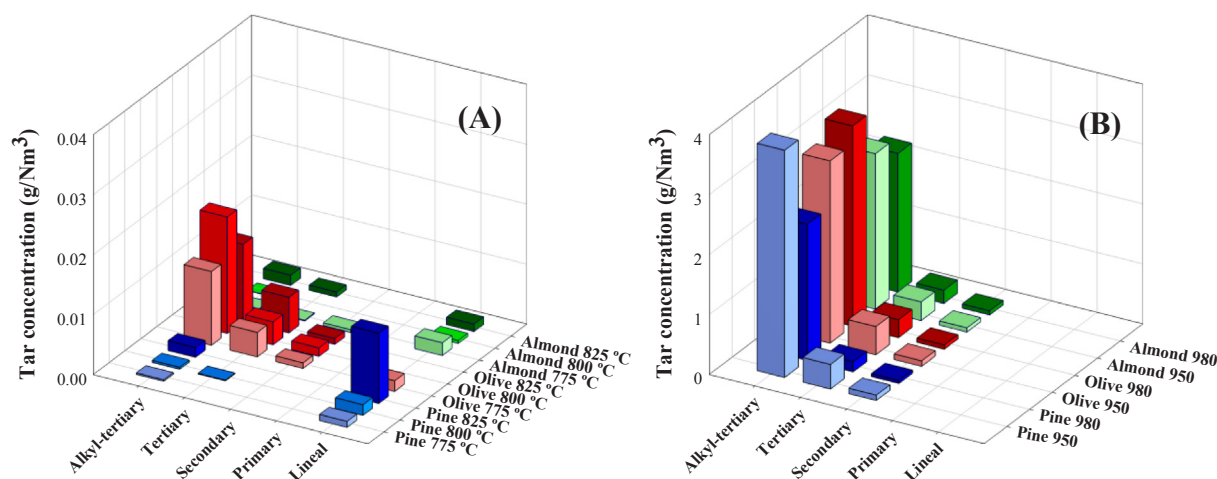
Fig. 8. Tar concentration for the three types of biomass tested at different fuel reactor temperatures operating under (A) CLOU mode and (B) iG-CLC mode.

found in the experiments with olive stone and almond shell. It should be taken into account that the NO present in the outlet stream of the air reactor can be considered an emission to the atmosphere and therefore, the levels should fulfil those specified in the current legislation [44]. The Directive 2010/75/EU on industrial emissions (integrated pollution prevention and control) sets the NO_x emission limit to 150 mg/Nm³ (normalized to 6% O_2) for new installations in the EU and for the highest power (> 300 MW). According to the values shown in Fig. 7(A), the NO_x level at the air reactor outlet was in the range 10–120 mg/Nm³ for the CLOU experiments and in the range 0–50 mg/Nm³ for iG-CLC experiments. Thus, no emission problems could be anticipated when biomass is used as fuel in a CLC system. Moreover, these values were obtained in the absence of a carbon striper, which would decrease the unconverted char bypassed to the air reactor and hence the NO_x formed in the air reactor.

3.3. Tar formation under iG-CLC and CLOU

Tar formation control during gasification represents one of the main challenges in the use of biomass. Tar has been reported to cause fouling problems downstream of the gasification chamber and strict limits have been imposed for its presence when the syngas produced is intended to be used for energy generation or chemicals production [45]. In the case of the CLC process, scarce information about tar formation can be found. The presence of tar is limited to the fuel reactor outlet and it is therefore affecting the quality of the CO_2 stream there generated and the further operations prior to CO_2 storage (compression and transport). In the recommendations summarized by de Visser et al. about CO_2 quality [42], there is no clear reference to tar. Nevertheless, in order to set a range of values for safe operation, the limit given by Reed et al. [46] for compressing and piping any distance a biomass gasification gas can be used. According to these authors, the tar content should be lower than 0.5 g/Nm³.

In the experiments under iG-CLC and CLOU modes, the tar compounds at the fuel reactor outlet were detected and quantified. In these experiments, steam was used in the fuel reactor as fluidizing agent in iG-CLC and nitrogen in CLOU. Most of the results from iG-CLC experiments were previously presented [15] and are included here to facilitate comparison with those obtained under CLOU mode. Fig. 8 plotted the tar compounds grouped as primary, secondary and tertiary tars [47,48] and also includes lineal hydrocarbons. The figure shows the concentration values for each group in the experiments with the different types of biomass.

The two most significant results when both operating CLC modes are compared are summarized next. First of all, the different levels of tar found. While in the iG-CLC operation, the total tar values oscillated

between 2.5 and 3.7 g/Nm³ at the highest temperature (980 °C), the values determined for CLOU were about two orders of magnitude lower (< 0.02 g/Nm³) in a lower fuel reactor temperature interval (775–850 °C). Therefore, in the case of iG-CLC additional measures should be considered in order to reduce the amount of tar present and to make it compatible with the < 0.5 g/Nm³ limit proposed by Reed et al. [46]. One of the possibilities is the combustion of tar in an oxygen polishing step after the fuel reactor together with the rest of unburnt compounds from the combustion process (CO, H_2 and CH_4) [15]. The tar levels found in the CLOU experiments are so low that it should not represent a problem in the CO_2 transport-storage chain. In any case, the combustion of biomass using both of any combustion modes results in lower tar content in the product gas stream than that expected in conventional processes such as biomass air-fired gasification. Note that for an air-blown circulating fluidized bed (CFB) gasifier a typical tar content of about 10 g/Nm³ has been reported [49].

The second relevant result is the tar composition found in the experiments. In the iG-CLC process the composition is similar for the three types of biomass tested and not clearly influenced by temperature (see [15]). The major compound is naphthalene accompanied by some other tertiary tars such as acenaphthylene and phenantrene. No benzene was detected, although the standard tar protocol followed to collect tar samples allows its collection as it was shown in previous works from the authors [35]. However, tar composition obtained in CLOU experiments showed some differences with respect to that obtained in iG-CLC. Table 6 shows the compounds identified in the CLOU experiments for different fuel reactor temperatures.

As it can be seen, low amounts of naphthalene are found but certain quantities of linear or branched hydrocarbons are detected, such as dodecane or tetradecane. This may indicate a different mechanism for the consumption/reforming of the tar under CLOU environment when compared to iG-CLC.

4. Conclusions

The two operating modes currently available to burn biomass using the Chemical Looping Combustion technology, namely iG-CLC and CLOU, were compared regarding two aspects in biomass combustion: NO_x and tar formation. Three different biomass residues were tested as fuels: pine sawdust, olive stone and almond shell.

Under similar operating conditions, fuel-N conversion seems to be favoured under iG-CLC mode. Although the combustion took place in different fuel reactor temperature ranges, in both combustion modes most the fuel-N appeared as N_2 at the fuel reactor outlet with only little presence of NO. The relation between N_2 and NO_x emitted in the fuel reactor was higher in the case of iG-CLC experiments due to the absence

Table 6

Tar composition for the CLOU tests with the three types of biomass (PN = pine sawdust; OS = olive stone; AS = almond shell).

Biomass	PN_4	PN_5	PN_6	OS_4	OS_5	OS_6	AS_4	AS_5	AS_6
Temperatures (°C)									
Fuel reactor	775	800	825	775	800	825	775	800	825
Air reactor	800	800	800	800	800	800	800	800	800
Tar composition (g/Nm^3 dry)									
Benzene, 1 propenyl	–	$1 \cdot 10^{-4}$	–	$1.7 \cdot 10^{-3}$	–	$1.9 \cdot 10^{-3}$	$1 \cdot 10^{-4}$	–	$5 \cdot 10^{-4}$
Dodecane	$4 \cdot 10^{-4}$	$1 \cdot 10^{-3}$	$6 \cdot 10^{-3}$	$1.8 \cdot 10^{-3}$	–	–	$9 \cdot 10^{-4}$	$2 \cdot 10^{-4}$	$7 \cdot 10^{-4}$
Indene	–	–	–	$6 \cdot 10^{-4}$	$1.1 \cdot 10^{-3}$	$1.4 \cdot 10^{-3}$	–	–	$3 \cdot 10^{-4}$
Tetradecane	$4 \cdot 10^{-4}$	$5 \cdot 10^{-4}$	$3.2 \cdot 10^{-3}$	–	–	–	$7 \cdot 10^{-4}$	$2 \cdot 10^{-4}$	$5 \cdot 10^{-4}$
Naphthalene	$2 \cdot 10^{-4}$	$3 \cdot 10^{-4}$	$7 \cdot 10^{-4}$	$10.5 \cdot 10^{-3}$	$19.4 \cdot 10^{-3}$	$11.9 \cdot 10^{-3}$	$1 \cdot 10^{-4}$	0.0000	$1.7 \cdot 10^{-3}$
2,6,10 trimethyltridecane	$2 \cdot 10^{-4}$	$3 \cdot 10^{-4}$	$2.5 \cdot 10^{-3}$	–	–	–	$5 \cdot 10^{-4}$	$1 \cdot 10^{-4}$	–
Naphthalene 2-methyl	–	–	–	$1.1 \cdot 10^{-3}$	$1.6 \cdot 10^{-3}$	$1.6 \cdot 10^{-3}$	–	–	–
Naphthalene 1-methyl	–	–	–	$7 \cdot 10^{-4}$	$1.1 \cdot 10^{-3}$	$1.1 \cdot 10^{-3}$	–	–	–
Biphenil	–	–	–	$9 \cdot 10^{-4}$	$1.4 \cdot 10^{-3}$	$1.0 \cdot 10^{-3}$	–	–	–
Benzophenone	–	–	–	–	–	–	$4 \cdot 10^{-4}$	–	–
Acenaphthylene	0.0000	–	–	$4 \cdot 10^{-4}$	–	$9 \cdot 10^{-4}$	–	–	–
Fluoranthene	–	–	–	–	–	–	–	–	–
Phenantrene	–	–	$9 \cdot 10^{-4}$	$1.4 \cdot 10^{-3}$	–	–	–	–	–
Total tar (g/Nm^3 dry)	0.001	0.002	0.013	0.019	0.025	0.020	0.003	0.001	0.004

of molecular oxygen that favours NO formation. Some differences between biomasses were observed regarding the amount of NO formed in the fuel reactor under CLOU mode and were attributed to the different char reactivity of the three types of biomass. Little amounts of N_2O were detected under CLOU mode at lower temperatures, but it disappeared at 850 °C. In the air reactor and for both combustion modes NO was detected and its concentration decreased when the fuel reactor temperature increased. However, its concentration never exceeded the current legal limits for power plants.

Regarding tar formation, total tar values between 2.5 and 3.7 g/Nm^3 were encountered under *i*G-CLC mode at the highest temperature (980 °C) at the fuel reactor outlet, mostly naphthalene. This makes a further oxygen polishing step necessary in order to condition the stream for subsequent transport and storage. Under CLOU, insignificant amounts were found although in this case also linear or branched hydrocarbons were detected.

Acknowledgments

References

[1] IPCC climate change 2014: synthesis report. Contribution of working groups I, II and III to the fifth assessment report of the intergovernmental panel on climate change. Geneva (Switzerland); 2014. p. 151.

[2] United Nations framework convention for climate change. The Paris agreement. http://unfccc.int/paris_agreement/items/9485.php; 2015.

[3] Azar C, Lindgren K, Obersteiner M, Riahi K, van Vuuren DP, den Elzen KMGJ, et al. The feasibility of low CO₂ concentration targets and the role of bio-energy with carbon capture and storage (BECCS). Clim Change 2010;100:195–202.

[4] IPCC. IPCC special report on carbon dioxide capture and storage. Cambridge, UK; 2005.

[5] Abanades JC, Arias B, Lyngfelt A, Mattisson T, Wiley DE, Li H, et al. Emerging CO₂ capture systems. Int J Greenhouse Gas Control 2015.

[6] Adanez J, Abad A, Garcia-Labiano F, Gayan P, De Diego LF. Progress in chemical-looping combustion and reforming technologies. Prog Energy Combust Sci 2012;38:215–82.

[7] Adánez J, Abad A, Mendiara T, Gayán P, de Diego LF, García-Labiano F. Chemical looping combustion of solid fuels. Prog Energy Combust Sci 2018;65:6–66.

[8] Kramp M, Thon A, Hartge EU, Heinrich S, Werther J. Carbon stripping – a critical process step in chemical looping combustion of solid fuels. Chem Eng Technol 2012;35:497–507.

[9] Cao Y, Pan WP. Investigation of chemical looping combustion by solid fuels. 1. Process analysis. Energy Fuels 2006;20:1836–44.

[10] Abad A, Adánez-Rubio I, Gayán P, García-Labiano F, de Diego LF, Adánez J. Demonstration of chemical-looping with oxygen uncoupling (CLOU) process in a 1.5 kW$_{th}$ continuously operating unit using a Cu-based oxygen-carrier. Int J Greenhouse Gas Control 2012;6:189–200.

[11] Adánez-Rubio I, Abad A, Gayán P, de Diego LF, Adánez J. CLOU process performance with a Cu-Mn oxygen carrier in the combustion of different types of coal with CO₂ capture. Fuel 2018;212:605–12.

[12] Schmitz M, Linderholm C, Lyngfelt A. Chemical looping combustion of sulphurous solid fuels using spray-dried calcium manganate particles as oxygen carrier. Energy Proc 2014;63:140–52.

[13] Mendiara T, García-Labiano F, Abad A, Gayán P, de Diego LF, Izquierdo MT, et al. Negative CO₂ emissions through the use of biofuels in chemical looping technology: A review. Appl Energy 2018. (accepted for publication).

[14] Mendiara T, Abad A, de Diego LF, García-Labiano F, Gayán P, Adánez J. Biomass combustion in a CLC system using an iron ore as an oxygen carrier. Int J Greenhouse Gas Control 2013;19:322–30.

[15] Mendiara T, Pérez-Astray A, Izquierdo MT, Abad A, de Diego LF, García-Labiano F, et al. Chemical looping combustion of different types of biomass in a 0.5 kW$_{th}$ unit. Fuel 2018;211:868–75.

[16] Shen L, Wu J, Xiao J, Song Q, Xiao R. Chemical-looping combustion of biomass in a 10 kW$_{th}$ reactor with iron oxide as an oxygen carrier. Energy Fuels 2009;23:2498–505.

[17] Linderholm C, Schmitz M, Knutsson P, Källén M, Lyngfelt A. Use of low-volatile solid fuels in a 100 kW chemical-looping combustor. Energy Fuels 2014;28:5942–52.

[18] Ströhle J, Ohlemüller P, Epple B. Chemical looping combustion of coal and biomass in a 1 MW$_{th}$ pilot plant using ilmenite and iron ore as oxygen carrier. 6th high temperature solid looping network meeting, Milano (Italy). 2015.

[19] Ohlemüller P, Ströhle J, Epple B. Chemical looping combustion of hard coal and torrefied biomass in a 1 MW$_{th}$ pilot plant. Int J Greenhouse Gas Control 2017;65:149–59.

[20] Berdugo Vilches T, Lind F, Rydén M, Thunman H. Experience of more than 1000 h of operation with oxygen carriers and solid biomass at large scale. Appl Energy 2017;190:1174–83.

[21] Abad A, Pérez-Vega R, Pérez-Astray A, Mendiara T, De Diego LF, García-Labiano F, et al. Biomass combustion with CO₂ capture by chemical looping: experimental results in a 50 kWth pilot plant. International conference on negative CO₂ emissions, Gothemburg (Sweden). 2018.

[22] Gu H, Shen L, Xiao J, Zhang S, Song T. Chemical looping combustion of biomass/coal with natural iron ore as oxygen carrier in a continuous reactor. Energy Fuels 2011;25:446–55.

[23] Adánez-Rubio I, Abad A, Gayán P, De Diego LF, García-Labiano F, Adánez J. Biomass combustion with CO₂ capture by chemical looping with oxygen uncoupling (CLOU). Fuel Process Technol 2014;124:104–14.

[24] Adánez-Rubio I, Pérez-Astray A, Mendiara T, Izquierdo MT, Abad A, Gayán P, et al. Chemical looping combustion of biomass: CLOU experiments with a Cu-Mn mixed oxide. Fuel Process Technol 2018;172:179–86.

[25] Schmitz M, Linderholm CJ. Performance of calcium manganate as oxygen carrier in chemical looping combustion of biochar in a 10 kW pilot. Appl Energy 2016;169:729–37.

[26] Schmitz M, Linderholm CJ, Lyngfelt A. Chemical looping combustion of four different solid fuels using a manganese-silicon-titanium oxygen carrier. Int J Greenhouse Gas Control 2018;70:88–96.

[27] Ishida M, Jin H. A novel chemical-looping combustor without NO$_x$ formation. Ind Eng Chem Res 1996;35:2469–72.

[28] Mendiara T, Izquierdo MT, Abad A, de Diego LF, García-Labiano F, Gayán P, et al. Release of pollutant components in CLC of lignite. Int J Greenhouse Gas Control 2014;22:15–24.

[29] Song T, Shen L, Xiao J, Chen D, Gu H, Zhang S. Nitrogen transfer of fuel-N in chemical looping combustion. Combust Flame 2012;159:1286–95.

[30] Song T, Shen T, Shen L, Xiao J, Gu H, Zhang S. Evaluation of hematite oxygen carrier in chemical-looping combustion of coal. Fuel 2013;104:244–52.

[31] Pérez-Vega R, Adánez-Rubio I, Gayán P, Izquierdo MT, Abad A, García-Labiano F, et al. Sulphur, nitrogen and mercury emissions from coal combustion with CO$_2$ capture in chemical looping with oxygen uncoupling (CLOU). Int J Greenhouse Gas Control 2016;46:28–38.

[32] Mendiara T, Adánez-Rubio I, Gayán P, Abad A, De Diego LF, García-Labiano F, et al. Process comparison for biomass combustion. *In situ* gasification-chemical looping combustion (*i*G-CLC) versus chemical looping with oxygen uncoupling (CLOU). Energy Technol 2016;4:1130–6.

[33] Zeng J, Xiao R, Zhang H, Wang Y, Zeng D, Ma Z. Chemical looping pyrolysis-gasification of biomass for high H$_2$/CO syngas production. Fuel Proc Technol 2017;168:116–22.

[34] Simell P, Ståhlberg P, Kurkela E, Albrecht J, Deutsch S, Sjöström K. Provisional protocol for the sampling and analysis of tar and particulates in the gas from large-scale biomass gasifiers. Version 1998. Biomass Bioenergy 2000;18:19–38.

[35] Virginie M, Adánez J, Courson C, De Diego LF, García-Labiano F, Niznansky D, et al. Effect of Fe-olivine on the tar content during biomass gasification in a dual fluidized bed. Appl Catal B Environ 2012;121–122:214–22.

[36] Adánez-Rubio I, Pérez-Astray A, Abad A, Gayán P, De Diego LF, Adánez J. Biomass combustion by chemical looping with oxygen uncoupling process: experiments with Cu-based and Cu-Mn mixed oxide as oxygen carriers. International Conference on Negative CO$_2$ Emissions, Gothemburg (Sweden). 2018.

[37] Abad A, Mendiara T, de Diego LF, García-Labiano F, Gayán P, Adánez J. A simple model for comparative evaluation of different oxygen carriers and solid fuels in iG-CLC processes. Fuel Process Technol 2018.

[38] Adánez-Rubio I, Izquierdo MT, Abad A, Gayán P, de Diego LF, Adánez J. Spray granulated Cu-Mn oxygen carrier for chemical looping with oxygen uncoupling (CLOU) process. Int J Greenhouse Gas Control 2017;65:76–85.

[39] Werther J, Saenger M, Hartge EU, Ogada T, Siagi Z. Combustion of agricultural residues. Prog Energy Combust Sci 2000;26:1–27.

[40] Glarborg P, Jensen AD, Johnsson JE. Fuel nitrogen conversion in solid fuel fired systems. Prog Energy Combust Sci 2003;29:89–113.

[41] Williams A, Jones JM, Ma L, Pourkashanian M. Pollutants from the combustion of solid biomass fuels. Prog Energy Combust Sci 2012;38:113–37.

[42] de Visser E, Hendriks C, Barrio M, Mølnvik MJ, de Koeijer G, Liljemark S, et al. Dynamis CO$_2$ quality recommendations. Int J Greenhouse Gas Control 2008;2:478–84.

[43] Pels JR, Wójtowicz MA, Moulijn JA. Rank dependence of N$_2$O emission in fluidized-bed combustion of coal. Fuel 1993;72:373–9.

[44] DIRECTIVE 2010/75/EU of the European Parliament and of the Council on industrial emissions (integrated pollution prevention and control); 2010.

[45] Milne TA, Evans RJ. Biomass gasifier 'tars': their nature, formation and conversion. 1998.

[46] Reed TB, Levie B, Graboski MS. Tar conversion. Fundamentals, development and scaleup of the air-oxygen stratified downdraft gasifier. Solar Energy Research Institute; 1987. SERI/PR-234-2571.

[47] Evans RJ, Milne TA. Molecular characterization of the pyrolysis of biomass. Energy Fuels 1987;1:123–37.

[48] Evans RJ, Milne TA. Molecular characterization of the pyrolysis of biomass. 2. Applications. Energy Fuels 1987;1:311–9.

[49] Anis S, Zainal ZA. Tar reduction in biomass producer gas via mechanical, catalytic and thermal methods: a review. Renewable Sustainable Energy Rev 2011;15:2355–77.